Proceedings of the

4th Patras Workshop on Axions, WIMPs and WISPs

June 18-21, 2008
Hamburg, Germany

Editors: Axel Lindner, Javier Redondo and Andreas Ringwald

Verlag Deutsches Elektronen-Synchrotron

Impressum

Proceedings of the 4th Patras Workshop on Axions, WIMPs and WISPs
June 18-21, 2008, Hamburg, Germany

Conference homepage
`http://axion-wimp2008.desy.de/`

Slides at
`http://axion-wimp2008.desy.de/e30`

Online proceedings at
`http://www-library.desy.de/confprocs.html`

The copyright is governed by the Creative Commons agreement, which allows for free use and distribution of the articels for non-commertial activity, as long as the title, the authors' names and the place of the original are referenced.

Editors:
Axel Lindner, Javier Redondo and Andreas Ringwald
August 2008
DESY-PROC-2008-02
ISBN 978-3-935702-26-3
ISSN 1435-8077

Published by
Verlag Deutsches Elektronen-Synchrotron
Notkestraße 85
22607 Hamburg
Germany

Organizing Committee

Laura Baudis,
Physik Institut,
University of Zurich
Winterthurerstr. 190
CH-8057 Zuerich

Joerg Jaeckel,
Department of Physics,
Durham University,
South Road
Durham DH1 3LE

Axel Lindner, Javier Redondo, Andreas Ringwald,
Deutsches Elektronen Synchrotron DESY,
Notkestraße 85,
D-22607 Hamburg

Konstantin Zioutas
Department of Physics,
University of Patras
26504 Rio

Conference Secretary and Local Organization

Julia Herrmann and Barbara Wittmann
Deutsches Elektronen Synchrotron DESY,
Notkestraße 85,
D-22607 Hamburg

Preface

The 4th Patras Workshop on Axion, WIMPs and WISPs took place from 18th to 21st June 2008 at DESY Hamburg. It was organized and supported by CERN, DESY and the Universities of Hamburg and Patras.

The original aim of this series of workshops was to provide academic training to the new generations of scientists working in the already mature field of axion physics. Since axions are one of the few prominent candidates for the dark matter in the universe it was quite natural to widen the scope already in the third workshop to include also its main alternative, weakly interacting massive particles (WIMPs), as another central topic. The interest was already moving from one concrete particle to one of the central questions of fundamental science today:

What is dark matter made of?

What hides beyond the successful Standard Model of particle physics?

In the present edition, this tendency has led us to include a third class of candidates for particles beyond the standard model, the so-called weakly interacting sub-eV particles (WISPs). Indeed, this mildly defined category naturally includes axions but also light hidden sector particles like hidden photons or mini-charged particles predicted in embeddings of the standard model in more unified theories, like string theory, which also includes gravity.

The spirit of these meetings has always been to bring together theorists and experimentalists, from every field in which our seek particles can manifest. The organizers of this workshop are especially proud of having gathered experts in cosmology, astrophysics and astroparticle physics, collider physics, optics, gravity and mathematics. This communion has always been extremely fertile in ideas, projects and collaborations. We sincerely believe that this workshop has even surpassed the expectations from previous events. We are looking forward to another boost from the 5th Patras Workshop to be held from 13th to 17th July 2009 in Durham.

Axel Lindner, Javier Redondo and Andreas Ringwald

Acknowledgements

The organizers would like to thank DESY for support and infrastructure and specially Julia Herrmann and Barbara Wittmann for their help with the organization what made the workshop run smoothly and helped to create a relaxing atmosphere.

The organizing committee.

Contents

Chapter 1

The Physics Case for WIMPs, Axions and WISPs

The Physics Case for Axions, WIMPs, WISPs and other Weird Stuff

Joerg Jaeckel

Institute for Particle Physics and Phenomenology, Durham University, Durham DH1 3LE, UK

We argue that there exists an excellent "physics case" motivating the search for axions, WIMPs, WISPs and other phenomena testable at low energies. This physics case arises from both experimental and observational evidence as well as the desire to test theoretical model building.

1 Introduction – Hints for new physics

Over the years both theoretical as well as experimental evidence has accumulated that strongly suggests the existence of physics beyond the current standard model of particle physics (SM). The Large Hadron Collider currently starting up at CERN will test many of the ideas for such physics beyond the standard model (BSM) and hopefully will provide us with a wealth of new information. In this note we argue that there is also a very good motivation to search for new physics in low energy experiments that can provide us with powerful complementary information on currently open questions and in particular on how the standard model is embedded into a more fundamental theory.

Let us begin by briefly repeating some of the main reasons why we believe that there must be physics beyond the standard model.

On the theoretical side there are a number of deficiencies in the SM. Some of them could be just aesthetic defects but some may go deeper. First of all the SM has a relatively large number $\mathcal{O}(30)$ free parameters that cannot be determined from theory alone but must be measured experimentally. Although this does not indicate an inconsistency of the theory it certainly is not in line with the hope that a fundamental theory of everything should have very few, possibly only 1 or even 0, free parameters. Moreover, some of the parameters seemingly need to require an enormous degree of finetuning or appear unnaturally small. Well known examples are the Higgs mass but also the θ parameter of QCD (which must be extremely small in order not to be in conflict with the observed smallness of strong CP violation). Another dissatisfying feature is that gravity is not incorporated into the SM but rather treated as a separate part. This is not just an aesthetic defect but also an expression of the fact that the quantization of gravity is still not (fully) understood. Finally, strictly speaking the SM will most likely not be valid up to arbitrary high energy scales. On the one hand this is due to our current inability to properly quantize gravity. But even the non-gravity parts are probably encountering problems in the form of Landau poles (places where the coupling becomes infinite) in the QED sector (at a very high scale much beyond the Planck scale) but probably also in the Higgs sector (where the problem is much more immediate and will occur at scales much below the Planck scale -

depending on the Higss mass possibly even not much above the electroweak scale).

Next there are quite a few phenomena which are experimentally well established but for which there is no good explanation within the standard model. The most shocking of which is probably the realization that most of the matter and energy in the universe actually is not made up of SM particles. Cosmological and astrophysical observations give strong evidence that about 70 % of the energy in the universe is dark energy and another 25 % is dark matter [1]. These are things that simply do not appear in the current SM (although they could be accommodated see, e.g., [2]). But even within the standard model there are things which are experimentally well established but for which a good explanation is lacking. These are, e.g., the existence of three generations of SM particles, the mass hierarchies for the SM particles and the small parameters such as, e.g., the already mentioned θ parameter [3]. The latter is, of course, a repetition of some of the problems already mentioned as 'theoretical' problems showing that they actually arise from experimental results.

Finally, there is the direct experimental evidence for BSM physics. At the moment most of this is still relatively circumstantial but it definitely demonstrates that low energy experiments can provide information on BSM physics as well as opening new directions which can be explored (or close others). Examples are the deviation [4] of the muon $(g-2)$ from the SM expectation, the excess in the event rate of the DAMA [5] experiment and the PVLAS anomaly [6] (which has been retracted [7] but, as we will see, has inspired a lot of fruitful experimental and theoretical activity).

2 Bottom-up/phenomenological arguments

In this section we will present several examples for physics at the low energy frontier that arise from more phenomenological arguments - a line of thought that could be called 'bottom-up' and that follows a hands-on approach on fixing problems step by step.

Axions are a good example for this approach [8]. The extreme smallness of the θ-angle is unexplained in the standard model. This can be solved by introducing a new symmetry - the Peccei Quinn symmetry. As a consequence one predicts a pseudo-Goldstone boson, the axion. This is already a good motivation to experimentally search for the axion, for example in light shining through a wall experiments [9, 10, 11], laser polarization experiments (as, e.g., PVLAS) [6, 7, 12] or axion helioscopes [13]. The case for this search is then strengthened by the finding that the axion is also a valid candidate for dark matter [14]. This prediction, however, not only strengthens the physics case for searching axions but it also opens new ways to do so. One can search for axion dark matter, for example using resonant cavity techniques [15] or looking in the sky for axions decaying into photons.

Another example are WIMPs (for a review see [16]). As a solution for the hierarchy problem in the SM one can, again, introduce a symmetry: SUSY. Introducing SUSY leads to many new particles, notably the heavy supersymmetric partners of the SM particles, which are weakly interacting and massive, i.e. WIMPs. Some of them are good candidates for dark matter. Again good motivation to perform a WIMP search. Another incentive is that SUSY also allows to explain the deviation of the muon $(g-2)$ from its SM value that was already mentioned in the introduction. SUSY might be discovered at a collider such as LHC. Such an experiment may even find a dark matter candidate. But in order to know that such a candidate really makes up all or most of the dark matter, i.e. if it was produced in sufficient quantities, one needs the low energy WIMP searches [5, 17] which therefore give us crucial information.

The PVLAS anomaly which was in contradiction to the SM expectation led to the introduction of several types of WISPs (weakly interacting slight (or sub-eV) particles). To check their result and to search for these WISPs the PVLAS group then improved their apparatus finding that the original result was probably an artifact of the apparatus [7]. However, this is not the end of the story. The introduction of WISPs also led people to realize that there is a large amount of unexplored parameter space for new physics that (e.g., due to the extremely weak interactions involved) cannot be tested in conventional colliders [18] [1]. Yet new ideas how to access this parameters space in low energy experiments and observations have been put forward [20]. Moreover, it was (re-)discovered that the extremely weak interactions of WISPs are often connected to very high energy scales $\gtrsim 10^5$ GeV, in some cases even as high as the string or the even Planck scale $\sim 10^{18}$ GeV. Showing that the new and improved low energy experiments can give us complementary information on very high energy physics.

3 Top-down/theory arguments

Instead of taking small steps and fixing the problems, in the process often creating a more and more baroque model, one can also go back to the drawing board and rethink the very principles on which the original model was based. One such attempt (among others) is string theory. One of the main motivations for string theory is to unify the SM with gravity. To achieve this point particles are replaced by extended strings. Currently string theory is not yet in a state where it provides a first principle derivation of the SM and corrections to the same. Nevertheless, it has a variety of general features that suggest avenues for model building and also specific phenomena.

One such general feature is that for consistency string theory likes SUSY. Following the arguments from the previous section SUSY provides a good physics case for WIMP searches. Accordingly string theory strengthens the physics case for such searches.

Another property of string theory is that in order to be consistent it needs the existence of extra (space) dimensions. In order to be in agreement with observation all except the well known three have to be compactified. However, compactification leaves its traces[2]. Shape and size deformations of the compactified dimensions correspond to scalar fields, so-called moduli. These could be very light (it is actually often difficult to give them any mass at all) and provide excellent WISP candidates (and may also be searched for in fifth force experiments [21]). In a similar manner also various types of axions appear in string theory (see, e.g., [22]). The physics of these particles (e.g. the small size of their interactions) is inherently linked to the string scale. Hence, suitable low energy experiments searching for such WISPs may give us the opportunity to probe the fundamental theory and its associated fundamental energy scale.

String theory also tends to have whole sectors of extra matter in addition to the ordinary SM matter. This matter often lives in so-called hidden sectors which have only extremely weak interactions with the SM particles. Accordingly particles in these sectors may avoid detection in collider experiments even if they are light, i.e. these hidden sector provide good candidates for WISPs[3]. Typical WISP candidates arising from such hidden sectors are extra 'hidden' U(1)

[1]Astrophysical arguments are, however, a different matter. For an overview over pre-PVLAS work in this direction see, e.g., [19].

[2]If the size of the extra dimension is large enough there could actually be a very direct consequence: the inverse square law of the gravitational force would be modified. This, too, can be tested in low energy experiments [21].

[3]If the hidden sector particles are somewhat heavier they can also be WIMP candidates [23] (which in some cases can also be searched for at colliders [23, 24]). However, this also depends on how strict one takes the

gauge bosons and 'hidden' matter charged under those U(1)s [25, 26][4]. In many models these hidden sectors are located at a different place in the extra dimension than the SM sector[5]. Accordingly searching and testing these hidden sectors can give us crucial global information on the compactification that can hardly be obtained from collider experiments which probe the local structure that has relatively strong interactions.

Finally, string theory also motivates some surprising things. In particular, some models predict non-commutativity and other Lorentz symmetry violating effects [30]. This then can also be tested in low energy experiments and observations such as, e.g., comparing the spectrum of hydrogen and anti hydrogen atoms [31] or by observing if light from gamma-ray bursts arrives at (slightly) different times depending on its polarization [32]. These experiments and observations (see [33] for an overview) again provide an ultra high precision that can then give us insights into the fundamental theory at very high energy scales.

4 Conclusions

Both the phenomenological bottom-up and the more theory oriented top-down approach provide an excellent physics case motivating further experiments at the low-energy frontier such as searches for axions, WIMPs and WISPs and other interesting effects such as Lorentz violation. These phenomena are often connected to energy scales much higher than those reachable in near future accelerators. They provide experimental access to hidden sectors that may contain crucial information on the underlying global structure of a more fundamental theory. Moreover, they give us reasons to challenge and experimentally check basic assumptions as, e.g., Lorentz symmetry. In conclusion, low energy but high precision experiments provide crucial complementary information to uncover the nature of a more fundamental theory beyond the standard model.

Final Note: Many of the things mentioned in these proceedings have been intensely discussed at the *Brainstorming and Calculationshop: The Physics Case for a Low Energy Frontier of Fundamental Physics* held at DESY in June 2008. More details from this collective effort can be found soon on http://alps-wiki.desy.de/e13/e42.

Acknowledgements

The author wishes to thank the organizers of the *4th Patras Workshop on Axions, WIMPs and WISPs* for a very enjoyable and stimulating meeting. Moreover, he is indebted to all participants of the *Brainstorming and Calculationshop: The Physics Case for a Low Energy Frontier of Fundamental Physics* for a great meeting on the subjects discussed in these proceedings.

'Weak' in the name WIMP. Often it is constraint to be the weak of electroweak. Then hidden sector particles cannot really be WIMPs.

[4]The hidden U(1)'s can interact with the SM via a kinetic or mass mixing with the ordinary photon [27, 28]. This kinetic mixing can then also lead to a small electric charge for the hidden matter [28].

[5]An alternative to truly hidden sectors are sectors with hyperweak interactions [29]. Although in these models the new particles can have tree-level interactions with the standard model particles these are extremely weak. Effectively they are diluted because the hyperweak sector extends more into the extra dimensions. Accordingly these, too, contain more information about the global structure.

References

[1] E. Komatsu *et al.* [WMAP Collaboration], arXiv:0803.0547 [astro-ph].

[2] H. Davoudiasl, R. Kitano, T. Li and H. Murayama, Phys. Lett. B **609** (2005) 117.

[3] N. F. Ramsay, Phys. Rept. **43** (1977) 409; C. A. Baker *et al.*, Phys. Rev. Lett. **97** (2006) 131801.

[4] G. W. Bennett *et al.* [Muon g-2 Collaboration], Phys. Rev. Lett. **92** (2004) 161802.

[5] R. Bernabei *et al.* [DAMA Collaboration], arXiv:0804.2741 [astro-ph].

[6] E. Zavattini *et al.* [PVLAS Collaboration], Phys. Rev. Lett. **96** (2006) 110406 [Erratum-ibid. **99** (2007) 129901].

[7] E. Zavattini *et al.* [PVLAS Collaboration], Phys. Rev. D **77** (2008) 032006.

[8] R. D. Peccei and H. R. Quinn, Phys. Rev. Lett. **38**, 1440 (1977); Phys. Rev. D **16**, 1791 (1977); S. Weinberg, Phys. Rev. Lett. **40**, 223 (1978); F. Wilczek, Phys. Rev. Lett. **40**, 279 (1978); J. E. Kim, Phys. Rept. **150** (1987) 1.

[9] P. Sikivie, Phys. Rev. Lett. **51**, 1415 (1983) [Erratum-ibid. **52**, 695 (1984)]; A. A. Anselm, Yad. Fiz. **42**, 1480 (1985); M. Gasperini, Phys. Rev. Lett. **59**, 396 (1987); K. Van Bibber, N. R. Dagdeviren, S. E. Koonin, A. Kerman and H. N. Nelson, Phys. Rev. Lett. **59**, 759 (1987).

[10] R. Cameron *et al.* [BFRT Collaboration], Phys. Rev. D **47** (1993) 3707;

[11] K. Ehret *et al.*, arXiv:hep-ex/0702023; C. Robilliard,*et al* [BMV Collaboration], Phys. Rev. Lett. **99** (2007) 190403; A. S. Chou *et al.* [GammeV (T-969) Collaboration], Phys. Rev. Lett. **100** (2008) 080402; P. Pugnat *et al.* [OSQAR Collaboration], arXiv:0712.3362 [hep-ex]. M. Fouche *et al.* [BMV Collaboration], Phys. Rev. D **78** (2008) 032013; A. Afanasev *et al.* [LIPSS Collaboration], arXiv:0806.2631 [hep-ex].

[12] S. J. Chen, H. H. Mei and W. T. Ni [Q& A Collaboration], Mod. Phys. Lett. A **22** (2007) 2815; P. Pugnat *et al.* [OSQAR Collaboration], Czech. J. Phys. **55**, A389 (2005); Czech. J. Phys. **56**, C193 (2006); R. Battesti *et al.* [BMV Collaboration], Eur. Phys. J. D **46**, 323333 (2008).

[13] K. Zioutas *et al.* [CAST Collaboration], Phys. Rev. Lett. **94** (2005) 121301; S. Andriamonje *et al.* [CAST Collaboration], JCAP **0704** (2007) 010; M. Minowa, Y. Inoue, Y. Akimoto, R. Ohta, T. Mizumoto and A. Yamamoto, arXiv:0809.0596 [astro-ph].

[14] L. F. Abbott and P. Sikivie, Phys. Lett. B **120** (1983) 133; J. Preskill, M. B. Wise and F. Wilczek, Phys. Lett. B **120** (1983) 127; M. Dine and W. Fischler, Phys. Lett. B **120** (1983) 137.

[15] P. Sikivie, Phys. Rev. Lett. **51** (1983) 1415 [Erratum-ibid. **52** (1984) 695]; S. Asztalos *et al.*, Phys. Rev. D **64** (2001) 092003; L. D. Duffy *et al.*, Phys. Rev. D **74** (2006) 012006.

[16] G. Jungman, M. Kamionkowski and K. Griest, Phys. Rept. **267** (1996) 195.

[17] F. Probst *et al.*, Nucl. Phys. Proc. Suppl. **110** (2002) 67; D. S. Akerib *et al.* [CDMS Collaboration], Phys. Rev. Lett. **93** (2004) 211301; G. Angloher *et al.* [CRESST Collaboration], Astropart. Phys. **23** (2005) 325; V. Sanglard *et al.* [The EDELWEISS Collaboration], Phys. Rev. D **71** (2005) 122002; J. Angle *et al.* [XENON Collaboration], Phys. Rev. Lett. **100** (2008) 021303; Z. Ahmed *et al.* [CDMS Collaboration], arXiv:0802.3530 [astro-ph].

[18] E. Masso and J. Redondo, JCAP **0509** (2005) 015; P. Jain and S. Mandal, Int. J. Mod. Phys. D **15** (2006) 2095; J. Jaeckel, E. Masso, J. Redondo, A. Ringwald and F. Takahashi, hep-ph/0605313; Phys. Rev. D **75** (2007) 013004; E. Masso and J. Redondo, Phys. Rev. Lett. **97** (2006) 151802; H. Gies, J. Jaeckel and A. Ringwald, Phys. Rev. Lett. **97** (2006) 140402; R. N. Mohapatra and S. Nasri, Phys. Rev. Lett. **98** (2007) 050402; P. Brax, C. van de Bruck and A. C. Davis, Phys. Rev. Lett. **99** (2007) 121103; P. Brax, C. van de Bruck, A. C. Davis, D. F. Mota and D. J. Shaw, Phys. Rev. D **76** (2007) 085010; I. Antoniadis, A. Boyarsky and O. Ruchayskiy, Nucl. Phys. B **793** (2008) 246; M. Ahlers, H. Gies, J. Jaeckel, J. Redondo and A. Ringwald, Phys. Rev. D **76** (2007) 115005; Phys. Rev. D **77** (2008) 095001.

[19] G. G. Raffelt, Stars As Laboratories For Fundamental Physics: The Astrophysics of Neutrinos, Axions, and other Weakly Interacting Particles, University of Chicago Press, Chicago, 1996; S. Davidson, S. Hannestad and G. Raffelt, JHEP **0005** (2000) 003.

[20] A. Dupays, C. Rizzo, M. Roncadelli and G. F. Bignami, Phys. Rev. Lett. **95** (2005) 211302; H. Gies, J. Jaeckel and A. Ringwald, Europhys. Lett. **76** (2006) 794; A. Badertscher *et al.*, Phys. Rev. D **75** (2007) 032004; A. Dupays, E. Masso, J. Redondo and C. Rizzo, Phys. Rev. Lett. **98** (2007) 131802; M. Fairbairn, T. Rashba and S. V. Troitsky, Phys. Rev. Lett. **98** (2007) 201801; E. G. Adelberger, B. R. Heckel, S. A. Hoedl, C. D. Hoyle, D. J. Kapner and A. Upadhye, Phys. Rev. Lett. **98** (2007) 131104; M. Ahlers, H. Gies, J. Jaeckel and A. Ringwald, Phys. Rev. D **75** (2007) 035011; S. N. Gninenko, N. V. Krasnikov and A. Rubbia, Phys. Rev. D **75** (2007) 075014; A. Mirizzi, G. G. Raffelt and P. D. Serpico, Phys. Rev. D **76** (2007) 023001; A. Melchiorri, A. Polosa and A. Strumia, Phys. Lett. B **650** (2007) 416; J. Jaeckel and A. Ringwald, Phys. Lett. B **653** (2007) 167; D. Hooper and P. D. Serpico, Phys. Rev. Lett. **99** (2007) 231102; J. Jaeckel and A. Ringwald, Phys. Lett. B **659** (2008) 509; A. De Angelis, O. Mansutti and M. Roncadelli, Phys. Lett. B **659** (2008) 847; K. A. Hochmuth and G. Sigl, Phys. Rev. D **76** (2007) 123011; M. Ahlers, A. Lindner, A. Ringwald, L. Schrempp and C. Weniger, Phys. Rev. D **77** (2008) 015018; H. Gies, D. F. Mota and D. J. Shaw, Phys. Rev. D **77** (2008) 025016; S. N. Gninenko, arXiv:0802.1315 [hep-ph]. S. N. Gninenko and J. Redondo, Phys. Lett. B **664** (2008) 180; J. Jaeckel, J. Redondo and A. Ringwald, arXiv:0804.4157 [astro-ph]; A. S. Chou *et al.*, arXiv:0806.2438 [hep-ex]; J. Jaeckel and J. Redondo, 0806.1115 [hep-ph]; P. L. Slocum, talk at the *4th Patras Workshop on Axions, WIMPs and WISPs* 2008, Hamburg, http://axion-wimp.desy.de/e30; M. Ahlers, J. Jaeckel, J. Redondo and A. Ringwald, arXiv:0807.4143 [hep-ph]; J. Jaeckel, arXiv:0807.5097 [hep-ph].

[21] C. D. Hoyle, U. Schmidt, B. R. Heckel, E. G. Adelberger, J. H. Gundlach, D. J. Kapner and H. E. Swanson, Phys. Rev. Lett. **86** (2001) 1418; J. Chiaverini, S. J. Smullin, A. A. Geraci, D. M. Weld and A. Kapitulnik, Phys. Rev. Lett. **90** (2003) 151101; V. V. Nesvizhevsky *et al.*, Nature **415** (2002) 297; E. G. Adelberger, B. R. Heckel and A. E. Nelson, Ann. Rev. Nucl. Part. Sci. **53** (2003) 77; J. C. Long, H. W. Chan, A. B. Churnside, E. A. Gulbis, M. C. M. Varney and J. C. Price, Nature **421** (2003) 922; V. V. Nesvizhevsky and K. V. Protasov, Class. Quant. Grav. **21** (2004) 4557; C. D. Hoyle, D. J. Kapner, B. R. Heckel, E. G. Adelberger, J. H. Gundlach, U. Schmidt and H. E. Swanson, Phys. Rev. D **70** (2004) 042004;

[22] P. Svrcek and E. Witten, JHEP **0606** (2006) 051.

[23] B. Kors and P. Nath, Phys. Lett. B **586** (2004) 366; B. Kors and P. Nath, JHEP **0507** (2005) 069; D. Feldman, B. Kors and P. Nath, Phys. Rev. D **75** (2007) 023503; D. Feldman, Z. Liu and P. Nath, AIP Conf. Proc. **939** (2007) 50; D. Feldman, Z. Liu and P. Nath, AIP Conf. Proc. **939** (2007) 50.

[24] C. Coriano, A. E. Faraggi and M. Guzzi, Phys. Rev. D **78** (2008) 015012.

[25] B. Batell and T. Gherghetta, Phys. Rev. D **73** (2006) 045016.

[26] K. R. Dienes, C. F. Kolda and J. March-Russell, Nucl. Phys. B **492** (1997) 104; D. Lüst and S. Stieberger, hep-th/0302221; S. A. Abel and B. W. Schofield, Nucl. Phys. B **685** (2004) 150; M. Berg, M. Haack and B. Kors, Phys. Rev. D **71** (2005) 026005; [arXiv:hep-th/0404087]; R. Blumenhagen, S. Moster and T. Weigand, Nucl. Phys. B **751** (2006) 186; S. A. Abel, J. Jaeckel, V. V. Khoze and A. Ringwald, Phys. Lett. B **666** (2008) 66; S. A. Abel, M. D. Goodsell, J. Jaeckel, V. V. Khoze and A. Ringwald, JHEP **0807** (2008) 124.

[27] L. B. Okun, Sov. Phys. JETP **56** (1982) 502 [Zh. Eksp. Teor. Fiz. **83** (1982) 892]; R. Foot and X. G. He, Phys. Lett. B **267** (1991) 509.

[28] B. Holdom, Phys. Lett. B **166** (1986) 196.

[29] C. P. Burgess, J. P. Conlon, L. Y. Hung, C. H. Kom, A. Maharana and F. Quevedo, JHEP **0807** (2008) 073.

[30] V. A. Kostelecky and S. Samuel, Phys. Rev. D **39** (1989) 683. N. Seiberg and E. Witten, JHEP **9909** (1999) 032; V. A. Kostelecky and R. Lehnert, Phys. Rev. D **63** (2001) 065008; M. S. Berger and V. A. Kostelecky, Phys. Rev. D **65** (2002) 091701; S. A. Abel, J. Jaeckel, V. V. Khoze and A. Ringwald, JHEP **0609** (2006) 074.

[31] R. Lehnert, hep-ph/0602097.

[32] V. A. Kostelecky and M. Mewes, Phys. Rev. Lett. **97** (2006) 140401.

[33] V. A. Kostelecky and M. Mewes, Phys. Rev. D **66** (2002) 056005; V. A. Kostelecky and N. Russell, arXiv:0801.0287 [hep-ph].

WIMPs: a Brief Bestiary

David G. Cerdeño

Departamento de Física Teórica C-XI & Instituto de Física Teórica UAM-CSIC,
Universidad Autónoma de Madrid, Cantoblanco, E-28049, Madrid, Spain

DOI: http://dx.doi.org/10.3204/DESY-PROC-2008-02/cerdeno_david

A brief overview of the motivation, viability and direct detection properties for some of the most popular candidates for WIMP dark matter is presented.

1 Introduction

The identification of the dark matter (DM) of the Universe constitutes one of today's major goals of modern Physics. This problem, once considered solely within the realm of Astrophysics is now deeply rooted in Particle Physics, since it is in the context of theories beyond the Standard Model (SM) where the most plausible candidates for DM arise. Given the outstanding advances in dark matter detection experiments, as well as the forthcoming onset of the LHC, an exciting near future can be anticipated in which this enigma might start being unveiled.

Given a DM candidate (stable and neutral particle), the size of its interaction with ordinary matter determines the resulting amount of DM in the Universe today. A relic density of particle DM is produced in the early Universe when its annihilation rate falls below the expansion rate. It can be estimated that in order to reproduce the present relic density of DM, a thermal candidate must have interactions of order of the Electroweak-scale. Not needing to introduce a new physical scale, such *weakly interacting massive particles*, WIMPs, constitute a very well-motivated general class of DM candidates. Moreover, an extremely attractive feature of WIMPs is that, despite their feeble interactions with ordinary matter, they could be detected directly on Earth experiments through their elastic scattering with nuclei in a detector.

Many models for new physics contain well-motivated DM candidates. In these notes I briefly comment on some of the most popular constructions, their viability and future detectability.

2 The beasts

Fourth generation neutrino. A *heavy neutrino* (Dirac or Majorana), belonging to a hypothetical fourth generation, was among the first proposals for WIMP dark matter. However, LEP limits on the invisible Z width pose a stringent lower bound on its mass, $m_\nu > M_Z/2$. Such neutrinos, having a too small relic density [1], would fail to account for all the dark matter in the Universe. Moreover, direct [2], as well as indirect DM searches [3], also ruled out $m_\nu \lesssim 1$ TeV. Some of these problems can be alleviated if the neutrino coupling to the Z boson is reduced, e.g., by considering mixing with a right-handed (sterile) component [4]. However, this renders the neutrino unstable, and although a large life time can be obtained by increasing the sterile composition, this leaves an extremely weakly interacting neutrino which therefore does not enter the WIMP category. An interesting possibility which allows to preserve the WIMP character of the heavy neutrino was recently explored within the context of a model with extra dimensions and an extended electroweak gauge group [5].

Supersymmetric WIMPs Supersymmetry (SUSY) was originally proposed as a solution to to the hierarchy problem in the SM and is nowadays regarded as one of the best motivated and most promising candidates for new physics. In SUSY extensions of the SM a discrete symmetry, known as R-parity, is often imposed in order to forbid lepton and baryon violating processes. A phenomenological implication of this is that SUSY particles are only produced or destroyed in pairs, thus rendering the lightest SUSY particle (LSP) stable.

Remarkably, in large areas of the parameter space of SUSY models, the LSP is an electrically neutral particle, the lightest *neutralino*, $\tilde{\chi}_1^0$, which therefore constitutes a very well motivated WIMP candidate [6]. The neutralino is a linear superposition of the fermionic partners of the neutral electroweak gauge bosons and of the neutral Higgs bosons (Higgsinos), and the resulting detection cross section is extremely dependent on its specific composition. The scalar part of the neutralino-proton cross section receives contributions from Higgs exchange in a t-channel and squark exchange in an s-channel. The latter also contributes to the spin-dependent part of the cross section, together with a Z boson exchange in a t-channel. The expressions for the different amplitudes can be found, e.g., in [7], and the conditions under which the neutralino detection cross section is enhanced are well understood [8]. In particular, a large Higgsino component induces an enhancement of both the Higgs and Z boson exchange diagrams, thereby leading to an increase in both the spin-dependent and independent cross sections. On the other hand, the presence of very light squarks leads to an enhancement of (mainly) the spin-dependent contribution [9]. As a consequence, current direct DM experiments are already sensitive to some areas of the SUSY parameter space and future detectors will explore deep into it.

Another possibility for a SUSY WIMP is the *sneutrino*, the scalar supersymmetric partner of the neutrino, since it is electrically neutral and weakly-interacting. However, given its sizable coupling to the Z boson, the left-handed sneutrino in the MSSM either annihilates too rapidly, resulting in a very small relic abundance, or gives rise to a large detection cross section, being excluded by direct DM searches [10]. Several models have been proposed to revive sneutrino DM by reducing its coupling with Z-boson with either the introduction of a mixture of left- and right-handed sneutrino [11] or by considering a purely right-handed sneutrino [12]. The latter cannot be thermal relics, since their coupling to ordinary matter is extremely reduced by the neutrino Yukawa coupling unless a new gauge interaction is introduced and would be unobservable in direct detection experiments.

Recently, an extension of the MSSM was studied where singlet scalar superfields are included, as in Ref. [13], simultaneously addressing the μ problem as in the Next-to-MSSM and generating non-vanishing Majorana neutrino masses with a (low-scale) see-saw mechanism. The associated presence of right-handed sneutrinos with a weak scale mass provides a new viable WIMP DM candidate. These can be thermally produced in sufficient amount to account for the CDM in the Universe through a direct coupling to the Higgs sector. Moreover their spin-independent detection cross section can be large enough to allow observation in future experiments [14].

Universal Extra Dimension models. Although theoretically very well motivated, SUSY is not the only possible extension of the SM leading to a viable DM candidate. An interesting alternative arises in theories with Universal Extra Dimensions (UED), in which all fields are allowed to propagate in the bulk [15]. These models predict an infinite tower of massive particles associated to each SM state. The masses of such KK excitations are related to the compactification scale, which can be chosen of order of the TeV. In the construction of realistic models the extra dimension has to be compactified in an orbifold in order to obtain chiral fermions. This leads to the occurrence of a conserved discrete symmetry, which is called KK-parity.

In this case, the *Lightest Kaluza-Klein Particle* (LKP) becomes stable and thus another viable DM candidate. The LKP usually corresponds to the first KK excitation of the hypercharge gauge boson [16, 17], $B^{(1)}$. In absence of spectral degeneracies, $B^{(1)}$ would achieve the appropriate relic density for masses in the 850–900 GeV range [17]. However, due to the quasi-degenerate nature of the KK spectrum, this range can be significantly modified, due to coannihilations with first and second KK-level modes. The allowed mass range was also found to depend significantly on the mass of the Standard Model Higgs boson.

In UED the leading contribution to the direct detection cross section of $B^{(1)}$ comes from the exchange of the Higgs (for spin-independent contribution) and of first level KK quarks $q^{(1)}$ (for both spin-dependent and independent) [18, 17]. The first diagram increases when the mass of the Higgs decreases, whereas the second contribution is very sensitive to the mass difference between the LKP and the exchanged KK quarks. In particular, when this mass difference is small, both the spin-independent and dependent detection cross section become large [9].

Little Higgs theories. These constructions were proposed in order to stabilize the Higgs mass through a collective symmetry breaking mechanism [19], in such a way that the Higgs would correspond to a pseudo-Goldstone boson. The inclusion of new Physics at the TeV scale, in particular of additional gauge bosons, gives rise to sizable contributions to low-energy observables and the model becomes severely constrained from electroweak precision fits. A discrete symmetry, called T-parity, can be introduced in order to alleviate these bounds [20]. The new gauge bosons would be odd under T-parity, thus forbidding tree-level corrections to precision electroweak observables. A phenomenological consequence of T-parity is that the *Lightest T-odd Particle* (LTP) becomes absolutely stable. Interestingly, the LTP is usually the partner of the hypercharge gauge boson [21], B_H. This is a neutral, weakly-interacting particle which therefore constitutes yet another candidate for WIMP dark matter.

The thermal relic abundance of B_H typically exceeds the WMAP constraint. The correct DM density is only obtained through the resonant annihilation of the Higgs s-channel or via coannihilation effects with another T-odd particle. The resulting direct detection cross section was found to be quite suppressed, given the fact that the heavy photon predominantly couples to SM particles through the Higgs boson, whose interactions with nucleons are weak. Thus, although the cross section increases when the Higgs mass decreases, only future dark matter experiments with targets of order 1 Ton would be sensitive to some regions of the parameter space [22]. Indirect detection, on the other hand, might better suited to study these candidates.

Other dark matter models Instead of looking for DM candidates in existing theories beyond the SM, a bottom-up approach can be adopted in which minimal additions to the SM are considered, involving the inclusion of a WIMP field (usually a new singlet) and new symmetries that protect their decay (in some occasions, also a new "mediator" sector that couples the WIMP to the SM). Examples in this direction include WIMPs with singlet mediation [23], models with an extended electroweak sector [24], models with additional gauge groups, and the *Secluded Dark Matter* scenario [25] in which WIMPs could escape direct detection.

3 Final comments

If WIMPs constitute the DM of the Universe we might have a good chance to detect them in the near future through a combination direct and indirect searches, as well as from the results of the search for new Physics with the LHC. Also, the combination of the results from these three different sources might help identifying this elusive ingredient of our Universe.

Acknowledgements

Work supported by the Spanish MEC under program "Juan de la Cierva" and Proyecto Nacional FPA2006-01105, the EU network MRTN-CT-2006-035863, the European Network of Theoretical Astroparticle Physics ILIAS/ENTApP under contract RII3-CT-2004-506222 and the project HEPHACOS P-ESP-00346 of the Comunidad de Madrid.

References

[1] B. W. Lee and S. Weinberg, Phys. Rev. Lett. **39** (1977) 165; P. Hut, Phys. Lett. B **69** (1977) 85; M. I. Vysotsky, A. D. Dolgov and Y. B. Zeldovich, JETP Lett. **26** (1977) 188 [P. Zh. Eksp. Teor. Fiz. **26** (1977) 200];

[2] S. P. Ahlen *et al.*, Phys. Lett. B **195** (1987) 603; D. O. Caldwell *et al.*, Phys. Rev. Lett. **61** (1988) 510; D. Reusser *et al.*, Phys. Lett. B **255** (1991) 143; J. Morales *et al.*, Nucl. Instrum. Meth. A **321** (1992) 410.

[3] M. Mori *et al.*, Phys. Lett. B **289** (1992) 463.

[4] S. Dodelson and L. M. Widrow, Phys. Rev. Lett. **72** (1994) 17.

[5] G. Belanger, A. Pukhov and G. Servant, JCAP **0801** (2008) 009.

[6] For a recent review, see: C. Muñoz, Int. J. Mod. Phys. **A19** (2004) 2093.

[7] J. R. Ellis, A. Ferstl and K. A. Olive, Phys. Lett. **B481** (2000) 304; J. R. Ellis, A. Ferstl and K. A. Olive.

[8] See, e.g,. D. G. Cerdeño and C. Muñoz, JHEP **0410** (2004) 015, and references therein.

[9] G. Bertone, D. G. Cerdeño, J. I. Collar and B. C. Odom, Phys. Rev. Lett. **99** (2007) 151301.

[10] T. Falk, K. A. Olive and M. Srednicki, Phys. Lett. B **339** 248 (1994).

[11] N. Arkani-Hamed *et al.*, Phys. Rev. D **64** 115011 (2001); D. Hooper, J. March-Russell and S. M. West, Phys. Lett. B **605** 228 (2005); C. Arina and N. Fornengo, JHEP **0711** (2007) 029; C. Arina *et al.*, arXiv:0806.3225.

[12] T. Asaka, K. Ishiwata and T. Moroi, Phys. Rev. D **73** 051301 (2006); Phys. Rev. D **75** 065001 (2007); S. Gopalakrishna, A. de Gouvea and W. Porod, JCAP **0605** (2006) 005; J. McDonald, JCAP **0701** (2007) 001; H. S. Lee, K. T. Matchev and S. Nasri, Phys. Rev. D **76** 041302 (2007).

[13] R. Kitano and K. y. Oda, Phys. Rev. D **61** 113001 (2000); B. Garbrecht *et al.*, JHEP **0612**, 038 (2006).

[14] D. G. Cerdeño, C. Muñoz and O. Seto, arXiv:0807.3029.

[15] T. Appelquist, H. C. Cheng and B. A. Dobrescu, Phys. Rev. D **64** (2001) 035002.

[16] H. C. Cheng, K. T. Matchev and M. Schmaltz, Phys. Rev. D **66**, 036005 (2002).

[17] G. Servant and T. M. P. Tait, Nucl. Phys. B **650** (2003) 391.

[18] H. C. Cheng, J. L. Feng and K. T. Matchev, Phys. Rev. Lett. **89** (2002) 211301.

[19] N. Arkani-Hamed, A. G. Cohen and H. Georgi, Phys. Lett. B **513** (2001) 232. N. Arkani-Hamed, A. G. Cohen, E. Katz and A. E. Nelson, JHEP **0207** (2002) 034.

[20] H. C. Cheng and I. Low, JHEP **0309** (2003) 051; JHEP **0408** (2004) 061. I. Low, JHEP **0410** (2004) 067.

[21] J. Hubisz and P. Meade, Phys. Rev. D **71** (2005) 035016.

[22] A. Birkedal, A. Noble, M. Perelstein and A. Spray, Phys. Rev. D **74** (2006) 035002 [arXiv:hep-ph/0603077].

[23] V. Silveira and A. Zee, Phys. Lett. B **161** (1985) 136. C. P. Burgess, M. Pospelov and T. ter Veldhuis, Nucl. Phys. B **619** (2001) 709 [arXiv:hep-ph/0011335]. J. McDonald, Phys. Rev. D **50** (1994) 3637.

[24] M. Cirelli, N. Fornengo and A. Strumia, Nucl. Phys. B **753** (2006) 178; R. Barbieri, L. J. Hall and V. S. Rychkov, Phys. Rev. D **74** (2006) 015007; L. Lopez Honorez *et al.* JCAP **0702** (2007) 028.

[25] M. Pospelov, A. Ritz and M. B. Voloshin, Phys. Lett. B **662** (2008) 53.

Axion Theory

Pierre Sikivie

Physics Department, University of Florida, Gainesville, FL 32611-8440, USA

The Strong CP Problem and its solution through the existence of an axion are briefly reviewed. The combined constraints from accelerator searches, stellar evolution and cosmology imply that the axion mass lies in the window $3 \cdot 10^{-3} > m_a \gtrsim 10^{-6}$ eV, with the lower bound being however much softer than the upper bound. If m_a is near the lower bound, axions are an important component of cold dark matter. I report briefly on the status of the ADMX dark matter search.

1 Introduction

The Standard Model of elementary particles present us with a puzzle. Indeed its action density includes, in general, a term [1]

$$\mathcal{L}_{\text{stand mod}} = ... \; + \; \frac{\theta g^2}{32\pi^2} G^a_{\mu\nu} \tilde{G}^{a\mu\nu} \tag{1}$$

where $G^a_{\mu\nu}$ are the QCD field strengths, g is the QCD coupling constant and θ is a parameter. One can show that QCD physics does depend on the value of θ and that this dependence enters only through the combination $\bar{\theta} \equiv \theta - \arg\det m_q$ where m_q is the quark mass matrix. If $\bar{\theta} \neq 0$ the strong interactions violate P and CP. Such P and CP violation is incompatible with the experimental upper bound on the neutron electic dipole moment [2] unless $|\bar{\theta}| < 10^{-10}$. The Standard Model does not provide a rationale for $\bar{\theta}$ to be small. Indeed P and CP violation are introduced by letting the elements of the quark mass matrix m_q be arbitrary complex numbers [3]. In that case, $\bar{\theta}$ is of order one. The puzzle why $\bar{\theta}$ is so small in reality is usually referred to as the "strong CP problem".

The puzzle is removed if the action density is instead

$$\mathcal{L}_{\text{stand mod + axion}} = ... \; + \; \frac{1}{2}\partial_\mu a \partial^\mu a + \frac{g^2}{32\pi^2} \; \frac{a(x)}{f_a} \; G^a_{\mu\nu} \tilde{G}^{a\mu\nu} \tag{2}$$

where $a(x)$ is a new scalar field, and the dots represent the other terms of the standard model. f_a is a constant with dimension of energy. In the theory defined by Eq. (2), $\bar{\theta} = \frac{a(x)}{f_a} - \det\arg m_q$ depends on the expectation value of $a(x)$. This field settles to a value that minimizes the effective potential. The strong CP problem is solved because the minimum of the QCD effective potential $V(\bar{\theta})$ occurs at $\bar{\theta} = 0$ [4]. The $aG \cdot \tilde{G}$ interaction in Eq. (2) is not renormalizable. However, there is a recipe for constructing renormalizable theories whose low energy effective action density is of the form of Eq. (2): construct the theory in such a way that it has a $U(1)$ symmetry which is a global symmetry of the classical action density, is broken by the color anomaly, and is spontaneously broken. Such a symmetry is called Peccei-Quinn symmetry after its inventors [5]. Weinberg and Wilczek [6] pointed out that a theory with a $U_{\rm PQ}(1)$ symmetry has a light pseudo-scalar particle, called the axion. The axion field is $a(x)$. f_a is of order the expectation value that breaks $U_{\rm PQ}(1)$, and is called the "axion decay constant".

The axion mass is given in terms of f_a by

$$m_a \simeq 6 \text{ eV } \frac{10^6 \text{ GeV}}{f_a} \ . \tag{3}$$

All axion couplings are inversely proportional to f_a. The axion coupling to two photons is:

$$\mathcal{L}_{a\gamma\gamma} = -g_\gamma \frac{\alpha}{\pi} \frac{a(x)}{f_a} \vec{E} \cdot \vec{B} \quad , \tag{4}$$

where $\vec{E}$ and $\vec{B}$ are the electric and magnetic fields, α is the fine structure constant, and g_γ is a model-dependent coefficient of order one. $g_\gamma = 0.36$ in the DFSZ model [7] whereas $g_\gamma = -0.97$ in the KSVZ model [8]. The axion has been searched for in many places, but has not been found [9]. Axion masses larger than about 50 keV are ruled out by particle physics experiments (beam dumps and rare decays) and nuclear physics experiments. The next range of axion masses, in decreasing order, is ruled out by stellar evolution arguments. The longevity of red giants rules out 200 keV $> m_a >$ 0.5 eV [10, 11] in case the axion has negligible coupling to the electron (such an axion is usually called 'hadronic'), and 200 keV $> m_a > 10^{-2}$ eV [12] in case the axion has a large coupling to electrons. The duration of the neutrino pulse from supernova 1987a rules out 2 eV $> m_a > 3 \cdot 10^{-3}$ eV [13]. Finally, there is a lower limit, $m_a \gtrsim 10^{-6}$ eV, from cosmology which will be discussed in the next section. This leaves open an "axion window": $3 \cdot 10^{-3} > m_a \gtrsim 10^{-6}$ eV. Note however that the lower edge of this window (10^{-6} eV) is much softer than its upper edge.

2 Axion cosmology

The implications of the existence of an axion for the history of the early universe may be briefly described as follows. At a temperature of order f_a, a phase transition occurs in which the $U_{\rm PQ}(1)$ symmetry becomes spontaneously broken. This is called the PQ phase transition. At these temperatures, the non-perturbative QCD effects which produce the effective potential $V(\overline{\theta})$ are negligible, the axion is massless and all values of $\langle a(x) \rangle$ are equally likely. Axion strings appear as topological defects. One must distinguish two scenarios, depending on wether inflation occurs with reheat temperature lower (case 1) or higher (case 2) than the PQ transition temperature. In case 1 the axion field gets homogenized by inflation and the axion strings are 'blown' away.

When the temperature approaches the QCD scale, the potential $V(\overline{\theta})$ turns on and the axion acquires mass. There is a critical time, defined by $m_a(t_1)t_1 = 1$, when the axion field starts to oscillate in response to the turn-on of the axion mass. The corresponding temperature $T_1 \simeq 1$ GeV. The axion field oscillations do not dissipate into other forms of energy. In case 1, their contribution to the cosmological energy density is [14, 15]

$$\Omega_a \sim 0.15 \left(\frac{f_a}{10^{12} \text{ GeV}} \right)^{7/6} \left(\frac{0.7}{h} \right)^2 \alpha(t_1)^2 \tag{5}$$

where $\alpha(t_1) \equiv a(t_1)/f_a$ is the initial misalignment angle. This contribution is called of 'vacuum realignment'. Note that the vacuum realignment contribution may be accidentally suppressed in case 1 because the homogenized axion field may happen to lie close to zero.

In case 2 the axion strings radiate axions [16, 17] from the time of the PQ transition till t_1 when the axion mass turns on. At t_1 each string becomes the boundary of N domain walls. If $N = 1$, the network of walls bounded by strings is unstable [18, 19] and decays away. If $N > 1$ there is a domain wall problem [20] because axion domain walls end up dominating the energy density, resulting in a universe very different from the one observed today. There is a way to avoid this problem by introducing an interaction which slightly lowers one of the N vacua with respect to the others, but there is very little room in parameter space for this to happen. More likely, the axion domain wall problem is solved by having $N = 1$ or by having inflation after the PQ phase transition (case 1).

In case 2 there are three contributions to the axion cosmological energy density. One contribution is from axions that were radiated by axion strings before t_1. A second contribution is from axions that were produced in the decay of walls bounded by strings after t_1 [21]. A third contribution is from vacuum realignment [14]. The contribution from axion string decay was the object of controversy for a number of years [22, 23, 24], but this controversy seems to have died away. Assuming it is resolved along the lines discussed in refs. [17, 24], the axion cosmological energy density is in case 2 [15]

$$\Omega_a \sim 0.7 \left(\frac{f_a}{10^{12}\ \mathrm{GeV}}\right)^{7/6} \left(\frac{0.7}{h}\right)^2 \quad . \tag{6}$$

It should be emphasized that there is considerable uncertainty in the estimates of Eqs. (5) and (6) because cosmology allows variations on the history of the universe before the time of nucleosynthesis.

3 Dark matter axion detection

An electromagnetic cavity permeated by a strong static magnetic field may be used to detect galactic halo axions [25]. The relevant coupling is given in Eq. (4). Galactic halo axions have velocities β of order 10^{-3} and hence their energies $E_a = m_a + \frac{1}{2}m_a\beta^2$ have a spread of order 10^{-6} above the axion mass. When the frequency $\omega = 2\pi f$ of a cavity mode equals m_a, galactic halo axions convert resonantly into quanta of excitation (photons) of that cavity mode.

Axion dark matter searches were carried out at Brookhaven National Laboratory [26], the University of Florida [27], Kyoto University [28], and by the ADMX collaboration [29] at Lawrence Livermore National Laboratory. The ADMX experiment has recently been upgraded to replace the HEMT (high electron mobility transistors) receivers used so far with SQUID microwave amplifiers. HEMT receivers have noise temperature $T_n \sim 3\ K$ [30] whereas $T_n \sim 0.05\ K$ was achieved with SQUIDs [31]. In a second phase of the upgrade, the experiment will be equipped with a dilution refrigerator to take full advantage of the lowered electronic noise temperature. When both phases of the upgrade are completed, the ADMX detector will have sufficient sensitivity to detect DFSZ axions at even a fraction of the local halo density.

4 Acknowledgments

This work was supported in part by the U.S. Deparment of Energy under grant DE-FG02-97ER41209.

References

[1] G. 't Hooft, Phys. Rev. Lett 37 (1976) 8, and Phys. Rev. D14 (1976) 3432; R. Jackiw and C. Rebbi, Phys. Rev. Lett. 37 (1976) 172; C.G. Callan, R.F. Dashen and D.J. Gross, Phys. Lett. B63 (1976) 334.

[2] I.S. Altarev et al., Phys. Lett. **B276** (1992) 242; K.F. Smith et al., Phys. Lett. **B234** (1990) 191.

[3] M. Kobayashi and K. Maskawa, Progr. Theor. Phys. **49** (1973) 652.

[4] C. Vafa and E. Witten, Phys. Rev. Lett. **53** (1984) 535.

[5] R. D. Peccei and H. Quinn, Phys. Rev. Lett. **38** (1977) 1440 and Phys. Rev. **D16** (1977) 1791.

[6] S. Weinberg, Phys. Rev. Lett. **40** (1978) 223; F. Wilczek, Phys. Rev. Lett. **40** (1978) 279.

[7] M. Dine, W. Fischler and M. Srednicki, Phys. Lett. **B104** (1981) 199; A. P. Zhitnitskii, Sov. J. Nucl. **31** (1980) 260.

[8] J. Kim, Phys. Rev. Lett. **43** (1979) 103; M. A. Shifman, A. I. Vainshtein and V. I. Zakharov, Nucl. Phys. **B166** (1980) 493.

[9] Axion reviews include: J.E. Kim, Phys. Rep. **150** (1987) 1; H.-Y. Cheng, Phys. Rep. **158** (1988) 1; R.D. Peccei, in 'CP Violation', ed. by C. Jarlskog, World Scientific Publ., 1989, pp 503-551; M.S. Turner, Phys. Rep. **197** (1990) 67; G.G. Raffelt, Phys. Rep. **198** (1990) 1.

[10] D. Dicus, E. Kolb, V. Teplitz and R. Wagoner, Phys. Rev. **D18** (1978) 1829 and Phys. Rev. **D22** (1980) 839.

[11] G. Raffelt and D. Dearborn, Phys. Rev. **D36** (1987) 2211.

[12] D. Dearborn, D. Schramm and G. Steigman, Phys. Rev. Lett. **56** (1986) 26.

[13] J. Ellis and K. Olive, Phys. Lett. **B193** (1987) 525; G. Raffelt and D. Seckel, Phys. Rev. Lett. **60** (1988) 1793; M. Turner, Phys. Rev. Lett. **60** (1988) 1797; H.-T. Janka et al., Phys. Rev. Lett. **76** (1996) 2621; W. Keil et al.. Phys. Rev. **D56** (1997) 2419.

[14] L. Abbott and P. Sikivie, Phys. Lett. **B120** (1983) 133; J. Preskill, M. Wise and F. Wilczek, Phys. Lett. **B120** (1983) 127; M. Dine and W. Fischler, Phys. Lett. **B120** (1983) 137.

[15] P. Sikivie, *Axion Cosmology*, Lect. Notes Phys. 741 (2008) 16.

[16] R. Davis, Phys. Rev. **D32** (1985) 3172 and Phys. Lett. **B180**

[17] D. Harari and P. Sikivie, Phys. Lett. **B195** (1987) 361.

[18] A. Vilenkin and A.E. Everett, Phys. Rev. Lett. **48** (1982) 1867.

[19] P. Sikivie in *Where are the elementary particles*, Proc. of the 14th Summer School on Particle Physics, Gif-sur-Yvette, 1982, edited by P. Fayet et al. (Inst. Nat. Phys. Nucl. Phys. Particules, Paris, 1983).

[20] P. Sikivie, Phys. Rev. Lett. **48** (1982) 1156.

[21] S. Chang, C. Hagmann and P. Sikivie, Phys. Rev. **D59** (1999) 023505.

[22] R.A. Battye and E.P.S. Shellard, Nucl. Phys. **B423** (1994) 260, Phys. Rev. Lett. **73** (1994) 2954 and erratum-ibid. **76** (1996) 2203.

[23] M. Yamaguchi, M. Kawasaki and J. Yokoyama, Phys. Rev. Lett. **82** (1999) 4578.

[24] C. Hagmann, S. Chang and P. Sikivie, Phys. Rev. **D63** (2001) 125018.

[25] P. Sikivie, Phys. Rev. Lett. **51** (1983) 1415 and Phys. Rev. **D32** (1985) 2988.

[26] S. DePanfilis et al., Phys. Rev. Lett. **59** (1987) 839 and Phys. Rev. **40** (1989) 3153.

[27] C. Hagmann et al., Phys. Rev. **D42** (1990) 1297.

[28] S. Matsuki, I. Ogawa, K. Yamamoto, Phys. Lett. **B336** (1994) 573;

[29] C. Hagmann et al., Phys. Rev. Lett. **80** (1998) 2043; S.J. Asztalos et al., Phys. Rev. **D64** (2001) 092003; L. Duffy et al., Phys. Rev. Lett. **95** (2005) 091304.

[30] R.F. Bradley, Nucl. Phys. B Proc. Suppl. **72** (1999) 137.

[31] M. Mück et al., Appl. Phys. Lett. **72** (1998) 2885; Nucl. Phys. B Proc. Suppl. **72** (1999) 145.

From Axions to other WISPs

Andreas Ringwald

DESY, Notkestraße 85, 22607 Hamburg, Germany

DOI: http://dx.doi.org/10.3204/DESY-PROC-2008-02/ringwald_andreas

We illustrate, taking a top-down point of view, how axions and other very weakly interacting sub-eV particles (WISPs) arise in the course of compactification of the extra spatial dimensions in string/M-theory.

It is a tantalizing question whether there is new physics *below* the Standard Model. That is to ask, whether there are new very light particles – apart from the known ones with sub-eV mass, the photon and the neutrinos – which are very weakly coupled to the Standard Model. In fact, embeddings of the latter into more unified theories, in particular into string theory, suggest their possible existence in a so-called hidden sector of the theory. Prominent examples of inhabitants of the latter are the axion and axion-like particles, arising as pseudo Nambu-Goldstone bosons associated with the breakdown of global anomalous U(1) symmetries. They occur generically in realistic string compactifications, as we will review below. Extra, hidden U(1) gauge bosons are also frequently encountered in string embeddings of the Standard Model, as we will summarize below. There is no reason why some of these hidden U(1) gauge bosons can not be massless or very light, in which case they also belong to the class of very weakly interacting sub-eV particles (WISPs). Further candidates for WISPs are very light hidden sector particles which are charged under the hidden U(1)s.

In this contribution, we will take a top-down point of view: we will illustrate how axions and other WISPs arise in the course of compactification of the extra dimensions of string theory. For the bottom-up point of view, i.e. for arguments and phenomenological as well as cosmological hints which point to the possible existence of WISPs, see the contributions of Joerg Jaeckel and Javier Redondo in these proceedings.

Axions from string compactifications.– The low-energy effective actions describing the dynamics of the massless bosonic excitations of the heterotic and type II string theories in 9+1 dimensions are summarized in Table 1. As we will see, after compactification of six of the

Heterotic	$S_{\rm H} = \frac{2\pi M_s^8}{g_s^2}\int d^{10}x\sqrt{-g}R - \frac{M_s^6}{2\pi g_s^2}\int \frac{1}{4}{\rm tr}F\wedge\star F - \frac{2\pi M_s^4}{g_s^2}\int\frac{1}{2}H\wedge\star H + \dots$
Type II	$S_{\rm II} = \frac{2\pi M_s^8}{g_s^2}\int d^{10}x\sqrt{-g}R - \frac{2\pi M_s^{p+1}}{g_s}\int d^{p+1}x{\rm tr}\sqrt{-\det\left(g+B+F/(2\pi M_s)\right)}$ $-2\pi{\rm i}M_s^{p+1}\int_{{\rm D}p}{\rm tr}\exp\left(B+F/(2\pi M_s)\right)\wedge\sum_q C_q + \dots$

Table 1: Low-energy effective actions describing the dynamics of the massless bosonic excitations in the weakly coupled heterotic (top) and type II string theories with Dp-branes in 9+1 dimensions. R is the Ricci scalar, F is the field strength of the gauge fields, and H is the field strength of the two-form field B. In our conventions, $M_s = 1/(2\pi\sqrt{\alpha'})$, with string tension α'.

spatial dimensions, pseudo-scalar fields a will generically arise which have a coupling $a\,\mathrm{tr}\,G\wedge G$ to the gluon field strength G in the effective Lagrangian describing the low-energy dynamics of the theory in 3+1 dimension and possess an anomalous Peccei-Quinn global shift symmetry, $a\to a+\epsilon$.

These are the properties needed for the axionic solution of the strong CP problem [1]. Indeed, the anomalous shift symmetry implies that the axion field can enter in the low-energy Lagrangian only through derivative and explicit symmetry violating terms originating from chiral anomalies,

$$\mathcal{L}_a=\frac{1}{2}\partial_\mu a\partial^\mu a+\mathcal{L}_a^{\rm int}\left[\frac{\partial_\mu a}{f_a};\psi\right]+\frac{r\alpha_s}{4\pi f_a}\,a\,\mathrm{tr}\,G^{\mu\nu}\tilde{G}_{\mu\nu}+\frac{s\alpha}{8\pi f_a}\,a\,F^{\mu\nu}\tilde{F}_{\mu\nu}+\dots\,, \tag{1}$$

with dimensionless constants $r\neq 0$ and s, the (conventionally normalized) electromagnetic (gluonic) field strength F (G), and the axion decay constant f_a. The CP violating term $\alpha_s/(4\pi)\,\bar\theta\,\mathrm{tr}\,G_{\mu\nu}\tilde{G}^{\mu\nu}$ in the QCD Lagrangian can then be eliminated by exploiting the shift symmetry, $a\to a-\bar\theta f_a/r$: the $\bar\theta$ dependence is wiped out by the axion, providing a natural explanation why e.g. the electric dipole moment of the neutron is so small. Finally, the topological charge density $\propto\langle\mathrm{tr}\,G^{\mu\nu}\tilde{G}_{\mu\nu}\rangle\neq 0$, induced by topological fluctuations of the gluon fields such as QCD instantons, provides a nontrivial potential for the axion field, giving a small mass to the axion [2], which can be inferred via current algebra and expressed in terms of the light (u,d) quark masses, the pion mass m_π and the pion decay constant f_π,

$$m_a=\sqrt{m_u m_d}/(m_u+m_d)\,m_\pi f_\pi/(f_a/r)\simeq 0.6\,\mathrm{meV}\times\left(10^{10}\,\mathrm{GeV}/(f_a/r)\right)\,. \tag{2}$$

For large axion decay constant f_a, we see that the axion is a prime example for a WISP: it is very weakly interacting (cf. Eq. (1)) and it is very light [3]. For various astrophysical, cosmological, and laboratory limits on f_a arising from the couplings of the axion to the Standard Model particles according to Eq. (1), see other contributions in these proceedings. Typically, for axions, the limit is $f_a/r\gtrsim 10^9$ GeV. Here, we will turn now to predictions of f_a in string embeddings of the Standard Model.

In the compactification of the weakly coupled heterotic string, a universal, *model-independent* axion appears as the dual of the antisymmetric tensor field $B_{\mu\nu}$ (whose field strength has been denoted by H in Table 1), $da\sim\star dB_{\mu\nu}$, with μ and ν tangent to 3+1 dimensional Minkowski space-time [4]. Its decay constant f_a is quite independent of the details of the compactification. In fact, after compactification of the theory, originally described in 9+1 dimensions by $S_{\rm H}$ in Table 1, on a 6 dimensional manifold with volume V_6, the resulting effective action can be matched to its standard normalization in 3+1 dimensions,

$$S_{3+1}=\frac{M_P^2}{2}\int d^4x\sqrt{-g}\,R-\frac{1}{4g_{\rm YM}^2}\int d^4x\sqrt{-g}\,\mathrm{tr}\,F_{\mu\nu}F^{\mu\nu}-\frac{1}{f_a^2}\int\frac{1}{2}H\wedge\star H+\dots\,, \tag{3}$$

with

$$M_P^2=(4\pi/g_s^2)M_s^8V_6;\quad g_{\rm YM}^2=4\pi g_s^2/(M_s^6V_6);\quad f_a^2=g_s^2/(2\pi M_s^4V_6)\,, \tag{4}$$

expressing the reduced Planck mass $M_P=2.4\times 10^{18}$ GeV, the gauge coupling $g_{\rm YM}$, and the axion decay constant f_a in terms of the string coupling g_s, the string scale M_s, and the volume V_6. Eliminating the volume V_6 and the string scale by means of the first two relations in Eq. 4, we end up with an axion decay constant of order of the GUT scale [5],

$$f_a/r=\alpha_{\rm YM}M_P/(2\pi\sqrt{2})\simeq 1.1\times 10^{16}\ \mathrm{GeV}\,,\ \text{for }\alpha_{\rm YM}=g_{\rm YM}^2/(4\pi)\sim 1/25\,. \tag{5}$$

Model-dependent axions arise in the context of weakly coupled heterotic strings from massless excitations of the two-form B-field on the 6 dimensional compact manifold [4]. Correspondingly, their properties depend much more on the details of the compactification. Nevertheless, a recent exhaustive study has elucidated [6] that also in this case the axion decay constant cannot be smaller than 10^{15} GeV. Similar conclusions have been drawn for the axions in strongly coupled heterotic string theory [6].

These findings can be easily understood physically: it is the string scale M_s which mainly determines the axion decay constant [7]. And in the heterotic case, this scale is large, e.g. $M_s = \sqrt{\alpha_{\rm YM}/(4\pi)}M_P$ for the weakly coupled heterotic string (cf. Eq. (4)).

This may be different in compactifications of type II string theories which give rise to "intersecting brane worlds". In these theories, the Standard Model lives on a stack of D($3{+}q$)-branes which are extended along the 3+1 non-compact dimensions and wrap q-cycles in the compactification manifold (see Fig. 1), while gravity propagates in the bulk, leading to a possibly smaller string scale at the expense of a larger compactification volume, $M_s \sim g_s M_P/\sqrt{V_6 M_s^6}$. In type II string theory, the axions come from the massless excitations of the q-form gauge field C_q (cf. Table 1). The precise predictions depend on the particular embedding of the Standard Model [7, 6], but generically one finds that the axion decay constant, $f_a \sim M_s$, can be substantially lower than in the heterotic case and in a phenomenologically very interesting range, e.g.

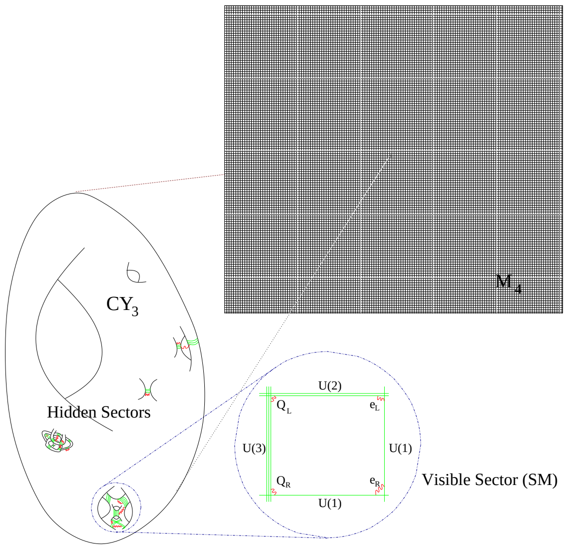

Figure 1: In compactifications of type II string theories the Standard Model is locally realized by a stack of D-branes wrapping cycles in the compact dimensions. In general, there are also hidden sectors localized at different places. Light visible and hidden matter particles arise from strings located at intersection loci and stretching between brane stacks. Adapted from Ref. [8].

$$f_a \sim M_P/\sqrt{V_6 M_s^6} \sim 10^{11}\ \text{GeV},\ \text{for}\ V_6 M_s^6 \sim 10^{14}\,, \tag{6}$$

in LARGE volume flux compactification models [7].

Other WISPs: Hidden U(1)s and hidden matter.– Additional hidden sector U(1) gauge factors are a generic feature of string compactifications. For example, in the "mini-landscape" of orbifold compactifications of the heterotic string [9] one encounters, at the compactification scale, a breaking of the gauge symmetry to a theory involving many hidden U(1)s, e.g. $\mathrm{E}_8\times\mathrm{E}_8 \to \mathrm{G}_{\rm SM}\times \mathrm{U}(1)^4 \times [\mathrm{SO}(8)\times\mathrm{SU}(2)\times\mathrm{U}(1)^3]$ and the like. Similarly, as illustrated in Fig. 1, the type II compactifications generically invoke hidden sector U(1)s[1], often also for global consistency requirements. Some of these hidden U(1)s may remain unbroken down to very small scales [11]. In this case their dominant interaction with the Standard Model will be through kinetic mixing

[1]Not shown are possible U(1)s arising from branes wrapping bulk cycles and intersecting the SM branes. For a large volume of the bulk, these interact very weakly with the SM [10] and are thus WISP candidates.

with the hypercharge $U(1)_Y$, described by the term

$$\mathcal{L} \supset \frac{\chi}{2gg'} \hat{Y}_{\mu\nu} \hat{X}^{\mu\nu} \,, \tag{7}$$

in the low energy effective Lagrangian, where $Y_{\mu\nu}$ ($X_{\mu\nu}$) is the hypercharge (hidden) U(1) field strength and g (g') is the hyper- (hidden-) charge. Often there is also light hidden matter charged under the hidden U(1)s, as illustrated for the type II compactifications in Fig. 1. After diagonalization of the gauge kinetic terms by a shift $\hat{X} \to \hat{X} + \chi\hat{Y}$ and a multiplicative hypercharge renormalization, one observes that the hidden sector particles acquire a minihypercharge $g_h = \chi g'$ [12]. There are strong astrophysical limits, $g_h \lesssim 10^{-14}$, for masses below a few keV, as reviewed by Javier Redondo in these proceedings, and there are a number of ideas to probe such values in the laboratory as summarized by Joerg Jaeckel. Here, we would like to concentrate on the string theory predictions for χ, which turn out to be comfortably small, but still of phenomenological interest.

Kinetic mixing is generated by the exchange of heavy messengers that couple both to the hypercharge U(1) as well as to the hidden U(1). In the context of compactifications of the heterotic string, its size has been estimated as [13]

$$\chi \sim gg'/(16\pi^2)\, C\, \Delta m/M_P \gtrsim 10^{-17}\,, \text{ for } C \gtrsim 10,\ \Delta m \gtrsim 100 \text{ TeV}\,, \tag{8}$$

where Δm is the mass splitting in the messenger sector. Small values for χ can also be accommodated in type II compactifications. Here, kinetic mixing can be understood as originating from the exchange of closed strings through the bulk [14]. Correspondingly, it can experience a volume suppression [11], e.g., from D3-brane mixing,

$$\chi \sim gg'/(16\pi^2)\, (V_6 M_s^6)^{-2/3} \sim 10^{-14}\,, \text{ for } V_6 M_s^6 \sim 10^{14}\,. \tag{9}$$

Exponentially suppressed values can be naturally obtained in flux compactifications with warped throats [11]. Intriguingly, values even as small as $\chi \sim 10^{-25}$ may be of phenomenological interest in the context of decaying dark matter [15].

References

[1] R. D. Peccei and H. R. Quinn, Phys. Rev. Lett. **38**, 1440 (1977).

[2] S. Weinberg, Phys. Rev. Lett. **40**, 223 (1978); F. Wilczek, Phys. Rev. Lett. **40**, 279 (1978).

[3] J. E. Kim, Phys. Rev. Lett. **43**, 103 (1979); M. Dine *et al.*, Phys. Lett. B **104**, 199 (1981).

[4] E. Witten, Phys. Lett. B **149**, 351 (1984).

[5] K. Choi and J. E. Kim, Phys. Lett. B **154**, 393 (1985); Phys. Lett. B **165**, 71 (1985).

[6] P. Svrcek and E. Witten, JHEP **0606**, 051 (2006).

[7] J. P. Conlon, JHEP **0605**, 078 (2006).

[8] J. P. Conlon, S. S. Abdussalam, F. Quevedo and K. Suruliz, JHEP **0701**, 032 (2007).

[9] O. Lebedev *et al.*, Phys. Lett. B **645**, 88 (2007).

[10] C. P. Burgess *et al.*, JHEP **0807**, 073 (2008).

[11] S. A. Abel *et al.*, Phys. Lett. B **666**, 66 (2008); S. A. Abel *et al.*, JHEP **0807**, 124 (2008).

[12] B. Holdom, Phys. Lett. B **166**, 196 (1986).

[13] K. R. Dienes, C. F. Kolda and J. March-Russell, Nucl. Phys. B **492**, 104 (1997).

[14] D. Lust and S. Stieberger, Fortsch. Phys. **55**, 427 (2007); S. A. Abel and B. W. Schofield, Nucl. Phys. B **685**, 150 (2004); M. Berg, M. Haack and B. Kors, Phys. Rev. D **71**, 026005 (2005).

[15] C. R. Chen *et al.*, arXiv:0809.0792 [hep-ph]; A. Ibarra *et al.*, arXiv:0809.3196 [hep-ph].

Chapter 2

Signals from Astrophysical Sources I: Solar Axions and Axion Dark Matter

Bounds on very Weakly Interacting Sub-eV Particles (WISPs) from Cosmology and Astrophysics

Javier Redondo

[1]DESY theory group, Notkestraße 85, 22607 Hamburg, Germany

DOI: http://dx.doi.org/10.3204/DESY-PROC-2008-02/redondo_javier

Many weakly interacting sub-electronVolt particles (WISPs) are easily accommodated in extensions of the standard model. Generally the strongest bounds on their existence come from stellar evolution and cosmology, where to the best of our knowledge observations seem to agree with the standard budget of particles. In this talk I review the most demanding constraints for axions and axion-like-particles, hidden photons and mini-charged particles.

There is little doubt in the particle physics community about the need of complementing the already very successful standard model (SM) to pursue a completely satisfactory final theory of elementary particles. On the other hand, and with the exception of the dark matter, our increasingly precise knowledge of the universe shows no trace of physics beyond the SM. If new light particles exist they should be very weakly interacting, probably only accessible to extremely precise experiments. Experiments such as the ones presented in this conference.

Astrophysics and cosmology are often strong probes of weakly interacting particles. The reason is clear: the huge magnitudes of the typical sizes, time scales, densities or temperatures in the early universe or in stars can convert a tiny "microscopic" effect in a big qualitative change in the evolution of the whole system. This conclusion is specially emphasized when we note that the only weakly interacting sub-eV particles (WISPs) in the standard model are neutrinos, whose production cross sections are strongly energy-dependent and therefore their role is increasingly inhibited as temperatures drop below the electroweak scale. Thus, in an non-extreme range of temperatures the early universe and stellar plasmas are very opaque to standard particles and WISPs can be the most efficient way of energy transfer. Whenever such an anomalous energy transfer has an observable implication we can derive strong constraints on the WISP interactions with the standard particles constituting the relevant plasma.

The oldest picture of the universe we have is a dense and hot plasma of elementary particles that expanded against gravity. As this plasma cooled down, the three long range forces clustered the particles into the structures which nowadays are found: the color force first confined quarks into protons and neutrons and later merged them into light nuclei (at BBN), the Coulomb force combined them with electrons into atoms (releasing the CMB) that gravity finally clustered into galaxies, then into clusters, etc... After the first galaxies formed, the conditions for stars to be born were settled. During all these steps of structure formation (in a broad sense) the role of WISPs can be constrained. Let us start this review in chronological order.

Big Bang Nucleosynthesis.- BBN left an invaluable probe of the early universe environment imprinted in today's observable light nuclei abundances [1]. Below $T \sim 0.7$ MeV the weak reactions $p+e^- \leftrightarrow n+\nu_e$ became ineffective, fixing the neutron/proton density ratio to $n/p \sim 1/7$. All particles present contribute to the energy density ρ which determines the speed of the cosmic expansion $H \propto \sqrt{\rho}$ and the "freeze-out" ratio n/p in turn. The larger H the sooner the p-n freezing and the higher n/p. Later, all neutrons are confined into ^{4}He nuclei whose primordial abundance can be measured today, leading to a bound on the non-standard energy density ρ_x during BBN, usually expressed as an effective number of thermal neutrino species, $N^{\rm eff}_{\nu,x} \equiv \frac{4}{7}\frac{30}{\pi^2 T^4}\rho_x = -0.6^{+0.9}_{-0.8}$ [2], where we assumed three standard neutrinos.

Therefore, while a spin-zero particle thermalized during BBN is allowed, this is not the case for other[1] WISPs like a mini-charged particle (MCP) ($N^{\rm eff}_{\nu,{\rm MCP}} \geq 1$) or a massive hidden photon γ' ($N^{\rm eff}_{\nu,\gamma'} = 21/16$). The interactions of MCPs and γ's with the standard bath should not allow thermalization before BBN. MCPs ψ are produced with a rate $\Gamma(e^+e^- \to \psi\overline{\psi}) \sim \alpha^2 Q^2_{\rm MCP} T/2$ ($Q_{\rm MCP}$ the MCP electric charge) while γ's with $\Gamma(\gamma e^\pm \to \gamma' e^\pm) \sim \chi^2_{\rm eff}\Gamma_{\rm C}$ with $\Gamma_{\rm C}$ the standard Compton scattering rate. Here $\chi_{\rm eff}$ is the effective $\gamma-\gamma'$ mixing in the plasma, which for sub-eV γ' masses is $\chi_{\rm eff} \simeq \chi(m_{\gamma'}/\omega_{\rm P})^2$. The ratio of the γ' mass to the plasma frequency $m_{\gamma'}/\omega_{\rm P}$ is extremely small before BBN so it suppresses γ' production with respect to other WISPs. Comparing with the expansion rate H we find that MCPs with $Q_{\rm MCP} < 2\times 10^{-9}$ would be allowed [3] but there are no significant bounds for hidden photons [4].

Cosmic Microwave background.- The today's measured CMB features an almost perfect blackbody spectrum with $\mathcal{O}(10^{-5})$ angular anisotropies. It is released at $T \sim 0.1$ eV but the reactions responsible of the blackbody shape freeze out much earlier, at $T \sim$ keV. Reactions like $\gamma + ... \to$WISP+... will deplete photons in a frequency dependent way, which can be constrained by the precise FIRAS spectrum measurements [5]. This has been used to constrain light MCPs [6] and HPs with $m_{\gamma'} \lesssim 0.2$ meV [7]. On the other hand, around $T \sim$ eV the primordial plasma is so sparse that WISPs would free-stream out of the density fluctuations, diminishing their contrast. Moreover, thermal WISPs contribute to the *radiation* energy density, delaying the matter-radiation equality and reducing the contrast growth before decoupling. In these matters they act as standard neutrinos [8] so ρ_x (and the couplings that would produce it) can again be constrained from the value of $N^{\rm eff}_\nu$ inferred from analysis of CMB anisotropies and other[2] large scale structure (LSS) data $\tilde{N}^{\rm eff}_{\nu,x} \equiv (4/11)^{4/3}\, N^{\rm eff}_{\nu,x} = -0.1^{-1.4}_{+2.0}$ [2]. This argument has been used to constraint axions [9] and meV γ's [7]. In this bound Ly-α forest data has been deliberately omitted. Ly-α has systematically favored values of $\tilde{N}^{\rm eff}_{\nu,x}$ larger than zero [10] which could be revealing the existence of a WISP relic density[3]. If this anomaly is due to a population of γ's created through resonant oscillations $\gamma-\gamma'$ between BBN and the CMB decoupling it can be tested in the near future by new laboratory experiments such as ALPS at DESY [7, 12].

Bounds from stellar evolution.- The production of WISPs in stellar interiors can substantially affect stellar evolution [13]. WISPs can be only scarcely produced in the dense plasmas of stellar interiors, but they will easily leave the star contributing directly to its overall luminosity. On the other hand, only photons of the photosphere (or neutrinos) contribute to the standard energy loss. Therefore, the WISP luminosity is enhanced at least by a volume/surface factor and a further $(d_{\rm inside}/d_{\rm surface})^n(T_{\rm inside}/T_{\rm surface})^m$ (d a relevant particle density, $n,m>1$) with respect to the standard luminosity. This can be a huge enhancement which certainly justifies the typical strong constraints.

[1] For details of these hypothetical particles and their embedding in theories beyond the SM the reader is refereed to the contributions of Andreas Ringwald and Joerg Jaeckel in these proceedings.

[2] One needs to complement CMB anisotropies with other LSS data to break the degeneracy of $\tilde{N}^{\rm eff}_{\nu,x}$ with other cosmological parameters such as the dark matter density.

[3] Probably because of an incorrect treatment of the bias parameter [11].

Stars evolve fusing increasingly heavier nuclei in their cores. Heavier nuclei require hotter environments, and when a nuclear species is exhausted in the core this slowly contracts and heatens up until it reaches the new burning phase. WISP emission shortens normal burning phases (the energy loss rate is higher than standard but the total energy is limited by the number of nuclei) but enlarges the intermediate (Red Giant) phases (WISP cooling delays reaching the appropriate temperature during the core contraction).

These effects have been used to constraint a variety of WISPs in different stellar environments [13] for which information on evolutionary time scales is available. The strongest limits for general axion-like-particles (ALPs) with a two photon coupling and MCPs come from observations of Horizontal Branch (HB) stars in globular clusters (GC) [14]. For the standard QCD axions, the best constraints come from White Dwarf cooling [15] through the coupling to electrons (DFSV axions) and from the duration of the SN1987A neutrino burst [13] through the nucleon coupling (KSVZ axions).

The Sun is less sensitive than these other stars to WISP emission, even though its properties are better known. Solar bounds have been obtained from studies of its lifetime, helioseismology and the neutrino flux [16], but being more precise they are also less demanding. Nevertheless, if WISPs are emitted from the Sun one can detect them with a dedicated laboratory experiment at earth [17]. One of the so-called Helioscope axion searches [18], CAST, has recently beaten the HB constraints for ALPs [19], and its results have been used to limit a possible solar γ' flux [20]. Following the now disclaimed PVLAS 2005 results [21], specific models were recently built that suppress WISP emission from stars [4, 22]. If this idea is realized, Helioscope bounds will gain terrain to energy loss arguments [23] (γ's are the minimal example of this case [20]).

In summary, cosmology and astrophysics provide the strongest constraints on the (minimal) WISP models described elsewhere in these proceedings, with the only exception of sub-meV γ's. Summary plots are shown in Figs. 1 and 2.

Acknowledgements

The author wishes to thank the participants of the "4th Patras Workshop on Axions, WIMPs and WISPs" and the "Brainstorming and Calculationshop on the Physics Case for a Low Energy frontier" for very stimulating discussions in a really friendly ambient.

References

[1] F. Iocco, G. Mangano, G. Miele, O. Pisanti, and P. D. Serpico, `arXiv:0809.0631 [astro-ph]`.

[2] V. Simha and G. Steigman, *JCAP* **0806** (2008) 016, `arXiv:0803.3465 [astro-ph]`.

[3] S. Davidson *et al.*, *JHEP* **05** (2000) 003; Z. Berezhiani and A. Lepidi, `hep-ph/0810.1317`.

[4] E. Masso *et al.*, *Phys. Rev. Lett.* **97** (2006) 151802; J. Redondo, `arXiv:0807.4329 [hep-ph]`.

[5] D. J. Fixsen *et al.*, *Astrophys. J.* **473** (1996) 576, `arXiv:astro-ph/9605054`.

[6] A. Melchiorri, A. Polosa, and A. Strumia. *Phys. Lett.* **B650**, 416–420 (2007), `hep-ph/0703144`.

[7] J. Jaeckel, J. Redondo, and A. Ringwald, *Phys. Rev. Lett.* **101** (2008) 131801, `astro-ph/0804.4157`.

[8] K. Ichikawa, T. Sekiguchi, and T. Takahashi, `arXiv:0803.0889 [astro-ph]`.

[9] S. Hannestad *et al.*, *JCAP* **0708** (2007) 015 and *JCAP* **0804** (2008) 019.

[10] U. Seljak *et al.*, *JCAP* **0610** (2006) 014; G. Mangano *et al.*, *JCAP* **0703** (2007) 006.

[11] J. Hamann, S. Hannestad, G. G. Raffelt, and Y. Y. Y. Wong, *JCAP* **0708** (2007) 021.

[12] J. Jaeckel and A. Ringwald, *Phys. Lett.* **B659** (2008) 509–514; J. Jaeckel, `arXiv:0809.3112 [hep-ph]`; J. Jaeckel, `arXiv:0807.5097 [hep-ph]`; J. Jaeckel and J. Redondo, `arXiv:0806.1115 [hep-ph]`.

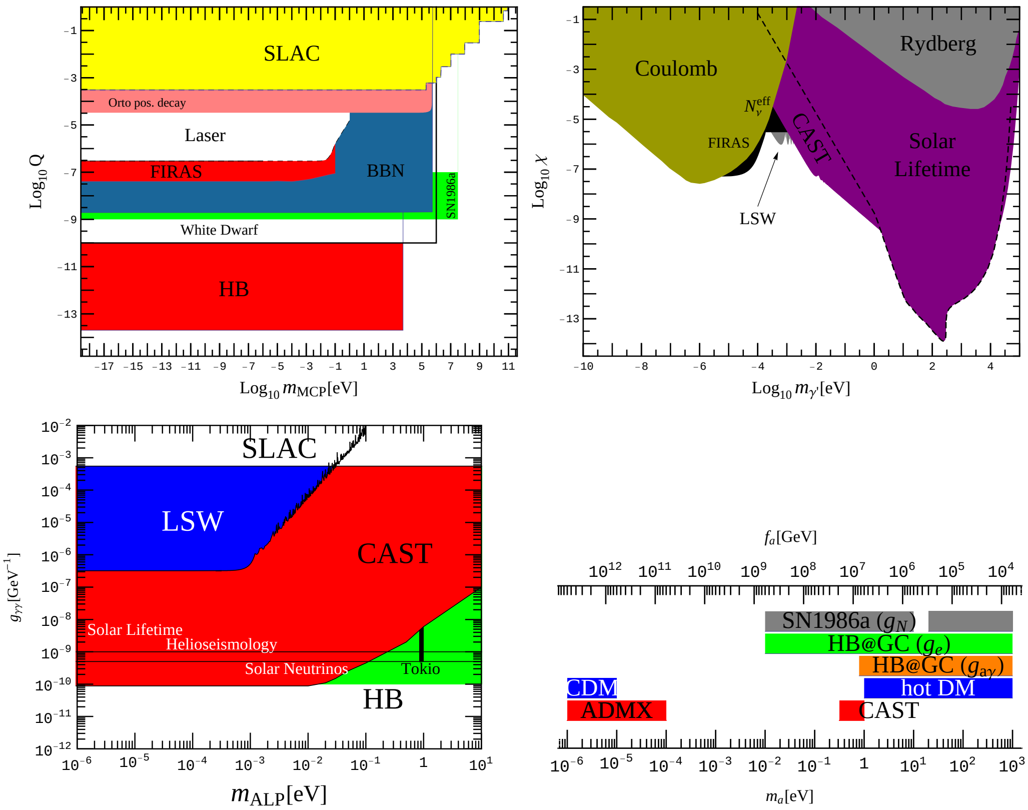

Figure 1: Summary of cosmological, astrophysical and some laboratory constraints for WISPs: minicharged particles (up left) (charge Q vd. mass $m_{\rm MCP}$) [24], hidden photons (up right) (kinetic mixing with photons χ vs. mass $m_{\gamma'}$) [24], axion-like-particles (down left) (two photon coupling $g_{\gamma\gamma}$ vs. mass $m_{\rm ALP}$) [16, 19] and axions (down right) (for decay constant f_a and mass m_a) [13]. See the text for details.

[13] G. G. Raffelt, *Stars as laboratories for fundamental physics.* The University of Chicago Press, 1996; G. G. Raffelt, *Lect. Notes Phys.* **741** (2008) 51–71, `arXiv:hep-ph/0611350`.

[14] G. G. Raffelt, *Phys. Rev.* **D33** (1986) 897; G. G. Raffelt *et al.*, *Phys. Rev.* **D36** (1987) 2211.

[15] G. G. Raffelt, *Phys. Lett.* **B166** (1986) 402; J. Isern *et al.*, `arXiv:0806.2807 [astro-ph]`.

[16] H. Schlattl *et al.*, *Astropart. Phys.* **10** (1999) 353–359; P. Gondolo *et al.*, `arXiv:0807.2926 [astro-ph]`.

[17] P. Sikivie, *Phys. Rev. Lett.* **51** (1983) 1415. [Erratum-ibid. **52**, 695 (1984)]. K. van Bibber *et al.*, *Phys. Rev.* **D39** (1989) 2089; E. A. Paschos *et al.*, *Phys. Lett.* **B323** (1994) 367–372.

[18] D. M. Lazarus *et al.*, *Phys. Rev. Lett.* **69** (1992) 2333–2336; S. Moriyama *et al.*, *Phys. Lett.* **B434** (1998) 147; Y. Inoue *et al.*, *Phys. Lett.* **B668** (2008) 93–97; K. Zioutas *et al.*, *Phys. Rev. Lett.* **94** (2005) 121301.

[19] **CAST** Collaboration, S. Andriamonje *et al.*, *JCAP* **0704** (2007) 010, `hep-ex/0702006`.

[20] J. Redondo, *JCAP* **0807** (2008) 008; S. N. Gninenko *et al.*, *Phys. Lett.* **B664** (2008) 180–184.

[21] E. Zavattini *et al.*, *Phys. Rev. Lett.* **96** (2006) 110406 and *Phys. Rev.* **D77** (2008) 032006.

[22] E. Masso *et al.*, *JCAP* **0509** (2005) 015; P. Brax *et al.*, *Phys. Rev. Lett.* **99** (2007) 121103; R. N. Mohapatra *et al.*, *Phys. Rev. Lett.* **98** (2007) 050402.

[23] J. Jaeckel *et al.*, *Phys. Rev.* **D75** (2007) 013004, `hep-ph/0610203`.

[24] M. Ahlers, J. Jaeckel, J. Redondo, and A. Ringwald, *Phys. Rev.* **D78** (2008) 075005.

Axion Hot Dark Matter Bounds

Georg Raffelt[1], *Steen Hannestad*[2] *Alessandro Mirizzi*[1], *Yvonne Y. Y. Wong*[1]

[1]Max-Planck-Institut für Physik, Föhringer Ring 6, D-80805 München, Germany
[2]Department of Physics and Astronomy, University of Aarhus, DK-8000 Aarhus C, Denmark

DOI: http://dx.doi.org/10.3204/DESY-PROC-2008-02/raffelt_georg

We derive cosmological limits on two-component hot dark matter consisting of neutrinos and axions. We restrict the large-scale structure data to the safely linear regime, excluding the Lyman-α forest. We derive Bayesian credible regions in the two-parameter space consisting of m_a and $\sum m_\nu$. Marginalizing over $\sum m_\nu$ provides $m_a < 1.02$ eV (95% C.L.). In the absence of axions the same data and methods give $\sum m_\nu < 0.63$ eV (95% C.L.).

1 Introduction

The masses of the lightest particles are best constrained by the largest cosmic structures. The well-established method of using cosmological precision data to constrain the cosmic hot dark matter fraction [1, 2] has been extended to hypothetical low-mass particles, notably to axions, in several papers [3, 4, 5, 6, 7]. If axions thermalize after the QCD phase transition, their number density is comparable to that of one neutrino family. Neutrino mass limits are in the sub-eV range so that axion mass limits will be similar and therefore of interest to experiments like CAST [8] or the Tokyo axion helioscope [9] that search for axions in the mass range around 1 eV. We here summarize our detailed limits on axions that were derived from the latest sets of cosmological data, including WMAP (5 years). Numerically our latest limit on m_a [7] is almost identical to one that some of us have derived several years ago [4]. The main difference is that in the older paper the Lyman-α data were used that we now consider "too dangerous" in that they are prone to systematic errors. So, the latest data, that are safely in the linear regime, now do as well as the older data where Lyman-α was included.

2 Axions

The Peccei-Quinn solution of the CP problem of strong interactions predicts the existence of axions, low-mass pseudoscalars that are very similar to neutral pions, except that their mass and interaction strengths are suppressed by a factor of order f_π/f_a, where $f_\pi \approx 93$ MeV is the pion decay constant, and f_a the axion decay constant or Peccei–Quinn scale [10]. In more detail, the axion mass is

$$m_a = \frac{z^{1/2}}{1+z}\,\frac{f_\pi m_\pi}{f_a} = \frac{6.0\ \text{eV}}{f_a/10^6\ \text{GeV}}\,, \tag{1}$$

where $z = m_u/m_d$ is the mass ratio of up and down quarks. A value $z = 0.56$ was often assumed, but it could vary in the range 0.3–0.6 [11]. A large range of f_a values is excluded by experiments and by astrophysical and cosmological arguments [12]. Axions with a mass of order 10 μeV could well be the cold dark matter of the universe [13] and if so will be found eventually by the ongoing ADMX experiment, provided that 1 $\mu\mathrm{eV} < m_a < 100\ \mu\mathrm{eV}$ [14].

In addition, a hot axion population is produced by thermal processes [15, 16]. Axions attain thermal equilibrium at the QCD phase transition or later if $f_a \lesssim 10^8$ GeV, erasing the cold axion population produced earlier and providing a hot dark matter component instead. If axions do not couple to charged leptons ("hadronic axions") the main thermalization process in the post-QCD epoch is [15] $a + \pi \leftrightarrow \pi + \pi$. The axion–pion interaction is given by a Lagrangian of the form [15] $\mathcal{L}_{a\pi} = (C_{a\pi}/f_\pi f_a)\,(\pi^0\pi^+\partial_\mu\pi^- + \pi^0\pi^-\partial_\mu\pi^+ - 2\pi^+\pi^-\partial_\mu\pi^0)\partial_\mu a$. In hadronic axion models, the coupling constant is [15] $C_{a\pi} = (1-z)/[3\,(1+z)]$. Based on this interaction, the axion decoupling temperature in the early universe was calculated in Ref. [4], where all relevant details are reported. In Fig. 1 we show the relic axion density as a function of f_a.

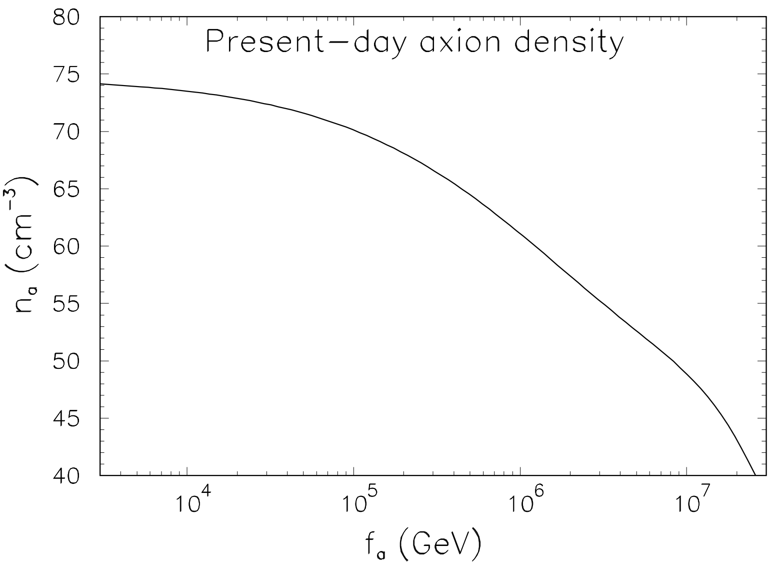

Figure 1: Axion relic density.

3 Cosmological model and data

We consider a cosmological model with vanishing spatial curvature and adiabatic initial conditions, described by six free parameters, the dark-matter density $\omega_{\rm dm} = \Omega_{\rm dm}h^2$, the baryon density $\omega_b = \Omega_b h^2$, the Hubble parameter $H_0 = h$ 100 km s^{-1} Mpc^{-1}, the optical depth to reionization τ, the amplitude of the primordial scalar power spectrum $\ln(10^{10}A_s)$, and its spectral index n_s. In addition we allow for a nonzero sum of neutrino masses $\sum m_\nu$ and a nonvanishing axion mass m_a which also determines the relic density shown in Fig. 1 by the standard relation between m_a and f_a. We show the priors on our parameters in Ref. [6].

We use the 5-year release of the WMAP cosmic microwave data [17, 18] that we analyze using version 3 of the likelihood calculation package provided by the WMAP team on the LAMBDA homepage [19], following closely the analyses of references [20, 21]. For the large-scale galaxy power spectra we use $P_{\rm g}(k)$ inferred from the luminous red galaxy (LRG) sample of the Sloan Digital Sky Survey (SDSS) [22, 23] and from the Two-degree Field Galaxy Redshift Survey (2dF) [24]. We only use data safely in the linear regime where a scale-independent bias is likely to hold true. For 2dF this is $k_{\rm max} \sim 0.09\ h\ {\rm Mpc}^{-1}$ (17 bands) and for SDSS-LRG $k_{\rm max} \sim 0.07\ h\ {\rm Mpc}^{-1}$ (11 bands). We do not use Lyman-α data at all. The baryon acoustic oscillation peak was measured in the SDSS luminous red galaxy sample [25]. We use all 20 points in the two-point correlation data and the corresponding analysis procedure [25]. We use the SN Ia luminosity distance measurements of provided by Davis et al. [26].

4 Results

We use standard Bayesian inference techniques and explore the model parameter space with Monte Carlo Markov Chains (MCMC) generated using the publicly available CosmoMC package [27, 28]. We find the 68% and 95% 2D marginal contours shown in Fig. 2 in the parameter plane of $\sum m_\nu$ and m_a. Marginalizing over $\sum m_\nu$ provides $m_a < 1.02$ eV (95% C.L.). In the absence of axions the same data and methods give $\sum m_\nu < 0.63$ eV (95% C.L.). These axion mass limits are nicely complementary to the search range of the CAST experiment [8] and the Tokyo helioscope [9] that can reach to 1 eV or somewhat above. While the hot dark matter limits are not competitive with the SN 1987A limits, it is intriguing that cosmology alone now provides both an upper and a lower limit for the allowed range of axion parameters.

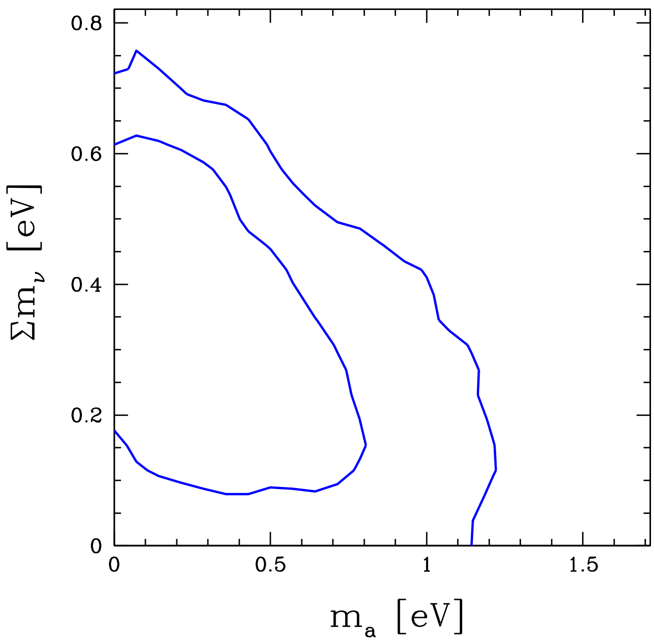

Figure 2: 2D marginal 68% and 95% contours in the $\sum m_\nu$–m_a plane.

Acknowledgements

We acknowledge use of computing resources from the Danish Center for Scientific Computing (DCSC) and partial support by the European Union under the ILIAS project (contract No. RII3-CT-2004-506222), by the Deutsche Forschungsgemeinschaft under the grant TR-27 "Neutrinos and Beyond" and by The Cluster of Excellence for Fundamental Physics "Origin and Structure of the Universe" (Garching and Munich).

References

[1] J. Lesgourgues and S. Pastor, Phys. Rept. **429** (2006) 307 [arXiv:astro-ph/0603494].

[2] S. Hannestad, Ann. Rev. Nucl. Part. Sci. **56** (2006) 137 [arXiv:hep-ph/0602058].

[3] S. Hannestad and G. Raffelt, JCAP **0404** (2004) 008 [arXiv:hep-ph/0312154].

[4] S. Hannestad, A. Mirizzi and G. Raffelt, JCAP **0507** (2005) 002 [arXiv:hep-ph/0504059].

[5] A. Melchiorri, O. Mena and A. Slosar, Phys. Rev. D **76**, 041303 (2007) [arXiv:0705.2695].

[6] S. Hannestad, A. Mirizzi, G. G. Raffelt and Y. Y. Y. Wong, JCAP **0708**, 015 (2007) [arXiv:0706.4198].

[7] S. Hannestad, A. Mirizzi, G. G. Raffelt and Y. Y. Y. Wong, JCAP **0804**, 019 (2008) [arXiv:0803.1585].

[8] S. Andriamonje *et al.* [CAST Collaboration], JCAP **0704**, 010 (2007) [arXiv:hep-ex/0702006].

[9] Y. Inoue, Y. Akimoto, R. Ohta, T. Mizumoto, A. Yamamoto and M. Minowa, arXiv:0806.2230 [astro-ph].

[10] R. D. Peccei, Lect. Notes Phys. **741** (2008) 3 [arXiv:hep-ph/0607268].

[11] W. M. Yao *et al.* [Particle Data Group], J. Phys. G **33** (2006) 1.

[12] G. G. Raffelt, Lect. Notes Phys. **741** (2008) 51 [arXiv:hep-ph/0611350].

[13] P. Sikivie, Lect. Notes Phys. **741** (2008) 19 [arXiv:astro-ph/0610440].

[14] S. J. Asztalos, *et al.*, Ann. Rev. Nucl. Part. Sci. **56** (2006) 293.

[15] S. Chang and K. Choi, Phys. Lett. B **316** (1993) 51 [arXiv:hep-ph/9306216].

[16] E. Massó, F. Rota and G. Zsembinszki, Phys. Rev. D **66** (2002) 023004 [arXiv:hep-ph/0203221].

[17] G. Hinshaw *et al.*, arXiv:0803.0732 [astro-ph].

[18] M. R. Nolta *et al.*, arXiv:0803.0593 [astro-ph].

[19] Legacy Archive for CMB Data Analysis (LAMBDA), http://lambda.gsfc.nasa.gov

[20] J. Dunkley *et al.* [WMAP Collaboration], arXiv:0803.0586 [astro-ph].

[21] E. Komatsu *et al.*, arXiv:0803.0547 [astro-ph].

[22] W. J. Percival *et al.*, Astrophys. J. **657** (2007) 645 [arXiv:astro-ph/0608636].

[23] M. Tegmark *et al.*, Phys. Rev. D **74** (2006) 123507 [arXiv:astro-ph/0608632].

[24] S. Cole *et al.* [2dFGRS Coll.], Mon. Not. Roy. Astron. Soc. **362** (2005) 505 [arXiv:astro-ph/0501174].

[25] D. J. Eisenstein *et al.* [SDSS Collaboration], Astrophys. J. **633** (2005) 560 [arXiv:astro-ph/0501171]; see also http://cmb.as.arizona.edu/∼eisenste/acousticpeak

[26] T. M. Davis *et al.*, Astrophys. J. **666** (2007) 716 [arXiv:astro-ph/0701510].

[27] A. Lewis and S. Bridle, Phys. Rev. D **66** (2002) 103511 [arXiv:astro-ph/0205436]

[28] A. Lewis, Homepage, `http://cosmologist.info`

Bounds on Light Dark Matter

Alexey Boyarsky[1,2], *Oleg Ruchayskiy*[3]
[1]ETHZ, Zürich, CH-8093, Switzerland
[2]Bogolyubov Institute for Theoretical Physics, Kiev 03780, Ukraine
[3]ÉPFL, FSB/ITP/LPPC, BSP 726, CH-1015, Lausanne, Switzerland

DOI: http://dx.doi.org/10.3204/DESY-PROC-2008-02/lindner_axel

In this talk we review the existing cosmological and astrophysical bounds on the light (with the mass in keV – MeV) range and super-weakly interacting dark matter candidates. A particular attention is paid to the sterile neutrino DM candidate.

The nature of Dark Matter (DM) is one of the most intriguing questions of particle astrophysics. Its resolution would have a profound impact on the development of particle physics beyond its Standard Model (SM). Although the possibility of having massive compact halo objects (MACHOs) as a dominant form of DM is still under debates (see recent discussion in [1] and references therein), it is widely believed that DM is made of non-baryonic particles. Yet the SM of elementary particles does not contain a viable DM particle candidate – massive, neutral and long-lived particle. Active neutrinos, which are both neutral and stable, form structures in a top-down fashion [2], and thus cannot produce observed large scale structure. Therefore, the DM particle hypothesis implies the extension of the SM. Thus, constraining properties of the DM, helps to distinguish between various DM candidates and may help to differentiate among different beyond the SM models (BSM). *What is known about the properties of DM particles?*

A lower bound on the mass of DM particle. The DM particle candidates have very different masses (for reviews see e.g. [3]). Quite a robust and model-independent *lower bound* on the mass of DM particles was suggested in [4]. The idea was based on the fact that for any fermionic DM the average phase-space density (in a given DM-dominated, gravitationally bound object) cannot exceed the phase-space density of the degenerate Fermi gas. This argument, applied to the most DM-dominated dwarf spheroidal satellites (dSph's) of the Milky Ways leads to the bound $m_{\rm DM} > 0.41\,\mathrm{keV}$ [5].

For particular DM models (with the known primordial velocity dispersion) and under certain assumptions about the evolution of the system which led to the observed final state, this limit can be strengthened. This idea was developed in a number of works (see e.g. refs. in [5]).

Decaying DM. For any DM candidate there should exist a mechanism of its production in the early Universe. Although it is possible that the DM is produced through interactions with the non-SM particles only (e.g. from the inflaton decay) and is inert with respect to all SM interactions, many viable DM candidates are produced via interaction with the SM sector. According to this interaction the DM candidates can be subdivided into *annihilating* and *decaying* ones. The annihilating DM candidates – WIMPs [6] – are well studied. A decaying DM candidate should be *superweakly* interacting (i.e. weaker than electroweak), otherwise it cannot have a cosmologically long lifetime. There are many examples of *super-WIMP* DM models: sterile neutrinos [7], gravitino in theories with broken R-parity [8], light volume modulus [9], Majoron [10]. All these candidate posses a 2-body decay channel: $\mathrm{DM} \to \gamma+\nu, \gamma+\gamma$. Therefore, searching for a monochromatic decay line in the spectra of DM-dominated objects provides a way of *indirect detection* of the DM or helps to *constrain* its interaction strength with the SM particles.

The astrophysical search for *decaying* DM is in fact more promising. Moreover, the positive result would be much more conclusive, than in the case of annihilating DM. Indeed, the decay signal is proportional to the *column density*: $\int \rho_{\rm DM}(r)dr$ along the line of sight and not to the $\int \rho^2_{\rm DM}(r)dr$ (as it is the case of the annihilating DM). As a result *(i)* a vast variety of astrophysical objects of different nature would produce roughly the same decay signal [11, 12]; *(ii)* this gives a freedom of choosing the observational targets, allowing to avoid the complicated astrophysical backgrounds (e.g. one does not need to look at the Galactic center, expecting a comparable signal from dark outskirts of galaxies and clusters and dark dSph's); *(iii)* if a candidate line is found, its surface brightness profile may be measured (as it does not decay quickly away from the centers of the objects), distinguished from astrophysical lines (which usually decay in outskirts) and compared among several objects with the same expected signal. This makes astrophysical search for decaying DM *another type of a direct detection experiment.*

A search of the DM decay signal was conducted both in the keV – MeV range [11, 13] and in GeV range [12]. The aggregate constraints on the decaying DM lifetime (towards the radiative decay) are shown on Fig. 1

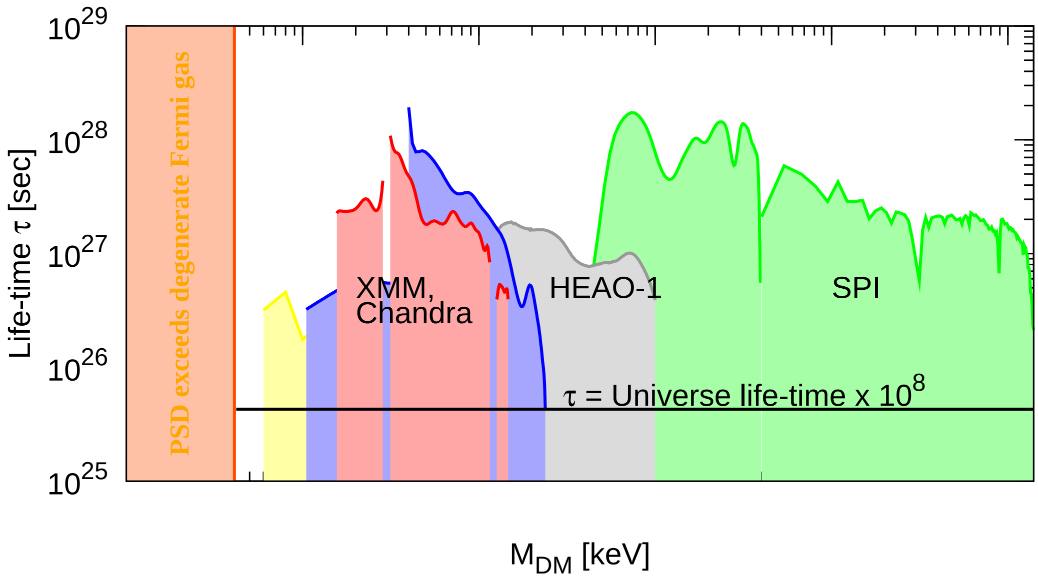

Figure 1: Restrictions on the lifetime of the radiatively decaying DM (based on [11, 13]). The lifetime exceeds the age of the Universe by at least 10^8.

Ly-α constraints. The fable strength of interaction of light super-WIMP particles often means that they were produced in the early Universe in a non-thermal way and decoupled deep into the radiation dominated (RD) epoch, while still being relativistic. This makes these particles *warm DM* candidates (WDM) (see e.g. [14]).

An important way to distinguish between WDM and CDM models is the analysis of the Lyman-α (Ly-α) forest data (for an introduction see e.g. [15]). Although very promising, the Ly-α method is very complicated and indirect. As at redshifts, probed by Ly-α, the evolution of structure already enters a non-linear stage, to relate measured power spectrum with the parameters of each cosmological model, one would have to perform prohibitively large number of numerical simulations. Therefore, various simplifying approximations have to be realized (see e.g. [16]). Apart from computational difficulties, the physics, entering the Ly-α analysis is not fully understood, as it is complicated and can be significantly influenced by DM particles [18]. Bayesian approach, used to fit the cosmological data, should also be applied with caution to put bounds on the particle physics parameters [17].

In many super-weakly interacting DM models, due to the non-thermal primordial velocity distribution, the linear powerspectrum (PS) (used as initial conditions in Ly-α analysis) has complicated non-universal form. The analysis of [26] assumed PS with a cut-off at small scales, defined by the particle's velocities. These results are not applicable for many models of decaying DM. For example, in a number of models (sterile neutrinos, gravitino) the primordial velocity distribution is a mixture of colder and warmer components and the PS develops a plateau at small scales. This makes much smaller masses compatible with Ly-α bounds. For these smaller masses it is important to take into account explicitly the primordial velocities of the particles (and not only their effect on the PS). See detailed analysis [17].

Sterile neutrino DM. Although known as a DM candidate for some 15 years [7], the sterile neutrino DM recently attracted a lot of attention. It was shown [19] that if one adds three right-handed (sterile) neutrinos to the SM, it is possible to explain simultaneously the data on neutrino oscillations, the DM in the Universe and generate the correct baryon asymmetry of the Universe without introducing any new physics *above electro-weak scale*. The lightest (DM) sterile neutrino can have mass in keV-MeV range and be coupled to the rest of the matter weakly enough to provide a viable (*cold* or *warm)* DM candidate. This model, explaining the three observed BSM phenomena within one consistent framework, is called *the νMSM* [19, 20].

There are several mechanisms of production of DM sterile neutrino in the early Universe: non-resonant active-sterile neutrino oscillations (**NRP**) [7, 21], resonant oscillations in the presence of lepton asymmetry (**RP**) [22, 23], decay of the gauge-singlet scalar field [24] (see also [25]). The Ly-α analysis was performed so far only for NRP scenario, and the results were claimed to be in the range $5 - 15\,\mathrm{keV}$ (see also [17]). Phase-space density bounds, applied to the NRP scenario lead to the $m_{\mathrm{NRP}} > 1.77 - 4\,\mathrm{keV}$.

Combining various constraints we see that there is a tension between the NRP scenario and the data (X-ray bounds and phase-space density arguments). For the RP mechanism a large window of allowed parameters remain open. These results are summarized on Fig. 2

References

[1] S. Calchi Novati (2007), 0711.4474.
[2] Y. B. Zel'dovich, A&A **5**, 84 (1970).

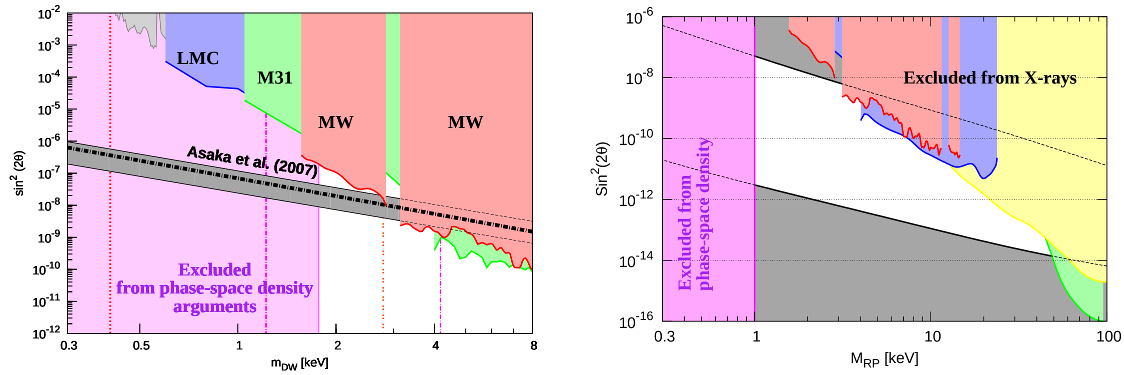

(a) (b)

Figure 2: Restrictions on sterile neutrino DM in NRP (left) and RP (right) scenarios.

[3] L. Bergstrom, Rept.Prog.Phys. **63**, 793 (2000); G. Bertone, D. Hooper, and J. Silk, Phys. Rep. **405**, 279 (2005); M. Taoso, G. Bertone, and A. Masiero, JCAP **0803**, 022 (2008).
[4] S. Tremaine and J. E. Gunn, Phys. Rev. Lett. **42**, 407 (1979).
[5] A. Boyarsky, O. Ruchayskiy, and D. Iakubovskyi `0808.3902`; D. Gorbunov, A. Khmelnitsky, and V. Rubakov `0808.3910`.
[6] B. W. Lee and S. Weinberg, Phys. Rev. Lett. **39**, 165 (1977).
[7] S. Dodelson and L. M. Widrow, Phys. Rev. Lett. **72**, 17 (1994).
[8] W. Buchmuller, et al., JHEP **03**, 037 (2007).
[9] J. P. Conlon and F. Quevedo, JCAP **0708**, 019 (2007), `0705.3460`.
[10] M. Lattanzi and J. W. F. Valle, Phys. Rev. Lett. **99**, 121301 (2007), `0705.2406`.
[11] A. Boyarsky, et al. Phys. Rev. Lett. **97**, 261302 (2006).
[12] G. Bertone, W. Buchmuller, L. Covi, and A. Ibarra (2007), `arXiv:0709.2299[astro-ph]`.
[13] A. Boyarsky, A. Neronov, O. Ruchayskiy, and M. Shaposhnikov, MNRAS **370**, 213 (2006); Phys. Rev. D **74**, 103506 (2006); S. Riemer-Sørensen, S. H. Hansen, and K. Pedersen, ApJ **644**, L33 (2006); C. R. Watson, et al. Phys. Rev. **D74**, 033009 (2006); A. Boyarsky, O. Ruchayskiy, and M. Markevitch, ApJ **673**, 752 (2008); K. N. Abazajian, M. Markevitch, S. M. Koushiappas, and R. C. Hickox, Phys. Rev. D **75**, 063511 (2007); A. Boyarsky, J. Nevalainen, and O. Ruchayskiy, A&A **471**, 51 (2007); A. Boyarsky, J. W. den Herder, A. Neronov, and O. Ruchayskiy, Astropart. Phys. **28**, 303 (2007; A. Boyarsky, D. Iakubovskyi, O. Ruchayskiy, and V. Savchenko, MNRAS **387**, 1361 (2008); A. Boyarsky, D. Malyshev, A. Neronov, and O. Ruchayskiy, MNRAS **387**, 1345 (2008).
[14] Bode, P., Ostriker, J. P., & Turok, N. 2001, ApJ, 556, 93.
[15] L. Hui, N. Y. Gnedin, and Y. Zhang, ApJ **486**, 599 (1997); N. Y. Gnedin and A. J. S. Hamilton, Mon.Not.Roy.Astron.Soc. **334**, 107 (2002).
[16] P. McDonald, et al., ApJS **163**, 80 (2006); M. Viel, J. Lesgourgues, M. G. Haehnelt, S. Matarrese, and A. Riotto, Phys. Rev. **D71**, 063534 (2005).
[17] A. Boyarsky, J. Lesgourgues, O. Ruchayskiy and M. Viel (2008), *to appear*.
[18] L. Gao and T. Theuns, Science **317**, 1527 (2007); J. Stasielak, P. L. Biermann, and A. Kusenko, ApJ **654**, 290 (2007).
[19] T. Asaka, S. Blanchet, and M. Shaposhnikov, Phys. Lett. **B631**, 151 (2005); T. Asaka and M. Shaposhnikov, Phys. Lett. B **620**, 17 (2005).
[20] M. Shaposhnikov (2007), `0708.3550`.
[21] T. Asaka, M. Laine, and M. Shaposhnikov, JHEP **01**, 091 (2007), `hep-ph/0612182`.
[22] X.-d. Shi and G. M. Fuller, Phys. Rev. Lett. **82**, 2832 (1999), `astro-ph/9810076`.
[23] M. Shaposhnikov, JHEP **08**, 008 (2008); M. Laine and M. Shaposhnikov, JCAP **6**, 31 (2008).
[24] M. Shaposhnikov and I. Tkachev, Phys. Lett. **B639**, 414 (2006), `hep-ph/0604236`.
[25] K. Petraki, Phys. Rev. D **77**, 105004 (2008), `arXiv:0801.3470`.
[26] M. Viel, et al. Phys. Rev. Lett. **97**, 071301 (2006); U. Seljak, A. Makarov, P. McDonald, and H. Trac, Phys. Rev. Lett. **97**, 191303 (2006); M. Viel, et al. Phys. Rev. Lett. **100**, 041304 (2008).

The Upgraded Performance of CAST.

Jaime Ruz[1] on behalf of the CAST Collaboration

[1]Instituto de Física Nuclear y Altas Energías, Universidad de Zaragoza, Zaragoza, Spain

DOI: http://dx.doi.org/10.3204/DESY-PROC-2008-02/ruz_jaime

CAST (CERN Axion Solar Telescope) is a helioscope looking for axions coming from the solar core to the Earth. The experiment, located at CERN, is based on the Primakoff effect and uses a magnetic field of 9 Tesla provided by a decommissioned LHC magnet. CAST is able to follow the Sun during sunrise and sunset and, therefore, four X-ray detectors are mounted on both ends of the magnet waiting for a photon from axion-to-photon conversion due to the Primakoff effect. During its First Phase, which concluded in 2004, CAST looked for axions with masses up to 0.02 eV. By using a buffer gas, CAST's Second Phase manages to re-establish the coherence needed to scan for axions with masses up to 1.20 eV. This technique enables the experiment to look into the theoretical regions for axions. During the years 2005 and 2006, the use of ^{4}He in CAST has already provided coherence in order to look for axions with masses up to 0.39 eV. At present time, CAST has managed to upgraded its experimental setup to alloy ^{3}He within the magnetic field and data concerning axions of masses up to 0.56 eV have already been taken.

1 Helioscope axion searches

The strong CP-problem of QCD might be solved by the introduction of a chiral symmetry that leads to the existence of a new pseudo-scalar particle [1]. Axions, as the new particles were named [2, 3], can be produced via the so-called Primakoff effect [4] in the presence of strong electromagnetic fields. The solar core is an ideal environment to produce them due to the strength of the solar plasma electric fields. In such conditions, a real photon (X-ray) and a virtual photon might couple and result in an axion that could be able to reach the Earth's surface. Those axions, could be reconverted into X-ray photons in a magnetic field and therefore detected by using a magnet pointing to the solar core and an X-ray detector attached to its end [5].

2 The CAST experiment

Twice per day, CAST (CERN Axion Solar Telescope) points in the direction of the Sun making use of a decommissioned superconducting LHC magnet of 9.26 m length and 9 Tesla field in order to look for a signal of axions according to the expected differential axion flux at the Earth's surface [6].

Four different X-ray detectors are mounted on both sides of the magnet. Each one of them is daily aligned with the solar core during 1.5 hours expecting a photon coming from an axion-to-photon conversion due to the Primakoff effect suitable to happen in the magnet of CAST. The detectors are: two sunset MICROMEGAS that replace the previously used Time Projection Chamber [7], a sunsrise MICROMEGAS [8] and a Charge Coupled Device [9], this last one together with an X-ray telescope that improves the signal to background ratio by a factor of about 200 for this detector.

Due to coherence requirements, during the data taking periods of 2003 [10] and 2004 [11] *(see Figure 1)* CAST was sensitive to axion masses under 0.02 eV. The loss of coherence over the full magnet length that CAST encountered during its First Phase when the magnet bores were under vacuum is restored for the Second Phase of the experiment by filling the magnet with a buffer gas such that the photon acquires an effective mass. By varying the gas and its pressure the search for axions with higher masses is possible.

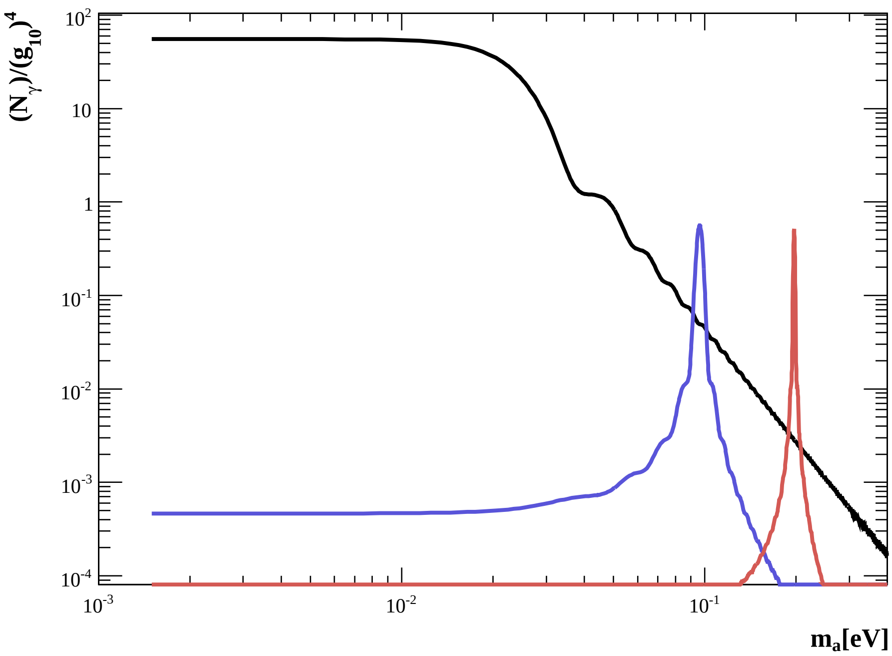

Figure 1: Expected photons arriving CAST for the First Phase (black line) and for two different settings of CAST's Second Phase (red and blue lines). Observe how CAST loss of coherence for axion with masses below 0.02 eV during the First Phase of the experiment is restored during the Second Phase with the help of ^{4}He and ^{3}He as buffer gases.

The CAST experiment has been upgraded in order to be able to have gases at various pressures in the magnet bores. Four cold windows have been developed and placed inside the magnet in order to keep the gas under the conditions needed. A complete gas system has been designed and built to deal with the buffer gas and control its pressure with the needed accuracy.

Cooling the super conducting CAST magnet down to 1.8 K by using superfluid Helium causes the employed gas in the magnet conversion region to saturate. ^{4}He for instance, is able to restore CAST's coherence for axions masses up to 0.39 eV but it saturates at ∼16.4 mbar. In order to achieve coherence for higher axion masses the use of lighter gases is required. ^{3}He allows a further search for axion masses up to 1.20 eV *(see figure 2)*. The Second Phase of CAST consists then of two different stages:

- ^{4}**He run:** allowing to look for axions with masses up to 0.39 eV. Completed during years 2005 and 2006.
- ^{3}**He run:** restoring coherence for axion masses up to 1.20 eV. Years 2007 to 2010.

CAST data taking procedure during its Second Phase has been chosen in a way such that allows to scan for axion masses from 0.02 to 1.20 eV in little steps.

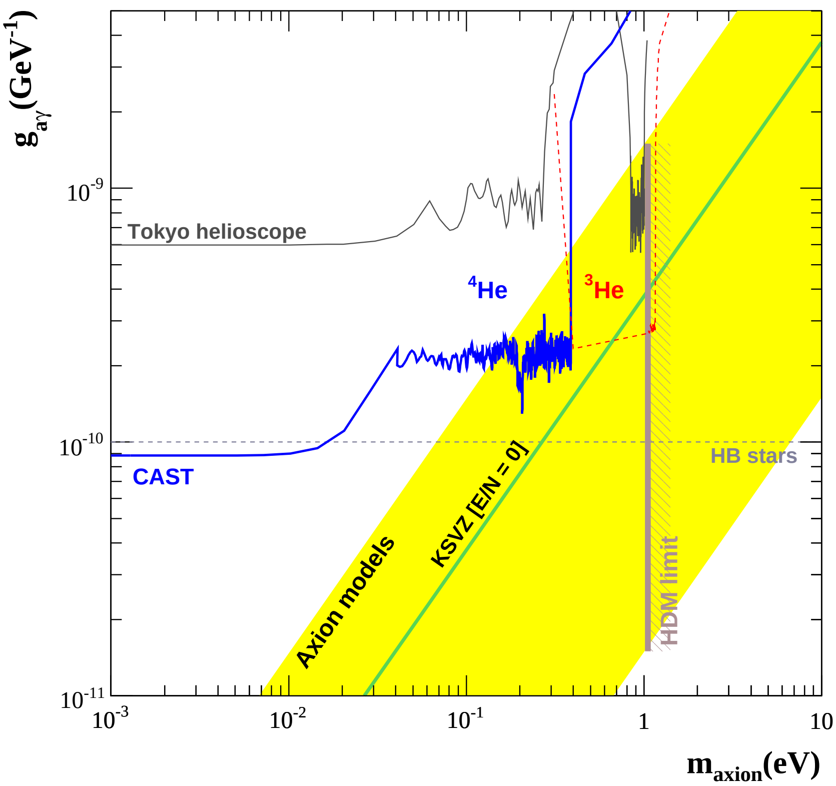

Figure 2: Preliminary CAST exclusion plot for axion mass versus coupling constant to photon in the experimental panorama of the rest of stelar axion search experiments. In the figure, it can be observed the result achieved by CAST during its first and the ^{4}He run of Second Phase [11] (thick blue line). The thin red line is the expectation for the ^{3}He run of CAST's Second Phase.

The procedure used for the ^{4}He run during 2005 and 2006 was to daily increase the ^{4}He gas density in the magnet bore by a certain amount of atoms. The overall range of pressure pressure inside the bore went from 0 to 13.43 mbar. This mechanism has already allowed CAST to restore the coherence of the Primakoff axion-to-photon conversion axion masses up to 0.4 eV *(see Figure 2)*. The ^{3}He run of CAST's Second Phase is ongoing and the Primakoff coherence condition has already been fulfilled for axions of masses up to 0.56 eV.

3 Conclusion

During its First Phase, while having vacuum in the magnet bores, CAST looked for traces of axion-to-photon conversions via the Primakoff effect for axions coming from the solar core. However, coherence restrictions constrained the axion mass search up to 0.02 eV [10, 11].

CAST's Second Phase has already started and the extension of sensitivity using ^{4}He gas has been explored by CAST during the years 2005 and 2006. The analysis of ^{4}He run is at its final stage and the preliminary results can be seen in the figure 2. The extension of sensitivity in CAST up to axions masses of 1.20 eV is being accomplished by using ^{3}He and the Primakoff coherence condition has already been fulfilled for axions of masses up to 0.56 eV.

References

[1] R. D. Peccei and H. R. Quinn, Physical Review Letters **38** (1977) 1440.

[2] S. Weinberg, Physical Review Letters **40** (1978) 223.

[3] F. Wilczek, Physical Review Letters **40** (1978) 279.

[4] H. Primakoff, Physical Review Letters **81** (1951) 899.

[5] P. Sikivie, Physical Review Letters **51** (1983) 1415 [Erratum ibid. **52** (1984) 695].

[6] K. van Bibber *et al*, Physical Review D. **39** (1989) 2089.

[7] D. Autiero *et al.*, New Journal of Physics **9** (2007) 171.

[8] P. Abbon *et al.*, New Journal of Physics **9** (2007) 170.

[9] M. Kuster *et al.*, New Journal of Physics **9** (2007) 169.

[10] K. Zioutas *et al.* [CAST Collaboration], Physical Review Letters **94** (2005) 121301.

[11] K. Zioutas *et al.* [CAST Collaboration], Journal of Cosmology and Astroparticle Physics **04** (2007) 010.

Tokyo Axion Helioscope

M. Minowa[1,4], *Y. Inoue*[2,4], *Y. Akimoto*[1], *R. Ohta*[1], *T. Mizumoto*[1], *A. Yamamoto*[3,4]

[1]Department of Physics, School of Science, University of Tokyo
[2]International Center for Elementary Particle Physics, University of Tokyo
[3]High Energy Accelerator Research Organization (KEK), 1-1 Oho, Tsukuba, Ibaraki 305-0801, Japan
[4]Research Center for the Early Universe (RESCEU), School of Science, University of Tokyo
[1,2,4] 7-3-1 Hongo, Bunkyo-ku, Tokyo 113-0033, Japan

DOI: http://dx.doi.org/10.3204/DESY-PROC-2008-02/minowa_makoto

A new search result of the Tokyo axion helioscope is presented. The axion helioscope consists of a dedicated cryogen-free 4T superconducting magnet with an effective length of 2.3 m and PIN photodiodes as x-ray detectors. Solar axions, if exist, would be converted into X-ray photons through the inverse Primakoff process in the magnetic field. Conversion is coherently enhanced even for massive axions by filling the conversion region with helium gas. The present third phase measurement sets a new limit of $g_{a\gamma\gamma} < 5.6\text{–}13.4 \times 10^{-10}\mathrm{GeV}^{-1}$ for the axion mass of $0.84 < m_a < 1.00\,\mathrm{eV}$ at 95% confidence level.

1 Introduction

The existence of axion is implied to solve the so-called strong CP problem [1, 2, 3, 4, 5]. Axions are expected to be produced in solar core through their coupling to photons with energies of order keV, and the so-called 'axion helioscope' technique may enable us to detect such axions directly [6, 7].

The differential flux of solar axions at the Earth is approximated by [8, 9]

$$\begin{aligned} \mathrm{d}\Phi_\mathrm{a}/\mathrm{dE} &= 6.020 \times 10^{10}[\mathrm{cm}^{-2}\mathrm{s}^{-1}\mathrm{keV}^{-1}] \\ &\times \left(\frac{g_{a\gamma\gamma}}{10^{-10}\mathrm{GeV}^{-1}}\right)^2 \left(\frac{E}{1\,\mathrm{keV}}\right)^{2.481} \exp\left(-\frac{E}{1.205\,\mathrm{keV}}\right), \end{aligned} \tag{1}$$

where $g_{a\gamma\gamma}$ is the axion-photon coupling constant. Their average energy is 4.2 keV reflecting the core temperature of the sun. Then, they would be coherently converted into X-rays through the inverse process in a strong magnetic field at a laboratory. The conversion rate in a simple case is given by

$$P_{a\to\gamma} = \left(\frac{g_{a\gamma\gamma} B_\perp L}{2}\right)^2 \left[\frac{\sin(qL/2)}{qL/2}\right]^2, \tag{2}$$

where $B_\perp$ is the strength of the transverse magnetic field, L is the length of the field along the axion path, $q = (m_\gamma^2 - m_a^2)/2E$ is the momentum transfer by the virtual photon, m_a is the axion mass, and m_γ is the effective mass of the photon which equals zero in vacuum.

If one can adjust m_γ to m_a, coherence will be restored for non-zero mass axions. This is achieved by filling the conversion region with gas. A photon in the X-ray region acquires a positive effective mass in a medium. In light gas, such as hydrogen or helium, it is well approximated by

$$m_\gamma = \sqrt{\frac{4\pi\alpha N_e}{m_e}}, \tag{3}$$

where α is the fine structure constant, m_e is the electron mass, and N_e is the number density of electrons. We adopted cold helium gas as a dispersion-matching medium. It is worth noting that helium remains at gas state even at 5–6 K, the operating temperature of our magnet. Since the bore of the magnet is limited in space, the easiest way is to keep the gas at the same temperature as the magnet. Moreover, axions as heavy as a few electronvolts can be reached with helium gas of only about one atmosphere at this temperature.

2 Experimental apparatus

The schematic figure of the axion helioscope is shown in Fig. 1. Its main components are identical to the ones used in the first [10] and second phase measurements [11] of the Tokyo Axion Helioscope performed in 1997 and 2000, respectively. It is designed to track the sun in order to achieve long exposure time. It consists of a superconducting magnet, X-ray detectors, a gas container, and an altazimuth mounting.

The superconducting magnet [12] consists of two 2.3-m long race-track shaped coils running parallel with a 20-mm wide gap between them. The magnetic field in the gap is 4 T perpendicular to the helioscope axis. The coils are kept at 5–6 K during operation. The magnet was made cryogen-free by making two Gifford-McMahon refrigerators to cool it directly by conduction, and is equipped with a persistent current switch. Thanks to these features, the magnet can be freed from thick current leads after excitation, and the magnetic field is very stable for a long period of time without supplying current.

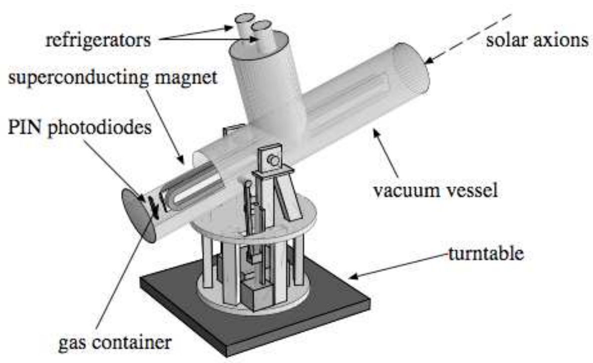

Figure 1: The schematic view of the axion helioscope.

The container to hold dispersion-matching gas is inserted in the $20 \times 92\,\mathrm{mm}^2$ aperture of the magnet. Its body is made of four 2.3-m long 0.8-mm thick stainless-steel square pipes welded side by side to each other.

Sixteen PIN photodiodes, Hamamatsu Photonics S3590-06-SPL, are used as the X-ray detectors [13], whose chip sizes are $11 \times 11 \times 0.5\,\mathrm{mm}^3$ each. In the present measurement, however, twelve of them are used for the analysis because four went defective through thermal stresses since the measurement of the previous phase. The effective area of a photodiode was measured formerly using a pencil-beam X-ray source, and found to be larger than $9 \times 9\,\mathrm{mm}^2$. It has an inactive surface layer of $0.35\,\mu$m [14].

The entire axion detector is constructed in a vacuum vessel and the vessel is mounted on an altazimuth mount. Its trackable altitude ranges from $-28°$ to $+28°$ and its azimuthal direction is designed to be limited only by a limiter which prevents the helioscope from endless rotation.

However, in the present measurement, the azimuthal range is restricted to about 60° because a cable handling system for its unmanned operation is not completed yet.

3 Measurement and Analysis

From December 2007 through April 2008, a measurement employing dispersion-matching gas was performed for 34 photon mass settings with about three days of running time per setting to scan around 1 eV.

Event reduction process is applied in the same way as the second phase measurement [11]. As a result, no significant excess was seen for any m_a, and thus an upper limit on $g_{a\gamma\gamma}$ at 95% confidence level was given. Fig. 2 shows the limit plotted as a function of m_a. Our previous limits from the first [10] and the second [11] phase measurements and some other bounds are also plotted in the same figure. The shown previous limits have been updated using newly measured inactive surface layer thickness of the PIN photodiode [14]; the difference is, however, marginal. The SOLAX [16], COSME [17] and DAMA [18] are solar axion experiments which exploit the coherent conversion on the crystalline planes [19] in a germanium and a NaI detector. The experiment by Lazarus et al. [15] and CAST [21] are the same kind of experiments as ours. The latter utilizes large decommissioned magnets of the LHC at CERN. Its limit is better than our previous limits by a factor of seven in low m_a region due to its larger B and L in Eq. (2). In the region $m_a > 0.14\,\text{eV}$, however, our previous and present limits surpass the limit of CAST[1]. The limit $g_{a\gamma\gamma} < 2.3 \times 10^{-9}\text{GeV}^{-1}$ is the solar limit inferred from the solar age consideration and the limit $g_{a\gamma\gamma} < 1 \times 10^{-9}\text{GeV}^{-1}$ is a more stringent limit reported by Schlattl et al. [20] based on comparison between the helioseismological sound-speed profile and the standard solar evolution models with energy losses by solar axions.

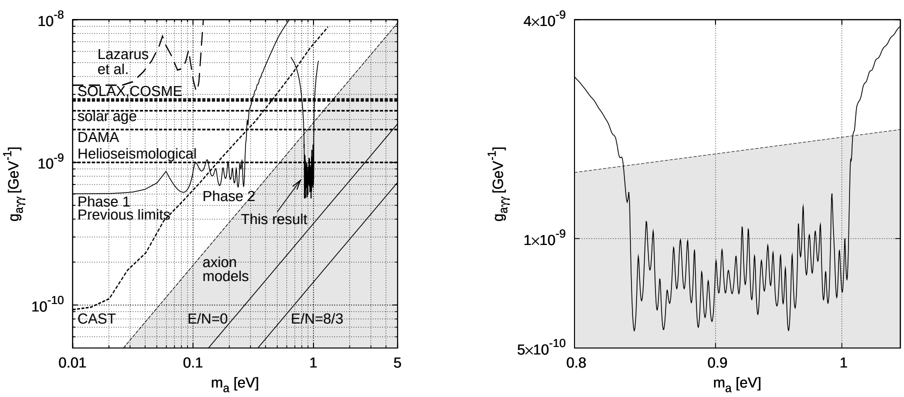

Figure 2: The left figure is the exclusion plot on $g_{a\gamma\gamma}$ to m_a. The new limit and the previous ones[10, 11] are plotted in solid lines. Dashed lines are explained in the text. The hatched area corresponds to the preferred axion models [22]. The right figure shows the magnified view of the new limit.

[1]CAST collaboration showed a preliminary limit in the region $m_a < 0.39\,\text{eV}$ in the present workshop.

4 Conclusion

The axion mass around 1 eV has been scanned with an axion helioscope with cold helium gas as the dispersion-matching medium in the $4\,\mathrm{T} \times 2.3\,\mathrm{m}$ magnetic field, but no evidence for solar axions was seen. A new limit on $g_{a\gamma\gamma}$ shown in Fig. 2 was set for $0.84 < m_a < 1.00\,\mathrm{eV}$. It is the first result to search for the axion in the $g_{a\gamma\gamma}$-m_a parameter region of the preferred axion models [22] with a magnetic helioscope. Full description of the present result is published in Ref. [23].

Acknowledgments

The authors thank the former director general of KEK, Professor H. Sugawara, for his support in the beginning of the helioscope experiment. This research was partially supported by the Japanese Ministry of Education, Science, Sports and Culture, Grant-in-Aid for COE Research and Grant-in-Aid for Scientific Research (B), and also by the Matsuo Foundation.

References

[1] R.D. Peccei, H.R. Quinn, Phys. Rev. Lett. 38 (1977) 1440.

[2] R.D. Peccei, H.R. Quinn, Phys. Rev. D 16 (1977) 1791.

[3] S. Weinberg, Phys. Rev. Lett. 40 (1978) 223.

[4] F. Wilczek, Phys. Rev. Lett. 40 (1978) 279.

[5] J.E. Kim, Phys. Rep. 150 (1987) 1.

[6] P. Sikivie, Phys. Rev. Lett. 51 (1983) 1415; 52 (1984) 695 (erratum).

[7] K. van Bibber et al., Phys. Rev. D 39 (1989) 2089.

[8] J. N. Bahcall and M. H. Pinsonneault, Phys. Rev. Lett. 92 (2004) 121301.

[9] G. G. Raffelt, Contribution to XI International Workshop on “Neutrino Telescope”, Venice, Italy, Feb. 22–25. 2005.

[10] S. Moriyama et al., Phys. Lett. B 434 (1998) 147.

[11] Y. Inoue et al., Phys. Lett. B 536 (2002) 18.

[12] Y. Sato et al., Development of a Cryogen-free Superconducting Dipole Magnet, in: Proc. of the 15th International Conference on Magnet Technology (MT-15) (Beijing, October 1997), eds.: L. Liangzhen, S. Guoliao, Y. Luguang (Science Press, Beijing, 1998) pp. 262–265; KEK-Preprint-97-202 (November, 1997).

[13] T. Namba et al., Nucl. Instr. Meth. A 489 (2002) 224.

[14] Y. Akimoto et al., Nucl. Instr. Meth. A 557 (2006) 684.

[15] D. M. Lazarus et al., Phys. Rev. Lett. 69 (1992) 2333.

[16] A. O. Gattone et al., Nucl. Phys. B(Proc. Suppl.)70 (1999) 59.

[17] A. Morales et al., Astropart. Phys. 16 (2002) 325.

[18] R. Bernabei et al., Phys. Lett. B 515 (2001) 6.

[19] E. A. Paschos, K. Zioutas, Phys. Lett. B323 (1994) 367.

[20] H. Schlattl, A. Weiss, G. Raffelt, Astropart. Phys. 10 (1999) 353.

[21] K. Zioutas et al., Phys. Rev. Lett. 94 (2005) 121301, C. Eleftheriadis, arXiv:0706.0637v1, and S. Andriamonje et al. (CAST Collaboration), J. Cosmol. Astropart. Phys. 04 (2007) 010.

[22] D. B. Kaplan, Nucl. Phys. B 260 (1985) 215, M. Srednicki, Nucl. Phys. B 260 (1985) 689, and S. L. Cheng, C. Q. Geng, W. -T. Ni, Phys. Rev. D 52 (1995) 3132.

[23] Y. Inoue, Y. Akimoto, R. Ohta, T. Mizumoto, A. Yamamoto, and M. Minowa, Phys. Lett. B (2008), doi:10.1016/j.physletb.2008.08.020.

Search for Low Energy Solar Axions with CAST

Giovanni Cantatore[1] for the CAST Collaboration[2]

[1]Università and INFN Trieste, Via Valerio 2, 34127, Trieste, Italy

[2]CAST Collaboration

E. Arik[17,*], S. Aune[2], D. Autiero[1,†], K. Barth[1], A. Belov[10], B. Beltrán[5,‡], S. Borghi[1], F. S. Boydag[17], H. Bräuninger[4], G. Cantatore[18], J. M. Carmona[5], S. Cebrián[5], S. A. Cetin[17], J. I. Collar[6], T. Dafni[2], M. Davenport[1], L. Di Lella[1,§], O. B. Dogan[17,*], C. Eleftheriadis[7], N. Elias[1], G. Fanourakis[8], E. Ferrer-Ribas[2], H. Fischer[9], J. Franz[9], J. Galán[5], E. Gazis[20], T. Geralis[8], I. Giomataris[2], S. Gninenko[10], H. Gómez[5], M. Hasinoff[11], F. H. Heinsius[9], I. Hikmet[17], D. H. H. Hoffmann[3], I. G. Irastorza[2,5], J. Jacoby[12], K. Jakovčić[14], D. Kang[9], T. Karageorgopoulou[20], M. Karuza[18], K. Königsmann[9], R. Kotthaus[13], M. Krčmar[14], K. Kousouris[8], M. Kuster[3], B. Lakić[14], C. Lasseur[1], A. Liolios[7], A. Ljubičić[14], V. Lozza[18], G. Lutz[13], G. Luzón[5], D. Miller[6], A. Morales[5,¶], J. Morales[5], T. Niinikoski[1], A. Nordt[3], A. Ortiz[5], T. Papaevangelou[1], M. Pivovaroff[16], A. Placci[1], G. Raiteri[18], G. Raffelt[13], H. Riege[1], A. Rodríguez[5], J. Ruz[5], I. Savvidis[7], Y. Semertzidis[15], P. Serpico[13], S. K. Solanki[19], R. Soufli[16], L. Stewart[1], M. Tsagri[15], K. van Bibber[16], J. Villar[5], J. Vogel[9], L. Walckiers[1], K. Zioutas[1,15]

1. European Organization for Nuclear Research (CERN), Genève, Switzerland
2. DAPNIA, Centre d'Études Nucléaires de Saclay (CEA-Saclay), Gif-sur-Yvette, France
3. Technische Universität Darmstadt, IKP, Darmstadt, Germany
4. Max-Planck-Institut für extraterrestrische Physik, Garching, Germany
5. Instituto de Física Nuclear y Altas Energías, Universidad de Zaragoza, Zaragoza, Spain
6. Enrico Fermi Institute and KICP, University of Chicago, Chicago, IL, USA
7. Aristotle University of Thessaloniki, Thessaloniki, Greece
8. National Center for Scientific Research "Demokritos", Athens, Greece
9. Albert-Ludwigs-Universität Freiburg, Freiburg, Germany
10. Institute for Nuclear Research (INR), Russian Academy of Sciences, Moscow, Russia
11. Department of Physics and Astronomy, University of British Columbia, Department of Physics, Vancouver, Canada
12. Johann Wolfgang Goethe-Universität, Institut für Angewandte Physik, Frankfurt am Main, Germany
13. Max-Planck-Institut für Physik (Werner-Heisenberg-Institut), Munich, Germany
14. Rudjer Bošković Institute, Zagreb, Croatia
15. Physics Department, University of Patras, Patras, Greece
16. Lawrence Livermore National Laboratory, Livermore, CA, USA
17. Dogus University, Istanbul, Turkey
18. Instituto Nazionale di Fisica Nucleare (INFN), Sezione di Trieste and Università di Trieste, Trieste, Italy
19. Max-Planck-Institut für Aeronomie, Katlenburg-Lindau, Germany
20. National Technical University of Athens, Athens, Greece

DOI: http://dx.doi.org/10.3204/DESY-PROC-2008-02/cantatore_giovanni_lea

We have started the development of a detector system, sensitive to single photons in the eV energy range, to be suitably coupled to one of the CAST magnet ports. This system should open to CAST a window on possible detection of low energy Axion Like Particles emitted by the sun. Preliminary tests have involved a cooled photomultiplier tube coupled to the CAST magnet via a Galileian telescope and a switched 40 m long optical fiber. This system has reached the limit background level of the detector alone in ideal conditions, and two solar tracking runs have been performed with it at CAST. Such a measurement has never been done before with an axion helioscope. We will present results from these runs and briefly discuss future detector developments.

1 Introduction

It has recently been pointed out [1] that many phenomena taking place in the sun, especially in its corona and in its magnetic field, are far from being completely understood. The production by the sun of Axion Like Particles (ALPs) and their subsequent interactions in the solar environment could provide a key to interpreting the physical mechanisms underlying these phenomena. These, and other considerations led to starting a search with the CAST magnetic helioscope [2] for hypothetical ALPs emitted by the sun in the energy range below 100 eV. The first step of this search, which will be reported here, has involved looking for 2-4 eV photons produced in the CAST magnet bore by the Primakoff [3] conversion into photons of solar ALPs in the latter energy range. The short term objective was to efficiently couple a detector system sensitive in the eV energy range to a CAST magnet bore and evaluate its background in normal operating conditions. The long term objective of the effort is attempting to detect, using sensors with the appropriate spectral sensitivity and good enough background, "low"-energy (tens of eV's) photons generated in the CAST helioscope by possible interactions of low-energy solar ALPs. We will briefly describe the detector system, which has been developed for this purpose under the BaRBE project financed by the Italian Istituto Nazionale di Fisica Nucleare (INFN), along with the coupling of this system to the CAST magnet. Finally, the data taking campaigns will be discussed and a summary of the data presented.

2 Preliminary tests and system set-up

The starting idea of the BaRBE project is to begin with readily available photon detectors sensitive in the visible range, test them in ideal laboratory conditions, and then design and build an optical system to couple the detectors to one of the bores of the CAST magnet. The devices used in this initial phase were a photomultiplier tube (PMT) (model 9893/350B made by EMI-Thorn) and an avalanche photodiode (APD) (model id100-20 made by idQuantique). The PMT had an active area dia. of 9 mm, with peak sensitivity at 350 nm. The APD had an active area dia. of 20 μm and peak sensitivity at 500 nm. For both detectors the Dark Count Rate (DCR) measured in the laboratory during preliminary tests was about 0.4 Hz. To measure the DCR, the PMT was biased at 1950 V and instrumented with an electronic readout

---

*Present address: Bogazici University, Istanbul, Turkey
†Present address: Institute de Physique Nucléaire, Lyon, France
‡Present address: Department of Physics, Queen's University, Kingston, Ontario
§Present address: Scuola Normale Superiore, Pisa, Italy
¶deceased

chain consisting of NIM standard modules. The APD readout module gave a 2 V, 10 ns wide, output signal which was transformed into a TTL pulse via a custom circuit. Both detectors were cooled by means of their built in Peltier coolers, operating at -20 ^{o}C, and were illuminated by a suitably attenuated blue LED source. To demonstrate single photon operation, the count histogram for each detector was fitted with a Poissonian distribution with average equal to 1. The DCR was then obtained after cutting the electronic noise pedestal using the fitted curve.

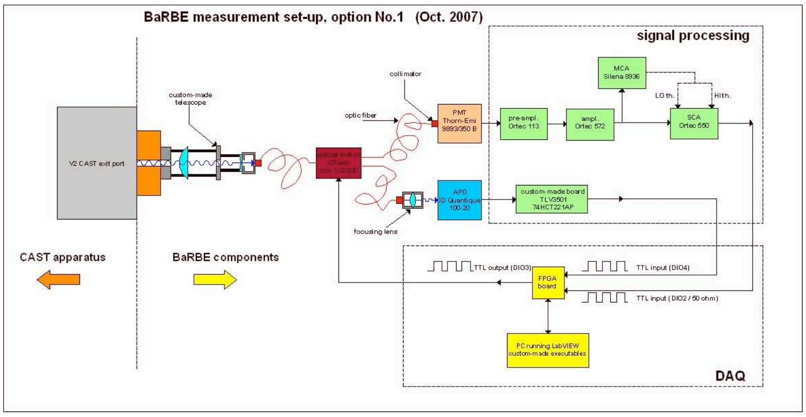

Figure 1: Schematic block-diagram of the BARBE setup at CAST (see text).

The basic elements of the coupling system were a Galileian telescope, a 40 m multimode optical fiber complete with input collimator and an optical switch (mod. 1x2 made by Leoni). The Galileian telescope consisted of a 2 inch dia., f = 200 mm, convex lens and of a 1 inch dia., f = - 30 mm, concave lens and was designed to optically couple the 40 mm dia. bore of the CAST magnet into the 9 mm dia. input collimator of the multimode fiber. The telescope was mounted directly onto one of the sunset side ports of the CAST magnet [1]. The detectors were placed far away from the magnet in the CAST experimental hall. The optical switch, which can be triggered by external TTL pulses, was used in order to share the light coming from the fiber between the PMT and the APD: each detector could then look at the magnet bore for 50% of the time and at the background for the remaining 50%. Figure 1 shows a block-diagram of the layout of the system as mounted on CAST. The overall light collection efficiency was about 50% for the PMT and less than 1% for the APD. The low efficiency of the APD channel was due to unresolved focussing difficulties. Since the APD data are of inferior quality, only the PMT measurements are considered. The total number of counts in each measurement is affected by afterpulses generated either by the PMT itself or by its readout electronic chain. It was found that afterpulses account for 11% of total counts. To eliminate the effect of the afterpulses the mean rate of counts is calculated, for both “light” and “dark” counts by solving for $x = 0$ the equation $N_x = A \cdot e^{-m} m^x / x!$, where x is the channel number, A is the total number of occurrences in all channels, N_x is the number of occurrences in the x-th channel measured experimentally. In this way occurrences in channel 0 are not affected by afterpulses.

[1] The telescope optical axis, determined before installation on a separate bench using an auxiliary laser beam, was aligned to the CAST magnet axis as established by the surveyors.

3 Measurement results

Two measurement campaigns were conducted. The first one in November 2007 with the telescope attached to the V2 port of the CAST magnet, while the second one was in March 2008 with the telescope on the V1 port.

In the first run each detector, PMT and APD, looked at the magnet bore for 50% of the time and at the background for the other 50%. Environmental checks and background measurements in different magnet positions and with field on and off were performed. A total of 45000 s of "live" data with the magnet on were taken, 10000 s of dummy solar tracking data and 35000 s of actual sun tracking data.

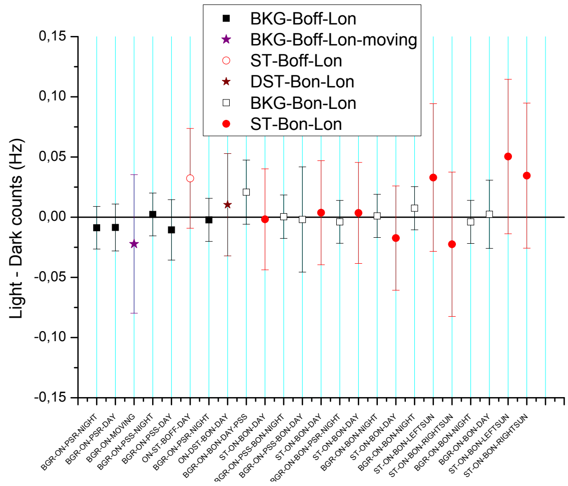

Figure 2: Difference between "light" and "dark" average count rates measured in the March 2008 run (PMT data only). Points on the abscissa axis correspond to different configurations of the entire apparatus, including background (BKG) tests and sun tracking (ST) periods with the magnet on (Bon). Error bars represent 1 σ intervals (see also text).

The second run was conducted using the PMT only, but keeping the switching system in order to have again the detector share its live time equally between signal and background. In this case 45000 s of live data were taken, of which 5000 s of dummy solar tracking data, 20000 s of actual solar tracking data and 20000 s of data with the magnet pointing off the sun center (10000 s pointing 0.25^o to the right and 10000 s pointing 0.25^o to the left). Figure 2 shows a plot of the difference of the measured average count rates between "light", when the PMT was looking at the magnet bore, and "dark", when the optical switch was toggled on the other position. The abscissa axis refers to the different conditions in which data were taken. Taking into account the 1 σ error bars reported in the plot, no statistically significant difference is found between "light" and "dark" count rates. The average background count rate measured for 3-4 eV photons during solar tracking was 0.35 ± 0.02 Hz for a total of 75000 s of data.

4 Conclusions and perspectives

The measurement runs conducted with the BaRBE detector system demonstrated that it is possible to couple two detectors to the CAST magnet via an optical fiber, while preserving a reasonable light collection efficiency (50% in the PMT case, that corresponds to 10% of overall system efficiency when taking into account the PMT spectral response curve), and without introducing additional noise sources. In 12 data sets taken during solar tracking (including 2 sets pointing off center) the background count rate for 3-4 eV photons was 0.35 $\pm$ 0.02 Hz and no significative excess counts over background were observed. This is the first time such a measurement has been done with an axion helioscope.

The challenge is now to progress to a new detector(s) with lower intrinsic background, possibly extending the spectral sensitivity to other regions of the energy interval below 100 eV . In the case of visible photons, one could also envision enclosing the CAST magnet bore in a resonant optical cavity in order to enhance the axion-photon conversion probability [4]. This would however require solving rather complex compatibility problems with the rest of the CAST apparatus.

Three types of detectors have at this moment been considered for future developments, a Transition Edge Sensor (TES) [5], a silicon sensor with DEPFET readout [6] and an APD cooled to liquid nitrogen temperatures. The TES sensor promises practically zero background, spectroscopic capability and sensitivity from less than 1 eV up to tens of eV's. It however requires operation at 100 mK and it has a small sensitive area (about 100μm $\times$ 100μm). The DEPFET sensors could reach a very low background if used in the Repetitive Non Destructive Readout (RNDR) mode, however they also have a small sensitive area. Finally, the cooled APD could be operated relatively easily if one accepts afterpulsing events, which should not pose a problem in a low expected rate environment. On the other hand, the sensitive area would only be about 300 μm^2 and the spectral sensitivity limited to the visible region. The present plan is to initially pursue all three possibilities in the hope of identifying the one where progress is faster.

5 Acknowledgments

Funding for the BaRBE project has been provided by INFN (Italy). The support by the GSRT in Athens is gratefully acknowledged. This research was partially supported by the ILIAS project funded by the EU under contract EU-RII3-CT-2004-506222. Special thanks to M. Karuza, V. Lozza and G. Raiteri of INFN Trieste for their excellent detector work, and to the entire CAST Collaboration for wonderful support and assistance. We also warmly thank the CERN staff for their precious help.

References

[1] See for instance K. Zioutas, "The enigmatic Sun: a crucible for new physics", Cern Courier, May 2008.

[2] S. Andriamonje *et al.* [CAST Collaboration], JCAP **0704** (2007) 010 [arXiv:hep-ex/0702006]; Kuster, M. *et al.*, New J. Phys., **9** (2007) 169; Abbon, P. *et al.*, New J. Phys. **9** (2007)170; Autiero, D. *et al.*, New J. Phys. **9** (2007) 171; Zioutas, K. *et al.* [CAST Collaboration], Phys. Rev Lett. **94** (2005) 121301.

[3] See for instance G. Raffelt and L. Stodolsky, Phys. Rev. D **37** (1988) 1237-1249.

[4] P. Sikivie, D. B. Tanner and K. van Bibber, Phys. Rev. Lett. **98** (2007) 172002 [arXiv:hep-ph/0701198].

[5] B. Cabrera, J Low Temp Phys **151** (2008) 82-93; D. Bagliani et al., J Low Temp Phys **151** (2008) 234-238.

[6] J. Kemmer and G. Lutz, Nucl. Instrum. Meth. A **253** (1987) 365; P. Fischer *et al.*, Nucl. Instrum. Meth. A **582** (2007) 843.

Hunting axions in low Earth orbit

Patrick Huber

Physics Department – IPNAS, Virginia Tech, Blacksburg VA 24061, USA

DOI: http://dx.doi.org/10.3204/DESY-PROC-2008-02/huber_patrick

We show that an x-ray observatory in low Earth orbit can, in principle, detect solar axion emission exploiting the same physics as experiments like CAST. We call this effect GECOSAX. The obtainable sensitivity strongly depends on the chosen orbit and time of year the observation is performed. We included the effects of the detailed geomagnetic field shape, precise orbit computation and the Earth atmosphere. Our background model is based on actual observations performed by the SUZAKU satellite. The final, limiting sensitivities we obtain for a realistic mission are at $2\,\sigma$: $g_{a\gamma} < (4.7-6.6)\times 10^{-11}\,\mathrm{GeV}^{-1}$, for axion masses $m_a < 10^{-4}\,\mathrm{eV}$, which significantly exceeds current laboratory sensitivities.

1 Introduction

The basic concept for the detection of solar axions was described by P. Sikivie in a seminal paper [1] in 1983. This very same technique is still employed today; the most recent incarnation being the CAST experiment [2]. The detection rate in these experiments is proportional to the conversion probability, which in the limit $m_a \to 0$ is given by

$$P^s_{a\gamma} = 2.45 \times 10^{-21} \left(\frac{g_{a\gamma}}{10^{-10}\,\mathrm{GeV}^{-1}}\right)^2 \left(\frac{B}{\mathrm{T}}\right)^2 \left(\frac{L}{\mathrm{m}}\right)^2 . \tag{1}$$

$P^s_{a\gamma}$ depends only on the product of $(B \cdot L)^2$, thus any experiments having similar values of $(B \cdot L)^2$ will have a similar conversion rate. The signal consists of x-ray photons in the energy range $2 - 10\,\mathrm{keV}$. As a reference value we can use the CAST values for $B \simeq 9\,\mathrm{T}$ and $L \simeq 10\,\mathrm{m}$, which yields $(B \cdot L)^2 \simeq 8000\,\mathrm{T}^2\mathrm{m}^2$. The basic idea of geomagnetic conversion of solar axions (GECOSAX), is to replace the strong but small magnet of CAST by the weak but large magnet, called Earth [3]. For the Earth, we have $B \sim 3 \cdot 10^{-5}\,\mathrm{T}$ and $L \sim 600\,\mathrm{km}$ and as a result $(B \cdot L)^2 \simeq 300\,\mathrm{T}^2\mathrm{m}^2$. This value is only about one order of magnitude smaller than the one of CAST, which *e.g.* could be compensated by a larger x-ray collection area. The obvious challenge for the GECOSAX approach is given by the x-ray emission directly from the Sun, which exceeds the GECOSAX signal by about 13 orders of magnitude. Here, following observation can be exploited: solar x-rays will be completely absorbed by the Earth or its atmosphere, whereas solar axion can pass it unattenuated. Therefore, on the night side of the Earth there will be solar axions but *no* solar x-rays. Thus, a GECOSAX experiment is indeed very similar to a terrestial experiment. In this contribution, we will explore the relevant effects, which need to be included for reliable computation of the expected GECOSAX signal. We also, will present a background estimate based on data of the SUZAKU satellite. Combined, this will allow us to arrive at a sensitivity to $g_{a\gamma}$ for such an experiment. A more detailed version of the material presented here can be found in Ref. [4].

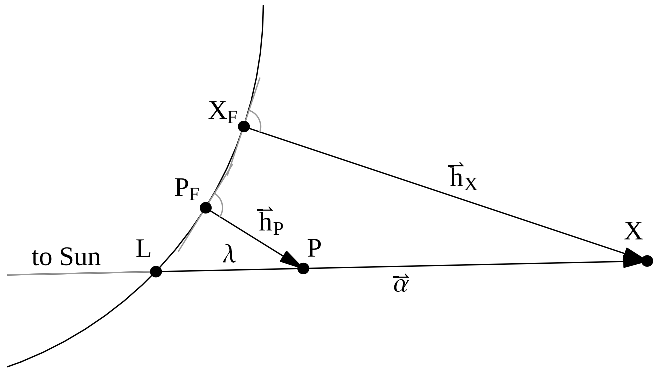

Figure 1: Geometry of the GECOSAX configuration drawn in the plane spanned by the center of the Earth, the center of the Sun and the satellite's position at t_0. Figure taken from [4].

2 Geometry & satellite position

The geometry of the GECOSAX configuration is depicted in Fig. 1, where X denotes the position of the satellite at t_0. The altitude of the satellite is then given by $\left|\vec{h}_X\right|$. Here, $\vec{\alpha} = \overline{LX}$ is the so called line of sight (LOS). The actual axion conversion will take place along the LOS, thus the axion conversion path length is given by $|\vec{\alpha}|$. Note, that $|\vec{\alpha}| \geq \left|\vec{h}_X\right|$, thus the altitude of the satellite is a lower bound on the available axion conversion path length. In order to to compute $P_{a\gamma}$ it is necessary to compute the position of the satellite, the Earth and the Sun relative to each other for a given time t_0. This is accomplished by using simple but accurate algorithms for the ephemeris of the Sun. The satellite's position is obtained from an analytic perturbation theory, which was developed to allow efficient tracking of a large number of objects in low Earth orbit on the very limited computers of the 60's. The algorithm we use yields errors of about 10 km, which are negligible for our purposes. Another advantage of this algorithm is that initial conditions for many satellites are easily available. In an actual satellite mission, the errors in the position of the satellite will be orders of magnitude smaller.

3 Magnetic field & Earth atmosphere

The magnetic field of the Earth is a complex and interesting system and its study is a whole field of research on its own. It is far from being a simple dipole field and its symmetry axis is not aligned with the rotation axis of the Earth, which leads to a diurnal modulation by the rotation of the Earth. Fortunately, for our purposes we only need to know the direction and magnitude of the $\vec{B}$-field along the LOS. This information is extracted from a global magnetic model which is based on ground and space observations of the magnetic field over an extended period of time. This data is then used to determine the coefficients of an expansion in spherical harmonics. Knowing these coefficients it is straightforward to retrieve the direction and magnitude of the $\vec{B}$-field. The field model we employ is accurate up to altitudes of about 1000 km and therefore, we will restrict our analysis to this range.

The effect of the Earth atmosphere on the propagation of x-rays is two-fold: First, there is refraction, which will create an effective mass m_γ for the photon. m_γ plays a crucial role in matching the momenta of the axion and the photon and therefore, has a strong effect on $P_{a\gamma}$. Secondly, there is absorption, which limits photon propagation to about one scattering length τ. Both effects scale with the air density ρ, which itself is a function of altitude h. The effects scale with density like $m_\gamma \propto \rho(h)^{\frac{1}{2}}$ and $\tau \propto \rho(h)^{-1}$. The proportionality constants are well know from laboratory experiments. Given $\rho(h)$ it is then straightforward to include both, the effect from refraction and absorption, into the computation of $P_{a\gamma}$. The density profile of the atmosphere follows a simple barometric height formula $\rho(h) \propto \exp h/h_0$ only up to $h \leq 50\,\mathrm{km}$. Beyond that, various other effects like diffusion or local heating by solar UV radiation, interaction of partially ionized air with the magnetic field *etc.* become important. There are various semi-empirical models available to describe the rich dynamics of the upper Earth atmosphere. Using a state of the art model we found that the total density variations encountered are insignificant for altitudes above $h > 70\,\mathrm{km}$ which determine the axion-photon conversion rate. Therefore, we use a static, average atmosphere which is approximated by an exponential of a higher order polynomial in h. This, greatly simplifies the treatment of atmospheric effects. Absorption is important up to altitudes of about 80 km, whereas refraction can not be neglected up about $h \simeq 120\,\mathrm{km}$.

4 Orbit choice

All the ingredients are then combined to computate $P_{a\gamma}$. As a result, the expected signal strength along each point of the orbit of a given satellite can be predicted with an error of about 10%. Clearly, orbits which provide the maximal signal strength are preferable over those ones which only yield a low signal strength. In any real experiment there will be background as well and thus the appropriate measure of signal strength is significance S, defined like this

$$S = \underbrace{A^{1/2} F^{-1/2}}_{=:Q} \underbrace{t^{1/2} \Phi_{10}}_{=:\Sigma} = Q\Sigma\,, \tag{2}$$

with A being the effective x-ray collection area, F the background rate integrated over the relevant energy range and source size. t is the available observation time, which is a sensitive function of the chosen orbit, since only those parts of the orbit in the Earth shadow count towards t. Here, Φ_{10} is the appropriately averaged flux of GECOSAX photons for $g_{a\gamma} = 10^{-10}\,\mathrm{GeV}^{-1}$. Note, that Σ depends only on the chosen satellite orbit, whereas Q depends only on the instrument used for x-ray observation. Thus, we can look for the best possible orbit without actually having to specify the instrument. On a typical orbit, the available conversion path length or length of the LOS will be largest at the entry and exit points of the Earth shadow for purely geometric reasons. Thus, the GECOSAX signal will be largest there as well. However, depending on the type of instrument aboard the satellite the observation cannot start at the point of entry and last till the point of exit. Therefore, we have to distinguish two types of missions: fixed mode missions, which can use the full duration of the dark orbit and turning mode missions, which have to discard the first and last 10 minutes of each dark orbit. Instead of designing an optimal orbit we chose to survey orbits of existing satellites and to identify the most suitable ones for the observation of GECOSAX. Naively, one would expect that high altitudes, to maximize the axion conversion path, with a high inclination, which carries the satellites over the magnetic poles, which have the highest $\vec{B}$-field, would be optimal. This expectation is well corroborated by our survey of 50 orbits with altitudes below 1000 km.

5 Sensitivity to $g_{a\gamma}$

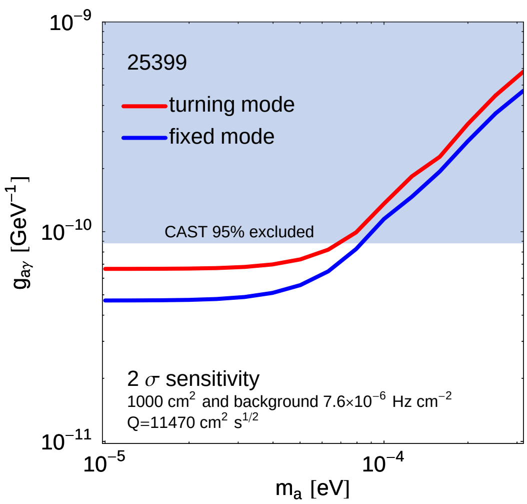

Figure 2: Sensitivity to $g_{a\gamma}$ as a function of the axion mass m_a at $2\,\sigma$ (95%) confidence level. The blue shaded region is excluded by the CAST experiment [2]. Figure taken from [4].

Using the optimal orbit, identified in the previous section, we now can compute the expected limiting sensitivity for an instrument of given size and background level. The background level, we assume corresponds to the one measured by the XIS FI sensor aboard the SUZAKU satellite [5]. The effective x-ray collection area is taken to be $1000\,\mathrm{cm}^2$ which is well within the range of currently in space used x-ray optical systems. The resulting sensitivity limit to $g_{a\gamma}$ as a function of the axion mass m_a is shown in Fig. 2. The number given in the left hand upper corner of this figure, is the US SPACECOM ID number of the satellite used. This orbit is nearly circular and has an average altitude of about 820 km and an inclination with the respect to the equator of 82°. Obviously, the fixed mode observation provides better sensitivity since it can use more observation time, which in addition has a higher signal strength. For $m_a < 2\cdot 10^{-5}\,\mathrm{eV}$ the sensitivity limit from a realistic, currently feasible mission is $4.6\cdot 10^{-11}\,\mathrm{GeV}^{-1}$. If one would envisage larger detectors and a dedicated mission limits of the order $(2-3)\cdot 10^{-11}\,\mathrm{GeV}^{-1}$ may be achievable.

Acknowledgments

It is my pleasure, to thank the organizers of Patras 08 for a very stimulating and interesting workshop.

References

[1] P. Sikivie. Experimental tests of the *invisible* axion. *Phys. Rev. Lett.*, 51:1415, 1983.

[2] S. Andriamonje et al. An improved limit on the axion-photon coupling from the CAST experiment. *JCAP*, 0704:010, 2007.

[3] Hooman Davoudiasl and Patrick Huber. Detecting solar axions using earth's magnetic field. *Phys. Rev. Lett.*, 97:141302, 2006.

[4] Hooman Davoudiasl and Patrick Huber. Feasibility Study for Measuring Geomagnetic Conversion of Solar Axions to X-rays in Low Earth Orbits. *JCAP*, 0808:026, 2008.

[5] K. Koyama et al. X-ray Imaging Spectrometer (XIS) on Board Suzaku. *Publ. Astron. Soc. Jap.*, 59:23–33, 2007.

Chapter 3

Signals from Astrophysical Sources II: High Energy Photon Experiments

Detection of Distant AGN by MAGIC: the Transparency of the Universe to High-Energy Photons

Marco Roncadelli[1], *Alessandro De Angelis*[2], *Oriana Mansutti*[3]

[1]INFN, Sezione di Pavia, via A. Bassi 6, I – 27100 Pavia, Italy

[2]Dipartimento di Fisica, Università di Udine, Via delle Scienze 208, I – 33100 Udine, and INAF and INFN, Sezioni di Trieste, Italy

[3]Dipartimento di Fisica, Università di Udine, Via delle Scienze 208, I – 33100 Udine, and INFN, Sezione di Trieste, Italy

The recent detection of blazar 3C279 by MAGIC has confirmed previous indications by H.E.S.S. that the Universe is more transparent to very-high-energy gamma rays than previously thought. We show that this fact can be reconciled with standard blazar emission models provided photon oscillations into a very light Axion-Like Particle occur in extragalactic magnetic fields. A quantitative estimate of this effect explains the observed spectrum of 3C279. Our prediction can be tested in the near future by the satellite-borne GLAST detector as well as by the ground-based Imaging Atmospheric Cherenkov Telescopes H.E.S.S., MAGIC, CANGAROO III, VERITAS and by the Extensive Air Shower arrays ARGO-YBJ and MILAGRO.

1 Introduction

As is well known, in the very-high-energy (VHE) band above 100 GeV the horizon of the observable Universe rapidly shrinks as the energy further increases. This comes about because photons from distant sources scatter off background photons permeating the Universe, thereby disappearing into electron-positron pairs [1]. The corresponding cross section $\sigma(\gamma\gamma \to e^+e^-)$ peaks where the VHE photon energy E and the background photon energy ϵ are related by $\epsilon \simeq (500\,\mathrm{GeV}/E)\,\mathrm{eV}$. Therefore, for observations performed by Imaging Atmospheric Cherenkov Telescopes (IACTs) – which probe the energy interval 100 GeV – 100 TeV – the resulting cosmic opacity is dominated by the interaction with ultraviolet/optical/infrared diffuse background photons (frequency band $1.2 \cdot 10^3$ GHz – $1.2 \cdot 10^6$ GHz, corresponding to the wavelength range $0.25\,\mu\mathrm{m} - 250\,\mu\mathrm{m}$), usually called Extragalactic Background Light (EBL), which is produced by galaxies during the whole history of the Universe. Neglecting evolutionary effects for simplicity, photon propagation is controlled by the photon mean free path $\lambda_\gamma(E)$ for $\gamma\gamma \to e^+e^-$, and so the observed photon spectrum $\Phi_{\rm obs}(E, D)$ is related to the emitted one $\Phi_{\rm em}(E)$ by

$$\Phi_{\rm obs}(E, D) = e^{-D/\lambda_\gamma(E)}\; \Phi_{\rm em}(E)\ . \tag{1}$$

Within the energy range in question, $\lambda_\gamma(E)$ decreases like a power law from the Hubble radius 4.2 Gpc around 100 GeV to 1 Mpc around 100 TeV [2]. Thus, Eq. (1) entails that the observed flux is *exponentially* suppressed both at high energy and at large distances, so that sufficiently far-away sources become hardly visible in the VHE range and their observed spectrum should anyway be *much steeper* than the emitted one.

Yet, observations have *not* detected the behavior predicted by Eq. (1). A first indication in this direction was reported by the H.E.S.S. collaboration in connection with the discovery of the two blazars H2356-309 ($z = 0.165$) and 1ES1101-232 ($z = 0.186$) at $E \sim 1\,\mathrm{TeV}$ [3]. Stronger evidence comes from the observation of blazar 3C279 ($z = 0.536$) at $E \sim 0.5\,\mathrm{TeV}$ by the MAGIC collaboration [4]. In particular, the signal from 3C279 collected by MAGIC in the region $E < 220$ GeV has more or less the same statistical significance as the one in the range 220 GeV $< E <$ 600 GeV (6.1σ in the former case, 5.1σ in the latter).

A suggested way out of this difficulty relies upon the modification of the standard Synchro-Self-Compton (SSC) emission mechanism. One option invokes strong relativistic shocks [5]. Another rests upon photon absorption inside the blazar [6]. While successful at substantially hardening the emission spectrum, these attempts fail to explain why *only* for the most distant blazars does such a drastic departure from the SSC emission spectrum show up.

Our proposal – usually referred to as the DARMA scenario – is quite different [7]. Implicit in previous considerations is the hypothesis that photons propagate in the standard way throughout cosmological distances. We suppose instead that photons can oscillate into a new very light spin-zero particle – named Axion-Like Parlicle (ALP) – and vice-versa in the presence of cosmic magnetic fields, whose existence has definitely been proved by AUGER observations [8]. Once ALPs are produced close enough to the source, they travel *unimpeded* throughout the Universe and can convert back to photons before reaching the Earth. Since ALPs do not undergo EBL absorption, the *effective* photon mean free path $\lambda_{\gamma,\mathrm{eff}}(E)$ gets *increased* so that the observed photons cross a distance in excess of $\lambda_\gamma(E)$. Correspondingly, Eq. (1) becomes

$$\Phi_{\mathrm{obs}}(E, D) = e^{-D/\lambda_{\gamma,\mathrm{eff}}(E)}\, \Phi_{\mathrm{em}}(E) \ , \tag{2}$$

from which we see that even a *slight* increase of $\lambda_{\gamma,\mathrm{eff}}(E)$ gives rise to a *huge* enhancement of the observed flux. It turns out that the DARMA mechanism makes $\lambda_{\gamma,\mathrm{eff}}(E)$ shallower than $\lambda_\gamma(E)$ although it remains a decreasing function of E. So, the resulting observed spectrum is *much harder* than the one predicted by Eq. (1), thereby ensuring agreement with observations even for a *standard* SSC emission spectrum. As a bonus, we get a natural explanation for the fact that only the most distant blazars would demand $\Phi_{\mathrm{em}}(E)$ to substantially depart from the emission spectrum predicted by the SSC mechanism.

Our aim is to review the main features of our proposal as well as its application to blazar 3C279.

2 DARMA scenario

Phenomenological as well as conceptual arguments lead to view the Standard Model of particle physics as the low-energy manifestation of some more fundamental and richer theory of all elementary-particle interactions including gravity. Therefore, the lagrangian of the Standard Model is expected to be modified by small terms describing interactions among known and new particles. Many extensions of the Standard Model which have attracted considerable interest over the last few years indeed predict the existence of ALPs. They are spin-zero light bosons defined by the low-energy effective lagrangian

$$\mathcal{L}_{\mathrm{ALP}} \ = \ \frac{1}{2}\,\partial^\mu\, a\, \partial_\mu\, a - \frac{1}{2}\, m^2\, a^2 - \frac{1}{4M}\, F^{\mu\nu}\, \tilde{F}_{\mu\nu}\, a \ , \tag{3}$$

where $F^{\mu\nu}$ is the electromagnetic field strength, $\tilde{F}_{\mu\nu}$ is its dual, a denotes the ALP field whereas m stands for the ALP mass. According to the above view, it is assumed $M \gg G_F^{-1/2} \simeq 250\,\mathrm{GeV}$. On the other hand, it is supposed that $m \ll G_F^{-1/2} \simeq 250\,\mathrm{GeV}$. The standard Axion [9] is the most well known example of ALP. As far as *generic* ALPs are concerned, the parameters M and m are to be regarded as *independent*.

So, what really characterizes ALPs is the trilinear γ-γ-a vertex described by the last term in $\mathcal{L}_{\mathrm{ALP}}$, whereby one ALP couples to two photons. Owing to this vertex, ALPs can be emitted by astronomical objects of various kinds, and the present situation can be summarized as follows. The negative result of the CAST experiment designed to detect ALPs emitted by the Sun yields the bound $M > 0.86 \cdot 10^{10}\,\mathrm{GeV}$ for $m < 0.02\,\mathrm{eV}$ [10]. Moreover, theoretical considerations concerning star cooling via ALP emission provide the generic bound $M > 10^{10}\,\mathrm{GeV}$, which for $m < 10^{-10}\,\mathrm{eV}$ gets replaced by the stronger one $M > 10^{11}\,\mathrm{GeV}$ even if with a large uncertainty [11]. The same γ-γ-a vertex produces an off-diagonal element in the mass matrix for the photon-ALP system in the presence of an external magnetic field $\mathbf{B}$. Therefore, the interaction eigenstates differ from the propagation eigenstates and photon-ALP oscillations show up [12].

We imagine that a sizeable fraction of photons emitted by a blazar soon convert into ALPs. They propagate unaffected by the EBL and we suppose that before reaching the Earth a substantial fraction of ALPs is back converted into photons. We further assume that this photon-ALP oscillation process is triggered by cosmic magnetic fields (CMFs), whose existence has been demonstrated very recently by AUGER observations [8]. Owing to the notorious lack of information about their morphology, one usually supposes that CMFs have a domain-like structure [13]. That is, $\mathbf{B}$ ought to be constant over a domain of size L_{dom} equal to its coherence length, with $\mathbf{B}$ randomly changing its direction from one domain to another but keeping approximately the same strength. As explained elsewhere [14], it looks plausible to assume the coherence length in the range $1 - 10\,\mathrm{Mpc}$. Correspondingly, the inferred strength lies in the range $0.3 - 1.0\,\mathrm{nG}$ [14].

3 Predicted energy spectrum

Our ultimate goal consists in the evaluation of the probability $P_{\gamma\to\gamma}(E,D)$ that a photon remains a photon after propagation from the source to us when allowance is made for photon-ALP oscillations as well as for photon absorption from the EBL. As a consequence, Eq. (2) gets replaced by

$$\Phi_{\mathrm{obs}}(E,D) = P_{\gamma\to\gamma}(E,D)\,\Phi_{\mathrm{em}}(E)\ . \tag{4}$$

We proceed as follows. We first solve exactly the beam propagation equation arising from $\mathcal{L}_{\mathrm{ALP}}$ over a single domain, assuming that the EBL is described by the "best-fit model" of Kneiske *et al.* [15]. Starting with an unpolarized photon beam, we next propagate it by iterating the single-domain solution as many times as the number of domains crossed by the beam, taking each time a *random* value for the angle between $\mathbf{B}$ and a fixed overall fiducial direction. We repeat such a procedure 10·000 times and finally we average over all these realizations of the propagation process.

We find that about 13% of the photons arrive to the Earth for $E = 500\,\mathrm{GeV}$, representing an enhancement by a factor of about 20 with respect to the expected flux without DARMA mechanism (the comparison is made with the above "best-fit model"). The same calculation gives a fraction of 76% for $E = 100\,\mathrm{GeV}$ (to be compared to 67% without DARMA mechanism) and a fraction of 3.4% for $E = 1\,\mathrm{TeV}$ (to be compared to 0.0045% without DARMA mechanism). The resulting spectrum is exhibited in Fig. 1. The solid line represents the prediction of the DARMA scenario for $B \simeq 1\,\mathrm{nG}$ and $L_{\rm dom} \simeq 1\,\mathrm{Mpc}$ and the gray band is the envelope of the results obtained by independently varying $\mathbf{B}$ and $L_{\rm dom}$ within a factor of 10 about such values. These conclusions hold for $m \ll 10^{-10}\,\mathrm{eV}$ and we have taken for definiteness $M \simeq 4 \cdot 10^{11}\,\mathrm{GeV}$ but we have checked that practically nothing changes for $10^{11}\,\mathrm{GeV} < M < 10^{13}\,\mathrm{GeV}$.

Our prediction can be tested in the near future by the satellite-borne GLAST detector as well as by the ground-based IACTs H.E.S.S., MAGIC, CANGAROO III, VERITAS and by the Extensive Air Shower arrays ARGO-YBJ and MILAGRO.

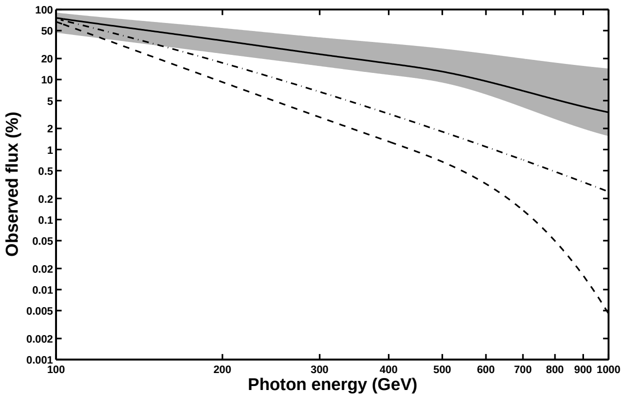

Figure 1: The two lowest lines give the fraction of photons surviving from 3C279 without the DARMA mechanism within the “best-fit model” of EBL (dashed line) and for the minimum EBL density compatible with cosmology (dashed-dotted line) [15]. The solid line represents the prediction of the DARMA mechanism as explained in the text.

References

[1] G. G. Fazio and F. W. Stecker, Nature **226** 135 (1970).

[2] P. Coppi and F. Aharonian, Astrophys. J. **487** L9 (1997).

[3] F. Aharonian *et al.* (H.E.S.S. Collaboration), Nature **440** 1018 (2006).

[4] J. Albert *et al.* (MAGIC Collaboration), Science **320** 1752 (2008).

[5] F. W. Stecker, M. G. Baring and E. J. Summerlin, Astrophys. J. **667** L29 (2007).
F. W. Stecker and S. T. Scully, Astron. Astrophys **478** L1 (2008).

[6] F. Aharonian, D. Khangulyan and L. Costamante, arXiv:0801.3198 (2008).

[7] A. De Angelis, M. Roncadelli and O. Mansutti, Phys. Rev. **D76** 121301 (2007).

[8] J. Abraham *et al.* [Pierre Auger Collaboration], Science **318** 939 (2007).

[9] J. H. Kim, Phys. Rep. **150** 1 (1987). H. Y. Cheng, Phys. Rep. **158** 1 (1988).

[10] K. Zioutas *et al.*, Phys. Rev. Lett. **94** 121301 (2005). S. Andriamoje *et al.*, JCAP 0704010 (2007).

[11] G. G. Raffelt, *Stars as Laboratories for Fundamental Physics* (University of Chicago Press, Chicago, 1996).

[12] P. Sikivie, Phys. Rev. Lett. **51** 1415 (1983); (E) ibid. **52** 695 (1984). L. Maiani, R. Petronzio and E. Zavattini, Phys. Lett. **B175** 359 (1986). G. G. Raffelt and L. Stodolsky, Phys. Rev. **D37** 1237 (1988).

[13] P. P. Kronberg, Rept. Prog. Phys. **57** 325 (1994). D. Grasso and H. Rubinstein, Phys. Rep. **348** 163 (2001).

[14] A. De Angelis, M. Persic and M. Roncadelli, Mod. Phys. Lett. **A23** 315 (2008).

[15] T. M. Kneiske, T. Bretz, K. Mannheim and D. H. Hartmann, Astron. Astrophys. **413** 807 (2004).

Indirect Search for Dark Matter with H.E.S.S.

Joachim Ripken for the H.E.S.S. Collaboration
Institut für Experimentalphysik der Universität Hamburg, Luruper Chaussee 149, 22761 Hamburg, Germany

The Universe is filled with non-baryonic Dark Matter which prevails the known form of matter (leptons and baryons). Indirect Dark Matter search methods are sensitive to self-annihilating Dark Matter candidates: among the spray of particles released in the self-annihilation process, gamma-rays and to some extent neutrinos can be used to trace regions with high overdensities of Dark Matter. The energy of these photons reaches up to the mass of the annihilating particles. For Dark Matter particles more massive than 100 GeV, atmospheric Cherenkov telescopes become sensitive to these radiation energies while for less massive particles, space-based detection techniques are favorable (e.g. with the recently commissioned Fermi mission). Here, we present a summary of results obtained with the H.E.S.S. experiment located in Namibia using four 100 m^2 optical telescopes to detect and image air Cherenkov light from extensive air showers. The experiment has been used to search for annihilation radiation from various candidate regions with enhanced Dark Matter density including the Galactic center, Sagittarius dwarf, M87, and clumps in the Galactic halo.

1 Introduction

A particularly interesting class of dark matter (DM) candidates are "weakly interacting massive particles" (WIMPs) which naturally arise in various extensions (or completions) of the standard model of elementary particle physics as e.g. the class of supersymmetric models or theories invoking extra dimensions. The simplest representative of the latter class of models is the widely studied Kaluza-Klein (KK) theory (see [7]). Some of these DM candidates are Majorana particles. In these specific cases, indirect search methods for DM are feasible. Self-annihilation could lead to an observable excess of γ-ray photons, neutrinos, and antimatter in cosmic-rays. Indirect search methods are complementary to direct search methods as well as to accelerator based methods. We are currently witnessing a rapid progress in the sensitivities reached in all domains including the commissioning/planning of new instruments for ground based gamma-ray astronomy (CTA), space-based gamma-ray satellites (Fermi, formerly known as GLAST, PAMELA), accelerator based experiments (LHC, ILC) and direct search methods (ZEPELIN, etc.).

Here, we present recently obtained results with the H.E.S.S. experiment. In the interpretation of the results we mainly focus on supersymmetric extensions of the standard model with the Neutralino as the lightest supersymmetric particle (LSP) as well as KK models, where the lowest excited state $B^{(1)}$ is the WIMP candidate.

There are two ways for the investigated WIMP candidates to produce γ-ray photons. In principle annihilation into monoenergetic photons is possible, but because of loop suppression unlikely and therefore not considered here. Most of the photons are produced in secondary reactions of the annihilation products following a continuous energy spectrum, which is challenging to distinguish from gamma-ray emission from more conventional sources (SNR, etc.).

We are considering a DM density profile with an inner slope $\varrho(r) \propto r^{-\gamma}$ (special cases: $\gamma = 1$ for an NFW-profile [12] and $\gamma = 1.5$ for a Moore-profile [10]), and a DM candidate with a mass m_{WIMP}. With an averaged velocity weighted annihilation cross section $\langle\sigma v\rangle$ (in the following text this parameter is only called "cross section") producing a photon spectrum dN_γ/dE per annihilation, the observed flux is $\Phi \propto \langle\sigma v\rangle \cdot dN_\gamma/dE \cdot \bar{J}(\Delta\Omega)\Delta\Omega$ with $\bar{J}(\Delta\Omega)\Delta\Omega \propto \int_{\Delta\Omega} d\Omega \int_{los} ds\, \varrho^2$.

Since the emissivity increases with ϱ^2, it is suggestive to search for this radiation from regions with a large density of DM.

2 Observations with H.E.S.S.

The H.E.S.S. experiment located in Namibia is an experiment investigating VHE γ-radiation. It consists of four imaging atmospheric Cherenkov telescopes observing stereoscopically the air showers initiated by energetic particles ($E > 100\,\mathrm{GeV}$) impinging on Earth's atmosphere. The shower images are used to distinguish between photon induced air showers and the much more abundant hadronic ones. The technique is sufficiently advanced to reconstruct the direction of the primary photon with an accuracy of 0.08° (per event), and to estimate the primary energy with a relative accuracy of around 15%. With this observatory it is possible to search for sources of VHE γ-ray photons with an energy $100\,\mathrm{GeV} < E < 100\,\mathrm{TeV}$ (the upper bound is limited by the collection area of the experiment of $\approx 10^5\,\mathrm{m}^2$: typically, non-thermal energy-spectra follow a power-law shape with $I(> E) \propto E^{-2\ldots-3}$). A considerable share of the observation time of the H.E.S.S. telescopes has been used to observe potential sites of detectable DM annihilation.
The Galactic center: The center of our Galaxy is an obvious target to search for γ-radiation from DM annihilation: the assumed Galactic density profile of the DM has there its maximum. H.E.S.S. has observed the super-massive black hole Sgr A* at the Galactic center for a total of 64 h. A steady, point-like VHE γ-ray source has been found, co-located within the astrometric uncertainties of the H.E.S.S. telescopes of $\approx 10\,\mathrm{arcsec}$ with the position of Sgr A*.

We consider an exclusive origin of the observed γ-rays from WIMP annihilation unlikely, because the required $m_{\mathrm{WIMP}} > 20\,\mathrm{TeV}$ and large cross section are difficult to reconcile with common WIMP models [9].

On the other hand only a part of the observed radiation could originate from DM annihilation, since there are several other possible sources of VHE γ-radiation in the observed region. In the following we derive an upper limit on the admixture of gamma-rays from DM annihilation and gamma-rays from astrophysical backgrounds. The measured spectrum is fitted with the sum $\Phi(E) = \Phi_{\mathrm{bg}}(E) + \Phi_{\mathrm{DM}}(E)$: $\Phi_{\mathrm{DM}}(E)$ describes the annihilation radiation, while $\Phi_{\mathrm{bg}}(E) \propto E^{-\Gamma}$ represents a background from other sources. In order to derive an upper limit, Φ_{DM} is increased until the minimal χ^2 of the fit of $\Phi(E)$ to the data reaches its 99% confidence limit. With these results an upper limit on $\bar{J}(\Delta\Omega)\Delta\Omega \cdot \langle\sigma v\rangle$ can be calculated. Assuming a density profile, limits on the annihilation cross section (see table 1) can be derived and vice versa. For these topics see also references [3, 13, 14]. More data have been taken in the meantime (under preparation).

The Sagittarius dwarf galaxy: The Sagittarius dwarf galaxy is a recently found dwarf galaxy in the halo of our galaxy at a heliocentric distance of 24 kpc. Since dwarf galaxies are dominated by DM, a realistic model of the density profile exists with less uncertainties than for the Galactic center (where baryonic matter dominates the stellar and gas dynamics). H.E.S.S. has observed this target. No indication for γ-radiation from Sgr Dwarf has been found so far. Upper limits on the annihilation cross section as function of the WIMP mass can be calculated.

For a cored density profile the limits on the cross section for neutralino annihilation have their minimum at $m_\chi \approx 200\,\mathrm{GeV}$ with $\langle\sigma v\rangle_{\mathrm{limit}} \approx 2 \cdot 10^{-25}\,\mathrm{cm}^3\mathrm{s}^{-1}$ not reaching into the area of WMAP compatible parameter sets. For $B^{(1)}$ annihilation the limits have their minimum at $m_{B^{(1)}} \approx 500\,\mathrm{GeV}$ with $\langle\sigma v\rangle_{\mathrm{limit}} \approx 4 \cdot 10^{-26}\,\mathrm{cm}^3\mathrm{s}^{-1}$. For this density profile a $B^{(1)}$ annihilation can be excluded for particle masses $m_{B^{(1)}} < 500\,\mathrm{GeV}$ (see reference [4]).

The unidentified source HESS J1303-631: The source of VHE γ-rays HESS J1303-631 was serendipitously found in the same field of view during observations of the pulsar binary system PSR B1259-63/SS 2883. HESS J1303-631 is a spatially extended source with no detected flux variability and no known counterpart at other wavelengths. This behavior is consistent with the expectations from DM accumulations. Therefore, the question was investigated whether this source could be a DM clump in the halo [11].

The considered energy spectra for annihilation radiation does not fit the measured spectrum well. In addition to this, we fit the measured luminosity profile with the line of sight integral of a given density profile ($\varrho \propto r^{-\gamma}$) convolved with the point spread function of the detector. The best fit is achieved with $\gamma = -0.8$. This would require a shell-like structure of the clump and is in contradiction with the expected NFW- ($\gamma = 1$) and the Moore-profile ($\gamma = 1.5$). Therefore, a DM nature of this source is very unlikely (see reference [15]).

Intermediate mass black holes: Intermediate mass black holes (IMBH) ($10 - 10^6 M_\odot$) in the Galactic halo can accumulate DM into so called mini-spikes [8]. This could lead to pointlike unidentified sources. H.E.S.S. has performed a systematic scan of the Galactic plane. No candidate of IMBH with a DM mini-spike was found. Depending on scenarios about the occurrence of IMBH and the mini-spike density profile, upper limits on the annihilation cross section can be derived. The upper limits rule out a massive WIMP with $m_{\mathrm{WIMP}} > 1\ TeV$. (see reference [5]).

The radio galaxy M87: The radio galaxy M87 is located in the center of the Virgo galaxy cluster. It is a giant elliptical (cD type) galaxy at a distance of 16 Mpc. VHE γ-rays from this source were detected in 1998/99 with HEGRA [1]. The detection was later confirmed in 2004 and 2005 by H.E.S.S. with a fast flux variability [2]. The variability immediately rules out an exclusive DM origin of of the radiation. Even when considering the possible quiescent flux level, it is still by orders of magnitude larger than the expectations from DM annihilation. The upper limits on the annihilation cross section (analogous to the calculations about the galactic center) are highly above the model cross sections. No DM is detectable from this source so far. With observations at lower energies (GLAST/Fermi or low-energy threshold Cherenkov telescopes) this could in principle be achieved.

3 Summary and outlook

So far, the indirect search for Dark Matter with H.E.S.S. has not produced any convincing evidence for gamma-ray emission from self-annihilating Dark Matter (with the possible exception of the Galactic center). The limits (listed in table 1) are however starting to constrain some models.

Future experiments will improve the abilities in the search for WIMP DM (mainly by lower sensitivity and wider energy reach). The lower energy window will be covered by the

	Galactic Center [1]	Sgr Dwarf [2]	M87 [3]	IMBH [4]
$\langle\sigma v\rangle_{\rm limit}(\chi\chi)$ [cm^{3}s^{-1}]	10^{-24}	$2\cdot 10^{-25}$	10^{-22}	10^{-28}
$\langle\sigma v\rangle_{\rm limit}(B^{(1)}B^{(1)})$ [cm^{3}s^{-1}]	10^{-24}	$4\cdot 10^{-26}$	10^{-22}	$3\cdot 10^{-29}$
$T_{\rm obs}$ $[h]$	64	11	89	~ 400

Table 1: Limits on the annihilation cross section of neutralino and $B^{(1)}$ annihilation. Typical annihilation cross sections are $\langle\sigma v\rangle_{\chi\chi} = 2\cdot 10^{-26}\,\text{cm}^3\text{s}^{-1}$ and $\langle\sigma v\rangle_{B^{(1)}B^{(1)}} = 1.7\cdot 10^{-26}\,\text{cm}^3\,\text{s}^{-1}/(m_{\rm WIMP}/1\,\text{TeV})^2$.

GLAST/Fermi satellite. The H.E.S.S. experiment will be upgraded with a central large Cherenkov telescope (H.E.S.S. Phase II) reducing the threshold from 100 GeV to $\approx$ 20 GeV. The multipronged approach (accelerator, direct and indirect search) to identify Dark matter will hopefully help to solve the origin of Dark Matter within the next decade.

References

[1] F. Aharonian *et al.*, A&A **404** L1 (2003)

[2] F. Aharonian *et al.* (H.E.S.S. collaboration), Science **314** 1424 (2006)

[3] F. Aharonian *et al.* (H.E.S.S. collaboration), Phys. Rev. Lett. **97** 221102 (2006)

[4] F. Aharonian *et al.* (H.E.S.S. collaboration), Astropart. Phys. **29** 55 (2008)

[5] F. Aharonian *et al.* (H.E.S.S. collaboration), arXiv:0806.2981v2 (2008); accepted for publication in Phys. Rev. D

[6] E. Baltz *et al.*, Phys. Rev. D **61** 023514 (2000)

[7] L. Bergström *et al.*, Phys. Rev. Lett. **94** 131301 (2005)

[8] G. Bertone *et al.*, Mod. Phys.Lett. A **20** 1021 (2005)

[9] D. Horns, Phys. Lett. B **607** 255 (2005)

[10] B. Moore *et al.*, ApJ **499** L5 (1998)

[11] B. Moore *et al.*, ApJ **524** L19 (1999)

[12] J. Navarro *et al.*, ApJ **426** 563 (1996)

[13] J. Ripken *et al.*, ICRC 2005 proceedings **4** 151 (2005)

[14] J. Ripken *et al.*, to appear in proceedings of the 30$^{\rm th}$ ICRC Merida (2007)

[15] J. Ripken *et al.*, to appear in proceedings of the 30$^{\rm th}$ ICRC Merida (2007)

[1] Assuming an NFW-profile
[2] Assuming a cored profile
[3] Profile considered in [6]
[4] Limits constraining for $m_{\rm WIMP} > 1\,\text{TeV}$

X-ray Constraints on Late Decaying Dark Matter Majorons (or Other Soft X-ray Emitting Candidates)*

Signe Riemer-Sorensen

Dark Cosmology Centre, Niels Bohr Institute, University of Copenhagen,
Juliane Maries Vej 30, DK-2100 Copenhagen, Denmark

DOI: http://dx.doi.org/10.3204/DESY-PROC-2008-02/riemer-sorensen_signe

An attractive way to generate neutrino masses is through the spontaneous breaking of lepton number. The resulting majoron can acquire a mass and thereby be the dark matter. Structure formation requires the dark matter mass to be ≈ 0.15 keV. The majorons can decay into two photons providing a mono-energetic emission line. Observing 0.1 keV photons is challenging, but we have obtained constraints in the 0.07-4.0 keV interval, which have been combined with earlier results and compared to realistic particle physics models for the majoron mass and interactions. The constraints applies to a wide range of dark matter candidates with radiative decays.

1 Introduction

In the Standard Model of particle physics the neutrinos are exactly massless which is in contradiction to the experimental evidence for neutrino oscillations. An attractive way to generate the neutrino masses involves spontaneous breaking of the global lepton symmetry. In this case the Goldstone boson associated to the broken symmetry, the majoron, can acquire a mass through quantum gravity effects. The idea of explicit violation of global symmetries by gravitational effects was originally put forward by R. Holman et al. [2] in the context of axions. This idea was applied to majorons by Akhmedov *et al.* [3] who first explored the possibility of a decaying keV mass singlet majoron. This paper was followed by Berezinsky and Valle [4] who proposed the majorons to be an excellent dark matter candidate with an observational signature. The majorons are unstable, decaying mostly to neutrinos but also to photons, with very long lifetimes, which may be longer than the lifetime of the Universe. Majorons with mass in the keV range could then constitute the bulk or a large part of the dark matter in the Universe. If so, cosmological observations can place interesting bounds on the coupling of this special type of majorons to neutrinos and photons.

*This talk was based on the paper by F. Bazzocchi, M. Lattanzi, S. Riemer-Sorensen and J. W. F. Valle, given in Ref. [1] which at the time of the workshop was accepted for publishing in JCAP.

2 Astrophysical constraints

The dominating majoron decay is into neutrinos. Lattanzi *et al.* [5] have studied the bounds imposed by the cosmic microwave background radiation on decaying keV mass majorons. The result is that the mass must lie in the interval 0.11 keV$< m_J <$ 0.18 keV and the decay rate must be smaller than $\Gamma_{J\nu\nu} < 10^{-19} s^{-1}$ in the case where the majorons are in thermal equilibrium in the early Universe and decouple very early.

The majorons are also allowed to decay into two photons providing a possible astrophysical signature from dark matter dominated regions in the Universe in terms of a mono-energetic emission line with an energy of half the majoron rest mass.

Current day X-ray observatories *Chandra* and *XMM-Newton* are only directly sensitive down to 0.3 keV, but by combining the High Resolution Camera onboard *Chandra* with a grating, a sensitivity down to 0.07 keV was obtained. However, using a grating has some disadvantages: i) The information of the origin of the photon is lost so it is not possible to optimize the signal to noise ratio. ii) The extension of the dark matter halo reduces the otherwise extremely high spectral resolution of the grating. iii) Gratings requires bright sources, so no X-ray faint dark matter dominated regions have been observed. We used observations of the Seyfert 1 galaxy NGC 3227. It is known there is a lot of baryonic emission from this galaxy, but the received flux is nonetheless a conservative upper limit on the flux from decaying dark matter, and due to the effects of the grating, no better target exists. The mass of the dark matter within the field of view was approximated to be 10^{10} $M_\odot$ and we assumed only one kind of dark matter. The obtained constraints on the decay rate is shown in Figure 1.

Allowing for non-equilibrium of the majorons in the early Universe, later decoupling or other production mechanism introduces a mass shift. We have expressed this ignorance in the parameter β, where the value of $\beta = 1$ was chosen for the scenario with thermal equilibrium and early decoupling. The CMB mass constraint from [5] discussed above then becomes $0.11 < \beta m_J < 0.18$keV. For non-thermal production mechanisms $\beta < 1$ so the mass constraint form CMB shift towards higher masses. Consequently we have compared our constraints to earlier line emission searches from dark matter (mainly performed in the context of sterile neutrinos, but applies to all dark matter candidates with a radiative decay) [6]. The constraints on the decay rate of the majorons into photons in the covered energy range of 0.07-4000 keV is shown in Figure 1. This have been compared to realistic particle physics models for the majoron mass and interactions.

In Figure 2 the diagonal lines gives the dependence of $\Gamma_{J\gamma\gamma}$ on m_J for different values of the triplet vacuum expectation value, v_3, which is one of the parameters of the underlying particle physics model. They single out the allowed strip in the $\Gamma_{J\to\gamma\gamma} - m_J$ plane consistent with neutrino oscillation data [7] and with the cosmological bounds on neutrino mass [8]. The left panel is for hierarchal neutrino masses while the right panel is for degenerate masses. The vertical bands in the figure indicate the mass region singled out by the CMB observations, for two different values of β. In both scenarios small m_J and v_3 values lead to decay rates well below the observational bounds.

However, for large values of v_3, e.g. 5 GeV, roughly corresponding to the maximum compatible with precision measurements of electroweak parameters [9], the radiative rates fall within the sensitivities of the Milky Way observations, and are thereby observationally excluded. For lower masses the observational sensitivities needs to be improved by about 20 orders of magnitude requiring completely new techniques from what is available today.

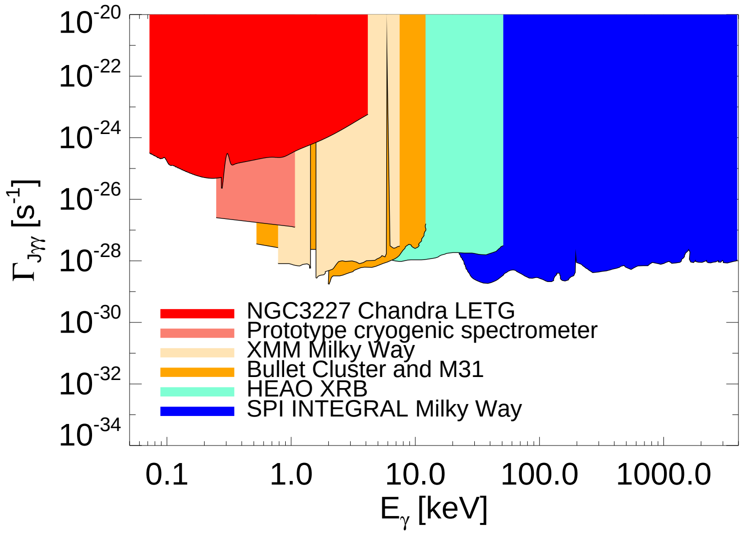

Figure 1: Upper limit on the decay rate (filled regions are excluded) from NGC3227 (red), the Milky Way halo observed with a prototype cryogenic spectrometer (salmon), *XMM* observations of the Milky Way (sand) and M31(orange), HEAO-1 observations of the diffuse x-ray background (aquamarine), INTEGRAL SPI line search in the Milky Way halo (blue) [6].

3 Summary

We have investigated the production of X-ray photons in the late-decaying dark matter scenario, and quantified the sensitivity of current observations to such a mono-energetic emission line. In particular, we have studied the constraints from the diffuse X-ray observations, as well as by considering the fluxes generated by dark matter dominated objects. These observations provide a probe of radiative dark matter decays and can be used as an *indirect detection* of the late decaying dark matter majoron scenario. We have illustrated this explicitly for the case where neutrinos get mass a la seesaw, where the majoron couples to photons through its Higgs triplet admixture. The constraints applies also to other dark matter candidates with radiative two-body decays emitting photons of energies of 0.07-4000 keV.

Acknowledgments

The Dark Cosmology Centre is funded by the Danish National Research Foundation.

References

[1] F. Bazzocchi, M. Lattanzi, S. Riemer-Sorensen and J. W. F. Valle, JCAP08(2008)013, arXiv:0805.2372 [astro-ph].

[2] R. Holman *et al.*, Phys. Lett. B **282** 132 (1992), arXiv:hep-ph/920306

[3] Akhmedov, Berezhiani, Mohapatra and Senjanovic, Phys. Lett. B **299** 90 (1993), arXiv:hep-ph/920985

[4] V. Berezinsky and J. W. F. Valle, Phys. Lett. B **318** 360 (1993) arXiv:hep-ph/9309214.

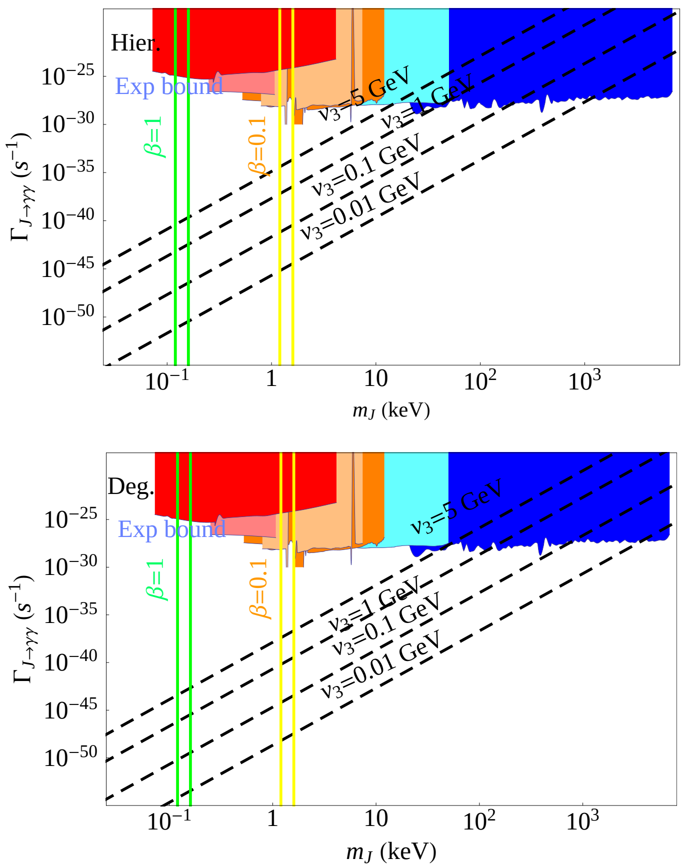

Figure 2: Majoron decay rate to photons as a function of the majoron mass m_J, for different values of the triplet vacuum expectation value, v_3. The left and right panels refer to hierarchical and degenerate neutrino mass spectra, respectively. The shaded regions are excluded by observations.

[5] M. Lattanzi and J. W. F. Valle, Phys. Rev. Lett. **99**, 121301 (2007), arXiv:0705.2406 [astro-ph].

[6] A. Boyarsky, J. W. den Herder, A. Neronov and O. Ruchayskiy, Astropart. Phys. **28**, 303 (2007), arXiv:astro-ph/0612219. A. Boyarsky, J. Nevalainen and O. Ruchayskiy, Astron. Astrophys. **471**, 51 (2007), arXiv:astro-ph/0610961. A. Boyarsky, O. Ruchayskiy and M. Markevitch, Astrophys. J. **673**, 752 (2008), arXiv:astro-ph/0611168. C. R. Watson, J. F. Beacom, H. Yuksel and T. P. Walker, Phys. Rev. D **74**, 033009 (2006), arXiv:astro-ph/0605424. arXiv:0709.2301 [astro-ph]. A. Boyarsky, A. Neronov, O. Ruchayskiy and M. Shaposhnikov, Mon. Not. Roy. Astron. Soc. **370**, 213 (2006), arXiv:astro-ph/0512509. A. Boyarsky, A. Neronov, O. Ruchayskiy, M. Shaposhnikov and I. Tkachev, Phys. Rev. Lett. **97**, 261302 (2006), arXiv:astro-ph/0603660. H. Yuksel, J. F. Beacom and C. R. Watson, arXiv:0706.4084 [astro-ph]. A. Boyarsky, D. Malyshev, A. Neronov and O. Ruchayskiy, arXiv:0710.4922 [astro-ph].

[7] M. Maltoni, T. Schwetz, M. A. Tortola and J. W. F. Valle, New J. Phys. **6**, 122 (2004), arXiv version 6 in hep-ph/0405172 provides updated neutrino oscillation results and references to previous works.

[8] J. Dunkley *et al.* [WMAP Collaboration], arXiv:0803.0586 [astro-ph].

[9] Particle Data Group, W. M. Yao *et al.*, J. Phys. **G33**, 1 (2006).

Polarization Measurements of Gamma Ray Bursts and Axion Like Particles

André Rubbia[1], *Alexander Sakharov*[1,2]

[1]Swiss Institute of Technology, ETH-Zürich, 8093 Zürich, Switzerland
[2]TH Division, PH Department, CERN, 1211 Geneva 23, Switzerland

DOI: http://dx.doi.org/10.3204/DESY-PROC-2008-02/sakharov_alexander

A polarized gamma ray emission spread over a sufficiently wide energy band from a strongly magnetized astrophysical object like gamma ray bursts (GRBs) offers an opportunity to test the hypothesis of axion like particles (ALPs). Based on evidences of polarized gamma ray emission detected in several gamma ray bursts we estimated the level of ALPs induced dichroism, which could take place in the magnetized fireball environment of a GRB. This allows to estimate the sensitivity of polarization measurements of GRBs to the ALP-photon coupling. This sensitivity $g_{a\gamma\gamma} \leq 2.2 \cdot 10^{-11}$ GeV^{-1} calculated for the ALP mass $m_a = 10^{-3}$ eV and MeV energy spread of gamma ray emission is competitive with the sensitivity of CAST and becomes even stronger for lower ALPs masses.

New very light spin-zero particles are predicted in many extensions of the Standard Model (see this proceedings for the references). Typically, such particles called axion like particles (ALPs) can arise as a result of a spontaneous breakdown of a continuos symmetry. A notable example of such breakdown is the Peccei-Quinn (PQ) mechanism [1], which remains perhaps the most natural solution to the CP problem in QCD. The most important phenomenological property of ALPs is their two-photon vertex interaction, which allows for ALP to photon conversion in the presence of an external electric and magnetic fields [2] through an interaction term

$$\mathcal{L}_{a\gamma} = -\frac{1}{4} g_{a\gamma\gamma} F_{\mu\nu} \tilde{F}^{\mu\nu} a = g_{a\gamma\gamma} \mathbf{E} \cdot \mathbf{B} a, \tag{1}$$

where a is the ALP field, F is the electromagnetic field strength tensor, $\tilde{F}$ its dual, $\mathbf{E}$, $\mathbf{B}$ the electric and magnetic fields respectively and $g_{a\gamma\gamma}$ is the ALP-photon coupling strength.

According to [3] the ALP-photon mixing (1) gives rise to vacuum dichroism. This dichroism results in the rotation of the polarization plane of an initially linearly polarized monochromatic beam by angle given in [3, 4]:

$$\epsilon = \frac{g^2_{a\gamma\gamma} B^2 \omega^2}{m_a^2} \sin^2 \left(\frac{m_a^2 L}{4\omega} \right) \sin 2\phi. \tag{2}$$

It is valid for a uniform magnetic field $\mathbf{B}$ lying at a nonvanishing angle ϕ with the wave vector $\mathbf{k}$ of photons with frequency ω. Here m_a is the mass of ALP, L is the length of the magnetized region. Such rotation, for instance, in case of ALPs, could be detected in a laser experiment like PVLAS [5, 6]. The validity of the approximation (2) is provided if the oscillation wavenumber

$$\Delta_{\rm osc}^2 = \left(\frac{m_a^2 - \omega_{\rm pl}}{2\omega}\right)^2 + B^2 g_{a\gamma\gamma}^2 \tag{3}$$

is dominated by the axion mass term. In fact, (3) pertains to the situation in which the beam propagates in a magnetized plasma, which gives rise to an effective photon mass set by the plasma frequency $\omega_{\rm pl} = \sqrt{4\pi\alpha n_e/m_e} \simeq 3.7\cdot 10^{-11}\sqrt{n_e/{\rm cm}^{-3}}$ eV, where n_e is the electron density and m_e is the electron mass.

The polarization of the prompt gamma ray emission has been measured in four bright GRBs: GRB021206, GRB930131, GRB960924 and GRB041219a. The first measurements made in [7] with Ranaty High Energy Solar Spectrometer Imager (RHESSI) satellite, found a linear polarization, $\Pi = (80 \pm 20)\%$, of the gamma rays from GRB021206 across the spectral window 0.15-2 MeV. The analysis techniques have been challenged in [8] and defended in [9]. Subsequent analyses made in [10] confirmed the results of [7] but at the lower level of significance. Later, in [11] the BATSE instrument on board of the Compton Gamma Ray Observatory (CGRO) has been used to measure, for two GRBs, the angular distribution of gamma rays back-scattered by the rim of the Earth's atmosphere: $35\% \leq \Pi \leq 100\%$ for GRB930131 and $50\% \leq \Pi \leq 100\%$ for GRB960924. The analysis technique of [11] is only sensitive to the energy range 3-100 keV. Finally, the analysis [12] of GRB041219a across the spectral window 100-350 keV has been performed using coincidence events in the SPI (spectrometer on board of the INTEGRAL satellite) and IBIS (the Imager on Board of the INTEGRAL satellite). The polarization fraction of $\Pi = 96^{+39}_{-40}\%$ was determined for this GRB.

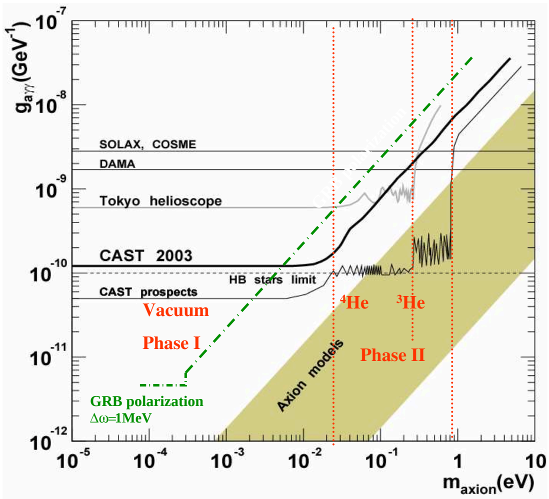

Figure 1: The plot of the regions of $(m_a, g_{a\gamma\gamma})$ space ruled out by various solar axion searches with the bound of the present letter, estimated for the inner part of the energy range 0.2-1.3 MeV applied for the polarization measurements of GRB021206 (dashed dotted line), superimposed.

According to the Hillas [14] diagram showing size and magnetic field strengths of different astrophysical object the typical magnetic field in a GRB's engine can be estimated as $B \simeq 10^9$ G over a region $L_{\rm GRB} \simeq 10^9$ cm. Moreover, the conservation of magnetic field energy at the rest wind frame of fireball shell model of the GRB's engine [15] implies at any radial distance r, in the fireball environment, $4\pi r_0^2 B_0^2 = 4\pi r^2 B^2$, leading to the relation $B = B_0(r_0/r)$, where B_0 and r_0 are the magnetic field strength and the size of the central part of the fireball. The minimal time scale of variability of GRBs light curves is estimated to be about 0.1 sec [1]. This implies that the typical extension of the GRB's engine is indeed compatible with $L_{GRB} \approx 10^9$ cm. Typically

[1] See, for example, the analysis in [16].

the central part of the fireball can be represented by a neutron star of radius $r_0 \approx 10^6$ cm with magnetic field of $B_0 \approx 10^{12}$ G. Therefore the strength of the magnetic field at the distance $r = L_{GRB}$ corresponds to $B \approx 10^9$ G, which is in a good agreement with the values taken from [14].

According to (2), the relative misalignment between the polarization planes of gamma radiation at two different energies ω_1 and ω_2 induced by ALPs (see for details [17]) is given by

$$\Delta\epsilon = \frac{L_{GRB}}{2\pi}\frac{g^2_{a\gamma\gamma}}{m_a^2}\Delta\omega B^2, \tag{4}$$

where $\Delta\omega = |\omega_2 - \omega_1|$. Therefore, one can observe that the constraint arises from the fact that if the ALP dichroism induced rotation of polarization plane (4) in the given magnetic field were to differ by more then $\pi/2$ over the energy range 0.2-1.3 MeV, as in the case of GRB021206, the instantaneous polarization in the detector would fluctuate significantly for the net time averaged polarization of the signal to be suppressed. This condition can be transformed into the bound on the ALP-photon coupling as

$$g_{a\gamma\gamma} \leq \pi \frac{m_a}{B\sqrt{\Delta\omega L_{\rm GRB}}} \approx 2.2 \cdot 10^{-8}\frac{m_a}{1\ \rm eV}\ (\rm GeV)^{-1}, \tag{5}$$

where the inner part of the spectral window 0.2-1.3 MeV ($\Delta\omega \approx 1$MeV) reported in polarization analysis of GRB021206 has been used. This constraint is obtained under the assumption that the correlation length of the magnetic field being initially defined by the typical size of the neutron star in the core of a GRB's engine is getting stretched out by the expansion of the fireball shell. So, at some moment of the expansion the correlation length becomes adjusted to the oscillation length. However, for the ALP's mass

$$m_a \leq m_{cr1} = \sqrt{\frac{2\pi\omega}{L_{GRB}}} \approx 3.5 \cdot 10^{-4}\ \rm eV \tag{6}$$

this condition does not hold anymore and the polarization planes misalignment angle should be calculated as

$$\Delta\epsilon = B^2 g^2_{a\gamma\gamma} L_{\rm GRB}\left(\frac{L_{\rm GRB}}{16} - \frac{\omega_1}{2\pi m_a^2}\right). \tag{7}$$

The expression (7) holds to be positive down to the mass (see for details [17]): $m_{\rm cr2} = 4\sqrt{\frac{\omega_1}{2\pi L_{GRB}}} \approx 8 \cdot 10^{-5}$ eV. Requiring again that the misalignment angle (7) does not exceed $\pi/2$ in the axion mass range between $m_{\rm cr1}$ and $m_{\rm cr2}$ one arrives to a bound, which can be well approximated by a constant [2]

$$g_{a\gamma\gamma} \leq \frac{2\sqrt{2\pi}}{BL_{\rm GRB}} \approx 5 \cdot 10^{-12}\ (\rm GeV)^{-1}. \tag{8}$$

In Fig. 1. we show the bounds (5) and (8) superimposed on the recent results of CAST [18] and other axion helioscope experiments [19]. The limit obtained becomes by factor $\sqrt{1\text{MeV}/\Delta\omega_{I,B}}$ weaker if we apply the width $\Delta\omega_I \approx 250$ keV of the energy bands for GRB041219a detected

[2]The electron number density in a GRB's environment can be estimated as $n_e \simeq 10^{10}$ cm^{-3} [15]. Therefore the expression (3) is still ALP mass dominated down to $m_a \approx m_{\rm cr}$ for the energy of the gamma radiation, $\omega \approx 1$ MeV, and constraints on $g_{a\gamma\gamma}$ calculated from (5) and (8).

by INTEGRAL or $\Delta\omega_B \approx 100$ keV for GRB930131 and GRB960924 detected by BATSE. This implies that $g_{a\gamma\gamma} \leq 4.4 \cdot 10^{-11}$ GeV^{-1} and $g_{a\gamma\gamma} \leq 6.9 \cdot 10^{-11}$ GeV^{-1} for INTEGRAL and BATSE measurements respectively calculated for the axion mass $m_a = 10^{-3}$ eV.

An improvement of the current estimations could be archived in further detection of gamma polarized signals from GRBs in the similar or higher energy ranges. For these reasons the POLAR [20] experiment as well as other numerous efforts to develop instruments with the sensitivity required for astrophysical polarimetry over 100 eV to 10 GeV band [21] become important probes for ALPs beyond Standard Model physics.

We thank K. Zioutas, H. Hofer and N. Produit for useful discussions on CAST, POLAR and related topics.

References

[1] R.D. Peccei and H. Quinn, Phys. Rev. Lett. **38** (1977) 1440

[2] D. A. Dicus, E. W. Kolb, V. L. Teplitz and R. V. Wagoner, Phys. Rev. D **18** (1978) 1829; P. Sikivie, Phys. Rev. Lett. **51** (1983) 1415 [Erratum-ibid. **52** (1984) 695].

[3] L. Maiani, R. Petronzio and E. Zavattini, Phys. Lett. B **175** (1986) 359.

[4] P. Sikivie, Phys. Rev. Lett. **51** (1983) 1415 [Erratum-ibid. **52** (1984) 695]; G. Raffelt and L. Stodolsky, Phys. Rev. **37** (1988) 1237.

[5] E. Zavattini *et al.* [PVLAS Collaboration], Phys. Rev. Lett. **96** (2006) 110406 [arXiv:hep-ex/0507107].

[6] E. Zavattini *et al.* [PVLAS Collaboration], arXiv:0706.3419 [hep-ex].

[7] W. Coburn and S.E. Boggs, Nature **423**, 415 (2003).

[8] R. E. Rutledge and D. B. Fox, Mon. Not. Roy. Astron. Soc. **350** (2004) 1272 [arXiv:astro-ph/0310385].

[9] S. E. Boggs and W. Coburn, arXiv:astro-ph/0310515.

[10] C. Wigger, W. Hajdas, K. Arzner, M. Gudel and A. Zehnder, Astrophys. J. **613** (2004) 1088 [arXiv:astro-ph/0405525].

[11] D. R. Willis *et al.*, arXiv:astro-ph/0505097.

[12] S. McGlynn *et al.*, arXiv:astro-ph/0702738.

[13] S. E. Boggs, C. B. Wunderer, K. Hurley and W. Coburn, Astrophys. J. **611** (2004) L77 [arXiv:astro-ph/0310307].

[14] A. M. Hillas, Ann. Rev. Astron. Astrophys. **22** (1984) 425; L. Anchordoqui, T. Paul, S. Reucroft and J. Swain, Int. J. Mod. Phys. A **18** (2003) 2229 [arXiv:hep-ph/0206072].

[15] T. Piran, Phys. Rept. **314** (1999) 575 [arXiv:astro-ph/9810256].

[16] J. R. Ellis, N. E. Mavromatos, D. V. Nanopoulos and A. S. Sakharov, Astron. Astrophys. **402** (2003) 409 [arXiv:astro-ph/0210124].

[17] A. Rubbia and A. S. Sakharov, Astropart. Phys. **29** (2008) 20.

[18] S. Andriamonje *et al.* [CAST Collaboration], JCAP **0704** (2007) 010 [arXiv:hep-ex/0702006]; K. Zioutas *et al.* [CAST Collaboration], Phys. Rev. Lett. **94** (2005) 121301 [arXiv:hep-ex/0411033].

[19] For review see: R. Battesti *et al.*, arXiv:0705.0615 [hep-ex]; D. Lazarus et al., Phys. Rev. Lett. **69** (1992) 2089; S. Moriyama et al., Phys. Lett. **B434** (1998) 147; R. Bernabei et al., Phys. Lett. **B515** (2001) 6; F.T. Avignone et al., Phys. Rev. Lett. **81** (1998) 5068; R.J. Creswick et al., Phys. Lett. **B427** (1998) 235.

[20] N. Produit *et al.*, Nucl. Instrum. Meth. A **550** (2005) 616 [arXiv:astro-ph/0504605];

[21] For reviews see: J.K. Black, 3rd Sympothium on Large TPCs for Low Energy Rare Event Detectors, Journal of Physics, Conference Series **65** (2007) 012005; A. Curioni, Ph.D. Dissertation Thesis, Columbia University (2004), unpublished; A. Rubbia, J. Phys. Conf. Ser. **39**, 129 (2006) [arXiv:hep-ph/0510320].

Spectroscopic Constraints on (pseudo-)Scalar Particles from Compact Astrophysical Objects

Doron Chelouche[1,2], *Raúl Rabadán*[2], *Sergey S. Pavlov*[3], *& Francisco Castejón*[4]

[1]Canadian Institute for Theoretical Astrophysics, University of Toronto, 60 Saint George Street, Toronto, ON M5S 3H8, Canada
[2]School of Natural Sciences, Institute for Advanced Study, Einstein Drive, Princeton 08540, USA
[3]Institute of Plasma Physics, Kharkov Institute of Physics and Technology, Kharkov, Ukraine
[4]Laboratorio Nacional de Fusión por Connamiento Magnético, Asociación Euratom-Ciemat para Fusión, 28040 Madrid, Spain

DOI: http://dx.doi.org/10.3204/DESY-PROC-2008-02/chelouche_doron

We propose a new method to search for light (pseudo-)scalar particles in the spectra of compact astrophysical objects such as magnetars, pulsars, and quasars. On accounts of compact astrophysical objects having intense magnetic fields extending over large volumes, they provide good conditions for efficient photon-particle oscillations via the Primakoff process. In particular, we show that if the coupling constant for light ($m_a < 10^{-2}$ eV) axions, $g > 10^{-13}\,\mathrm{GeV}^{-1}$ then it is likely that absorption-like features would be detectable in the spectrum of compact astrophysical sources.

1 Why are compact astrophysical objects interesting?

Compact astrophysical sources, by our definition, are those objects whose size is of order their Schwartzschild radius and include black holes and neutron stars. Neutron stars are thought to be the end stages of (not too massive) stars wherein the stellar core of the progenitor object collapsed dragging with it magnetic field lines from large volumes (and amplifying them via dynamo effects) resulting in a highly magnetized object [1]. Another example is that of supermassive black holes which grow by matter accretion over cosmic times during which phase they become very luminous and give rise to the quasar phenomenon [2]. While neutron star masses are of order a solar mass, supermassive black holes at the centers of galaxies may be several billion solar masses.

The photon-axion conversion probability is given, in the limit of small values, by (e.g., [3]):

$$P_{\gamma\to a} \simeq \frac{1}{4} g^2 B^2 R^2 \tag{1}$$

where B is the magnetic field intensity and R is the coherence size of the field which, for compact objects, is also the size of the system. It is instructive to compare the expected $P_{\gamma\to a}$ for compact objects and for terrestrial experiments: for the CAST experiment the product, B^2R^2 is of order $10^{16}\,[\mathrm{G}^2\cdot\mathrm{cm}^2]$. In comparison, for pulsars whose magnetic field is of order 10^{13} G and whose size is ~ 10 km (e.g., [4]), this product is of order $\sim 10^{36}\,[\mathrm{G}^2\cdot\mathrm{cm}^2]$! Therefore, pulsars are many orders of magnitude more efficient in converting photons to axions (and vice-versa). As such, one can potentially probe down to much lower values of g using compact objects than is possible using CAST (see e.g., [5] and references therein).

2 Spectral oscillation features

Efficient photon-axion oscillations occur when the momentum transfer in the conversion process is negligible. This occurs when the effective mass of the photon, as it propagates through a refractive medium (e.g., magnetized vacuum or plasma), equals that of the axion. As the refractive index for photons is frequency dependent, this condition is met only for certain frequencies and is of resonance nature. In particular, it necessitates the presence of plasma (for which the refractive index is smaller than unity) and does not occur in pure vacuum.

For a medium with uniform conditions (e.g., plasma density, magnetic field intensity), the photon energy where resonances occur,

$$\omega_0 = \omega_p \frac{B}{B_c} \sqrt{\frac{F_{||}(\omega_0) - m_a^2/\omega_p^2}{7\alpha/45\pi}}. \tag{2}$$

ω_p is the plasma frequency, $B_c \simeq 4 \times 10^{13}\,\mathrm{G}$ is the critical magnetic field, $F_{||}$ is the normalized refractive index for photons whose polarization is parallel to the direction of the (projected) magnetic field, and α is the fine structure constant (this expression holds for sub-critical magnetic fields; for the more general case see [6]). Resonance occurs only if $F_{||} - m_a^2/\omega_p^2 > 0$ which sets an upper limit on the axion mass which can be efficiently probed by a given environment. For $m_a/\omega_p \ll 1$ and setting $F_{||} = 1$ (as appropriate for cold plasma), we find that resonances are expected to occur around infrared to optical energies for pulsars, hard X-ray and gamma ray energies for quasars, and sub-mm to infrared energies for magnetars (note that the above expression does not hold for magnetars for which $B > B_c$; see [6] for the general case).

The photosphere of compact objects emits over a broad spectral range and one therefore expects to detect photon deficits at photon-axion resonance energies. Phenomenologically, such features would look like absorption features although the physics is very different. Making accurate spectral predictions for such features requires one to follow the evolution of the coupled photon-axion system with time from the photosphere where photons are created to the telescope. The details of the equations of motion involved and their solution are fully discussed in [6]. We only mention that the important refractive processes to include are due to plasma (whether active or inactive, cold or hot) as well as vacuum birefringence.

Here we focus on one example being that of magnetars. In those objects, the magnetic field and plasma density, ρ, vary with distance from the photosphere such that $B \propto \rho \propto R^{-3}$ (dipolar field configuration; [4]). Judging from Eq. 2, it is clear that photons of different energy will undergo resonance conversion at different locations in the atmosphere. In particular, the predicted spectral feature is broad as B and ρ decay monotonically with distance with ω_0 spanning a wide energy range. For all cases considered here the variations in the magnetospheric conditions are slow enough (adiabatic) so that considerable photon to axion conversion occurs (see [7]).

Some examples of the predicted spectral oscillation features are shown in Fig. 1 for several values of g. At the current upper limit given by CAST of $g \sim 10^{-10}\,\mathrm{GeV}^{-1}$, a very broad absorption-like spectral feature should be easily detectable (extending from infrared to optical

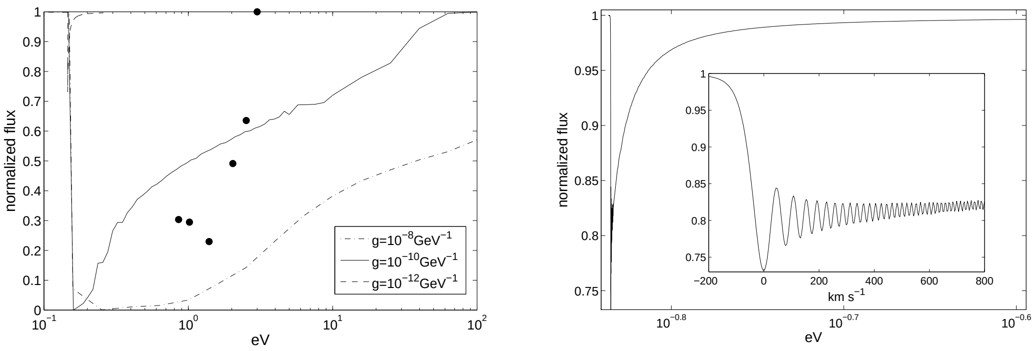

Figure 1: *Left:* Spectral oscillation feature as predicted for magnetars ($B = 10^{15}$ G and $n(r_\star) = 10^{15}\,\mathrm{cm}^{-3}$ (with the photospheric radius, $r_\star = 10\,\mathrm{km}$) for several values of g. Note the prominent absorption-like feature which can be observed for $g = 10^{-10}\,\mathrm{GeV}^{-1}$ which is the best current limit on g from CAST and horizontal branch stars. Also shown for comparison is (normalized) photometric data for a magnetar (circles; adopted from [8]). *Right:* Zoom in on the spectral oscillation feature for $g = 10^{-12}\,\mathrm{GeV}^{-1}$. The feature is broad and can be detected using low resolution spectra. The inset shows a high resolution blow up of the feature revealing oscillatory pattern being a trademark of photon-particle spectral conversion features.

energies in the example shown). For lower values of g ($\sim 10^{-12}\,\mathrm{GeV}^{-1}$), the feature is narrower yet can be easily detected using broad band photometry and low to medium resolution spectra. Using high resolution spectra one may be able to identify the oscillatory pattern, a trademark of photon-particle conversion and is not expected to arise from atomic emission and absorption processes (see Fig. 1). In cases where the properties of the object along the line of sight change with time (e.g., a rotating star), the spectral oscillation feature would be time-dependent. In particular, the energy and strength of the spectral feature would vary with rotation phase of the star and phase-sensitive observations may be crucial for correctly identifying it. In addition, plasma composition, photon polarization, magnetic field direction with respect to the photon propagation direction as well as the plasma temperature could all affect the predicted spectral oscillation features. A full treatment of these issues is given in [6].

In the above, we have given spectral predictions for the specific case of magnetars. However, a similar line of reasoning applies also to pulsars, magnetars, and other types of compact objects. In all cases relatively broad spectral oscillation features are predicted and can be detected down to low values of g. Such spectral features may be identified by **(a)** their broad band shape, **(b)** the presence of small energy-scale oscillations, **(c)** distinct variability pattern which is intimately connected with time variations in the mean magnetic field strength and plasma density in the magnetosphere along the line of sight. In particular, the spectral properties of such features are very different from those characterizing atomic features.

3 Implications for axion physics

The calculated spectral oscillation features for compact objects depend on their intrinsic properties. Assuming that the current understanding of such systems is qualitatively correct then it is possible to define the axion parameter space which can be probed by spectroscopic studies

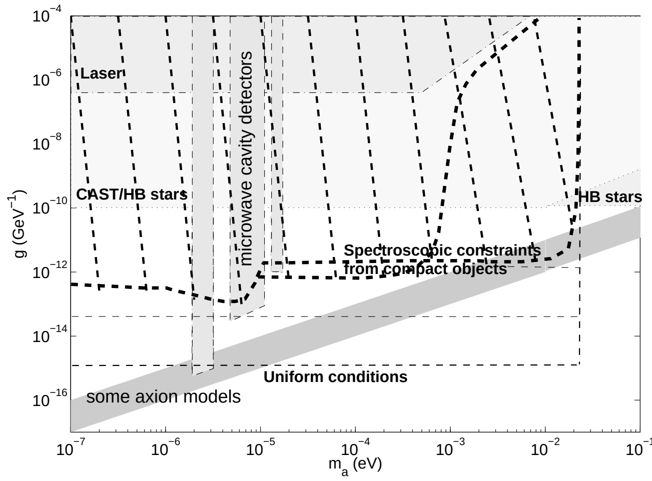

Figure 2: The particle parameter space which can be probed by observations of compact astrophysical sources assuming flux decrements of 10% can be detected. Clearly, the proposed spectroscopic method can probe down to much lower values of g (for axion mass of $< 10^{-2}$ eV it is possible to probe down to $g \lesssim 10^{-12}\,\mathrm{GeV}^{-1}$) than is accessible by other methods (thick hatched dashed region). Also, the proposed method does not require axions to be dark matter particle. For comparison we show the parameter space probed by systems of size $r_\star$ with uniform magnetic and plasma density size (thin hatched dashed region). See [6] for further details.

of these sources (more details can be found in [6]). Assuming one can detect flux decrements of order 10% in the data (as noted before, this requires low to medium resolution spectra), the sensitivity limit in g and m_a is shown in Fig. 2. Clearly, this method can, in principal, increase our sensitivity to light ($m_a < 10^{-2}$ eV) axions by 2-3 orders of magnitude using certain types of objects. Furthermore, the regions of parameter space which can be probed by different classes of objects overlap allowing to reduce systematic effects and corroborate the results. We emphasize that the proposed method works equally well for scalar and pseudo-scalar particles and does not require axions to be dark matter candidates.

References

[1] Spruit, H. C. 2007 (astro-ph/0711.3650).

[2] Rees, M. & Volonteri, M. 2007 (astro-ph/0701512).

[3] Raffelt, G., & Stodolsky, L. 1988, Phys. Rev. D, 37, 1237;
Sikivie, P. 1983, Phys. Rev. Lett., 51, 1415.

[4] Goldreich, P., & Julian, W. H. 1969, ApJ, 157, 869;
Harding, A. K. 2005 (astro-ph/0510134).

[5] Raffelt, G. G., 2005 (hep-ph/0504152);
Raffelt, G. G., 2006 (hep-ph/0611350);
Zioutas et al., 2005, Phys. Rev. Lett., 94, 121301.

[6] Chelouche, D. et al. 2008, ApJ Supp., in press (astro-ph/0806.0411).

[7] Lai, D., & Heyl, J. 2006, Phys. Rev. D, 74, 123003 (astro-ph/0609775).

[8] Durant, M., & van Kerkwijk, M. H. 2005, ApJ, 627, 376 (astro-ph/0502027)

Chapter 4

Direct Searches for Dark Matter WIMPs

First results from DAMA/LIBRA

R. Bernabei[1], *P. Belli*[1], *F. Cappella*[2], *R. Cerulli*[3], *C.J. Dai*[4], *A. d'Angelo*[2], *H.L. He*[4], *A. Incicchitti*[2], *H.H. Kuang*[4], *J.M. Ma*[4], *F. Montecchia*[1], *F. Nozzoli*[1], *D. Prosperi*[2], *X.D. Sheng*[4], *Z.P. Ye*[4]

[1]Dip. di Fisica, Università di Roma "Tor Vergata" and INFN, sez. Roma "Tor Vergata", I-00133 Rome, Italy
[2]Dip. di Fisica, Università di Roma "La Sapienza" and INFN, sez. Roma, I-00185 Rome, Italy
[3]Laboratori Nazionali del Gran Sasso, I.N.F.N., Assergi, Italy
[4]IHEP, Chinese Academy, P.O. Box 918/3, Beijing 100039, China

DOI: http://dx.doi.org/10.3204/DESY-PROC-2008-02/incicchitti_antonella

The highly radiopure $\simeq$ 250 kg NaI(Tl) DAMA/LIBRA set-up is running at the Gran Sasso National Laboratory of the I.N.F.N.. Here first results obtained by this second generation experiment exploiting the model-independent annual modulation signature for Dark Matter particles in the galactic halo are mentioned (exposure of 0.53 ton x yr). The DAMA/LIBRA data confirm the evidence for the presence of Dark Matter particles in the galactic halo as observed by the former DAMA/NaI experiment. The combined analysis of the data of the two experiments (total exposure 0.82 ton x yr) gives a C.L. at 8.2 sigma.

The former DAMA/NaI [1, 2, 3, 4, 5], and the present DAMA/LIBRA set-ups [6, 7], have been developed inside the DAMA project [1, 2, 3, 4, 5, 6, 7, 8] and both present unique features in order to investigate the presence of Dark Matter (DM) particle in the galactic halo by exploiting the model-independent annual modulation signature (originally suggested more than twenty years ago [9]).

In particular, this signature exploits the effect of the Earth revolution around the Sun on the number of events induced by DM particles in a suitable low background set-up placed deep underground. In fact, as a consequence of its annual revolution, the Earth should be crossed by a larger flux of DM particles around roughly June 2^{nd} (when its rotational velocity is summed to the one of the solar system with respect to the Galaxy) and by a smaller one around roughly December 2^{nd} (when the two velocities are subtracted). Thus, the contribution of the signal to the counting rate in the k–th energy interval can be written as [2]: $S_k = S_{0,k} + S_{m,k} \cos\omega(t - t_0)$, where: i) $S_{0,k}$ is the constant part of the signal; ii) $S_{m,k}$ is the modulation amplitude; iii) $\omega = \frac{2\pi}{T}$ with period T; iv) t_0 is the phase.

This signature is very distinctive since a seasonal effect induced by DM particles must satisfy all the following requirements: 1) the rate must contain a component modulated according to a cosine function; 2) with one year period; 3) with a phase roughly around June 2^{nd} in case of usually adopted halo models (slight variations may occur in case of presence of non thermalized DM components in the halo [3, 10]); 4) this modulation must be present only in a well-defined low energy range, where DM particles can induce signals; 5) it must be present only in those events where just a single detector, among all the available ones in the used set-up, actually "fires" (*single-hit* events), since the probability that DM particles experience multiple interactions is negligible; 6) the modulation amplitude in the region of maximal sensitivity has to be $\lesssim 7\%$ in case of usually adopted halo distributions, but it may be significantly larger in case of some particular scenarios such as *e.g.* those of reference [11]. To mimic such a signature spurious effects or side reactions should be able not only to account for the observed modulation amplitude but also to contemporaneously satisfy all the requirements of the signature [2, 7].

The DAMA/LIBRA set-up, its main features and radiopurity have been discussed in details in reference [6], while the model-independent experimental results obtained by DAMA/LIBRA (exposure of 0.53 ton×yr over 4 annual cycles) and those combined with DAMA/NaI (exposure of 0.29 ton×yr over 7 annual cycles), just mentioned in the following, are presented in details in reference [7]. In fact, a clear annual modulation of the *single-hit* events (i.e. events in which just one detector fires) satisfying all the several peculiarities expected for a dark matter particle induced effect has also been observed in DAMA/LIBRA [7]. A cumulative 8.2 σ C.L. is reached when considering the data of the two experiments all together. In particular, Figure 1 shows the time behaviour (over three energy intervals) of the model-independent experimental residual rates for *single-hit* events collected by the DAMA/NaI and the new DAMA/LIBRA experiments over eleven annual cycles (0.82 ton×yr); when the phase and the period are free in the best fit procedure, an amplitude equal to (0.0131 ± 0.0016) cpd/kg/keV, a phase $t_0 = (144 \pm 8)$ days and a period $T = (0.998 \pm 0.003)$ year are measured in the (2-6) keV energy range [7], well in agreement with the expectations. The experimental data have been investigated by various analyses as reported in details in reference [7].

In order to verify absence of annual modulation in other energy regions and, thus, to also verify the absence of any significant background modulation, the energy distribution measured during the data taking periods has been investigated up to MeV region; in particular the analyses described in reference [7] exclude the presence of a background modulation in the whole energy spectrum at a level much lower than the effect found in the lowest energy region for the *single-hit* events.

A further investigation has also been performed on the *multiple-hits* events (i.e. events in which more than one detector fire). The *multiple-hits* events class – on the contrary of the *single-hit* one – does not include events induced by DM particles since the probability that a DM particle interacts in more than one detector is negligible. The fitted modulation amplitude is $A = -(4 \pm 6) \cdot 10^{-4}$ cpd/kg/keV for the *multiple-hits* residual rate in the (2-6) kV energy range [7]. Summarising, evidence of annual modulation with proper features is present in the *single-hit* residuals (events class to which the DM particle-induced signals belong), while it is absent in the *multiple-hits* residual rate (event class to which only background events belong). Since the same identical hardware and the same identical software procedures have been used to analyse the two classes of events, the obtained result offers an additional strong support for the presence of DM particles in the galactic halo, further excluding any side effect either from hardware or from software procedures or from background. Details can be found in reference [7].

Obviously as previously done for DAMA/NaI [2], careful investigations on absence of any significant systematics or side reaction effect in DAMA/LIBRA have been quantitatively carried out. In fact, in order to continuously monitor the running conditions, several pieces of information are acquired with the production data and quantitatively investigated [7]. No modulation has been found in any possible source of systematics or side reactions for DAMA/LIBRA as well; thus, cautious upper limits (90% C.L.) on the possible contributions to the DAMA/LIBRA measured modulation amplitude have been estimated [7]. They cannot account for the measured modulation amplitude and contemporaneously satisfy all the requirements of the signature. For

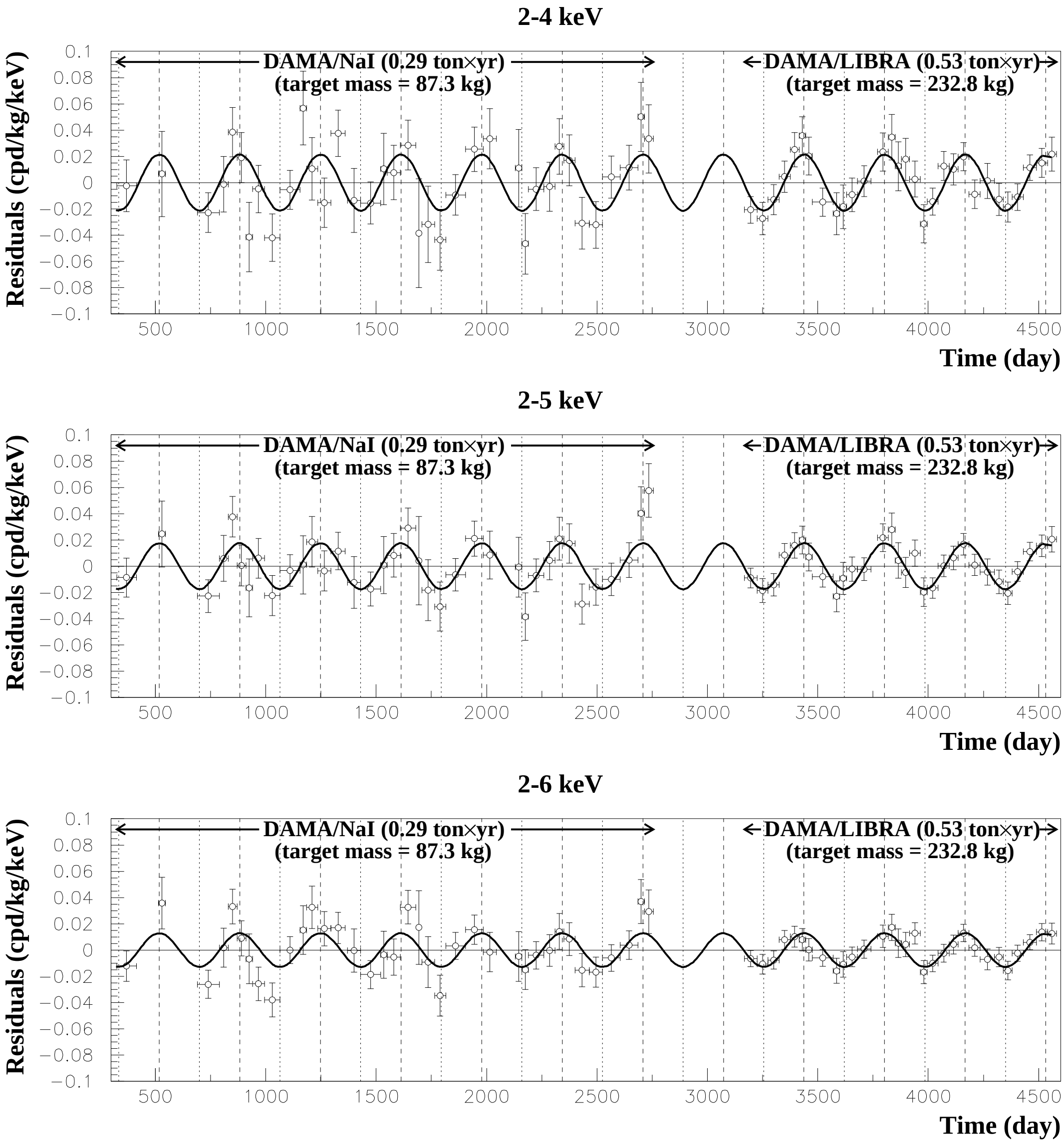

Figure 1: Model-independent experimental residual rate of the *single-hit* scintillation events, measured by DAMA/NaI and DAMA/LIBRA in the (2 – 4), (2 – 5) and (2 – 6) keV energy intervals as a function of the time. The zero of the time scale is January 1^{st} of the first year of data taking of the former DAMA/NaI experiment. The experimental points present the errors as vertical bars and the associated time bin width as horizontal bars. The superimposed curves represent the cosinusoidal function behaviours $A\cos\omega(t-t_0)$ with a period $T = \frac{2\pi}{\omega} = 1$ yr, with a phase $t_0 = 152.5$ day (June 2^{nd}) and with modulation amplitudes, A, equal to the central values obtained by best fit over the whole data, that is: (0.0215 ± 0.0026) cpd/kg/keV, (0.0176 ± 0.0020) cpd/kg/keV and (0.0129 ± 0.0016) cpd/kg/keV for the (2 – 4) keV, for the (2 – 5) keV and for the (2 – 6) keV energy intervals, respectively. The dashed vertical lines correspond to the maximum of the signal (June 2^{nd}), the dotted vertical lines correspond to the minimum. The total exposure is 0.82 ton $\times$ yr. For details and for more results see reference [7].

detailed discussions on all the related topics and for results see the devoted paper [7]. In conclusion, also the data of the first four annual cycles of DAMA/LIBRA as previously those of DAMA/NaI, fulfil the requirements of the DM annual modulation signature.

The corollary question about the nature of the DM particle(s) detected by the annual modulation signature and the related astrophysical, nuclear and particle Physics scenarios requires subsequent model-dependent corollary analyses as those performed [2, 3, 4]; few examples have been given in reference [7], while an update of allowed volumes/regions in various scenarios is in preparation. One should stress that it does not exist any approach to investigate the nature of the candidate in the direct and indirect DM searches which can offer these information independently on astrophysical, nuclear and particle Physics assumptions. It is also worth noting that no experiment exists whose result can be directly compared in a model-independent way with the DAMA/NaI and DAMA/LIBRA experimental results; some related arguments have been addressed e.g. in references [2, 3, 4, 6, 7, 12].

Finally, the collection of a larger exposure with DAMA/LIBRA (and with the possible DAMA/1ton, which is at R&D stage) and the possible lowering of the energy threshold below 2 keV will allow further investigations on DM features and will offer higher sensitivities.

References

[1] R. Bernabei *et al.*, Phys. Lett. **B389** 757 (1996); Phys. Lett. **B424** 195 (1998); Phys. Lett. **B450** 448 (1999); Phys. Lett. **B480** 23 (2000); Phys. Lett. **B509** 197 (2001); Eur. Phys. J. **C23** 61 (2002); P. Belli *et al.*, Phys. Rev. **D61** 023512 (2000); Phys. Rev. **D66** 043503 (2002).

[2] R. Bernabei *et al.*, La Rivista del Nuovo Cimento **26** n.1, 1-73 (2003); Int. J. Mod. Phys. **D13** 2127 (2004).

[3] R. Bernabei *et al.*, Eur. Phys. J. **C47** 263 (2006).

[4] R. Bernabei *et al.*, Il Nuovo Cim. **A112** 545 (1999); Eur. Phys. J. **C18**, 283 (2000); Int. J. Mod. Phys. **A21** 1445 (2006); Int. J. Mod. Phys. **A22** 3155 (2007); Eur. Phys. J. **C53** 205 (2008); Phys. Rev. **D77** 023506 (2008); Mod. Phys. Lett. **A23** 2125 (2008).

[5] R. Bernabei *et al.*, Phys. Lett. **B408** 439 (1997); Phys. Rev. Lett. **83** 4918 (1999); Il Nuovo Cimento **A112** 1541 (1999);
P. Belli *et al.*, Phys. Lett. **B460** 236 (1999); Phys. Rev. **C60** 065501 (1999); Phys. Lett. **B515** 6 (2001);
F. Cappella *et al.*, Eur. Phys. J.-direct **C14** 1 (2002);
R. Bernabei *et al.*, Eur. Phys. J. **A23** 7 (2005); Eur. Phys. J. **A24** 51 (2005).

[6] R. Bernabei *et al.*, Nucl. Instr. & Meth. **A592** 297 (2008).

[7] R. Bernabei *et al.*, Eur. Phys. J. **C** DOI 10.1140/epjc/s10052-008-0662-y, arXiv:astro-ph/0804.2741.

[8] R. Bernabei *et al.*, Eur. Phys. J. **A27** s01 35 (2006); Phys. Lett. **B546** 23 (2002); Phys. Lett. **B527** 182 (2002); Nucl. Instrum. & Meth. **A482** 728 (2002); Eur. Phys. J. direct **C11** 1 (2001); Phys. Lett. **B493** 12 (2000); New Journal of Physics **2** 15.1 (2000); Phys. Lett. **B436** 379 (1998); Eur. Phys. J. **A36** 167 (2008); Phys. Lett. **B658** 193 (2008); ROM2F/2008/17, to appear on the Proc. of the Int. conf. NPAE 2008, Kiev, Ukraine; Phys. Rev. **C76** 064603 (2007); Nucl. Phys. **A789** 15 (2007); Ukr. J. Phys. **51** 1037 (2006); Nucl. Instrum. & Meth. **A555** 270 (2005); Nucl. Phys. **A705** 29 (2002); Astropart. Phys. **7** 73 (1997); Il Nuovo Cim. **A110** 189 (1997);
R. Cerulli *et al.*, Nucl. Instrum. & Meth. **A525** 535 (2004);
P. Belli *et al.*, Nucl. Instrum. & Meth. **A498** 352 (2003); Astropart. Phys. **10** 115 (1999); Nucl. Phys. **B563** 97 (1999); Phys. Rev. **D61** 117301 (2000); Phys. Lett. **B465** 315 (1999); Phys. Lett. **B387** 222 (1996); Phys. Lett. **B389** 783 (err.) (1996); Il Nuovo Cim. **19** 537 (1996); Astropart. Phys. **5** 217 (1996).

[9] K.A. Drukier, K. Freese and D.N. Spergel, Phys. Rev. **D33** 3495 (1986);
K. Freese, J. Frieman and A. Gould, Phys. Rev. **D37** 3388 (1988).

[10] F.S. Ling, P. Sikivie and S. Wick, Phys. Rev. **D70** 123503 (2004).

[11] D. Smith and N.. Weiner, Phys. Rev. **D64** 043502 (2001);
D.. Tucker-Smith and N. Weiner, Phys. Rev. **D72** 063509 (2005).

[12] R. Bernabei *et al.*, arXiv:astro-ph/0806.0011 (2008).

Status of the KIMS Experiment

Seung Cheon Kim for the KIMS Collaboration

Department of Physics and Astronomy, Seoul National University,Seoul 151-747

DOI: http://dx.doi.org/10.3204/DESY-PROC-2008-02/kim_seungcheon

KIMS (Korea Invisible Mass Search) Collaboration has carried out WIMP search using CsI(Tℓ) crystal scintillators. The experiment was conducted in YangYang underground laboratory(Y2L), of which the water equivalent depth is about 2000m. Besides CsI main detectors, we are operating neutron detector and muon detector to understand the background events other than WIMP. Recently the CsI main detector was upgraded to 104.4 kg. The current status of KIMS project is reported.

1 Introduction

Dark matter problem is a long-standing, open question about the missing mass which isn't identified yet, but whose gravitational effect is evident [1]. Furthermore, it is supposed to occupy most part of the matter component in the universe. By recent astronomical observation, like bullet cluster [2], the existence of exotic dark matter, not ordinary like atom or other known particle, is supported more than before. WIMP (Weakly Interacting Massive Particle) is one of strong candidates of the dark matter since it is introduced naturally from the supersymmetry theory. LSP (lightest supersymmetric particle) can be the stable, massive and weakly interacting particle so that it can explain the relic dark matter density for present large scale structure of the universe [3]. WIMP is expected to recoil the nucleus and deposit a few tens keV of recoil energy. All over the world, many experiments to detect WIMP are going on. KIMS(Korea Invisible Mass Search) is one of these projects, using CsI(Tℓ) crystal scintillator, which has been carried out in Yangyang underground laboratory (Y2L) in Korea.

Atomic mass number	$Cs = 133,\ I = 127$
Density(g/cm^3)	4.53
Decay constant(ns)	~ 1000
Peak emission(nm)	550
Light yield($photon/MeV$)	~ 60000
Hygroscopicity	Slight
Spin expectation value(Cs)	$< Sp >= -0.370,\ < Sn >= 0.003$
Spin expectation value(I)	$< Sp >= 0.309,\ < Sn >= 0.075$

Table 1: Properties of CsI(Tℓ) crystal.

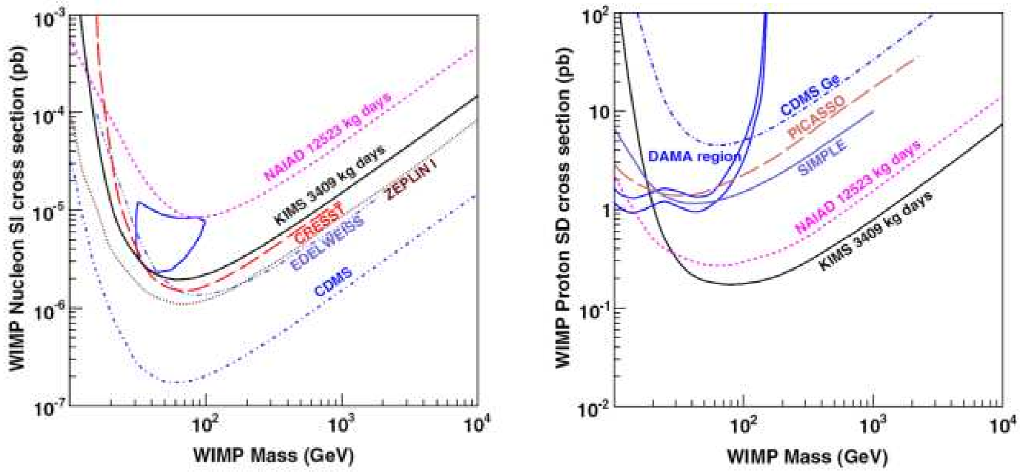

(a) (b)

Figure 1: SI exclusion limit (a). SD exclusion limit for pure proton (b).

CsI(Tℓ) is a very popular scintillator, which has high light yield and weak hygroscopicity. Table 1 shows the some properties of CsI(Tℓ) crystal. CsI(Tℓ) crystal enables pulse shape discrimination so that we can statistically separate the electron recoil background from nuclear recoil signals. Since CsI(Tℓ) has high spin expectation value, especially for proton, it is quite sensitive to the Spin Dependent(SD) interaction of WIMP with nucleus, which makes this project distinguished. But, because of internal radio-isotopes, ^{137}Cs , ^{134}Cs , ^{87}Rb , we have made serious efforts to reduce these impurities, and now we can obtain $\sim$ 2cpd level of crystal [4]. Using these crystal, we have performed the experiment in Y2L, whose water-equivalent-depth is 2000m, with proper passive and active shieldings, and neutron monitoring detector. The full description about the detector system can be found in other documents [5].

2 Latest WIMP search results

Each detector module is composed of a crystal and two PMTs which are mounted at both ends of the crystal. The crystal weighs 8.7kg, and its size is 8cm $\times$ 8cm $\times$ 30cm. The PMT is green-enhanced and the light yield is around 5 photoelectron per keV. Each event was recorded for a period of 32 μs with 500 MHz FADC. We required 2 photoelectrons in 2 μs in each PMT for an event condition. With 4 detector modules, we obtained 3409 kg·days of data.

At the energy range of interest, 3–11 keV, PMT noise events significantly limits the sensitivity. So, to understand the PMT background events, we took some data after replacing CsI(Tℓ) crystals with clean acrylic boxes. With this experiment, we found following facts. Firstly, PMT background event decays faster than scintillation signals from the crystal. Secondly, it decays as one exponential function rather than two components of exponential. Thirdly, it is asymmetric across 2 PMTs. According to the cuts developed by PMT-only-test, we could reject all the PMT background events. And, we selected only single hit events, which fire only one detector module, since WIMP doesn't do the multiple scattering.

We applied pulse shape discrimination method to the selected events to calculate the nuclear recoil event rate, using the mean time calibration with ^{137}Cs Compton scattering γ and neutron from Am-Be source. In determining the nuclear recoil event rate, we considered various factors for systematic error, i.e, variation according to different crystals and temperature. From this careful estimation, we concluded that our nuclear recoil event rates are consistent with zero and we set the limit of WIMP-Nucleon cross section at 90% confidential level [6].

Through this result, we can cross-check DAMA experiment which claims the observation of WIMP by annual modulation technique with NaI(Tℓ) crystals. As shown in Figure 1(a), our result is not compatible with DAMA signal region. At least, we can say that we ruled out the DAMA signal region contributed from ^{127}I , the dominant target of SI interaction for DAMA experiment. And, as shown in Figure 1(b), for SD interaction in the case of pure proton coupling, we could set the most stringent limit around 100GeV WIMP mass. However, DAMA / LIBRA recently confirmed their annual modulation signature with higher statistics. Therefore the annual modulation remains to be checked independently by other experiments. KIMS with higher mass may be able to check annual modulation directly.

3 Study of background event which mimics WIMP

Because neutrons also make nuclear recoil, it's very hard to distinguish neutron signals from WIMP signal. So, neutron background must be suppressed as much as possible. Main sources of neutron are spontaneous fission of ^{238}U, (α, n) reactions and neutrons induced by cosmic muons. Neutrons from these natural radioactivity except cosmic muon, can be blocked through proper passive shield sufficiently. But, high energy cosmic ray can produce the neutron inside of the shield structure. Furthermore, since when high energy muon hits the crystal, it produces an event with very long tail like a few tens of millisecond for CsI(Tℓ) , this tail event can be detected as the low energy signal (Figure 2). A detailed study for the rejection of these tail events is in progress.

To understand the neutron and cosmic muon background, we installed neutron monitoring detector made of BC501A scintillator inside and outside of the detector shield. And,we made detector's outmost layer which covers the detector shield in 4π direction with the mineral oil mixed with liquid scintillator for the muon veto. The measured muon flux in our experimental hall is 2.7×10^{-7} /cm^2/s . The neutron flux at the experimental hall is measured as 8×10^{-7}/cm^2/s for 1.5MeV–6MeV neutron. We measured the muon induced neutron rate inside of the shield from the coincidence between neutron detector and muon detector. The measurement is $(3.8 \pm 0.7) \times 10^{-2}$ counts/day/liter for 0.4MeV–2.75MeV neutron. This is more or less consistent with our GEANT4 simulation result, $(2.0 \pm 0.2) \times 10^{-2}$ counts/day/liter. The neutrons induced by cosmic muons are thereby not affecting our WIMP search at the level of the current sensitivity.

4 Current status

Recently, The total detector mass is increased to 104.4kg, which consists of 12 modules. A preliminary study shows the background levels are 2–4 cpd depending on the crystal. We have took the data from the end of 2007, and some minor optimization has been done. After one year, we expect to see some important messages about the annual modulation.

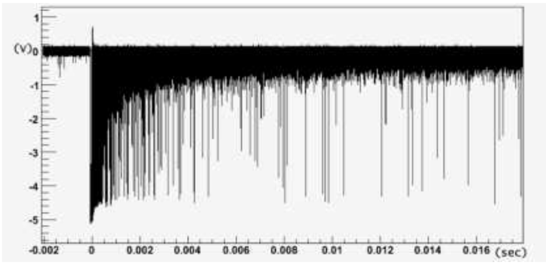

Figure 2: High energy muon event with long tail observed by CsI(Tℓ) detector. The time scale shown in the figure is up to 17ms and one can still see the photoelectrons.

References

[1] F.Zwicky, Helv. Phys. Acta **6**, L110 (1933)

[2] D.Clowe *et al.*, ApJL. **648**, L109-L113 (2006), arXiv:astro-ph/0608407v1

[3] G. Jungman,M. Kamionkowski, K. Griest, Phys. Rep. **267** 195 (1996).

[4] H.S.Lee *et al.*, Nucl. Instrum. Methods A **571** 644 (2007).

[5] H.S.Lee, "Dark Matter Search with CsI(Tℓ) Crystals", Ph.D, Dissertation, Department of Physics, Seoul National University, (2007)

[6] H.S.Lee *et al.*, Phys. Rev. Lett. **99** 091301 (2007).

The XENON100 Dark Matter Experiment

Marc Schumann[1], *Eirini Tziaferi*[2] for the XENON100 collaboration

[1]Rice University, 6100 Main St., Houston TX, USA

[2]University of Zürich, Winterthurerstr. 190, Zürich, Switzerland

DOI: http://dx.doi.org/10.3204/DESY-PROC-2008-02/schumann_marc

The XENON collaboration searches for Dark Matter using a dual-phase liquid xenon (LXe) TPC to measure nuclear recoils from WIMPs scattered off Xe nuclei. The next step of the XENON program is XENON100, a 170 kg detector with a fiducial mass of about 50 kg surrounded by an active LXe veto. It is currently installed underground at LNGS (Italy). First test measurements have started, and it will be operational in fall 2008. This paper introduces XENON100, describes all major components, and focuses on the studies of the expected gamma and neutron background. All used materials have been screened to obtain their intrinsic radioactivity, which allows to predict the background and determines the final sensitivity.

1 Introduction

There is overwhelming observational evidence that about 25% of the universe consists of cold Dark Matter [1]. The nature of the Dark Matter particle, however, remains unknown. One of the best motivated candidates is the WIMP (weakly interacting massive particle) that arises naturally in particle physics theories beyond the Standard Model like Supersymmetry, Large Extra Dimensions, and Little Higgs [2].

The XENON Dark Matter experiment searches for nuclear recoils from WIMPs scattering elastically off xenon nuclei in a two-phase (liquid/gas) time projection chamber (TPC).

Xenon as Dark Matter target The expected WIMP interaction rate is < 0.1 events/kg/day and the nuclear recoils have energies < 50 keV, showing a steeply falling featureless spectrum. The noble gas xenon – an efficient and fast scintillator (178 nm) without any long lived isotopes – is an ideal choice for the target material: its high mass number $A \sim 131$ enhances the interaction probability for spin-independent WIMP-nucleon interactions ($\sigma \propto A^2$) and its high $Z = 54$ and high density ($\rho = 3$ g/cm^3) provide powerful self-shielding in a compact detector geometry.

XENON is a two-phase TPC with two arrays of photomultipliers (PMTs) above and below the target region [3]. The principle of operation is illustrated in Fig. 1: a particle interacting with the xenon generates primary scintillation light ($S1$). The electrons from ionization in the target are drifted upwards by a strong electric field ($\sim$1 kV/cm) applied at the cathode, and are extracted to the gas phase (extraction field $\sim$10 kV/cm) where they create secondary scintillation light ($S2$). The primary vertex can be reconstructed within $\sim$3 mm using the electron drift time and the hit pattern information on the PMT arrays.

Important information for an event-by-event discrimination of signal and background events is obtained from the ratio of secondary and primary scintillation light, $S2/S1$. This ratio is much

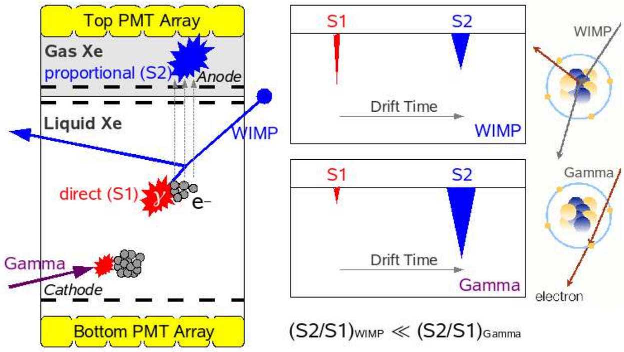

Figure 1: In a XENON TPC, primary ($S1$) and secondary scintillation light ($S2$) are different for electron recoil (β, γ) and nuclear recoil-like events (WIMPs, neutrons), and their ratio $S2/S1$ can be used for effective event-by-event discrimination. The event vertex can be reconstructed in the TPC to make fiducial volume cuts.

smaller for nuclear recoils (WIMPs, neutrons) than for electron recoils (electrons, gammas) making up most of the background.

Results from XENON10 The XENON Dark Matter Search program is a phased program: it aims to run a ton scale liquid Xenon (LXe) detector, but it proceeds step by step to gain experience from the operation of smaller detectors. The first Dark Matter Search step was the very successful operation of XENON10 at Laboratori Nazionali del Gran Sasso (LNGS), Italy, from 2005-2007. XENON10 was a 15 kg LXe detector with a fiducial mass of 5.4 kg. A blind analysis of 58.8 live days, corresponding to an exposure of 136 kg days, lead to the best WIMP search limit in 2007, with a spin independent WIMP-nucleon cross section of 8.8×10^{-44} cm^2 at a WIMP mass of 100 GeV/c^2, and 4.5×10^{-44} cm^2 at 30 GeV/c^2 (90% C.L.) [4].

The same data sample was also analyzed in terms of spin-dependent interactions [5]: this is possible since natural xenon contains about 50% odd isotopes: 26.5% ^{129}Xe (spin 1/2) and 21.2% ^{131}Xe (spin 3/2). XENON10 excludes previously unexplored parameter space for neutralinos, where it is in particular sensitive to pure neutron couplings. Moreover, it excludes a heavy Majorana neutrino in the mass range of $9.4 - 2200$ GeV/c^2 as a Dark Matter candidate.

XENON10 was limited by background since its materials were not chosen according to low intrinsic radioactivity. The main purpose of the experiment was to prove that this detector type works successfully and gives competitive results. XENON100, the next step in the phased program, is improved in terms of radioactivity and design.

2 XENON100

The aim of XENON100 is a sensitivity increase by a factor of ~50 compared to XENON10. This can be achieved by reducing the background in the fiducial volume by two orders of magnitude and increasing the detector mass by a factor of 10: it has a total mass of 170 kg LXe, where 70 kg are inside the TPC and the rest in an active veto region. We expect to have about 50 kg in the fiducial volume after geometric cuts.

The background reduction is achieved by a careful choice of materials and by using an improved detector design: all components with a known higher intrinsic radioactivity (cryogenics, feedthroughs) are now located outside the passive shielding. The shield of XENON10 was improved for this experiment: it now consists of 20 cm lead (inner 5 cm are low radioactivity lead, 17 ± 5 Bq/kg from ^{210}Pb), 20 cm of polyethylene, and an inner layer of up to 5 cm of copper.

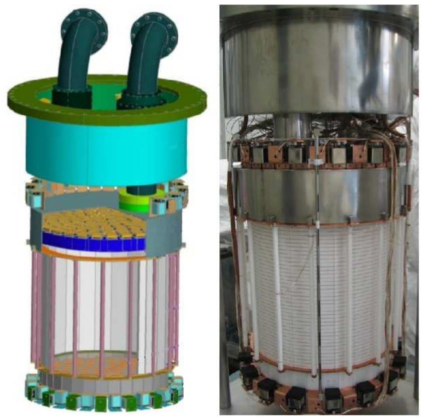

Figure 2: The XENON100 detector. The TPC contains 70 kg of LXe and is surrounded by an active LXe shield of 100 kg. The detector is fully assembled and installed underground at LNGS since February 2008. The materials used for the detector were carefully chosen upon their low radioactivity and the detector design is such that all radioactive "hot" components are located far away from the sensitive volume, outside the shield.

Cryostat, cooling, and xenon purification The double wall cryostat is made out of low radioactivity stainless steel and has a weight of 70 kg only. Cooling is provided by a 170 W PTR cryocooler (Iwatani CryoMini Coldhead PC150) that liquefies the xenon gas outside the shield continuously.

In order to achieve high electron lifetimes in the liquid – a necessary requirement to drift charges over large distances – the number of electronegative impurities in the xenon has to be small. XENON100 uses a high temperature getter (SAES getters Mono Torr) to remove these impurities during constant xenon recirculation.

Xenon has no long lived isotopes that could give rise to intrinsic background. However, it contains a tiny fraction of radioactive ^{85}Kr ($T_{1/2} = 10.756$ y). In order to remove the krypton to the ppt level, the xenon gas was purified commercially and a sophisticated krypton distillation system (Taiyo Toyo Sanso Ltd.) was procured. This instrument allows us to purify the Xe from Kr on site.

TPC design, electric field configuration The XENON100 TPC is a cylinder with 15 cm radius and 30 cm height, made out of PTFE (teflon) to improve light collection (Fig. 2). The active volume is viewed by two PMT arrays: the top array consists of 98 PMTs arranged in concentric rings to improve radial fiducial volume cuts. 80 PMTs on the bottom array are placed as closely as possible to optimize light collection which finally determines the low energy threshold of the experiment. All light detectors are $1'' \times 1''$ Hamamatsu R8520 low radioactivity PMTs. The bottom PMTs have an increased quantum efficiency of ∼33% with respect to the top array of PMTs.

A layer of LXe of about 3 cm thickness surrounds the whole TPC. This veto is made active with 64 more PMTs: 2×16 PMTs monitor the LXe above and below the target volume, respectively, and 32 PMTs look at the sides. We expect to gain an additional factor of ∼3−4 in background reduction compared to using a passive veto.

The cathode at the lower end of the TPC is a 75 μm thick stainless steel (SS) mesh in hexagonal geometry, the mesh pitch is 5 mm. A cathode high voltage of −30 kV generates a drift field of 1 kV/cm, corresponding to a maximal electron drift time of ∼160 μs. On the other side, the TPC is closed with a stack of 3 hexagonal SS meshes: the anode (125 μm, 2.5 mm pitch) is located between two grounded meshes, the spacing is 5 mm. An extraction field of 10 kV/cm is obtained by applying +5 kV to the anode. The whole stack is optimized for optical transparency and minimal impact on the $S2$ energy resolution ($\sim 4\%$). 40 equidistant double ring field shaping rings are used to optimize the homogeneity of the drift field inside the TPC.

In order to ensure that the signal strength does not depend on the xy-position, the liquid gas interface has to be placed parallel to the anode. Four levelmeters measuring the capacitance of LXe filled SS tubes are used to level the TPC. The height of the liquid level can be adjusted since the anode stack is placed inside a "diving bell" with a gas outlet whose height can be changed by a motion feedthrough. The diving bell technique also allows to put a veto layer of xenon above the TPC and the top PMT array.

Data Acquisition and Slow Control system The XENON100 data acquisition system (DAQ) must be capable to digitize the full waveform of 242 PMTs, where the time window for an event is 320 μs. (This is the doubled maximal drift time to not miss an event when the DAQ triggered on $S1$ instead of $S2$.) At the same time, the maximal trigger rate has to be large enough to allow fast calibration.

We solved this issue by using CAEN V1724 flash ADC modules. This 14bit ADC with 10 ns time resolution has a circular buffer for a measurement without deadtime in Dark Matter mode. Additionally, it features an on-board FPGA used to decrease the data amount by removing the baseline between peaks which contains no interesting information: it only writes samples above an adjustable threshold into the output buffer and stores the time when the sample exceeded the threshold, thus the full waveform can be reconstructed. This allows to calibrate the detector at $\sim$400 Hz for $S1$ pulses only, and with $\sim$50 Hz if $S1$ and $S2$ signals are measured simultaneously.

XENON100 is continuously monitored with a dedicated Slow Control system that records all relevant parameters of the experiment, such as temperatures (inside the cryostat in liquid and in gas, at the PTR, environment), pressures, flow rate (recirculation, filling, N_2 purge), LXe levels, cryostat vacuum, Rn activity, high voltages, PMTs, etc.

3 Expected backgrounds of XENON100

For every dark matter experiment, an a-priori knowledge of its background has to be obtained in order to predict its sensitivity. This background can be mostly gammas, which produce electron recoils and neutrons, which produce nuclear recoils. A WIMP scattering off the target nucleus produces a nuclear recoil, therefore it cannot be distinguished from a neutron. The gamma background is reduced with an efficiency of 99.5%−99.9% [4] using the $S2/S1$ ratio. Nevertheless it is crucial to minimize both kinds of background, in order to realize a factor of 100 reduction over XENON10, which had a gamma background of 0.6 dru in the WIMP search region. (1 dru = 1 event/kg/day/keV, where keV is measured with the proper energy scale for nuclear recoils.) XENON100 achieves this by:

- placing hot materials, such as the cryogenics and the feedthroughs, outside the shielding. These materials were found to have a high radioactivity in XENON10, therefore they were moved far away from the detector;
- careful selection of ultra low background materials (c.f. Sec. 3.1);
- using 100 kg of LXe as an active shield. Events in the fiducial volume which are detected in coincidence with events in the veto will be rejected in the analysis.

3.1 Material screening

The selection of most of the materials in XENON100 was done based on their low intrinsic radioactivity. XENON100 operates a dedicated screening facility underground at LNGS, consisting of a 2.2 kg high purity Ge crystal in an ultra-low background Cu cryostat, which is surrounded by a low background shielding (Cu and Pb). Moreover, we also use the LNGS screening facility with some of the most sensitive Ge detectors in the world.

All the materials in XENON100 were screened in order to know their ^{238}U, ^{235}U, ^{232}Th, ^{40}K, and ^{60}Co contamination. Several low-activity materials were identified, such as the stainless steel used for the cryostat and the TPC. Table 1 shows the results from the screening of a subset of materials.

Material	Unit	U [mBq/unit]	Th [mBq/unit]	K [mBq/unit]	Co [mBq/unit]
PTFE	kg	< 0.31	< 0.16	< 0.11	NA
Stainlees steel (SS)	kg	< 1.9	< 1.0	8.5 ± 0.9	10.5 ± 4.2
PMT bases	base	0.71 ± 0.05	0.10 ± 0.03	NA	NA
22 high QE PMTs	PMT	< 0.24	0.18 ± 0.05	11.5 ± 2.0	0.55 ± 0.10
SS Screws for PMT bases	kg	< 9.2	16 ± 4	9 ± 3	< 46.4
Copper	kg	< 0.020	< 0.023	NA	NA
Polyethylene	kg	< 3.80	< 2.69	< 5.88	<0.684
Outer Pb (516 ± 90 Bq/kg)	kg	< 5.7	< 1.6	< 1.1	14 ± 6
Inner Pb (17 ± 5 Bq/kg)	kg	< 6.8	< 3.9	< 0.19	< 28

Table 1: A subset of materials screened with the Ge detectors of XENON100 and LNGS. The last four materials are used for the shielding of XENON100. The dominating activity for the two types of lead (given in the brackets) is due to ^{210}Pb.

3.2 Gamma and neutron background studies

The results from the material screening were used to predict the gamma and neutron induced background in XENON100. The geometry of the detector and its shielding was coded with the GEANT4 toolkit [6].

Gamma background Gammas from U, Th, K, and Co (and ^{210}Pb for lead) were simulated for the detector and shielding materials. The rate of electron recoils which are generated in liquid xenon in the WIMP search region was estimated and is shown in Table 2. The detector position resolution (few mm) and the activity of each material were taken into account. Fiducial volume cuts were applied to cut events at the edges of the detector, reducing the target mass to ~ 50 kg. The total rate of single scatters (WIMPs will never double scatter because of their low cross section) due to gammas is expected to be around 10 mdru before $S2/S1$ discrimination, which is indeed about a factor of 100 lower than in XENON10.

Neutron background Neutrons are the most crucial background for many underground experiments. Experiments searching for WIMPs work with a very low energy threshold and are sensitive to − and should be protected from − neutrons from two possible sources:

Material	Single scatter rate [mdru]
PTFE	0.18 ± 0.02
SS	2.01 ± 0.22
PMTs	4.91 ± 0.60
Copper	0.026 ± 0.002
Polyethylene	2.50 ± 0.29
Lead	negligible
Total	9.63 ± 0.70

Table 2: Predicted gamma background rate in the WIMP search region (4.5−26.9 keVnr). The differential rate unit is defined as 1 dru = 1 event/kg/day/keV.

1. Rock, detector, and shielding components, the so called local radioactivity: these neutrons have energies less than 10 MeV and are produced via spontaneous fission and (α,n) reactions of ^{238}U and ^{232}Th on light elements.

2. Muons, the only cosmic-ray particles that can penetrate the rock down to hundreds of meters, produce high energy neutrons with a spectrum extending to GeV in spallations and electromagnetic and hadronic cascades. The neutron yield from cosmic-ray muons depends strongly on the depth of the underground laboratory [7].

Each of these background sources is studied separately in order to estimate the total neutron background of XENON100.

Radioactivity from detector and shielding materials: The local radioactivity from detector and shielding materials was calculated by generating the neutron spectra from spontaneous fission and (α,n) reactions following U/Th-decays and by propagating these neutrons into the fiducial volume. The neutron fluxes and the energy spectra from U/Th contamination in each material were calculated by the modified SOURCES4A code [8]. Figure 3 shows the neutron spectra from polyethylene (left) and Cu (right), assuming 10 ppb U contamination. It is obvious that (α,n) reactions contribute much less to the neutron spectrum of Cu, since it is a high-Z material.

Table 3 (2^{nd} column) shows the simulated neutron production rate for each material. These neutrons were propagated into the detector and the single scatter recoils in the fiducial volume

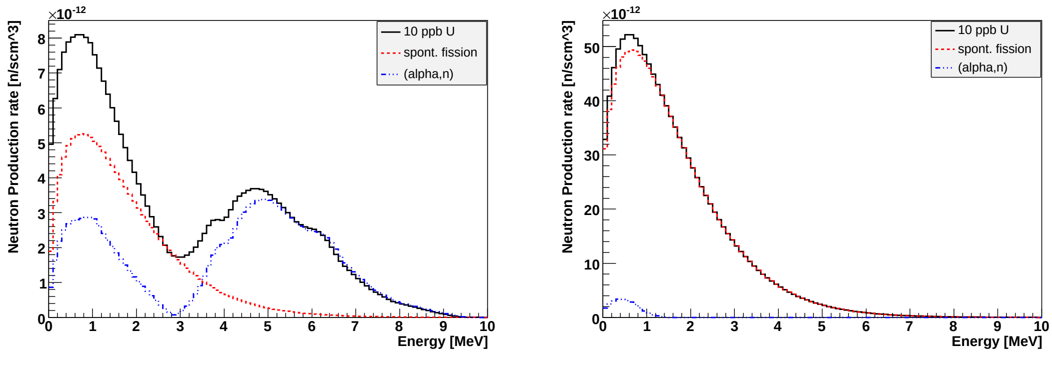

Figure 3: Neutron spectra from 10 ppb U in polyethylene (left) and in Cu (right). The dashed line shows the contribution from spontaneous fission, the dotted-dashed line from (α,n) reactions, and the solid line illustrates the total neutron production rate.

Material	n/year	Single Scatters [10^{-7}dru]
PTFE	10.10	5.84± 0.03
SS	15.04	1.83± 0.02
PMTs	7.02	3.18± 0.02
Copper	1.58	0.11± 0.002
Polyethylene	416.26	4.89± 0.10
Lead	7384 .56	0.38 ± 0.02
Total	–	16.23 ± 0.11

Table 3: Neutrons from detector materials: Column 2: Neutrons produced in detector and shielding material per year. Column 3: Mean rate of single scatter nuclear recoils in the WIMP search region (4.5−26.9 keVnr).

were recorded as shown in Fig. 4. Table 3 (3^{rd} column) also gives the mean single scatter nuclear recoil rate in the WIMP search region. The fraction of single recoils is ∼44%. The total rate of nuclear single scatters from local radioactivity is estimated to be 1.6 μdru, which corresponds to 0.6 single nuclear recoils per year in the fiducial volume.

Radioactivity from the cavern: The neutron background from the experimental environment is calculated in a similar way as above. The cavern in which the XENON100 detector is located is simulated to consist of 30 cm concrete followed by rock. Material composition and activities were taken from [10]. Since the detector is located close to LNGS Hall A, the same activity values were assumed for the XENON100 cavern. The rock thickness is considered to be 3 m, since no neutrons from larger distances can reach the rock-cavern boundary. Using the SOURCES4A code, the neutron production rate was calculated to be 1.7 and 7.1 per year per gram from concrete and rock, respectively. Even if the production rate from rock is higher, the dominant contribution is expected to be from concrete, which reduces the neutron flux from the rock significantly. These simulations, however, are still in progress.

Event rate from cosmic-ray muons: The muon transportation through the Gran Sasso rock down to a depth of 3600 m.w.e. was done with the MUSIC code [7]. Muon energy and angular distribution were calculated with MUSUN [7]. The mean muon energy, which increases with

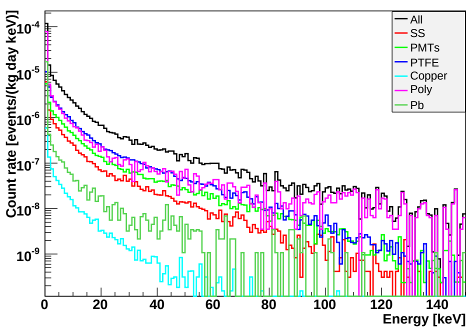

Figure 4: Single scatter nuclear recoils in the fiducial volume of XENON100 due to U/Th contamination in the detector and shielding materials. The spectra correspond to the total rate generated in PTFE, polyethylene, PMTs, SS, Pb, Cu, and LXe (top to bottom).

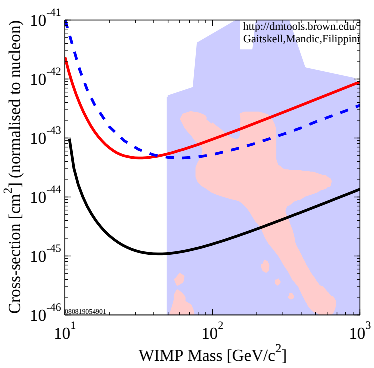

Figure 5: Projected sensitivity of XENON100 (black), reaching a sensitivity of $2 \cdot 10^{-45}$ cm^2 for a 100 GeV WIMP. Additionally, the current limits of XENON10 (red) [4] and CDMS (dashed blue) [9] are shown.

the lab depth, is 270 GeV in LNGS, and the muon flux is 1.17 $m^{-2}h^{-1}$. For this simulation, the rock thickness is assumed to be 6 m, which is a sufficient distance for all the hadronic cascades to develop and to produce neutrons. These neutrons then were propagated into the detector. It is known that neutron production from muons is more favored in high-Z materials [7], therefore many neutrons will be produced inside the shielding. These simulation are in progress and final results are not available yet, but it is expected to be a sub-dominant neutron background compared to the local radioactivity.

4 Summary and outlook

The XENON100 detector is installed underground at LNGS, Italy, in a depth of 3600 m water equivalent since February 2008. Since then, almost all components have been tested successfully and calibration and background data are taken continuously in order to characterize the response and performance of the experiment. The first Dark Matter run is scheduled for the end of 2008.

Based on the detailed background studies using the measured activities of the detector components, we expect a gamma background of about 0.01 events/keVee/kg/day and less than 0.6 neutrons/year (from local radioactivity) in the fiducial volume and the WIMP search region. Assuming the same energy threshold as achieved in XENON10 and the same electron recoil rejection power, we will be able to run XENON100 background free for about 2 months with $\sim$50 kg fiducial mass, reaching a sensitivity of $2 \cdot 10^{-45}$ cm^2 for a 100 GeV WIMP (Fig. 5).

At the same time, the XENON collaboration already started to study the design and the backgrounds of a larger LXe detector which will probe a large fraction of the predicted WIMP parameter space.

References

[1] W.-M. Yao *et al.* (PDG), Journ. of Phys. **G33** 1 (2006) and references therein.

[2] A. Bottino *et al.*, Phys. Rev. **D69** 037302 (2004);
J. Ellis *et al.*, Phys. Rev. **D71** 095007 (2005);
H. C. Cheng *et al.*, Phys. Rev. Lett. **89** 211301 (2002);
A. Birkedal-Hansen and J. G. Wacker, Phys. Rev. **G69** 065022 (2004).

[3] E. Aprile *et al.*, New Astron. Rev. **49** 289 (2005).

[4] J. Angle *et al.* (XENON10), Phys. Rev. Lett. **100** 021303 (2008).

[5] J. Angle *et al.* (XENON10), Phys. Rev. Lett. **101** 091301 (2008).

[6] S. Agostinelli *et al.*, Nucl. Instr. Meth. **A506** 250 (2003).

[7] P. Antonioli *et al.*, Astrop. Physics **7** 357 (1997);
V. A. Kudryavtsev *et al.*, Phys. Lett. **B471** 251 (1999);
V. A. Kudryavtsev *et al.*, Nucl. Instr. Meth. **A505** 688 (2003).

[8] Wilson *et al*, Phys. Lett. **B645** 153 (2007);
M. Carson *et al*, Astrop. Physics **21** 667 (2004);
R. Lemrani *et al*, Nucl. Instr. Meth. **A560** 454 (2006);
V. Tomasello *et al*, doi:10.1016/j.physletb.2003.10.071.

[9] Z. Ahmed *et al.* (CDMS), arXiv:0802.3530 (2008).

[10] H. Wulandari *et al.*, Astrop. Physics **22** 313 (2004).

Recent Results from the CDMS-II Experiment

Tobias Bruch[1] for the CDMS Collaboration

[1]University of Zürich, Winterthurerstr 190, 8047 Zürich, Switzerland

DOI: http://dx.doi.org/10.3204/DESY-PROC-2008-02/bruch_tobias

The Cryogenic Dark Matter Search experiment (CDMS) employs low-temperature Ge and Si detectors to detect WIMPs via their elastic scattering interaction with the target nuclei. The current analysis of 397.8 kg-days Ge exposure resulted in zero observed candidate events, setting an upper limit on the spin-independent WIMP-nucleon cross-section of $6.6 \times 10^{-44}\,\mathrm{cm}^2$ ($4.6 \times 10^{-44}\,\mathrm{cm}^2$, when previous CDMS Soudan data is included) at the 90% confidence level for a WIMP mass of 60 GeV. To increase the sensitivity, new one inch thick detectors have been developed which will be used in the SuperCDMS phase. SuperCDMS 25kg will be operated at SNOLAB with an expected sensitivity on the spin-independent WIMP-nucleon elastic scattering cross-section of $1 \times 10^{-45}\,\mathrm{cm}^2$.

1 Introduction

The Cryogenic Dark Matter Search (CDMS) experiment operates 19 Ge (250 g each) and 11 Si (100 g each) detectors at the Soudan underground laboratory (MN, USA) to search for non-luminous, non-baryonic Weakly Interacting Massive Particles (WIMPs), that could form the majority of the matter in the universe [1, 2] . Each detector is a disk 7.6 cm in diameter and 1 cm thick. The detectors are operated at cryogenic temperatures $\sim$ 40 mK to collect the athermal phonons created upon an interaction in the crystal in four independent sensors. In addition, the electron hole pairs created by a recoil are drifted in a field of 3 V/cm (Ge), 4 V/cm (Si) towards two concentric electrodes lithographically patterned on one flat side of the crystals [3]. In the analysis events from the outer part of the detectors are removed by a fiducial volume cut based on the partitioning of energy between the two concentric charge electrodes. The simultaneous measurement of the phonon and ionization recoil energy of an interaction in the crystals not only allows an accurate measurement of the recoil energy independent of recoil type (nuclear/electron recoil), but also allows the discrimination between nuclear and electron recoils by the so called ionization yield parameter, which is the ratio of the ionization and phonon energy, providing a rejection factor of $> 10^4$. Nuclear recoils produce fewer charge pairs, and hence less ionization energy than do electron recoils of the same energy. The ionization yield for electron and nuclear recoils is determined from ^{133}Ba and ^{252}Cf calibrations respectively, providing the bands shown in Fig. 1.

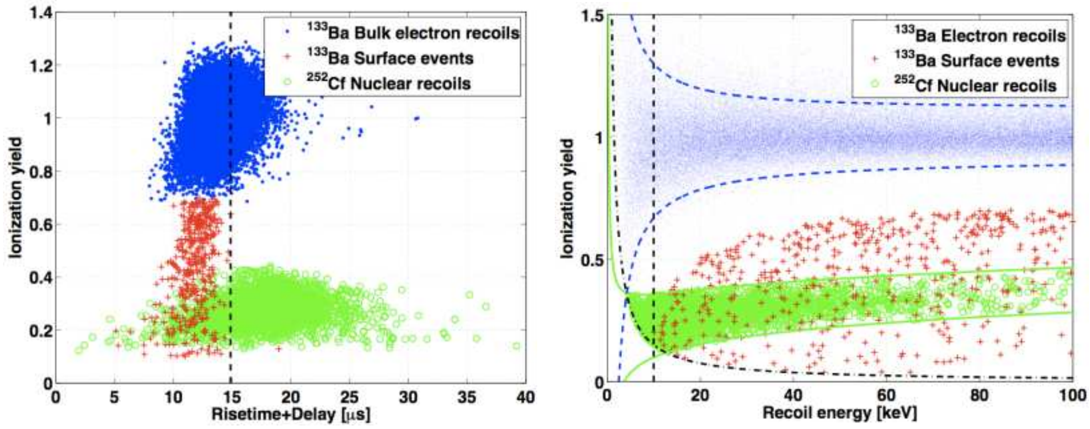

Figure 1: Ionization yield as a function of the recoil energy (left panel) and phonon-timing parameter (right panel) for calibration data in a germanium detector. Three different classes of events are identified: ^{133}Ba gamma-calibration bulk (blue dots) and surface (red crosses) events, as well as nuclear recoils (green circles) from ^{252}Cf neutron-calibration data. In the left plot the nuclear - (green line) and electron-recoil band (blue/dashed) are shown with the analysis threshold (dashed/vertical) of 10 keV and the ionization threshold (black/dot dash). The vertical dashed line in the right plot indicates the position of the timing cut, efficiently cutting out surface events.

2 Backgrounds

Passive shielding, consisting of lead and polyethylene layers, are used to reduce external gamma and neutron backgrounds, leaving decays of radioactive contamination inside the shielding as the dominant natural background. Monte Carlo simulations with the GEANT4 Toolkit of the radioactive contamination (isotopes of the ^{238}U and ^{232}Th chain as well as ^{60}Co and ^{40}K) of materials inside the experimental apparatus match the observed background spectra very well, revealing no unidentified spectral lines, which would indicate an additional contamination. The whole experimental setup is surrounded by an active scintillator veto to reject events caused by cosmogenic muons or showers. Neutrons induced by radioactive processes or cosmogenic muons interacting near the experimental apparatus, can generate nuclear recoils which cannot be distinguished from possible dark matter interactions on an event-by-event basis. Monte Carlo simulations of both sources give a conservative upper limit of < 0.1 events in the current WIMP-search data from each source.

Particle interactions may suffer from a suppressed ionization signal if the interactions occur in the first few microns of the crystal surfaces. For events interacting in the first few microns the ionization loss is sufficient to missclassify these as nuclear recoils. These events, referred to as surface events, can be identified as a third population between the electron and nuclear band in Fig.1. Surface events mainly occur due to radioactive contamination on detector surfaces, or as a result of external gamma ray interactions releasing low-energy electrons from surfaces near the detectors. A correlation analysis between alpha-decay and surface-event rates provides evidence that ^{210}Pb is a major component of our surface event background. The remaining surface-event rate is compatible with the rate expected from photon induced events [4].

To discriminate surface events against nuclear recoil events the timing properties of the phonon pulses are used. The two parameters used to cut out surface events and select nuclear recoils are the delay of the slower phonon signal with respect to the ionization signal and the risetime of the leading phonon pulse (which is the one with the highest amplitude), since surface events have smaller delays and faster risetimes than bulk nuclear-recoils. The cut, based on the sum of risetime and delay provides good surface event rejection, improving the overall rejection of electron recoils to $> 10^6$. The cut is designed for each detector independently by using calibration data only as shown in Fig.1. Only single scatters with a timing parameter value greater than the cut value are considered as WIMP candidates. A single scatter is required to deposit energy in one and only one detector. In the analysis the signal window is constrained by the 2σ nuclear recoil band.

3 Results

The current analysis used data (397.8 kg-days of germanium exposure) from two periods (run 123 and 124) between October 2006 and July 2007. Of the 19 Ge detectors, three suffering reduced performance from readout failures and one with relatively poor energy resolution have been left out. The remaining 15 Ge detectors were used for the run 123 analysis. The data taken with eight detectors in run 124 is not considered in this analysis, since they have differences in performance between the two runs.

Surface events present in ^{133}Ba calibration data or naturally present in WIMP search data, were studied to determine the surface event leakage into the signal region after the timing cut is applied. The estimated surface event leakage, based on the observed numbers of single- and multiple- scatter events within and surrounding the 2σ nuclear recoil region in each detector, is $0.6^{+0.5}_{-0.3}(stat.)^{+0.3}_{-0.2}(syst.)$ [5] events. After all analysis cuts were finalized and leakage estimation schemes selected, the single recoil blinded WIMP signal region was unmasked on February 4th, 2008. No event was observed within the signal region. The WIMP search data of all detectors is shown in Fig.2. The four events passing the timing cut (red crosses in the figure) are outside of the 2 σ nuclear recoil signal region. From this data the 90% CL upper limit on the spin-independent WIMP-nucleon cross section shown as the red dashed line in Fig. 3 is derived [5]. The inclusion of a reanalysis of previous CDMS data [6] (shown as the red solid line), sets the world's most stringent upper limit on the spin-independent WIMP-nucleon cross section for WIMP masses above 42 GeV/c^2 with a minimum of 4.6×10^{-44} cm^2 for a WIMP mass of 60 GeV/c^2.

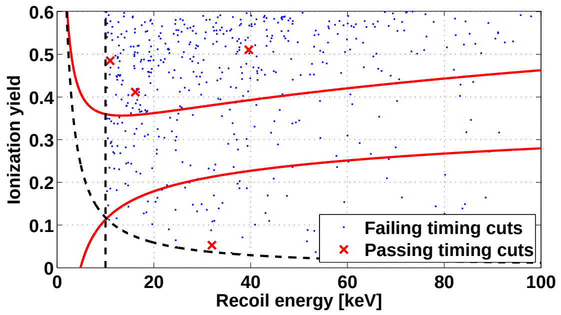

Figure 2: Low background events around the 2σ nuclear recoil signal region (red band) from all detectors used in this analysis, failing (blue dots) and passing (red crosses) the timing cuts. The four events passing the timing cuts are outside of the nuclear recoil region

To further increase the sensitivity the total accumulated exposure has to be increased. This can be achieved by increasing the detector mass and the runtime of the experiment. So far the CDMS-II setup has acquired 1500 kg-days of Ge raw exposure (including run 123/124) and is expected to accumulate an additional exposure of ~ 500 kg-days until the end of 2008. For the SuperCDMS setup new 1 inch thick detectors have been developed and tested, providing an increase of a factor 2.54 in mass with respect to the 1 cm thick detectors used in CDMS-II. The redesign of the phonon readout, which maximizes the active phonon collection area, and new sensor configurations are expected to improve the discrimination between surface events and nuclear-recoils. The first two super towers consisting each of six 1 inch thick detectors will be installed at the Soudan site by 2009 to demonstrate the improved discrimination capabilities, and show that the operation with a background free signal region can be maintained. At the SuperCDMS 25 kg stage seven super towers will be installed and operated at SNOLAB. As shown in Fig.3, SuperCDMS 25 kg aims to reach a sensitivity of $1 \times 10^{-45}\,\mathrm{cm}^2$ at a WIMP mass of $60\,\mathrm{GeV/c}^2$.

4 Conclusions

The CDMS-II experiment has maintained high dark matter discovery potential by limiting expected backgrounds to less than one event in the signal region. The current data sets the world's most stringent upper limit on the spin-independent WIMP-nucleon cross-section for WIMP masses above $42\,\mathrm{GeV/c}^2$ with a minimum of $4.6 \times 10^{-44}\,\mathrm{cm}^2$ for a WIMP mass of $60\,\mathrm{GeV/c}^2$. Ongoing runs aim to accumulate roughly 2000 kg-days of WIMP search exposure until the end of 2008. By this the CDMS-II experiment is expected to reach a sensitivity of $1 \times 10^{-44}\,\mathrm{cm}^2$. The first two super towers with new 1 inch thick detectors will be installed at the Soudan site by 2009 demonstrating the improved discrimination capabilities. The next upgrade of the CDMS experiment to SuperCDMS 25 kg operating seven super towers will be installed at SNOLAB, increasing the sensitivity by one order of magnitude.

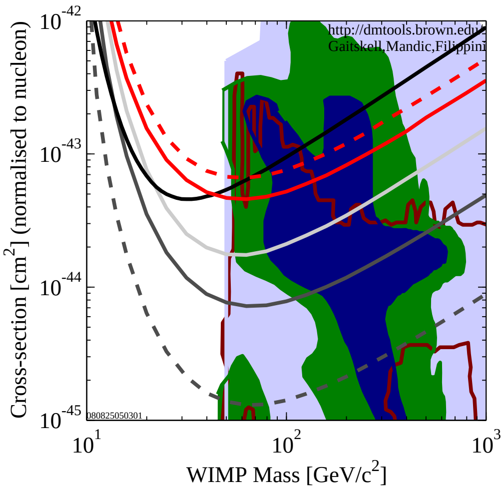

Figure 3: Upper limits on the spin independent WIMP-nucleon cross-section from the current analysis (red dashed) and the combined limit by including previous CDMS data (red solid) [5]. Also shown are the limit from the XENON10 experiment [7] (black solid) and expected sensitivities of the CDMS-II setup until the end of 2008 (light gray); two super towers operated at Soudan (dark gray/solid) and the SuperCDMS 25 kg stage (dark gray/dashed). Filled regions indicate CMSSM models [8, 9].

References

[1] D.N. Spergel *et al.*, Astrophys. J. Suppl. 148, 175 (2003).

[2] G. Jungman *et al.*, Phys. Rep. 267, 195 (1996).

[3] T. Saab *et al.*,Nucl. Inst. and Meth. A 444, 300 (2000)

[4] CDMS Collab., in preparation.

[5] Z. Ahmed *et al.*, submitted to Phys. Rev. Lett. arXiv:astro-ph/0802.3530 (2008).

[6] CDMS Collab., in preparation; R.W. Ogburn, Ph.D. thesis. Stanford University, 2008.

[7] J. Angel *et al.*, Phys. Rev. Lett. 100, 021303 (2008).

[8] E.A. Baltz and P. Gondolo, JHEP 10, 052 (2004).

[9] L. Roszkowski *et al.*, JHEP 07, 075 (2007).

Results of the CRESST Commissioning Run 2007

G. Angloher[1], M. Bauer[4], I. Bavykina[1], A. Bento[1,7], A. Brown[3], C. Bucci[5],C. Ciemniak[2], C. Coppi[2], G. Deuter[4], F. von Feilitzsch[2], D. Hauff[1], S. Henry[3], P. Huff[1], J. Imber[3], S. Ingleby[3], C. Isaila[2], J. Jochum[4], M. Kiefer[1], M. Kimmerle[4], H. Kraus[3], J.-C. Lanfranchi[2], R. F. Lang[1], B. Majorovits[3,6], M. Malek[3], R. McGowan[3], V. B. Mikhailik[3], E. Pantic[1], F. Petricca[1], S. Pfister[2], W. Potzel[2], F. Pröbst[1], W. Rau[2,8], S. Roth[2], K. Rottler[4], C. Sailer[4], K. Schäffner[1], J. Schmaler[1], S. Scholl[4], W. Seidel[1], L. Stodolsky[1], A. J. B. Tolhurst[3], I. Usherov[4], W. Westphal[2,9]

[1]Max-Planck-Institut für Physik, Föhringer Ring 6, D-80805 München, Germany
[2]Physik-Department E15, Technische Universität München, D-85747 Garching, Germany
[3]Department of Physics, University of Oxford, Oxford OX1 3RH, United Kingdom
[4]Eberhard-Karls-Universität Tübingen, D-72076 Tübingen, Germany
[5]INFN, Laboratori Nazionali del Gran Sasso, I-67010 Assergi, Italy
[6]now at: Max-Planck-Institut für Physik, Föhringer Ring 6, D-80805 München, Germany
[7]on leave from: Departamento de Fisica, Universidade de Coimbra, P3004 516 Coimbra, Portugal
[8]now at: Department of Physics, Queen's University,Ontario K7L 3N6, Canada
[9]Deceased

DOI: http://dx.doi.org/10.3204/DESY-PROC-2008-02/lanfranchi_jc

CRESST (Cryogenic Rare Event Search with Superconducting Thermometers) is a low-temperature experiment dedicated to the direct dark matter detection via nuclear recoil. It is located in Hall A of the Laboratori Nazionali del Gran Sasso, Italy. Scintillating $CaWO_4$ crystals operated at a few mK are utilized as target for WIMPs (Weakly Interacting Massive Particles), which are expected to scatter predominantly on the heavy tungsten nuclei. As for background rejection, CRESST uses the phonon-light technique, where two different quantities of an interaction are recorded: the heat production in the $CaWO_4$ crystal and the simultaneous emission of scintillation light, which is monitored by a second low-temperature detector, the light detector. The information provided by both detectors allows a powerful background discrimination on an event by event basis. After a major upgrade phase, CRESST-II has now successfully completed a commissioning run during 2007, the results of which are presented in this article.

Introduction.- CRESST (Cryogenic Rare Event Search with Superconducting Thermometers) is an experiment aimed at the direct detection of dark matter in the form of WIMPs (Weakly Interacting Massive Particles). It is located at a depth of 3500 m.w.e. (meter water equivalent) in Hall A of the Laboratori Nazionali del Gran Sasso, Italy. Highly sensitive low-temperature detectors operated at a few mK are used to measure the small recoil energies of a few keV expected in a WIMP-nucleus scattering. In the past, CRESST [1] was already able to obtain competitive results along with other direct detection low-temperature experiments like CDMS [2] and EDELWEISS [3]. However, the experiment necessitated major changes concerning the experimental setup in order to face the challenges connected to the next phase of exploration of the WIMP-nucleon scattering cross section scenario. First results obtained during the commissioning phase in 2007 are presented in this article.

Detection Principle.- CRESST uses detector modules as depicted in Fig. 1. Each module consists of two individual low-temperature detectors. A large detector with scintillating $CaWO_4$ as target provides an accurate measurement of the total energy deposited by an interaction, while the simultaneous measurement of the light yield with the second detector allows a powerful rejection of events that are not nuclear recoils [4]. This method, which is referred to as the heat-scintillation or light-phonon technique is the key to our rare event search since a background discrimination on an event by event level is realized. Nine such detector modules were installed for the commissioning run in 2007; whereas only two were used for the dark matter analysis presented in section Results.

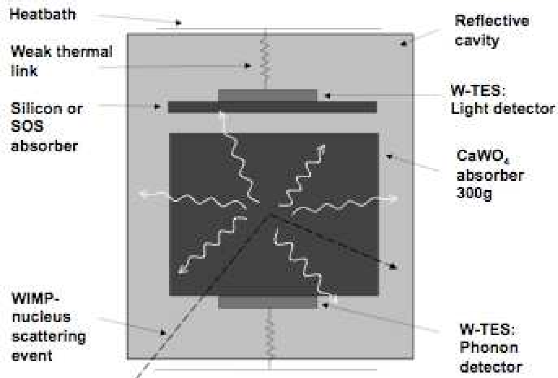

Figure 1: Schematic setup of a CRESST detector module. The module is made of two independent low-temperature detectors: one consisting of a $CaWO_4$ target crystal, which provides a total energy measurement (phonon channel), and one silicon-on-sapphire (SOS) or pure silicon wafer for measuring the scintillation light emitted by the target crystal (light channel). For a highly efficient light collection the two detectors are enclosed in a reflective and scintillating cavity.

Experimental Setup.- The setup of CRESST prior to the upgrade is described in detail in [5]. The changes made during the upgrade to CRESST-II included the installation of a PE neutron shield, a muon veto, a new detector support structure, a new 66-channel SQUID read out with associated data acquisition (DAQ), and a calibration source lift. Figure 2 shows the setup after the upgrade and is described in detail in [6]. The CRESST-II setup now allows to operate a total of 33 detector modules, i.e. 33 phonon and 33 light channels simultaneously, i.e. $\sim$10kg of target mass.

Results.- As discussed in more detail in Ref. [6], for the dark matter analysis, data taken with the two detector modules (Zora/SOS23) and (Verena/SOS21) between March 27th and July 23rd 2007 was used. The results are shown in Fig. 3. The cumulative exposure was 47.9 kg-days. For tungsten only, this corresponds to an exposure of 30.6 kg-days. The analysis is performed on the assumption of coherent or spin-independent scattering for the WIMP. This process strongly favors tungsten recoils due to the $\sim A^2$ factor in the WIMP-nucleus cross section. The acceptance region on the plots is based on: firstly, the quenching factor for the light yield and secondly, on the maximum energy expected for tungsten recoils. A similar region for "all nuclear recoils" can be defined using the quenching factors for Ca and O. The quenching factor boundaries are shown on the plots of Fig. 3. Below the dashed curve 90% of all nuclear recoils are expected, and below the solid curve 90% of the tungsten recoils are expected. The energy boundaries are indicated by the vertical lines. The upper limit at 40 keV is set by form-factor [7] effects, which effectively limit the energy transfer to the tungsten nucleus. The lower limit is set at 10 keV, where "leakage" from the electron recoil band becomes evident and recoil discrimination between electron and nuclear recoils becomes inefficient.

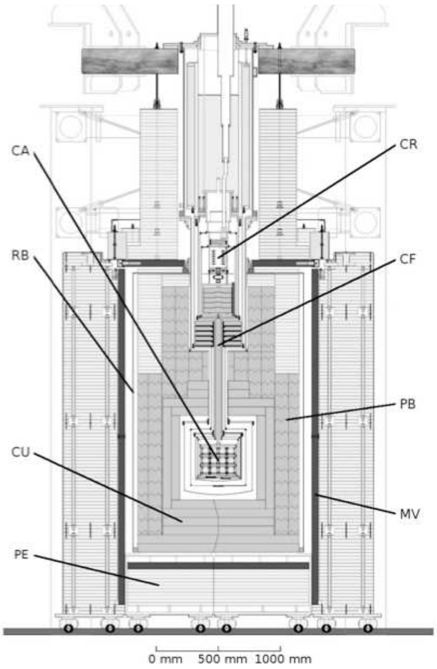

Figure 2: ^{3}He-^{4}He dilution refrigerator and shielding as upgraded for CRESST-II. The detector carousel (CA) is connected to the mixing chamber of the cryostat (CR) by a long copper cold finger (CF) in order to reduce background originating from the dilution refrigerator itself. The gas-tight radon box (RB) encloses the low-background copper (CU) and low-background lead shielding (PB). It is covered by a plastic scintillator muon-veto (MV) and a 45 cm thick polyethylene neutron moderator (PE). Additional granular PE is placed between the baffles in the upper part of the cryostat to close the line of sight for neutrons coming from the top.

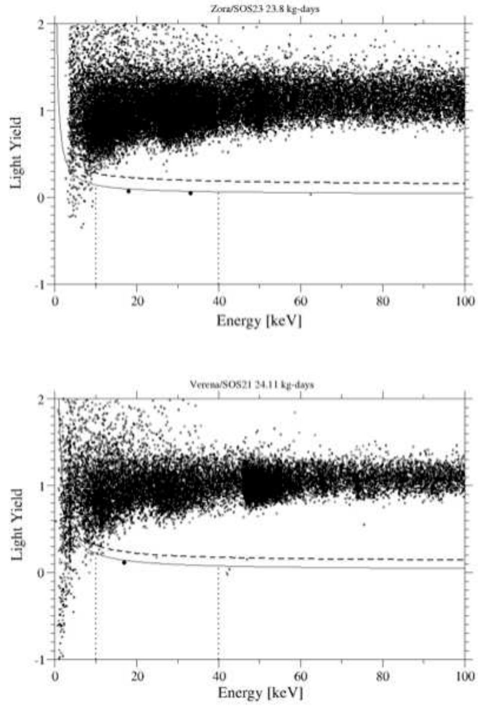

Figure 3: Low-energy event distribution measured with two 300 g $CaWO_4$ detector modules during the commissioning run. The vertical axis represents the light yield, and the horizontal axis the total energy, as measured by the phonon channel. Below the dashed curve 90 % of all nuclear recoils, and below the solid curve 90 % of the tungsten recoils are expected. The heavy black dots show the events in the "tungsten recoils" acceptance region. The intense regions of the electron recoil bands are due to γ and β-background.

In the data presented, three candidate events (heavy black dots) are observed in Fig. 3 for the "tungsten recoils" acceptance region. The individual events are at 16.89 keV (Verena/SOS21) and at 18.03 keV and 33.09 keV (Zora/SOS23). The corresponding rate is 0.063 per kg-day. From this rate and using standard assumptions on the dark matter halo [8, 9] (WIMP mass density of 0.3 GeVcm^{-3}), an upper limit for the coherent or spin-independent WIMP-nucleon scattering cross-section may be obtained using the maximum energy gap method [10]. This limit is plotted as the solid curve in Fig. 4. The minimum of the curve, for a WIMP mass of $\sim$60 GeV, is at 4.8×10^{-7} pb.

The question arises, however, as to the nature of the three observed tungsten or nuclear recoil candidates. One possibility could be remaining neutrons. Simulations [15] would give a rate of only $\sim 10^{-5}$ per kg-day and therefore much less than the few observed events. A possibility could be that during the run a weak spot in the neutron shielding above the muon veto was identified and patched only after data taking was completed. Another conceivable source for neutrons could be some non-operational modules which were present during the run. These can act as non-vetoable neutron sources for the operational modules. However, an estimate for the background events from an inactive detector module is well below 1.4×10^{-5} per kg-day. Apart from neutrons, another possibility arises from incomplete coverage of the inner surfaces of the detector module with scintillator, which could lead to unvetoed nuclear recoils from surface α-decays [16]. Therefore, it is now planned to paint some possibly uncovered areas (e.g. springs that hold the $CaWO_4$ crystals) with scintillating material.

Concerning the impact of muons, estimates [15] of muon-induced neutrons in the setup result in only 2.8×10^{-3} per kg-day. No muon signals were found in coincidence with nuclear recoil events.

In conclusion no satisfactory explanation for the few candidate events from conventional radioactive or particle sources can be given. Further work such as the enhancement of the reflective cavities is underway to clarify this issue.

Conclusions.- New elements of the CRESST-II apparatus were installed and operated. CRESST-II successfully completed its commissioning run in 2007. Data were taken with two detector modules for a total of ~48 kg-days. Three candidate events of uncertain origin are present in the acceptance region for tungsten recoils, yielding a rate of 0.063 per kg-day. A factor of ~ 10 improved performance is found with respect to previous work for the "all nuclear recoils" acceptance region. A limit on coherent WIMP-nucleon scattering, is obtained, which at its lowest value, assuming $M_{\mathrm{WIMP}} \approx 60\mathrm{GeV}$, is 4.8×10^{-7} pb.

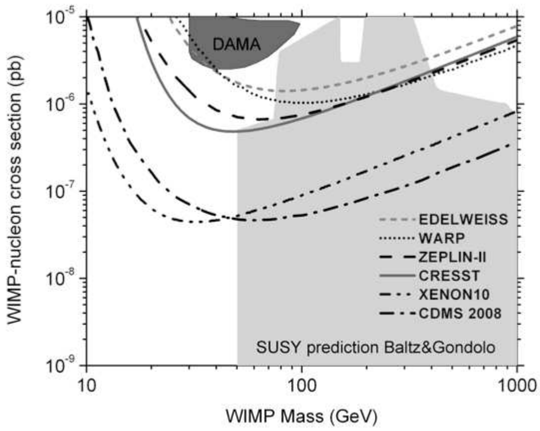

Figure 4: Coherent or spin-independent scattering cross section exclusion limit derived from the data of Fig. 3 using the maximum energy gap method. For comparison the limits from other experiments [2],[11],[12], [3],[13] and the range predicted by some supersymmetry models [14] are also shown.

References

[1] G. Angloher et al., Astropart. Phys. **23** (2005) 325.

[2] Z. Ahmed et al, arXiv:0802.3530v2 [astro-ph].

[3] V. Sanglard et al., Phys.Rev. **D 71** (2005) 122002.

[4] P. Meunier et al, Appl. Phys. Let. **75** (1999) 1335.

[5] G. Angloher et al., Astropart. Phys. **18** (2002) 43.

[6] G. Angloher et al., arXiv:0809.1829v1[astro-ph].

[7] R. H. Helm, Phys. Rev. **104** (1956) 1466.

[8] F. Donato, N. Fornengo and S. Scopel, Astropart. Phys. **9** (1998) 247.

[9] J. D. Lewin and P. F. Smith, Astropart. Phys. **6** (1996) 87.

[10] S. Yellin, Phys. Rev. D **66** (2002) 032005.

[11] J. Angle et al., Phys. Rev. Lett. **100** (2008) 021303.

[12] P.Benetti et al., arXiv:astro-ph/0701286v2.

[13] G. J. Alner et al., Astropart. Phys. **28** (2007) 287.

[14] E. A. Baltz and P. Gondolo: Physical Review **D 67** (2003) 063503.

[15] H. Wulandari, J. Jochum, W. Rau, F.von Feilitzsch, Astropart. Phys. **22** (2004) 313, hep-ex/0312050v2.

[16] W. Westphal et al., J. Low Temp. Phys.,**151** (2008) 824.

The Argon Dark Matter Experiment (ArDM)

Christian Regenfus[1] on behalf of the ArDM collaboration

[1]Physik-Institut der Universität Zürich, CH–8057 Zürich, Switzerland

DOI: http://dx.doi.org/10.3204/DESY-PROC-2008-02/regenfus_christian

The ArDM experiment, a 1 ton liquid argon TPC/Calorimeter, is designed for the detection of dark matter particles which can scatter off the spinless argon nuclei. These events producing a recoiling nucleus will be discerned by their light to charge ratio, as well as the time structure of the scintillation light. The experiment is presently under construction and will be commissioned on surface at CERN. Here we describe the detector concept and give a short review on the main detector components.

1 Introduction

Recent developments in noble liquid detectors give a promising outlook for this scalable technology which is favored by high scintillation and ionization yields. For the first time, a liquid xenon detector [1] is producing limits that are competitive with the currently well established dark matter searches of cryogenic semiconductor detectors [2]. Gross target masses of around 50 kg are currently employed and are pushing the effective exposures for experiments with event by event background recognition into the range of 100 kg·d. Upcoming larger noble liquid experiments [3, 4, 5] will naturally have to fight more and more background events, not only for the feedthrough in the phase space of the data but also in terms of maximal tolerable trigger rates. However, selfshielding should improve performance for larger and larger target sizes, which is one of the strongest motivations to go to large masses. Above all, the number of single scattering neutrons can then be determined (on a statistical base) from the distribution of multiple interacting neutrons of a given background spectrum. Figure 1 shows the frequency distribution of neutron interactions on the example of the ArDM geometry [6].

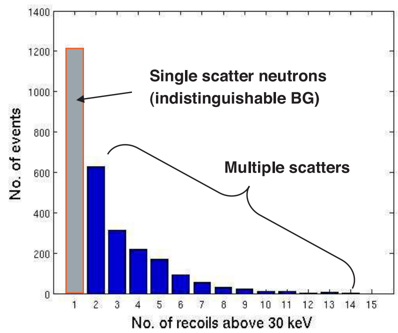

Figure 1: Interaction multiplicity of background neutrons in ArDM (MC).

The best recognition of electron recoils (usually background) should generally be achieved in a two phase configuration of a noble liquid detector allowing for the multiplication and hence the measurement of small ionization charges. In the case of liquid argon, both, the scintillation light to charge ratio and the temporal structure of the light emission itself [7, 8, 9] can be used for electron recoil discrimination. This is due to the ionization-density-dependent population of the two ground states of argon excimers ($^1\Sigma_u^+$ and $^3\Sigma_u^+$) which are responsible for the VUV luminescence of liquid argon. The large ratio of their radiative lifetimes ($\approx 10^2$) allows for a good discrimination between electron and nuclear recoils, even at energies below 20 keV on the electron equivalent scale [10]. A drawback of the argon technology is the short wavelength of the scintillation light (128 nm) and the presence of the ^{39}Ar β-emitter. However, because of form factors, argon is less sensitive to the threshold of the nuclear recoil energy, than is e.g. xenon. For the same reason the recoil energy spectra of argon and xenon are quite different. These liquids are therefore complementary in providing a crosscheck once a WIMP signal has been found.

2 Conceptual design

The main design goal of the ArDM project [5] was the construction of a ton scale liquid argon detector for spectroscopy of nuclear recoils above 30 keV. Three dimensional imaging and event by event interaction type identification will be used to reach a very high background suppression. An estimate of the final sensitivity and its extrapolation to larger LAr projects is one of the main subjects of this R&D program which is a prototype unit for future large LAr detectors. With current MC calculations we expect a sensitivity in the range of $10^{-44}\,\mathrm{cm}^2$ for a measurement of the spin independent cross section for weakly interacting dark matter particles.

In liquid argon about 400 VUV photons and a few free elementary charges[1] are typically produced in a WIMP interaction at 30 keV. Background rejection will be achieved by the combination of cuts on the fiducial volume, the event topology (e.g. no multiple scatter), the scintillation light to charge ratio, and the temporal structure of the light emission. This requires a large homogeneous electric field over the full detector volume, a large area position sensitive charge readout (3rd dimension from drift time), a large area light readout with good time resolution, and an efficient liquid argon purification system. The event trigger is generated by the fast light signal. Figure 2 shows a sketch of the two-phase operating mode of the detector. An interaction in the liquid produces VUV radiation (128 nm) by a complicated process of excitation and ionization of argon atoms, which results in the formation and subsequent radiative decay of the argon excimers [8]. This light can not be absorbed by neutral argon atoms and hence propagates to the side walls of the experiment which are coated with the wave shifting material tetraphenylbutadiene (TPB). The VUV light is absorbed and re-emitted with high efficiency at wavelengths around 430 nm, which is a region of high quantum efficiency of standard bialkali photomultipliers (PMTs). By diffusive reflection on the side walls, the light is transported to the bottom of the apparatus where an array of 14 hemispherical 8" PMTs is located. The strong electric field is capable of preventing free electrons in the densely ionized region around a nuclear recoil from recombining and sweeps them to the surface of the liquid. Here there they are extracted into the gaseous phase and multiplied ($\approx 10^4$) in the high field regions ($\approx 30\,\mathrm{kV/cm}$) of a rigid large gas electron multiplier (LEM) which extends over the full detector surface.

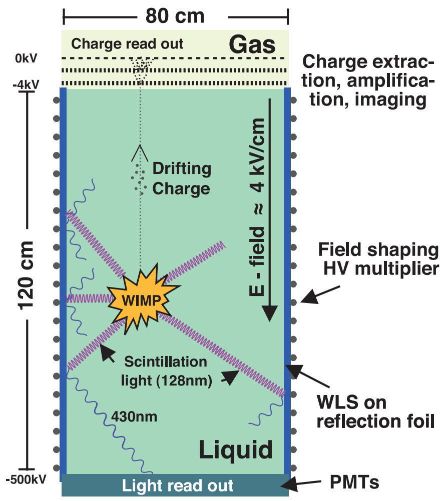

Figure 2: Conceptual design of ArDM.

[1]if the electrical field is above 1 kV/cm

3 Main experimental components and status

Figure 3 left shows the mechanical arrangement of the cryogenic cooling and cleaning system together with the main stainless steel dewar (containing roughly 1800 kg of liquid argon). An inner cylindrical volume of 80 cm diameter and 120 cm height is delimited by round ring electrodes (field shapers). It is instrumented and used as a 850 kg active LAr target in a vertical TPC configuration (Fig. 3 right). The field shaper rings are connected to a HV diode-capacitor charge pump system (Cockroft-Walton circuit) which is fully immersed in the liquid argon. It consists of 210 stages and is designed to reach a voltage of -500 kV at its end creating an approximately 4 kV/cm vertical electric field. This design avoids an electrical HV feedthrough

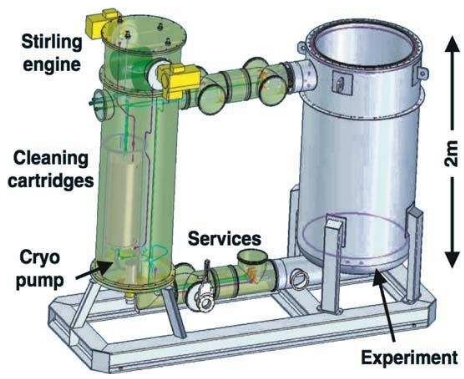

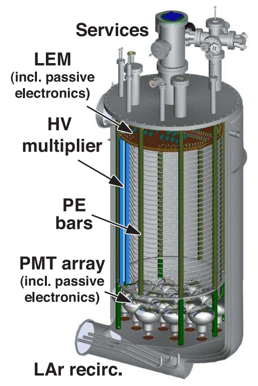

Figure 3: Left: 3D drawing of cryo-system and main dewar, right: view inside the main dewar with arrangement of the detector components hanging from the top flange on polyethylene bars.

into the liquid phase, as well as a (lossy) voltage divider. The system was tested successfully and takes advantage of the high dielectric breakdown voltage of liquid argon.

Another unique feature of the experiment is the realization of charge readout by a two-stage LEM manufactured by standard printed circuit board (PCB) methods. It will be placed 5 mm millimetres above the liquid level in the argon gas. It consists of two 1.6 mm thick 3 mm spaced Vetronite boards with holes of 0.5 mm diameter and a readout anode. A stable overall gain of 10^3 is routinely attained by prototypes. The positional readout is achieved by segmenting the upper LEM surface and the anode plate with 1.5 mm wide x and y-strips respectively. In total there are 1024 readout channels which are AC coupled to charge sensitive preamplifiers located externally on the top flange of the apparatus. Because it is operated in pure argon gas, which cannot quench charge avalanches, the LEM is built with considerable attention to HV discharges.

The readout for the 128 nm scintillation light was designed with the constraint that large VUV sensitive photosensors (e.g. MgF_2 windowed PMTs) are commercially not available. To keep the system simple and scalable, we chose an approach similar to a light diffusion cell with an array of PMTs in the liquid argon at the bottom (Figure 4). To shift the light into the range of high quantum efficiency of the borosilicate windowed bialkali PMTs, we evaporated a thin layer ($\approx$1 mg/cm^2) of tetraphenylbutadiene (TPB) onto the 15, cylindrically arranged, 25 cm wide reflector sheets which are located in the vertical electric field. These sheets, which are made out of the PTFE fabric Tetratex^{TM} (TTX), are clamped to the upper- and lowermost field shaper rings. The Hamamatsu PMTs R5912-02MOD-LRI, sensitive to single photons, are made from particularly radiopure borosilicate glass and feature bialkali photocathodes with Pt-underlay for operation at cryogenic temperatures. This ineluctably reduces their quantum efficiency by roughly one third to a value of approximately 15% [11]. The PMT glass windows are also coated with TPB to convert directly impinging VUV photons. The average number of detected photoelectrons per produced 128 nm photon of the overall detector is currently under investigation. From laboratory measurements we expect a value around 2-5%. The development of this light detection system and particularly the operation of (gaseous) argon test cells with α particle excitation were described in earlier work [12, 13]. A more detailed description of the present experimental state can be found in [14].

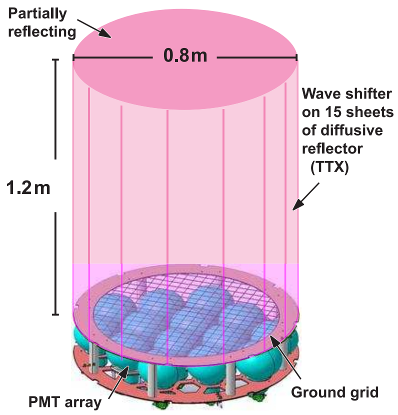

Figure 4: ArDM light diffusion cell.

Outlook

While R&D work for sub detector parts is finalizing, the main mechanical components are set together on surface at CERN, allowing for their commissioning. Following a successful operation at surface and later on at shallow depth (CERN), we consider a deep underground operation.

Acknowledgements

This work is supported by grants from the Swiss National Science Foundation and ETH Zürich.

References

[1] J. Angle *et al.* (XENON10 collaboration), Phys. Rev. Lett. 100, 021303 (2008).
[2] Z. Ahmed *et al.* (CDMS collaboration), arXiv:0802.3530v2 [astro-ph] (2008).
[3] XENON100 server at Univ. of Zürich, http://www.physik.uzh.ch/groups/groupbaudis/xenon/
[4] WARP: Experimental Proposal (2004) http://warp.lngs.infn.it/papers/proposal.pdf
[5] ArDM, A.Rubbia J. Phys. Conf. Ser. 39: 129-132,2006
[6] L. Kaufmann, Doctoral thesis, ETH IPP (2008)
[7] S. Kubota et al., J. Phys. C 11, 2645 (1978)
[8] M. Suzuki et al., NIM 192, 565 (1982)
[9] A. Hitachi et al., Phys. Rev. B 27, 9, 5279 (1983)
[10] W. Lippincott *et al.*, Phys. Rev. C 78, 035801 (2008).
[11] A. Bueno *et al.*, JINST 3 P01006 (2008)
[12] C. Regenfus, Proc. of the sixth Int. workshop on the identification of dark matter (IDM2006), Rhodes, Greece 11-16 September 2006, page 325, World Scientific 2007
[13] C. Amsler *et al.*, JINST 3 P02001 (2008)
[14] V. Boccone, Proc. of the International Conference on Calorimetry in High Energy Physics (CALOR08), Pavia, Italy 26-30 May 2008, to be published in: Journal of Physics Conference Series (JPCS)

Head-Tail in the DRIFT-II Dark Matter Detector

N.J.C. Spooner[1] on behalf of the DRIFT Collaboration

[1]Department of Physics and Astronomy, University of Sheffield, Sheffield, S3 7RH, UK.

DOI: http://dx.doi.org/10.3204/DESY-PROC-2008-02/spooner_neil

We introduce the concepts and techniques relevant to determining evidence for the so-called Head-Tail asymmetry from neutron-induced nuclear recoil tracks in the DRIFT-II dark matter detector. The back-to-back dual TPC arrangement in DRIFT makes this detector ideal for Head-Tail tests, allowing systematic errors to be reduced. The detection of Head-Tail asymmetry can open a powerful new means of searching for a galactic signature from WIMPs.

1 Introduction

A world-wide effort to observe WIMP-induced nuclear recoils in terrestrial materials is underway [1]. Annual modulation [2] provides one route towards a galactic signature based on the non-terrestrial nature of WIMPs but it is known that a more powerful galactic signal, impossible to mimic by terrestrial backgrounds, could come from a device capable of tracking the direction of WIMP-induced recoil ions, down to low (∼1 keV/amu) energies, event by event [3]. The only method established for observing these powerful but difficult to extract signatures, is to use a low density, large volume, target with sufficient spatial resolution to do the necessary tracking [4]. The DRIFT (Directional Recoil Identification From Tracks) experiment at Boulby mine [5], is designed to achieve this using a low pressure CS_2 gas Negative Ion Time Projection Chamber (NITPC) [6]. Previous studies have shown that only ∼100 WIMP events are, in principle, needed to demonstrate the galactic nature of such a range component signature [7]. However, reconstruction of the full recoil direction vector, to distinguish the "tail" from the "head", as opposed to the direction axis alone, critically influences this sensitivity, lowering the required number of events to ∼10. Confirmation that this is possible would open prospects for a new generation of experiment sensitive to the galactic WIMP velocity distribution.

To achieve this signature requires measurement of the variation in ionization density along the track. Based on use of a 1 m^3 DRIFT module with realistic energy threshold and size for WIMP searches, we present here a new technique for achieving such a measurement. Results from application of the methods introduced here will be published in the near future. The technique is based on measuring the integrated ionization loss split between the head and tail of sulfur recoil tracks down to 1.5 keV/amu, induced by ^{252}Cf neutrons [8]. We show how the energy loss can be measured and hence how it is possible to measure track orientation.

2 DRIFT concept and dead-tail experiment

The idea behind DRIFT is to make use of the Earth's motion through the stationary Galactic WIMP halo which will tend to produce a WIMP wind from the direction Cygnus, declination $\sim 45°$. Recoil tracks produced will preferentially be aligned with this wind vector [3]. A detector on Earth at a latitude $\sim 45°$, like Boulby, will thus see the WIMP wind vector oscillate over a sidereal day, from pointing south to pointing to the Earth's center, repeating each sidereal day and going rapidly out of phase with the terrestrial day. The recoils produced are extremely low energy with the electronic stopping power, energy loss to electrons, expected to decrease from tail to head [9], (more ionization at the tail than head). However, as the ion slows the energy loss to nuclear recoils also becomes important. Also, ions at the end of their range scatter frequently and so tend to ball up, losing their last energy over a small region, possibly creating an ionization spike at the track-head, observable depending on the topology relative to the readout [10]. Even if these effects yield a theoretical head-tail asymmetry, the detector resolution and diffusion to a readout could swamp the effect.

Descriptions of the DRIFT-II design, operation and analysis are given in [11, 12], the specific module used here, DRIFT-IIc, being essentially identical to IIa,b. The device comprises a 1.5 m^3 low background stainless steel vessel filled with 40 Torr CS_2 and containing two identical back-to-back TPCs with a common 1 m^2 central cathode plane. Recoil events can form in two identical drift regions of 1 m^2 by 50 cm depth. Ionization tracks are drifted in each TPC away from the central cathode, to be read out by either of two MWPCs. We defined here the direction perpendicular to the MWPCs as the z-direction, this being horizontal, the +z direction defined as left to right viewed from the front with the origin on the central cathode. Each MWPC comprises 448 grid (y-direction) and 448 anode wires (x-direction) of 2 mm pitch, grouped into 8 signal lines per readout plane. 52 wires at the edges provide veto signals against, for instance, alphas [12]. The fiducial volume is 0.80 m^3 (134 g of CS_2) and each drift volume has a retractable ~ 100 μmCi ^{55}Fe source for gain monitoring.

The head-tail technique here is based on use of a 202 μCi ^{252}Cf source to produce neutrons headed in the +x, -y, +z and -z directions. Simulations [13] have shown such exposures mimic WIMPs quite well. For instance, Figure **??** compares the S recoil spectrum from ^{252}Cf neutrons (using GEANT) and 1000 GeV WIMPs. Thus the head-tail signature in either +z or -z neutron exposure, should if present be seen through production of a different degree of ionization at the head or tail revealed as an asymmetry in the time distribution of ionization arrival at the MWPC planes. For instance, if the effect produces more ionization at the head then for a -z directed neutron run, events on the right TPC will have, on average, more ionization earlier than later. Events on the left TPC will have the reverse. For the +z run the effect will be opposite. For x and y runs, with neutrons parallel to the MWPCs, the ionization on average will appear the same at the beginning and end.

3 Head-tail analysis procedure

A simple event-by-event analysis has been developed to quantify this, where the voltage integral over the first and second half of each accepted ionization time profile is calculated and the ratio taken as an asymmetry measure. In DRIFT, the voltage integral is proportional to the Number of Ionizing Pairs (NIPs), convertible to event energy using source calibrations. For instance, 1000 NIP S recoils have energies of 47 keV [13]. We thus introduce a so-called asymmetry quantity given by: $NIPsRatio = NIPs_1/NIPs_2$, where indices refer to the first and second half of the pulse. Determination of NIPsRatio follows by locating the highest voltage and using this to find the first time that the waveform crosses 25% of this value on either side (to minimizes potential biases from waveform noise and baseline shifts). The middle of the track is defined as midway between these times. NIPs_1 is the integral voltage above 25% of the peak value at minimum time to the middle and NIPs_2 the integral from there to 25% of peak value at maximum time. Prior to this a first stage analysis is used to extract the recoil signals from unwanted backgrounds, like sparks and alphas see [14] and for general concepts see [15]. Figure 2 shows a typical NIPs energy spectrum for neutron-induced S recoils selected by the analysis. Here, the hardware threshold and the analysis cuts produced an effective threshold of $\sim$1000 NIPs, 47 KeV S recoil [13].

Experiments can proceed using this technique with neutrons alternately directed along the +x, -y, +z and -z directions. For a given number of events passing cuts for each exposure and direction, the means of the NIPsRatio distribution for left and right TPC can be recorded along with their difference and the significance (difference divided by combined error). It is expected, for instance, that for the +x run the average NIPsRatio=1.0 since equal numbers of events are headed towards or away from the detectors. It is likely however that in practice the mean ratio is not 1.0 because there will be amplifier overshoot that tends to shorten the second half of the event. However, because we have two detectors, identical except for the opposing electric drift fields, with identical electronic shaping on both sides, the left and right mean NIPsRatios should be in statistical agreement. The +y run should show the same result within the errors. The technique will then allow the +z run to be compared with the +x and -y runs to determine whether the events on the left side have, for instance, a larger NIPsRatio and events on the right, smaller. The sign here is of course a signature that indicates if there is more ionization at the tail than head or vice-versa. As a check the -z run results for the left should agree with those for the right from the +z run.

As a better measurement of the effect events on the left(right) of the +z(-z) runs for which the NIPsRatio measures the ratio of the ionization at the head of the track to the tail, can be combined, as also for the events on the right(left) of the +z(-z) runs for which the NIPsRatio measures the ratio of the ionization at the head to the tail. The difference in these average ratios can be used as a better measure of the effect. As a further check the same procedure can be applied to the +x and -y runs, where a null result is expected.

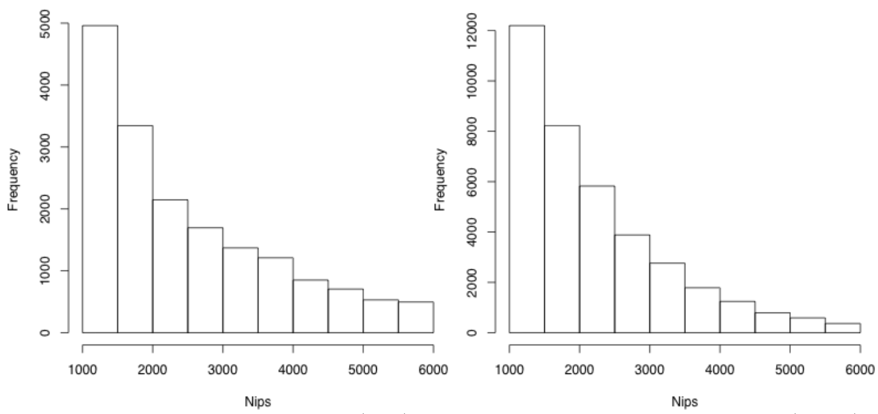

Figure 1: Predicted NIPs spectrum for (left) neutron induced S recoils; and (right) from 1000 GeV WIMPs (using GEANT).

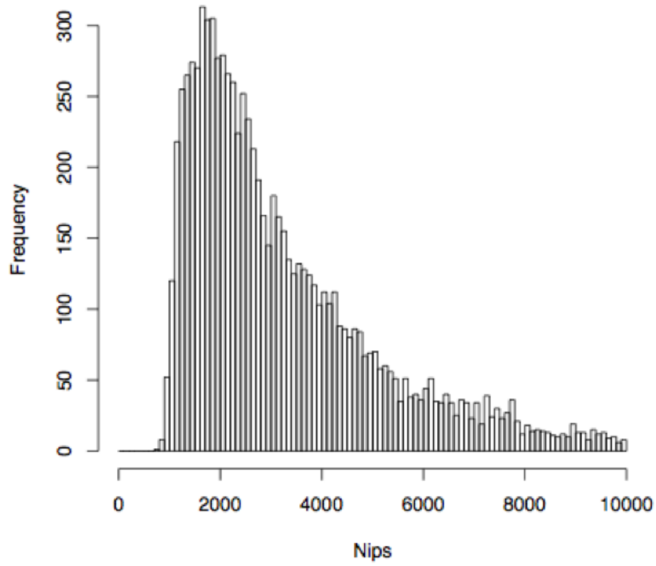

Figure 2: Example neutron S recoils NIPs spectrum.

4 Conclusion

In summary, we have developed a new technique for determining the existence or not of a head-tail asymmetry in nuclear recoils at low energy in DRIFT. The DRIFT II detector is designed well for this type of measurement since it comprises two detectors identical except for the direction of the drift field. Results form a directed neutron run using the technique are expected to be published soon [16]. We thank J. Martoff for useful discussions, CPL for access to Boulby and NSF and ILIAS EU contract RII3-CT-2004-506222 for support.

References

[1] N.J.C. Spooner, J. Phys. Soc. Japan, 76 (2007) 11101

[2] R. Bernabei et al., arXiv:0804.2741v1

[3] D.P. Snowden-Ifft, et al., Phys. Rev. D61 (2000) 101301

[4] G.J.Alner et al., Nucl. Instr. and Meth. A535 (2004) 644

[5] E. Tziaferi et al., Astropart. Phys. 27 (2007) 326

[6] S. Burgos et al., Astropart. Phys. 28 (2007) 409

[7] B. Morgan et al., Phys. Rev. D71 (2005) 103507

[8] N.J.C. Spooner (for DRIFT), Proc. 6th Int. Heidelberg Conf, Ed. H.V. Klapdor-Kleingrothaus, WS (2008) 104

[9] A. Hitachi, Rad. Phys. Chem. (2008), arXiv:0804.1191

[10] P. Majewski et al., Astropart. Phys. arXiv:xxx

[11] G.J. Alner et al., Nucl. Instr. and Meth. A555 (2005) 173

[12] S. Burgos et al., Nucl. Instr. and Meth. A584 (2008) 114

[13] D.P.Snowden-Ifft et al., Nucl. Instr. and Meth. A498 (2003) 155

[14] S. Burgos et al., Astropart. Phys. arXiv:xxx

[15] D. Muna, PhD. Thesis, University of Sheffield (2008)

[16] S. Burgos et al. arXiv:0809.1831 (2008)

Chapter 5

Laboratory Searches for Axions and WISPs

LIPSS Results for Photons Coupling to Light Neutral Scalar Bosons

Andrei Afanasev[1], *Oliver K. Baker*[2], *Kevin Beard*[3], *George Biallas*[4] *James Boyce*[4], *Minarni Minarni*[5], *Roopchan Ramdon*[1], *Michelle Shinn*[4] *and Penny Slocum*[2]

[1]Department of Physics, Hampton University, Hampton, VA 23668
[2]Department of Physics, Yale University, P.O. Box 208120, New Haven, CT 06520
[3]Muons, Inc., 552 N. Batavia Avenue, Batavia, IL 60510
[4]FEL Division, Jefferson Laboratory, 12000 Jefferson Avenue, Newport News, VA 23606
[5]Department of Physics, Universitas Riau (UNRI), Pekanbaru, Riau 28293 Indonesia

DOI: http://dx.doi.org/10.3204/DESY-PROC-2008-02/baker_keith

The LIPSS search for a light neutral scalar boson coupling to optical photons is reported. The search covers a region of parameter space of approximately 1.0 meV and coupling strength greater than 10^{-6} GeV^{-1}. The LIPSS results show no evidence for scalar coupling in this region of parameter space.

1 Introduction

Several theories in particle physics as well as cosmology predict the existence of at least one scalar, that is, spin-zero, boson [1, 2, 3, 4, 5, 6, 7, 8]. Many theories of physics beyond the SM (BSM) can accommodate scalars with very small masses and weak couplings to SM fields [9, 10, 11]. For the latter, there is renewed interest in experimental searches for sub-electron volt mass, spin-zero, weakly interacting particles, triggered in large part by the recent PVLAS collaboration claims [12], now disclaimed [13], of an anomalous rotation of polarized laser light when it propagates through a magnetic field. The experimental programs that explore the parameter space of weakly interacting, light, spin-zero, bosons by and large all use the "light shining through a wall" (LSW) technique of photon regeneration [14]: laser photons are sent through a strong magnetic field where some of them can convert into low-mass, weakly interacting bosons. These bosons then pass through a wall that serves to block the incident laser light, and reconvert into photons in a second magnetic field in a similar manner.

The Light Pseudoscalar and Scalar Particle Search (LIPSS) collaboration searched for evidence of photons coupling to light, neutral bosons (LNBs) in a series of measurements that took place at Jefferson Lab (JLab) in the Spring of 2007. The results reported here are the LIPSS collaboration's direct search for the scalar coupling of photons to a hypothetical LNB in an LSW experiment. This is contrasted to the search for pseudoscalar couplings between photons and a LNB that has already recently been reported by the BMV collaboration [15], and as carried out originally by the BFRT collaboration [16]. The GammeV collaboration at Fermi National Accelerator Laboratory (FNAL) [17] and the OSQAR collaboration at the European Center for Nuclear Research (CERN) [18] reported first results for both scalar and pseudoscalar couplings to photons in this same region of coupling-mass parameter space. It is to be emphasized that the LIPSS collaboration took data using near-infrared photons continuously over extended periods as compared with the previously reported LSW experiments. Thus, it is most sensitive to phenomena discussed in the context of hypothetical chameleon particles [19]. The limits presented here can also be compared with the results from the CAST collaboration [20] that searches for solar produced axions (light, weakly interacting, pseudoscalar bosons, [6]) using the regeneration technique, to sensitive searches for dark matter halo axions in the galaxy [21], and to constraints on BSM couplings and masses from tests of the gravitational inverse-square law [22].

2 Experimental setup and data analysis

The experimental setup is described in [23]. Laser light from the JLab Free Electron Laser (FEL) facility was used over a period of one week of running. The FEL creates light that is more than 99.9% linearly polarized in pulses that are 150 fs long with a repetition rate of up to 75 MHz. For the LIPSS runs, it was tuned to a wavelength of 0.935 ± 0.010 microns with an intensity of 180 watts on average.

The LIPSS beam line consists of an upstream (generation) magnetic field region and an identical (regeneration) magnetic field region placed downstream of it. Between the generation and regeneration magnets is an optical beam dump that also serves as a power meter; the beam dump in combination with a stainless steel vacuum flange on the input to the downstream beam line blocks all incident FEL light from the regeneration magnet. Both generation and regeneration magnets had dipole fields of 1.77 ± 0.04 Tesla and effective lengths of 1.01 ± 0.02 meters. In all of the results presented here, the laser light polarization direction was perpendicular to the magnetic field; the experiment was therefore sensitive to scalar (positive parity) couplings between photons and LNBs.

The camera system was a Princeton Instruments Spec-10:400BR with WinView32 software. It consisted of a back-illuminated CCD with 1340×400 pixels imaging area (a single pixel was $20\ \mu \times 20\mu$ in area). The CCD array was cooled to -120^o C resulting in a typical dark current of less than one single electron per pixel per hour. Stray light from all sources was shown to be less than one count per pixel per hour during the experiment. The read noise was determined to be 2.7 ± 0.2 counts per pixel per readout. Cosmic rays (CRs) that strike the pixel array leave clear ionization signals in the pixels that they strike and are easily subtracted from the data. Runs that contain a CR hit on any pixel within an area of 100×100 pixels around the signal region were discarded.

The data were analyzed by defining a signal region where any regenerated photons would be observed, and background regions where no signal was expected. The signal region for the pixel array was taken to be a 3×3 pixel area at the aligned-beam location. Tests performed subsequent to the data runs confirmed that the beam focus on the signal region wandered by at most one pixel vertically and horizontally; the 3×3 pixel area defined as the signal region did not change during the data runs.

The nine pixels in the signal area were binned together in software for each run. All other pixels and pixel groupings outside the signal region were used to define the background region(s). The difference between the counts in the signal region and the counts in the background region (normalized to the number of pixels in the signal region) was determined for all data runs [24]. No excess events above background were seen in any single run, or if all runs were combined.

3 Results and conclusions

The rate of regenerated photons is given by [14]

$$\mathrm{R} = \mathrm{r}_\gamma\ \mathrm{P}_{\gamma\to\mathrm{LNB}}\ \mathrm{P}_{\mathrm{LNB}\to\gamma}\ \frac{\Delta\Omega}{\Omega}\ \epsilon_\mathrm{c}\ \epsilon_\mathrm{d} \tag{1}$$

where r_γ is the FEL (incident) photon rate, $\Delta\Omega$ is the solid angle for detection, ϵ_c is the photon collection efficiency, ϵ_d is the detector quantum efficiency, and

$$\mathrm{P}_{\gamma\to\mathrm{LNB}} = \mathrm{P}_{\mathrm{LNB}\to\gamma} = \frac{(\mathrm{gB})^2}{\frac{\mathrm{m}^4}{4\omega^2}}\ \sin^2\left(\frac{\mathrm{m}^2\mathrm{L}}{4\omega}\right) \approx \frac{1}{4}(\mathrm{gBL})^2 \tag{2}$$

is the probability of scalar boson generation from the incident photons for magnets not too long for a given wavelength of light; photon regeneration from these scalar particles is given by the identical expression as shown. Here ω is the photon energy, m (g) is the LNB mass (coupling strength to photons), and B (L) is the magnetic field strength (length). The significance of the result is defined as $\mathrm{S} = \mathrm{signal}/\sqrt{\mathrm{background}}$ where signal is the number of events expected based upon Equation (1) and that would show up in the signal region as described above. The results indicate no coupling of photons to a LNB at any significance..

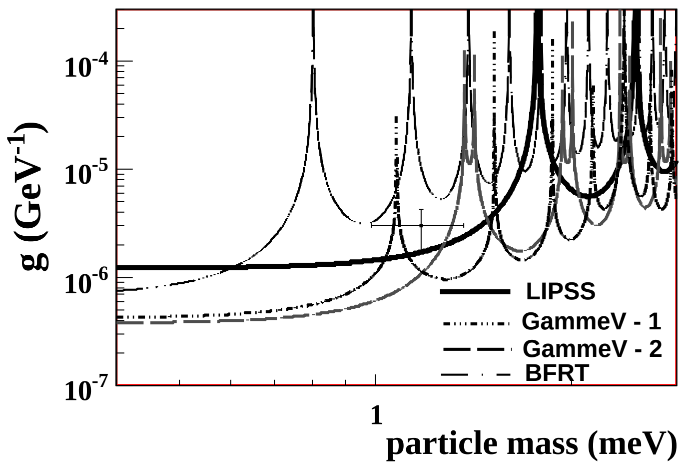

Figure 1: The new LIPSS limits on scalar coupling, g, of photons to a hypothetical LNB (in inverse giga-electron-volts) versus the LNB mass in milli-electron-volts. The curves show the LIPSS result for a significance of 2.2 (full) along with the results from previous measurements at different photon energies: GammeV-1 (using magnet lengths 5.0 m and 1.0 m), GammeV-2 (using magnet lengths 3.1 m and 2.9 m), and BFRT, as indicated. The data point is the region claimed (now disclaimed) by the PVLAS collaboration [12, 13]. The LIPSS photon energy was 1.33 eV while those of GammeV and BFRT were 2.34 eV and 2.44 eV, respectively.

The results from this run can therefore be used to set the new limits on the scalar coupling of photons to a hypothetical LNB shown in Figure 1. This represents the most stringent limits to date on this scalar coupling in a generation-regeneration experiment in this range of parameters for a long, continuously-running LSW experiment using optical photons. The region above the S=2.2 (full) is ruled out in the present experiment. These are similar limits already set by the BMV [15], BFRT [16], GammeV [17], and OSQAR [18] collaborations for pseudoscalar and scalar couplings, but under slightly different LSW experimental conditions. The LIPSS measurement was made with photons closest to that of the original PVLAS wavelength. This result therefore would rule out any energy dependence of the result at this level for this energy range.

4 Acknowledgments

The authors thank the technical staff of the JLab FEL Division, especially F. Dylla, G. Neil, G. Williams, R. Walker, D. Douglas, S. Benson, K. Jordan, C. Hernandez-Garcia, and J. Gubeli, as well as M.C. Long of Hampton University for their excellent support of the experimental program. Funding from the Office of Naval Research Award N00014-06-1-1168 is gratefully acknowledged.

References

[1] M. Ahlers *et. al.*, Phys. Rev. D**75**, 035011 (2007); A. Ringwald, J. Phys. Conf. Ser. **39**, 197 (2006).

[2] J. Khoury and A. Weltman, Phys. Rev. Lett. **93**, 171104 (2004), Phys. Rev. D**69**, 044026 (2004); D.F. Mota and D.J. Shaw, Phys. Rev. D**75**, 063501 (2007), Phys. Rev. Lett. **97**,151102 (2006).

[3] Ph. Brax, C. van de Bruck, A.-C. Davis, J. Khoury, and A. Weltman, Phys. Rev. D**70**, 123518 (2004); Ph. Brax, C. van de Bruck, A.-C. Davis, J. Khoury, and A.M. Green, Phys. Lett. B**633**, 441 (2006).

[4] K. Choi, Phys. Rev. D **62**, 043509 (2000).

[5] I. Waga and J. Frieman, Phys. Rev. D**62**, 043521 (2000); J. Frieman *et. al.*, Phys. Rev. Lett. **75**, 2077 (1995); J.A. Frieman, C.T. Hill, and R. Watkins, Phys. Rev. D**46**, 1226 (1992).

[6] R.D. Pecci and H.R. Quinn, Phys. Rev. Lett. **38**, 1440 (1977); Phys. Rev. D**16**, 1791 (1977); S. Weinberg, Phys. Rev. Lett. **40**, 223 (1978); F. Wilczek, Phys. Rev. Lett. **40**, 279 (1978).

[7] G.G. Raffelt, in W.-M. Yao *et. al.*, (Particle Data Group), J. Phys. G**33**, 1 (2006).

[8] P.W. Higgs, Phys. Lett. **12**, 132 (1964).

[9] B. Holdom, Phys. Lett. B**166**, 196 (1986); R. Foot and X. G. He, Phys. Lett. B**267**, 509 (1991); K.R. Dienes *et. al.*, Nucl. Phys. B**492**, 104 (1997); S.A. Abel and B.W. Schofield, Nucl. Phys. B**685**, 150 (2004); L.B. Okun, Sov. Phys. JETP **56**, 502 (1982).

[10] J. Jaeckel and A. Ringwald, Phys. Lett. B**659**, 509 (2008); M. Ahlers *et. al.*, Phys. Rev. D**77**, 095001 (2008).

[11] V.V. Popov and O.V. Vasil'ev Europhys. Lett. **15**, 7 (1991); D. Maity, S. Roy, and S. SenGupta, Phys. Rev. D**77**, 015010 (2008).

[12] E. Zavattini *et. al.*, Phys. Rev. Lett. **96**, 110406 (2006).

[13] E. Zavattini *et. al.*, Phys. Rev. D**77**, 032006 (2008); http://axion-wimp.desy.de/index_eng.html (2007).

[14] K.V. Bibber *et. al.*, Phys. Rev. Lett. **59**, 759 (1987).

[15] C. Robilliard *et. al.*, Phys. Rev. Lett. **99**, 190403 (2007).

[16] R. Cameron *et. al.*, Phys. Rev. D**47**, 3707 (1993).

[17] A.S. Chou *et. al.*, Phys. Rev. Lett. **100**, 080402 (2008); GammeV collaboration http://gammev.fnal.gov.

[18] R. Ballou *et. al.*, CERN Report CERN-SPSC-2007-039 (2007); SPSC-M-762 (2007).

[19] M. Ahlers *et. al.*, Phys. Rev. D**77**, 015018 (2008); H. Gies *et. al.*, Phys. Rev. D**77**, 025016 (2008).

[20] S. Andriamonje *et. al.*, J. Cosmol. Astropart. Phys. **04**, 010, (2007).

[21] R. Bradley *et. al.*, Rev. Mod. Phys. **75**, 777 (2003); P. Sikivie, Phys. Rev. Lett. **51**, 1415 (1983).

[22] G.L. Smith *et. al.*, Phys. Rev. D**61**, 022001 (2000); R. Schlamminger *et al.*, Phys Rev. Lett. **100**, 041101 (2008); A. Dupays, E. Masso, J. Redondo, and C. Rizzo, Phys. Rev. Lett. **98**, 131802 (2007).

[23] LIPSS collaboration, Phys. Rev. Lett. (accepted for publication) (2008).

[24] K.B. Beard, Jefferson Laboratory Technical Note, JLAB-TN-07-012 (2007).

GammeV: Fermilab Axion-like Particle Photon Regeneration Results

William Wester

Fermilab, MS222, Batavia IL, USA
presented on behalf of the GammeV *Collaboration*

DOI: http://dx.doi.org/10.3204/DESY-PROC-2008-02/wester_william

GammeV is an axion-like particle photon regeneration experiment conducted at Fermilab that employs the light shining through a wall technique. We obtain limits on the coupling of a photon to an axion-like particle that extend previous limits for both scalar and pseudoscalar axion-like particles in the milli-eV mass range. We are able to exclude the axion-like particle interpretation of the anomalous PVLAS 2006 result by more than 5 standard deviations.

1 Introduction

The question, *What are the particles that make up the dark matter of the universe?*, is one of the most fundamental scientific questions today. Besides weakly interacting massive particles (WIMPs) such as neutralinos, axion-like particles or other weakly interacting sub-eV particles (WISPs) are highly motivated dark matter particle candidates since they have properties that might explain the cosmic abundance of dark matter. The milli-eV mass scale is of particular interest in modern particle physics since that mass scale may be constructed with a see-saw between the Planck and TeV mass scales, and may be related to neutrino mass differences, the dark energy density expressed in (milli-eV)^4, and known dark matter candidates such as gravitinos and axion-like particles. In 2006, the PVLAS experiment reported [1] anomalous polarization effects in the presence of a magnetic field including polarization rotation and ellipticity generation that could be interpreted as being mediated by an axion-like particle in the milli-eV mass range with a unexpectedly strong coupling to photons. It is noted that additional data recorded by PVLAS no longer observe the anomalous effects [2].

A previous laser experiment conducted in the early 1990's by a collaboration Brookhaven, Fermilab, Rochester, and Trieste (BFRT) used a "light shining through a wall" (LSW) [3] technique to set limits on sub-eV axion-like particles [4]. However, their utilization of existing 4.4m long magnets happened to result in a minimum with no sensitivity for an axion-like particle in the mass range suggested by the anomalous PVLAS result. The GammeV experiment [5] has been proposed to examine the milli-eV mass scale for an axion-like particle that couples to photons to resolve the possible mystery of the anomalous PVLAS result and to extend the search for an axion-like particle in the milli-eV mass scale.

2 GammeV apparatus

The GammeV apparatus is shown schematically in Fig. 1 and is used in a LSW configuration where, in the presence of an external magnetic field, a laser photon might oscillate into an axion-like particle that can traverse a "wall" and then have a small probability to regenerate back into a detectable photon. The formula for the probability of this regeneration is given by the following:

$$\begin{aligned}
P_{regen} &= \frac{16B_1^2B_2^2\omega^4}{M^4m_\phi^8}\sin^2\left(\frac{m_\phi^2L_1}{4\omega}\right)\cdot\sin^2\left(\frac{m_\phi^2L_2}{4\omega}\right) \\
&= (2.25\times10^{-22})\times\frac{(B_1/\mathrm{Tesla})^2(B_2/\mathrm{Tesla})^2(\omega/\mathrm{eV})^4}{(M/10^5\ \mathrm{GeV})^4(m_\phi/10^{-3}\ \mathrm{eV})^8} \\
&\quad\times\sin^2\left(1.267\frac{(m_\phi/10^{-3}\ \mathrm{eV})^2(L_1/\mathrm{m})}{(\omega/\mathrm{eV})}\right)\sin^2\left(1.267\frac{(m_\phi/10^{-3}\ \mathrm{eV})^2(L_2/\mathrm{m})}{(\omega/\mathrm{eV})}\right)
\end{aligned}$$

where ω is the photon energy, M is a high mass scale inverse to the coupling to photons $g_{a\gamma\gamma}$, m_ϕ is the mass of the axion-like particle, and B_1, L_1, B_2 and L_2 are the magnetic field strengths and lengths in the photon conversion and regeneration regions, respectively.

The GammeV experiment utilizes two novel aspects in order to have increased sensitivity over the region of interest. The plunger is constructed so that it can place the "wall" either in the middle ($L_1 = L_2$) of the magnet or toward one end of the magnet ($L_1 \neq L_2$). This changes the magnetic baseline over which axion-like particles can be generated and regenerated back into photons which is dependent on the mass through the $\sin^2$ terms in the above formula. Thus, the regions of insensitivity will be shifted from each other when the plunger is put in two distinct positions and the entire region of interest in the milli-eV mass range can be probed with high sensitivity. The second aspect is to utilize time correlated single photon counting techniques in order to have high efficiency for signal and very low noise. In this technique, the time of each 10 ns wide laser pulse is recorded and correlated to the time of PMT pulses (also about 10 ns wide) which include dark pulses at approximately 100 Hz. The chance of a random PMT pulse being in time with a laser pulse is very small compared with the expected rate of in-time signal events if the PVLAS anomalous signal was due to an axion-like particle with large coupling to photons.

3 Calibration

GammeV recorded calibration data called the "leaky mirror" sample where the wall was removed, photons were generated from the laser, the intense laser burst was attenuated by a factor of $\sim 10^{19}$, and then single photons were recorded by the PMT. The attenuation involved shining the laser onto a highly reflective mirror - that was leaky by a factor approximately 10^{-4}. A second mirror, a 10 μm pin hole, and several neutral density filters completed the attenuation. The end result was that we could observe single photons generated by the laser, confirm the speed of light travel of those photons through the GammeV apparatus, and establish a 10 ns-wide window *a priori* for our search region since regenerated photons from an axion-like particle would have the same relative timing. By putting a polarizing filter before the PMT, we also verified that polarization of the laser light was parallel or perpendicular to the magnetic field depending on whether we inserted a 1/2-wave plate into the optical path.

We would thus be able to probe either scalar or pseudoscalar axion-like particles which differ in that the coupling requires the polarization to be aligned or perpendicular to the magnetic field.

4 Data taking and results

Data were acquired in four configurations: two polarizations and two positions of the "wall." In each configuration, approximately 20 hours of data was acquired - nearly 1.5M pulses with 4×10^{17} photons per pulse. The time of each laser pulse was recorded along with the time of each pulse detected by the PMT. In an offline analysis of the data, the timing of PMT pulses relative to the laser pulse could be examined in the temporal region where the "leaky mirror" calibration photons were also recorded. Fig. 2 shows the data recorded in the four configurations where 1, 0, 1, and 2 signal candidates are observed in the 10 ns wide search window. The expected background is obtained from the data by looking at the number of PMT pulses within 10000 ns of the laser firing and indicates that we should have expected approximately 1.5 events of expected background in each of the four configurations. Our observation of 4 signal candidates is consistent with the expectation of 6 background PMT pulses; hence, the data show no indication of regenerated photons. We use the determined efficiencies of the PMT and optical transport along with the measured laser power for each pulse to obtain the normalization on the number of incident photons and the expectation of the signal rate.

The non-observation of an excess signal allows us to set limits at 3σ of the axion-like particle coupling to photons versus the mass that extend the previously excluded region. In addition, we exclude at more than 5σ the axion-like particle interpretation of the PVLAS anomaly. Figures 3, 4 show the resulting limits for the coupling of scalar and pseudoscalar axion-like particles to photons in milli-eV mass region.

Acknowledgments

This work is supported by the U.S. Department of Energy under Contract No. DE-AC02-07CH11359. The project is made possible through the work of technical resources including a mechanical team within the Fermilab Particle Physics Division and a magnet team within the Fermilab Technical Division.

References

[1] E. Zavattini *et al.* [PVLAS Collaboration], Phys. Rev. Lett. **96**, 110406 (2006) [arXiv:hep-ex/0507107].

[2] E. Zavattini *et al.* [PVLAS Collaboration], arXiv:0706.3419 [hep-ex].

[3] K. Van Bibber, N. R. Dagdeviren, S. E. Koonin, A. K. Kerman and H. N. Nelson, Phys. Rev. Lett. **59**, 759 (1987).

[4] R. Cameron *et al.*, Phys. Rev. D **47**, 3707 (1993).

[5] A.S. Chou *et al.* [GammeV Collaboration], Phys. Rev. Lett. **100**, 080402 (2008). Additional description may be found at: http://gammev.fnal.gov.

[6] P. Sikivie, Phys. Rev. Lett. **51**, 1415 (1983) [Erratum-ibid. **52**, 695 (1984)]. P. Sikivie, Phys. Rev. D **32**, 2988 (1985) [Erratum-ibid. D **36**, 974 (1987)].

[7] C. Robilliard, it et al. [BMV Collaboration], Phys. Rev. Lett. **99**, 190403 (2007) [arXiv:0707.1296 [hep-ex]].

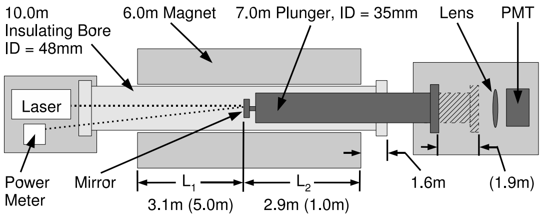

Figure 1: Schematic diagram of the GammeV experimental apparatus showing a Nd:YAG laser sending 20Hz of 10 ns wide laser pulses down the warm bore of a Tevatron dipole magnet. In either the middle of the magnet or toward one end is the "wall" which reflects the laser back onto a power meter. The "wall" is mounted on a sliding vacuum tube, the plunger, which is welded light-tight inside the magnet and which extends into a PMT dark box. If an axion-like particle did traverse the wall, it could regenerate in the plunger back into a detectable photon that could be focused onto the PMT. photocathode.

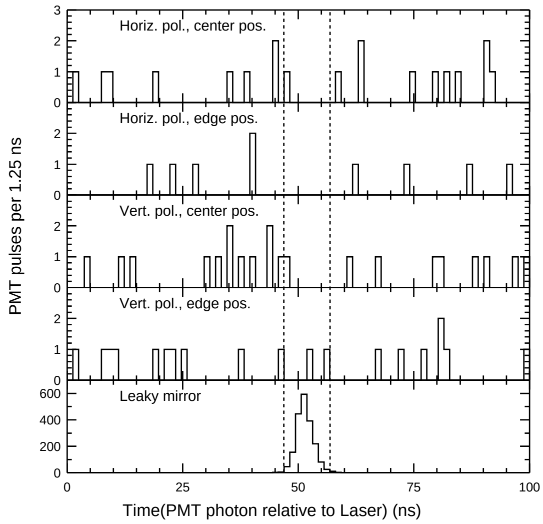

Figure 2: PMT pulse time relative to laser pulse time for the four run configurations shown relative to the expected time distribution of photons form the "leaky mirror" calibration data. The *a priori* search region for signal candidates is between the two dotted lines.

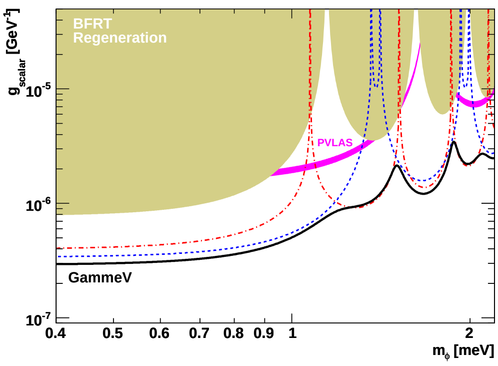

Figure 3: Exclusion region obtained by GammeV for the coupling to photons versus the mass of a scalar axion-like particle. The dashed lines show the limits obtained separately for the data recorded with the "wall" in the middle and near one end of the magnet. Also shown is the anomalous PVLAS region of interest. Finally,the shaded region indicates the previous exclusion from the BFRT.

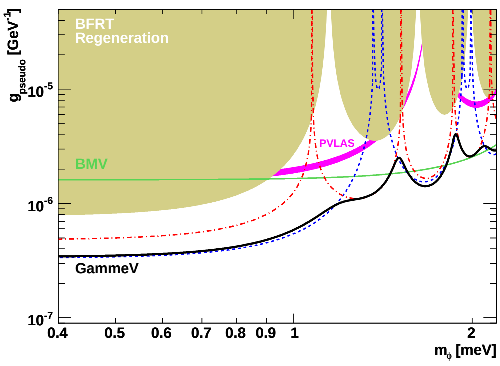

Figure 4: Exclusion region for the case that the axion-like particle couples to photons as a pseudoscalar. Also shown is a recent limit obtained by the BMV [7] experiment.

Open Access in High Energy Physics: Overview and Future Challenges

Martin Köhler

DESY, Notketraße 85, 22607 Hamburg, Germany

DOI: http://dx.doi.org/10.3204/DESY-PROC-2008-02/koehler_martin

This paper describes a business model for the 'golden' road to Open Access which is specifically tailored for High Energy Physics (HEP), but can possibly be extended to other disciplines: SCOAP^3 - the **S**ponsoring **C**onsortium for **O**pen **A**ccess **P**ublishing in **P**article **P**hysics. We also report on the status of INSPIRE, the designated successor of the well-established SPIRES database, and a complete HEP e-Infrastructure. Finally, aspects of the challenges involved in HEP data preservation are discussed.

1 Introduction to Open Access

According to Wikipedia "*Open Access* (OA) is free, immediate, permanent, full-text, online access, for any user, web-wide, to digital scientific and scholarly material." The immediate and permanent access to the full-text of (research) articles for anyone webwide is made possible by consent of the author and/or the copyright holder. One should note that the concept of OA is compatible with peer review and publishing in non OA-journals. Furthermore, OA is not free to produce and there is much debate about the economics of its funding. In general, specific business models depend on the way OA is delivered (see below). The most prominent roads to OA are *Open Access publishing* - the 'golden' road - and *Open Access self-archiving* - the 'green' road.

2 Open Access and the role of journals in the High Energy Physics community

The idea of Open Access is well known and long established in the HEP community. For over forty years, HEP institutes have shipped preprints of their authors worldwide at their own expenses. In 1991, the HEP community saw the launch of arXiv –http://xxx.lanl.gov at that time– the archetype of Open Archives. With the establishment of arXiv, OA became second nature to HEP scientists and nowadays posting on arXiv before even submitting to a journal is quite a common practice. It is worth mentioning that this process has always been purely author driven, without mandate, even without debate.

As an 'all-arXiv discipline' and due to spiralling subscription costs HEP is at a risk to see numerous journal subscriptions cancelled by large multidisciplinary university libraries (if that is not already the case). On the other hand, high quality peer-reviewed journals are the basis for academic evaluation of institutes and (young) researchers. The main role of journals is to assure high-quality peer-review and act as keepers-of-the-records.

Since OA obviously is incompatible with the traditional subscription model, publishers and customers have experimented with new OA compatible business models. In the *hybrid model*, for an additional fee in the range from $\approx 900 - 3.000$ US$, it is possible to make individual articles openly accessible. The subscription costs might get reduced, but for institutions and libraries, the hybrid model is generally more expensive than the traditional subscription model and hence has had very little success up to now. In the *sponsoring model* institutions pay for the journals through annual sponsoring fees; there are no author charges and the whole journal content is open access. Another prominent model, which is very successful in life science is the *author charge* model. Here a publishing fee is due for all accepted articles and again the whole journal is then open access.

3 The SCOAP^3 consortium

In 2008 the Large Hadron Collider (LHC) at CERN, will begin to operate. It will be the only HEP experiment worldwide of this size and most HEP publications will be related to this machine and the results of the experiments done with it. It is therefore very significant that in 2007 all the LHC collaborations, i.e. more than 5400 scientists, have signed a statement strongly encouraging the usage of electronic publishing methods and supporting the principle of Open Access. To support this goal CERN and other leading HEP laboratories, DESY among them, have started SCOAP^3, - the **S**ponsoring **C**onsortium for **O**pen **A**ccess **P**ublishing in **P**article **P**hysics. SCOAP^3 plans to make the approx. 20,000 articles/year published by the HEP community freely accessible by re-directing subscription money on a budget of approx. 10M€/year. This money will be raised from about 50 funding bodies and roughly 10 publishers will be involved[1]. Note that this scale is much smaller than that of e.g. the currently well established ATLAS HEP experiment, where the budget is approx. 400M€ and more than 1000 contracts have been signed. At the moment about 38% of the needed funds have been pledged and another 15% are coming soon. The substantial goal is to have SCOAP^3 operational for the first LHC articles.

4 HEP databases

A recent poll[2] of the HEP community with more than 2.000 participants, which is roughly 10% of the whole community has demonstrated that more than 90% of the users use community-based services, e.g. subject repositories and laboratory-supported databases. The use of Google and Google scholar correlates with experience. While almost 22% of the younger people with less than two year career experience use these database for information recovery, this drops to 6% for people with more than six years of experience. The use of (other) commercial databases is marginal. With almost 50%, the well-established SPIRES database is by far the largest of the laboratory-supported databases and was one of the first on the 'market'. It has been initially built by SLAC and is today maintained in collaboration by SLAC, DESY and FERMILAB.

While the quality of the data contained in SPIRES is undoubtedly extremely high, the user-interface and the underlying software architecture is due for a major update. Moreover, according to the above-mentioned poll, the scientists obviously do not only need a modern user-interface for SPIRES, but also a tighter integration of the various different HEP information systems and new features, i.e. they need a new HEP e-Infrastructure, which includes text- and data-mining applications, as well as Web 2.0 technology. To achieve this goal, in Spring 2008, the SPIRES collaboration and CERN have signed an expression of interest to build such a system, called INSPIRE, with CERN's Invenio as the underlying software. The first alpha test of the new system is due in autumn 2008, a tighter collaboration with publishers and other data providers will follow soon, and public beta tests will start in 2009.

5 The next frontier: Preservation of research data

During the last decades, the HEP experiments became more and more complex and more expensive. Given the fact that e.g. the LHC has cost about 6 billion Euros in public money, it is obvious that one can not repeat these experiments later to obtain new or validate the old data, put new theories to test or to combine the data with some future experiments. The only feasible option is storage and re-use of the collected data. In fact, if this data cannot re-used after the experiment has been stopped and disbanded, the investment into the experiment will not have been exploited to its full capacity. Only an additional and relatively small fraction of the funds is needed to preserve a large fraction of knowledge. CERN Director General Elect Rolf-Dieter Heuer suggests that in order to preserve the HEP data the community should follow a *parallel way*: In addition to experiment data models, a parallel format for (re-)usable high-level objects is to be elaborated. This approach has successfully worked in the past to combine data of 'competing' experiments. 'Oral' and 'additional' knowledge is embedded into such a format to make it understandable and hence re-usable by practitioners in other experiments as well as by theorists.

Unfortunately, there are issues with the 'parallel way': First of all even a small fraction of a big number still gives a large number, so substantial funds are needed. Elaboration of a parallel format competes with research time and the thousands of person-years needed for the 'parallel way' need enormous academic incentives and motivation for realization. This can only succeed if the issues of (open) access, credibility, accountability, reproducibility of results and depth of peer reviewing have been addressed.

To summarize: A monolithic way of doing business needs rethinking.

6 Conclusion

After more than forty years of preprints, sixteen years of repositories and the web, SCOAP^3 –a model for Open Access Publishing– is the next logical step in HEP publishing. On the information retrieval side, the time is ripe for INSPIRE, an e-Infrastructure for HEP communication. The next challenge is the preservation of HEP data.

References

[1] S. Mele *et al.*,J. High Energy Phys. **12** S01 (2006).

[2] A. Gentil-Beccot*et al.* arXiv:0804.2701 [cs.DL].

Hunting for Chameleons in ALP Searches

Amanda Weltman

Department of Applied Mathematics and Theoretical Physics, Cambridge University, Cambridge CB2 0WA, United Kingdom.
Department of Mathematics and Applied Mathematics,
University of Cape Town, Private Bag, Rondebosch, South Africa, 7700

DOI: http://dx.doi.org/10.3204/DESY-PROC-2008-02/lindner_axel

We discuss some recent developments in chameleon models. In particular we discuss the possibility of searching for chameleons in axion-like particle searches performed in the laboratory. Such chameleons may couple to both photons and matter with different coupling strengths. We discuss the exciting possibility of searching for these dark energy candidates in quantum vacuum experiments - in particular for the GammeV experiment at Fermilab.

1 Introduction

Without doubt, one of the most riveting problems of modern physics is the cosmological constant problem. The remarkable observation that the universe is accelerating in its expansion has pushed theorists to propose ever more creative theories while at the same time pushing observational cosmologists to probe the detailed nature of so-called Dark Energy with increasingly sophisticated equipment and techniques.

In this short article, based on a talk given at the IV^{th} Patras Workshop, we will discuss one of the many Dark Energy models that is perhaps most compelling because of the predictions it makes for non-cosmological experiments. So-called chameleon models [1] can be tested both in space and in the laboratory in varied instantiations. These complementary probes allow us to learn about a dark energy model without any cosmological measurements within the settings of experiments that are all designed for other purposes. As such they provide both added motivation and a low cost per physics output quotient for such experiments.

2 Chameleon theories

Chameleon fields have been introduced in recent years [1, 2] to allow for cosmologically evolving light scalar fields that do not violate any known local fifth force or Equivalence Principle tests. Most enticingly, they offer a dark energy candidate whose properties may be probed in our local environment; via local tests of gravity in space and tests of quantum field theory in the lab. The essential feature of these fields is that due to their couplings to matter they acquire an effective potential and thus an effective mass that depends quite sensitively on the background energy density. In this way they have managed to satisfy all tests of the equivalence principle and fifth force experiments so far [1, 3]. Not only can these fields use their local environment to hide from our tests but their properties change depending on their environment thus allowing for both nontrivial predictions for tests of gravity in space and for cosmological effects. For extensive details on chameleon physics see [1, 2, 4].

2.1 Ingredients

In [2] an action of the following form is proposed for Chameleon fields coupled to matter and photons;

$$S = \int d^4x\sqrt{-g}\left(\frac{1}{2M_{pl}^2}R - \partial_\mu\phi\partial^\mu\phi - V(\phi)\right) - \frac{e^{\phi/M_\gamma}}{4}F^{\mu\nu}F_{\mu\nu} + S_m(e^{2\phi/M_m^i}g_{\mu\nu}, \psi_m^i)\ , \quad (1)$$

where S_m is the action for matter and in general the chameleon field, ϕ can couple differently to different matter types ψ_i, and $V(\phi)$ is the chameleon self interaction. For simplicity here we will consider a universal coupling to matter defined by $\beta_m = M_{\rm Pl}/M_m$ while allowing for a different coupling to electromagnetism, $\beta_\gamma = M_{\rm Pl}/M_\gamma$, through the electromagnetic field strength tensor $F_{\mu\nu}$.

The non-trivial coupling to matter and the electromagnetic field induces an effective potential

$$V_{\rm eff}(\phi, \vec{x}) = V(\phi) + e^{\beta_m\phi/M_{\rm Pl}}\rho_m(\vec{x}) + e^{\beta_\gamma\phi/M_{\rm Pl}}\rho_\gamma(\vec{x}), \quad (2)$$

where we have defined the effective electromagnetic field density $\rho_\gamma = \frac{1}{2}(|\vec{B}^2 - |\vec{E}|^2)$ rather than the energy density. An essential insight of chameleon models is noticing that the presence of matter and electromagnetic fields induces a minimum $\phi_{\rm min}$ in $V_{\rm eff}$ where V can be a monotonic function. The dependence of this minimum on the background matter and electromagnetic fields causes the effective mass of the chameleon field to change in response to its environment. In turn we find varied chameleon phenomenology depending on the experimental setup and hence the environment.

We can see explicitly that for an exponential potential, the effective mass of the field ϕ is dependent on the local density of matter and electromagnetic fields,

$$V(\phi) = \Lambda^4\exp\left(\frac{\Lambda^n}{\phi^n}\right),\ \phi_{\rm min} \approx \left(\frac{nM_{\rm Pl}\Lambda^{n+4}}{\beta_{\rm m}\rho_m + \beta_\gamma\rho_g}\right)^{\frac{1}{n+1}} \text{ and } m_\phi^2 \approx \frac{(n+1)}{(n\Lambda^{n+4})^{\frac{1}{n+1}}}\left(\beta_m\rho_m + \beta_\gamma\rho_\gamma\right)^{\frac{n+2}{n+1}}$$

where the next to leading order terms are suppressed by factors of $\beta_i\phi/M_{\rm Pl} \ll 1$.

3 Tests in the lab : The GammeV experiment

In their initial realization [1], chameleon theories held the enticing promise of being observable in space based tests of gravity. Such models studied scalar fields coupled with gravitational strength to matter, i.e. $\beta_m \sim \mathcal{O}(1)$. Their unique properties explained why they have not yet been observed in earth-based tests of gravity. However, in recent years, it has been realized that even very strongly coupled chameleons, i.e. $\beta \sim \mathcal{O}(10^{10})$ even could evade tests of gravity on earth [4]. While strongly coupled models are essentially not testable in space they do open up the possibility for tests in the laboratory to reveal chameleons. Quantum vacuum experiments hold the promise for observing chameleons or constraining strongly coupled chameleons. In particular searches for axions or axion like particles (ALPS) through photon to ALP conversion in the presence of a magnetic field offer a window into constraining strongly coupled chameleon theories [5, 6, 7, 8, 9]. A word of caution - it is important to realize that even though such experiments are probing the chameleon-photon coupling, β_γ (and not the matter coupling directly), at their current stage, they can only constrain a theory that has strong coupling to both photons and matter [10]. Future experiments may broaden this range to include $\mathcal{O}(1)$ couplings to matter, which would be most interesting

Consider a vacuum chamber, whose walls, of density $\rho_{\rm wall}$, are much thicker than the chameleon Compton radius associated with the density $\rho_{\rm wall}$. Chameleons in the vacuum will be nearly massless and unaffected by the chameleon field in the chamber wall. As a chameleon particle approaches the wall, its mass will increase. If its momentum is less than the chameleon mass inside the wall, then it will bounce elastically off the wall. Thus the vacuum chamber will serve as a "bottle" for chameleon particles.

The GammeV experiment at Fermilab [5] is just such a chameleon bottle [6]. If the chameleon field couples to photons as well as to baryonic matter, then a photon interacting with a magnetic field in the vacuum chamber will oscillate into a chameleon particle, analogous to an ALP. When this superposition of photon and chameleon states hits a glass window on one side of the chameleon bottle, it will be measured in the quantum mechanical sense; photons pass through the glass window, while chameleons are reflected. A continuous source of photons entering the bottle will gradually fill it with a gas of chameleon particles. After the photon source is turned off, chameleons will decay back into photons, which can escape the bottle through the glass window. GammeV looks for this "afterglow" effect, a unique signature of photon-coupled chameleon particles [7]. See figure 1 for a schematic of the experiment apparatus. For a more detailed discussion of the GammeV experiment and the first results see [5, 10].

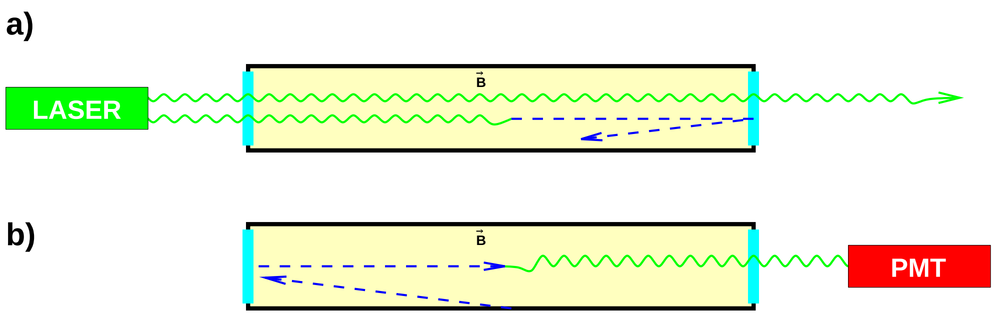

Figure 1: Schematic of the GammeV apparatus. a) Chameleon production phase: photons propagating through a region of magnetic field oscillate into chameleons. Photons travel through the glass endcaps whereas chameleons see the glass as a wall and are trapped. b) Afterglow phase: chameleons in the chamber gradually decay back into photons and are detected by a photomultiplier tube.

4 Conclusions

In this short article we have reviewed the intriguing possibility that a scalar field may couple directly to both matter and photons. The rich phenomenology of these chameleon models makes concrete predictions for tests in space as well as in the laboratory possible providing us with complementary ways of testing the theory by probing different regions of parameter space. Most excitingly, there is a very real possibility that within the coming decade chameleon fields could either be observed or ruled out entirely using the space tests, laboratory tests and astrophysical observations becoming available to us. It is worth emphasizing that regions of parameter space that have already been ruled out for axions will not necessarily be ruled out for chameleons. This was the lesson of [11] where it was shown that the CAST experiment and the original PVLAS signal are perfectly compatible for chameleons though not for axions. The nature of chameleon fields - i.e. their differing mass depending on environment means that we cannot blindly apply the regions of exclusion from axion searches but rather these studies need to be readdressed to apply constraints to the chameleon parameter space.

Acknowledgments

A.W would like to thank the Organizers and the participants of the Fourth Patras Workshop for truly excellent and productive meeting. A.W. gratefully acknowledges her many collaborators on Chameleon models in particular - Justin Khoury, Anne Davis, Phillipe Brax, Carsten van de Bruck and most recently the GammeV collaboration, especially Amol Upadhye and Aaron Chou for many useful discussions and for their insights onto chameleon phenomenology.

References

[1] J. Khoury and A. Weltman, Phys. Rev. Lett. **93**, 171104 (2004); Phys. Rev. D **69**, 044026 (2004).

[2] Ph. Brax, C. van de Bruck, A.-C. Davis, J. Khoury and A. Weltman, Phys. Rev. D **70**, 123518 (2004).

[3] A. Upadhye and S. S. Gubser and J. Khoury, Phys. Rev. D **74** (2006).

[4] D. F. Mota and D. J. Shaw, Phys. Rev. D. **75**, 063501 (2007); Phys. Rev. Lett. **97** 151102, (2006).

[5] http://gammev.fnal.gov/

[6] The chameleon experiment described here was developed with Aaron Chou, Jason Steffen, Amol Upadhye, and William Wester, working closely with the GammeV collaboration.

[7] The "particle trapped in a jar" technique was developed as part of the GammeV experiment and independently realised in [8, 9]

[8] M.Ahlers, A. Lindner, A. Ringwald, L. Schremp and C. Weninger. Phys. Rev D., **77**, 015018, (2008).

[9] H. Gies, D.F. Mota and D. J, Shaw, Phys. Rev D., **77**, 025016, (2008).

[10] The GammeV Collaboration - `arXiv:0806.2438 [hep-ex].`

[11] Ph. Brax, C. van de Bruck, A. C. Davis, Phys.Rev.Lett. bf 99 , 121103, (2007).

Search for Chameleon Particles via Photon Regeneration

Aaron S. Chou[1] for the GammeV Collaboration

[1]Center for Cosmology and Particle Physics, New York University, 4 Washington Place, New York, NY 10003.

DOI: http://dx.doi.org/10.3204/DESY-PROC-2008-02/chou_aaron

We report the first results from the GammeV search for chameleon particles, which may be created via photon-photon interactions within a strong magnetic field. The chameleons are assumed to have matter effects sufficiently strong that they reflect from all solid surfaces of the apparatus, thus evading detection in our previous search for weakly-interacting axion-like particles. We implement a novel technique to create and trap the reflective particles within a jar and to detect them later via their afterglow as they slowly convert back into photons. These measurements provide the first experimental constraints on the couplings of chameleons to photons.

1 Chameleons

Cosmological observations over the past decade have demonstrated with increasing significance the existence of a cosmic acceleration, usually attributed to a negative pressure substance known as *dark energy*. The chameleon mechanism, in which field gains an environment-dependent effective mass, has been proposed as a possible explanation of dark energy [1, 2].

Chameleons may also have axion-like couplings to photons such as $\beta_\gamma(\phi/M_{\rm Pl})F^{\mu\nu}F_{\mu\nu}$ or $\beta_\gamma(\phi/M_{\rm Pl})\tilde{F}^{\mu\nu}F_{\mu\nu}$ where β_γ is a dimensionless coupling parameter. Such a coupling allows photons to oscillate into chameleons and back in the presence of an external magnetic field. The couplings of chameleons to matter and the electromagnetic field induce an effective potential

$$V_{\rm eff}(\phi,\vec{x}) = V(\phi) + e^{\beta_{\rm m}\phi/M_{\rm Pl}}\rho_{\rm m}(\vec{x}) + e^{\beta_\gamma\phi/M_{\rm Pl}}\rho_\gamma(\vec{x}), \tag{1}$$

where $\rho_{\rm m}$ is the background matter density and we have defined the effective electromagnetic field density $\rho_\gamma = \frac{1}{2}(|\vec{B}^2| - |\vec{E}|^2)$ (for scalars) or $\rho_\gamma = \vec{E}\cdot\vec{B}$ (for pseudoscalars) rather than the energy density. Thus the effective mass of the chameleon, $m_{\rm eff} \equiv \sqrt{d^2V_{\rm eff}/d\phi^2}$, evaluated at the minimum of the potential, will depend on the background energy density. A chameleon with large coupling $\beta_{\rm m}$ to matter will become massive inside typical laboratory materials. A chameleon may be trapped inside a "jar" if its total energy ω is less than what its effective mass would be within the material of the walls of the jar. In this case, the walls reflect the incoming chameleons. Chameleons produced from photon oscillation in an optically transparent chamber will be confined until they regenerate photons, which emerge as an afterglow once the original photon source is turned off [3, 4, 5]. The GammeV experiment in its second incarnation is designed to search for such an afterglow and to measure or constrain the possible coupling of chameleons to photons.

2 Afterglow from a jar of chameleons

The GammeV apparatus, described in [6, 7], consists of a long stainless steel cylindrical vacuum chamber inserted into the bore of a $B = 5$ T, $L = 6$ m Tevatron dipole magnet. The entrance and exit of the chamber are sealed with BK7 vacuum windows. A 20 Hz pulsed Nd:YAG laser emits $\omega = 2.33$ eV photons into the chamber at a rate of $F_\gamma \sim 10^{19}$ photons/sec. The 1 cm^{-1} laser linewidth is sufficiently large to span the discrete energy levels of the trapped chameleons.

Interactions with the magnetic field cause each photon to oscillate into a superposition of photon and chameleon states. This superposition can be measured in a quantum mechanical sense through collisions with the windows; chameleons bounce, while photons pass through. The probability for producing a chameleon is obtained from the usual photon-axion oscillation formula $\mathcal{P}_{\rm pr} = \frac{4\beta_\gamma^2 B^2 \omega^2}{M_{\rm Pl}^2 m_{\rm eff}^4} \times \sin^2\left(\frac{m_{\rm eff}^2 L}{4\omega}\right)$. In order to populate the jar with chameleons, the laser is operated continuously for $\tau_{\rm pr} \approx 5$ h. After emerging through the exit window of the chamber, the beam is reflected back through the chamber in order to increase the chameleon production rate and facilitate monitoring of the laser power.

During the afterglow phase of the experiment, the laser is turned off and a low-noise photomultiplier tube placed at the exit window is uncovered. Chameleons interacting with the magnetic field oscillate back into photons, some of which escape to be detected by the PMT. Data are taken in two separate runs, with the polarization vector of the laser either aligned with or perpendicular to the magnetic field, to search for pseudoscalar as well as scalar chameleons.

Throughout the production and afterglow phases, a pressure $P_{\rm chamber} \approx 10^{-7}$ Torr is maintained inside the vacuum chamber using a turbomolecular pump connected to a roughing pump. Because the low-mass chameleons are highly relativistic inside the chamber, the turbo pump simply acts as extra volume (0.026 m^3) for the chameleons. The positive displacement roughing pump is however the weakest "wall" of the chamber, and chameleons must be able to reflect ($m_{\rm eff} > \omega$) on the higher pressure $P_{\rm rough} = 1.9 \times 10^{-3}$ Torr residual gas at the intake of the roughing pump. Furthermore, our experiment is only sensitive to models in which the chameleon is sufficiently light for coherent oscillation in the chamber, $m_{\rm eff} \ll m_{\rm osc} = \sqrt{4\pi\omega/L} = 9.8 \times 10^{-4}$ eV at $P = P_{\rm chamber}$. For a variety of chameleon models, the effective chameleon mass scales with ambient density as $m_{\rm eff}(\rho) \propto \rho^\alpha$, for α of order unity. Our limits on the coupling β_γ will only be valid for models in which the predicted density scaling is strong enough to satisfy both the containment condition at higher ambient density and the coherence condition ant lower ambient density. If $m_{\rm eff}$ is dominated by interactions with the residual gas rather than by interactions with the magnetic energy density, then $m_{\rm eff} = m_0(P/P_{\rm rough})^\alpha$, our constraints on β_γ are valid for models with $\alpha \gtrsim 0.8$ and $\omega < m_0 < m_{\rm osc}(P_{\rm rough}/P_{\rm chamber})^\alpha$. Otherwise, the range of sensitivity in α is even more restricted. Since in our apparatus, $\rho_{\rm m} \approx \rho_\gamma \approx 2 \times 10^{-13}$g/cm^3, the experiment is mainly sensitive to models in which $\beta_{\rm m} \gg \beta_\gamma$ which in addition predict large α.

The prediction of the afterglow rate is complicated by the fact that repeated bounces from imperfectly aligned windows and chamber walls cause chameleon momenta to become isotropic. The coupled photon-chameleon equations must then be integrated along all possible trajectories within the chamber. We model a bounce from the chamber wall as a partial measurement in which the regenerated photon amplitude is attenuated by a factor of $f_{\rm ref}^{1/2}$, where $f_{\rm ref}$ is the reflectivity. The mean decay rate $\Gamma_{\rm dec}$ per chameleon is found by averaging over all trajectories and accounting for losses due to escape or absorption of regenerated photons. Although the cylinder walls are not polished, a low absorptivity $1-f_{\rm ref} = 0.1$ is assumed in order to overpredict the coherent build-up of photon amplitude over multiple bounces. This overprediction of the decay rate of the signal results in a more conservative limit on the coupling constant. We obtain an afterglow decay rate $\Gamma_{\rm dec} = 9.0 \times 10^{-5}$ Hz for $\beta_\gamma = 10^{12}$, with $\Gamma_{\rm dec} \propto \beta_\gamma^2$.

The signal itself is conservatively underpredicted as follows. While the laser is on, new chameleons are produced at the rate of $F_\gamma \mathcal{P}_{\rm pr}$ and decay at the rate of $N_\phi \Gamma_{\rm dec}$. After a time $\tau_{\rm pr}$ the laser is turned off, and the chamber contains $N_\phi^{(\rm max)} = F_\gamma \mathcal{P}_{\rm pr} \Gamma_{\rm dec}^{-1}(1 - e^{-\Gamma_{\rm dec}\tau_{\rm pr}})$ chameleon particles. For our apparatus, this saturates at 3.6×10^{12} for $\beta_\gamma \gtrsim 10^{12}$ and small $m_{\rm eff}$. The contribution to the afterglow photon rate from non-bouncing chameleon trajectories is

$$F_{\rm aft}(t) = \frac{\epsilon_{\rm det} f_{\rm vol} f_{\rm esc} F_\gamma {\mathcal{P}_{\rm pr}}^2 c}{\ell_{\rm tot}\Gamma_{\rm dec}} \left(1 - e^{-\Gamma_{\rm dec}\tau_{\rm pr}}\right) e^{-\Gamma_{\rm dec} t}, \tag{2}$$

for $t \geq 0$, where $t = 0$ is the time at which the laser is turned off. The detector efficiency $\epsilon_{\rm det}$ contains the 0.92 optical transport efficiency, as well as the 0.387 quantum efficiency and 0.7 collection efficiency of the PMT. Because chameleons in the turbo pump region do not regenerate photons, we consider only the chameleons in the cylindrical chamber, which represents a volume fraction $f_{\rm vol} = 0.40$ of the total population. A fraction $f_{\rm esc} = 5.3 \times 10^{-7}$ of chameleons travel the entire distance $\ell_{\rm tot}$ from entrance to exit windows without colliding with the chamber walls, and are focussed by a 2" lens onto the photocathode. While many chameleons that bounce from the walls may also produce photons which reach the detector (indeed, most of the photons that can reach the detector are on bouncing trajectories), such collisions result in a model-dependent chameleon-photon phase shift [8] which can affect the coherence of the oscillation on bouncing trajectories. Our goal here is to present results that are independent of the chameleon model and can thus be applied more generally. We therefore consider only the direct light from non-bouncing trajectories in order to predict the minimum possible afterglow rate for any β_γ and $m_{\rm eff}$. Furthermore, we apply the maximum possible decay rate $\Gamma_{\rm dec}$ in Eq. 2 to allow for the possibility that the afterglow could disappear before we can turn on the detector. Figure 1 shows the expected photon afterglow rate for several values of the photon-chameleon coupling β_γ. Non-observation of this underpredicted rate sets the most conservative limits.

3 Results

No significant excess above the PMT dark rate is seen. In order to minimize the effects of systematic uncertainties due to fluctuations in the dark rate, we compare the expected afterglow signal averaged over the entire observation time to the mean signal observed by the PMT. The dominant uncertainty in our measurements of the chameleon afterglow rate is the systematic uncertainty in the PMT dark rate. We estimate this quantity, using data from [6], by averaging the count rate in each of 55 non-overlapping samples approximately one hour in length. The dark rate, computed by averaging the sample means, is 115 Hz, with a standard deviation of 12.0 Hz. This systematic variation in the dark rate is significantly larger than the statistical uncertainty in the individual sample means. Thus our 3σ upper bound on the mean afterglow rate is 36 Hz above the mean of the data rate for each run, after the 115 Hz average dark rate has been subtracted.

For each $m_{\rm eff}$ and β_γ we predict the total number of excess photons expected within the observation time window. Figure 2 shows the regions excluded by GammeV in the $(m_{\rm eff}, \beta_\gamma)$ parameter space for scalar and pseudoscalar chameleon particles. At $m_{\rm eff}$ near $\sqrt{4\pi\omega/L} = 9.8\times$

10^{-4} eV, our exclusion region is limited by destructive interference in chameleon production. At higher $m_{\rm eff}$, a larger β_γ is needed to produce an equivalent non-bouncing minimum signal rate. However, for $\beta_\gamma \gtrsim 10^{13}$ our sensitivity diminishes because, as shown in Fig. 1, the chameleon decay time $\Gamma_{\rm dec}^{-1}$ in GammeV could be less than the few hundred seconds required to switch on the PMT. In summary, GammeV has carried out the first search for chameleon afterglow, a unique signature of photon-coupled chameleons. Figure 2 presents conservative constraints in a model-independent manner, over a restricted range of chameleon models.

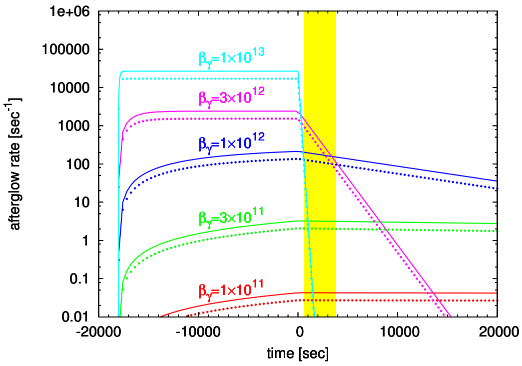

Figure 1: Expected chameleon to photon conversion rate for various values of the coupling to photons β_γ. The solid curves are for chameleons with masses of 10^{-4} eV while the dotted curves are for 5×10^{-4} eV chameleons. Our observation time window for pseudoscalar chameleons is shown shaded in yellow; the corresponding time window for scalar chameleons is shifted to the right by about 700 sec.

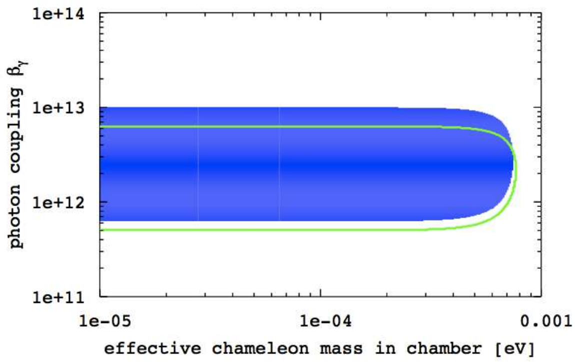

Figure 2: Region excluded by GammeV to 3σ for pseudoscalar (solid blue region) and scalar particles (region between green lines). Constraints worsen at $m_{\rm eff} \gtrsim 10^{-3}$ eV as photon-chameleon oscillation becomes incoherent. These constraints are valid only for models in which the mass scales quickly enough with background density that both the containment and coherence conditions are satisfied.

Acknowledgements: This work is supported by the U.S. Department of Energy under contract No. DE-AC02-07CH11359 and by the U.S. National Science Foundation by NSF-PHY-0401232.

References

[1] J. Khoury and A. Weltman. *Phys. Rev. Lett.*, 93, 2004. 171104.

[2] J. Khoury and A. Weltman. *Phys. Rev. D*, 69, 2004. 044026.

[3] The "particle trapped in a jar" technique was developed as part of the GammeV experiment, and independently realized in [4, 5].

[4] M. Ahlers, A. Lindner, A. Ringwald, L. Schrempp, and C. Weniger. *Phys. Rev. D.*, 77, 2008. 015018 [arXiv:0710.1555 [hep-ph]].

[5] H. Gies, D. F. Mota, and D. J. Shaw. *Phys. Rev. D.*, 77, 2008. 025016 [arXiv:0710.1556 [hep-ph]].

[6] A. S. Chou and others [GammeV (T-969) Collaboration]. *Phys. Rev. Lett.*, 100, 2008. 080402 [arXiv:0710.3783 [hep-ex]].

[7] Aaron S. Chou et al. [arXiv:0806.2438 [hep-ex]].

[8] P. Brax, C. van de Bruck, A. C. Davis, D. F. Mota, and D. J. Shaw. *Phys. Rev. D*, 76, 2007. 085010 [arXiv:0707.2801 [hep-ph]].

Status of the ALPS Experiment

Klaus Ehret[1] for the ALPS Collaboration

[1]DESY, Notketraße 85, 22607 Hamburg, Germany

DOI: http://dx.doi.org/10.3204/DESY-PROC-2008-02/ehret_klaus

The ALPS experiment at DESY searches for light particles which are coupling very weakly to photons. Primary physics goal is the search for axion like particles in a photon regeneration experiment. Central part of the experimental setup is a five Tesla strong superconducting HERA dipole magnet. During two operation periods in the years 2007 and 2008 we have collected first data and explored the sensitivity of the setup. A Fabry Perot laser cavity is being set up in order to increase the sensitivity by more than one order of magnitude.

One of the most exciting quest in particle physics is the search for new particles beyond the standard model. Extensions of the standard model predict not only new particles with masses above the electroweak scale ($\sim$ 100 GeV) but also the so called WISPs (**W**eakly **I**nteracting **S**ub-eV **P**articles). Several possible candidates are axions [1] or axion like particles (ALPs), light spin 1 particles called "hidden sector photons" [2] or light minicharged particles [3]. For a summary on their role in physics beyond the standard model see the contributions of J. Jaeckel and A. Ringwald to these proceedings [4]. It is certainly an important and fundamental question whether any of these light particles exist. Unfortunately, the predictions for the masses and couplings of WISPs are typically not precise and extensive searches in broad parameter spaces have to be performed. Of course, any experimental measurement which gives new indications or new limitations is highly welcome. Nowadays, the strongest constraints come from astrophysical and cosmological arguments (see the contribution of J. Redondo in these proceedings [5]) and from dedicated laboratory experiments [6]. Very recently, the observations of PVLAS [7] triggered the interest, exploration and setup of new low energy experiments using high photon fluxes combined with strong electromagnetic fields.

The **ALPS** experiment, located at DESY in Hamburg, uses a spare superconducting HERA dipole magnet and a strong laser beam for "**A**xion **L**ike **P**article **S**earch". In fact, the experiment has also a large sensitivity for other WISPs so the acronym ALPS should stand more precisely for "**A**ny **L**ight **P**article **S**earch". The primary goal is the indirect detection of a light ALP in a "light shining through a wall" (LSW) experiment [8]. A small fraction of the incident photons from our laser can convert to ALPs ϕ in the presence of the magnetic field by the so-called Primakoff effect [9]. Being ϕs very weakly interacting with ordinary matter, they cross light-tight walls without significant absorption. Behind the absorber, some of these ALPs will reconvert via the inverse-Primakoff process into photons with the initial properties.

The probability of the Primakoff transition $P_{\gamma\to\phi}$ is the same as for the inverse-Primakoff $P_{\phi\to\gamma}$ in the ALPs symmetric setup. Therefore the LSW probability is just the square of $P_{\gamma\to\phi} = g^2B^2E^2/(4m_\phi^4)\sin^2 m_\phi^2 L/(4E)$ with B the magnetic field strength, L the length of the conversion region and E the photon energy. The ALP parameters: mass (m_ϕ) and two photon

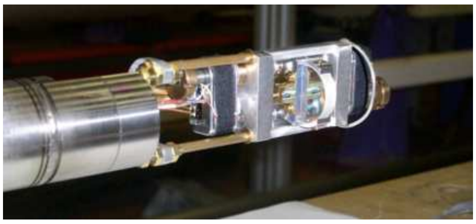

Figure 1: Adjustable mirror with custom made pico-motors attached to the laser tube.

coupling (g) are assumed to be unrelated (see [4] for the relevant definitions).

The transition probability is maximal in the limit $m_\phi^2/E \to 0$ where it is coherent along the full length, reaching $g^2B^2L^2/4$. The mass reach of the experiment is determined therefore by E through the coherence condition $m_\phi^2 < 2\pi E/L$. The polarization of the beam allows to distinguish between scalar and pseudo scalar ALPs.

After the submission of the Letter of Intent [10] the ALPS experiment was approved by the DESY directorate in January 2007. The ALPS collaboration comprises also the Laser Zentrum Hannover (LZH), the Hamburg observatory (HO) and the Albert Einstein Institute(AEI).

The Experimental Setup: The ALPS experiment is built up around the HERA dipole which features a field $B = 5.16$ T and a length of 8.42 m. Its beam pipe is bent with a remaining clear aperture of only 18 mm, which implies serious demands on the beam quality of the laser. The interior is insulated against the cold part of the magnet, allowing to perform the experiment at room temperature. In order to keep the temperature stable the beam pipe is flushed with nitrogen. Inside the dipole beam pipe we place two further tubes which bound the $\gamma - \phi$ conversion and reconversion regions and are operated under vacuum conditions. This is crucial since an index of refraction $n > 1$ suppresses the conversion probabilities [11]. Both tubes range from either side approximately to the middle of the magnet and can be easily removed. A removable light-tight absorber wall is mounted on the inner end of the **detector tube** while an adjustable mirror is attached to the inner side of the **laser tube**, cf. Fig. 1, because dissipating the high laser power inside the magnet could produce dangerous quenches of the magnet. On both sides of the laser tube there are vacuum sealed windows. Custom made pico-motors based on piezo actuators allow a very precise remote adjustment of the inner mirror within the strong magnetic field. This was a very important precondition for the later setup of a laser cavity inside the superconducting magnet.

The laser: The laser setup, built on an solid optical table inside our laser hut, allows to adjust the intensity and the polarization of the beam. A low intensity reference beam is guided in a beam tube outside the magnet parallel to the main beam to the detector setup. Due to the small aperture of the magnet and the requirement to focus the beam on a few pixels of the used camera a small laser beam width with a very good beam quality factor $M^2 \sim 1$ is required. Both, the beam divergence θ and the minimal spot size σ_{min} are proportional to M^2.

There exist high power infrared lasers but the demanding request on the beam quality excludes many industry devices. Furthermore, it is a challenging enterprise to get affordable high efficient and low noise detectors for infrared photons. In summer 2007 we setup the experiment with a 3.5 W Verdi-Coherent CW green laser with $\lambda = 532$ nm and $M^2 < 1.1$ and a commercial camera with good efficiency for green light. Based on the experience of a test run in autumn 2007 we abandoned the initial plan to use an infrared laser.

By the end of the year 2007 we setup and operated successfully a LIGO type pulsed laser system [12] with a pulse-length of 15 nsec and a repetition rate of 20 kHz. The system delivered

14 W of green laser light, which corresponds to a photon flux of $4 \cdot 10^{19} s^{-1}$. During an extensive commissioning phase in spring 2008 we operated the complete setup and explored its sensitivity (details are discussed later on). Based on this experience, it became clear that we had to increase the photon flux by one order of magnitude to become competitive with other experiments and to reach a sensitivity which allows the exploration of yet untouched areas in the parameter phase space of ALPs (cf. Fig. 2). Together with our new collaborators from the AEI we setup a resonant optical cavity in the first half of the HERA magnet. An enhanced LIGO (eLIGO) laser, developed at the LZH for gravitational experiments delivers 35 W 1064 nm laser light with excellent beam characteristics. This is converted into 532 nm green laser light and fed into the 8.62 m long cavity, which is bounded by the outer mirror, mounted on the optical table inside the laser hut, and the mirror at the inner end of the laser beam tube cf. Fig. 1.

The resonant cavity is locked by adopting the frequency of the eLIGO laser to compensate the length fluctuations of the setup. It was a major success and very important proof of principle, that the cavity could be locked over days and operates stable also when the magnet is powered. Recently we studied details of this ambitious setup in order to improve the performance and to exploit the full capability. Two major upgrade steps are under preparation: a second resonant laser cavity around the frequency doubling crystal and the inclusion of the outer mirror into the cavity vacuum system. You may find several details concerning the laser setup and cavity in the contributions of M. Hildebrand to these proceedings.

Detector: As photon detector we used so far the commercial astronomy CCD camera SBIG ST-402ME with $765 * 510$ 9 μm $\times$ 9 μm pixels and a quantum efficiency of 60% for $\lambda = 532$ nm. We operate the camera at -5 C. It has a low dark current and a small readout noise of 17 e^-. The camera allows sampling times between 0.04 s and 1 h. The beam is focused on a small area ≈ 10 μm, i.e. a few pixels.

In order to improve the sensitivity we ordered the camera PIXIS 1024-BL (Princeton Instruments) with a quantum efficiency of 95 % for $\lambda = 532$ m. This camera operates at -70 C, featuring a lower dark current of 0.001 e^- pixel$^{-1}s^{-1}$ and a readout noise of less than 4 e^-. The camera was delivered by the end of August and its performance is now under investigation.

Commissioning Run 2008 & Exploration of Sensitivity: During the commissioning run in spring 2008 we used the 14 W LIGO laser and the SBIG camera to collect ~ 100 h of data with magnet and laser on. The magnet, the camera and the laser worked very reliably. In order to minimize the impact of readout noise we used a sampling time of 20 min or one hour. The absorber was removed a few times in order to test the alignment. Unfortunately the front and back surfaces of the mirror inside the magnet were not sufficiently parallel, causing a deflection of the light passing the mirror used for the alignment of the setup. This limits the knowledge of the beam spot, i.e. the position of potential re-converted photons on the CCD and prohibits to use the data for real physics. The troubling mirror was immediately replaced.

The acquired data were nevertheless used to go through the complete data analysis chain. Around 10 % of the frames are rejected by visual inspection because they contain intense tracks (likely from ambient radioactivity or cosmics) close to the signal region. As measurement we use the sum of the pixel values in a 3×3 array around the beam spot region. After the correction of baseline shifts, which are presumably correlated with varying temperatures of the surroundings, the remaining fluctuations corresponds to the expectations of uncorrelated dark currents and the read-out noise of the individual pixels. The classification of data depends on the physics. Data with magnet on and vertical (horizontal) laser polarization are signals for pseudo-scalar (scalar) ALPs. All other data including dark frames are background. The final observable is the difference in the mean of the distribution of many signal measurements to the mean of the

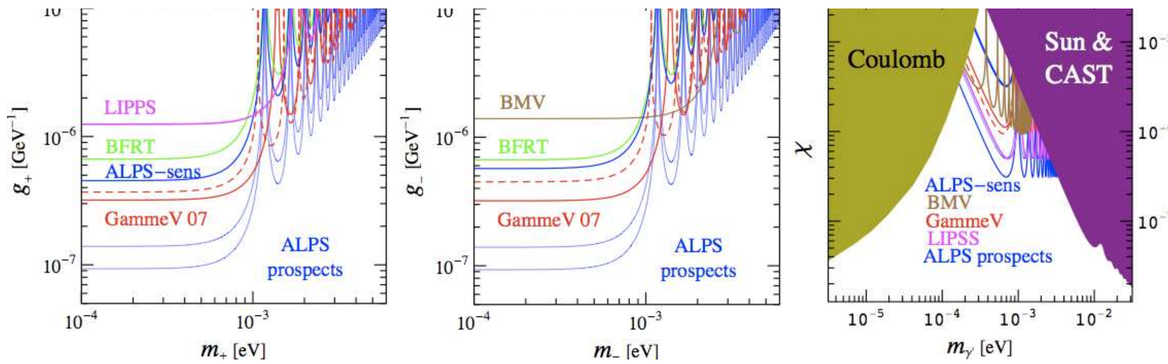

Figure 2: Comparison of sensitivities of ALPS and other axion-like-particle searches for scalar ALPs, pseudo scalar ALPs and "hidden sector photons" [3, 6].

distribution of many background measurements. We see no signal, i.e. no significant difference between signal and background distributions.

Taking into account the conversion factors and a conservative estimate for the efficiencies the sensitivity for the reconverted photon flux is around 40 mHz. This leads together with the initial laser photon flux of $4 \cdot 10^{19}\gamma/\mathrm{s}$ to a detection probability $P_{\gamma\to\phi\to\gamma} \approx 10^{-21}$. The deduced sensitivity in the ALP and in the "hidden sector photon" parameter space is plotted in Fig. 2.

Outlook: Exploiting the two major improvements of the setup which are under preparation, the resonant cavity and a high performance camera, increases the sensitivity of the setup by nearly one order of magnitude. The lower curves in Fig. 2 show the expected ALPS sensitivity with 300 W of green laser light and this together with the additional improved detector. We expect to have the improved setup by the end of the year in operation, allowing us to explore yet untouched areas in the parameter space of the low energy frontier.

References

[1] S. Weinberg, *Phys. Rev. Lett.* **40** (1978) 223–226; F. Wilczek, *Phys. Rev. Lett.* **40** (1978) 279–282.

[2] L. B. Okun, *Sov. Phys. JETP* **56** (1982) 502; M. Ahlers, H. Gies, J. Jaeckel, J. Redondo and A. Ringwald, Phys. Rev. D **76** (2007) 115005 [arXiv:0706.2836 [hep-ph]].

[3] B. Holdom, *Phys. Lett.* **B166** (1986) 196; H. Gies et al., *Phys. Rev. Lett.* **97** (2006) 140402, `hep-ph/0607118`; M. Ahlers, H. Gies, J. Jaeckel, J. Redondo and A. Ringwald, Phys. Rev. D **77** (2008) 095001, [arXiv:0711.4991 [hep-ph]].

[4] A. Ringwald, `arXiv:0810.3106 [hep-th]`; J. Jaeckel, `arXiv:0809.3112 [hep-ph]`.

[5] J. Redondo, `arXiv:0810.3200 [hep-ph]`.

[6] **PDG** Col., C. Amsler *et al.*, *Phys. Lett.* **B667** (2008) 1; **BRFT** Coll., R. Cameron *et al.*, *Phys. Rev.* **D47** (1993) 3707; **GammeV** Coll., A. S. Chou *et al.*, *Phys. Rev. Lett.* **100** (2008) 080402; **BMV** Coll., C. Robilliard *et al.*, *Phys. Rev. Lett.* **99** (2007) 190403; **LIPPS** Coll., A. Afanasev *et al.*, *Phys. Rev. Lett.* **101** (2008) 120401; M. Fouche *et al.*, Phys. Rev. D **78** (2008) 032013 [arXiv:0808.2800 [hep-ex]].

[7] **PVLAS** Coll., E. Zavattini *et al.*, *Phys. Rev. Lett.* **96** (2006) 110406 and *Phys. Rev.* **D77** (2008) 032006.

[8] P. Sikivie, *Phys. Rev. Lett.* **51** (1983) 1415; K. Van Bibber et al. *Phys. Rev. Lett.* **59** (1987) 759.

[9] H. Primakoff, *Phys. Rev.* **81** (1951) 899.

[10] **ALPS** Collaboration, K. Ehret *et al.*, `hep-ex/0702023`.

[11] G. Raffelt and L. Stodolsky, *Phys. Rev.* **D37** (1988) 1237.

[12] M. Frede et al. *Optics Express* **Vol.15 Issue 2** (2007) 459.

Chapter 6

New Theoretical Developments

Axions and Photons In Terms of “Particles” and “Anti-Particles”

Eduardo I. Guendelman[1], *Idan Shilon*[1]

[1]Physics Department, Ben-Gurion University of the Negev, Beer-Sheva 84105, Israel

The axion photon system in an external magnetic field, when for example considered with the 1+1 geometry of the experiments exploring axion photon mixing displays a continuous axion-photon duality symmetry in the limit where the axion mass is neglected. The conservation law that follows from this symmetry is obtained. The magnetic field interaction is seen to be equivalent to first order to the interaction of a complex charged field with an external electric potential, where this fictitious ”electric potential” is proportional to the external magnetic field. Generalizing the scalar QED formalism to 2+1 dimensions makes it clear that a photon and an axion split into two components in an inhomogeneous magnetic field.

Introduction.- The possible existence of a light pseudo scalar particle is a very interesting possibility. For example, the axion [1, 2, 3] which was introduced in order to solve the strong CP problem has since then also been postulated as a candidate for the dark matter. A great number of ideas and experiments for the search this particle have been proposed [4, 5].

Here we are going to focus on a particular feature of the axion field ϕ: its coupling to the photon through an interaction term of the form $g\phi\epsilon^{\mu\nu\alpha\beta}F_{\mu\nu}F_{\alpha\beta}$. It was recognized by Sikivie that axion detection exploiting axion to photon conversion in a magnetic field was a possibility [6] and afterwards, further developments were carried out in [7, 10].

We will study here properties of the axion-photon system in the presence of a strong magnetic field. By representing axions and photons as particles and anti particles we will show also that photons and axions split in the presence of an external magnetic field, in a way that we will make more precise. By this we mean that from a beam of photons we will get two different kinds of scattered components (plus the photons that do not suffer any interactions), each of the scattered beams has also an axion component, but each of the beams is directly observable due to its photon component and an observable process is obtained to first order in the axion photon interaction (unlike the “light shining through a wall” phenomena).

Action and Equations of Motion.- The action principle describing the relevant light pseudoscalar coupling to the photon is

$$S = \int d^4x \left[-\frac{1}{4}F^{\mu\nu}F_{\mu\nu} + \frac{1}{2}\partial_\mu\phi\partial^\mu\phi - \frac{1}{2}m^2\phi^2 - \frac{g}{8}\phi\epsilon^{\mu\nu\alpha\beta}F_{\mu\nu}F_{\alpha\beta} \right]. \tag{1}$$

We now specialize to the case where we consider an electromagnetic field with propagation along the y and z directions and where a strong magnetic field pointing in the x-direction is present. This field may have an arbitrary space dependence in y and z, but it is assumed to be time independent. In the case the magnetic field is constant, see for example [11] for general solutions. For the small perturbations, we consider only small quadratic terms in the action for the axion and the electromagnetic fields, following the method of Ref. [11]. This means that the interaction between the background field , the axion and photon fields reduces in our current set-up to

$$S_I = -\int d^4x \left[\beta\phi E_x\right], \tag{2}$$

where $\beta = gB(y,z)$. Choosing the temporal gauge for the photon excitations and considering only the x-polarization for the electromagnetic waves (since only this polarization couples to the axion) we get the following 2+1 effective dimensional action (A being the x-polarization of the photon, so that $E_x = -\partial_t A$)

$$S_2 = \int dydzdt \left[\frac{1}{2}\partial_\mu A\partial^\mu A + \frac{1}{2}\partial_\mu\phi\partial^\mu\phi - \frac{1}{2}m^2\phi^2 + \beta\phi\partial_t A\right]. \tag{3}$$

Since we consider only $A = A(t,y,z)$, $\phi = \phi(t,y,z)$, we have avoided the integration over x. For the same reason μ runs over t, y and z only. This leads to the equations

$$\partial_\mu\partial^\mu\phi + m^2\phi = \beta\partial_t A \quad \text{and} \quad \partial_\mu\partial^\mu A = -\beta\partial_t\phi. \tag{4}$$

As is well known, when choosing the temporal gauge the action principle cannot reproduce the Gauss constraint (here with a charge density obtained from the axion photon coupling) and has to be imposed as a complementary condition. However, this constraint is automatically satisfied here just because of the type of dynamical reduction employed and does not need to be considered anymore.

The continuous axion photon duality symmetry and the scalar QED analogy.- Without assuming any particular y and z-dependence for β, but still insisting that it will be static, we see that in the case $m = 0$, we discover a continuous axion photon duality symmetry, since: 1) The kinetic terms of the photon and axion allow for a rotational $O(2)$ symmetry in the axion-photon field space, 2) the interaction term, after dropping a total time derivative, can also be expressed in an $O(2)$ symmetric way as follows:

$$S_I = \frac{1}{2}\int dydzdt\beta\left[\phi\partial_t A - A\partial_t\phi\right]. \tag{5}$$

The axion photon symmetry is (in the infinitesimal limit)

$$\delta A = \epsilon\phi, \delta\phi = -\epsilon A, \tag{6}$$

where ϵ is a small number. Using Noether‘s theorem, this leads to the conserved current, with components given by

$$j_0 = A\partial_t\phi - \phi\partial_t A - \frac{\beta}{2}(A^2 + \phi^2) \quad \text{and} \quad j_i = A\partial_i\phi - \phi\partial_i A. \tag{7}$$

Here $i = y, z$ coordinates. Defining now the complex field ψ as $\psi = \frac{1}{\sqrt{2}}(\phi + iA)$, we see that in terms of this complex field, the axion photon density takes the form

$$j_0 = i(\psi^*\partial_t\psi - \psi\partial_t\psi^*) - \beta\psi^*\psi. \tag{8}$$

We observe that (to first order in β) (5) represents the interaction of the magnetic field with the "axion photon density" 7, (9) and also that this interaction has the same form as that of scalar QED with an external "electric " field to first order. In fact the magnetic field (or more precisely $\beta/2$) appears to play the role of external electric potential that couples to the axion photon density (7), (9) which appears then to play the role of an electric charge density. From this analogy one can obtain without effort the scattering amplitudes, just using the known results from the scattering of charged scalar particles under the influence of an external static electric potential (see for example [13]).

One should notice however that the natural initial states used in a real experiment, like an initial photon and no axion involved, is not going to have a well defined axion photon charge in the second quantized theory (although its average value appears zero), so the S matrix has to be presented in a different basis than that of normal QED . This is similar to the difference between working with linear polarizations as opposed to circular polarizations in ordinary optics, except that here we talk about polarizations in the axion photon space. In fact pure axion and pure photon initial states correspond to symmetric and antisymmetric linear combinations of particle and antiparticle in the analog QED language. The reason these linear combinations are not going to be maintained in the presence on B in the analog QED language, is that the analog external electric potential breaks the symmetry between particle and antiparticle and therefore will not maintain in time the symmetric or antisymmetric combinations.

From the point of view of the axion-photon conversion experiments, the symmetry (6) and its finite form, which is just a rotation in the axion-photon space, implies a corresponding symmetry of the axion-photon conversion amplitudes, for the limit $\omega >> m$.

In terms of the complex field, the axion photon current takes the form

$$j_k = i(\psi^* \partial_k \psi - \psi \partial_k \psi^*). \tag{9}$$

The Particle Anti-Particle Representation of Axions and Photons and their Splitting in an External Magnetic Field.- Introducing the charge conjugation [14],

$$\psi \to \psi^*, \tag{10}$$

we see that the free part of the action is indeed invariant under (11). The A and ϕ fields when acting on the free vacuum give rise to a photon and an axion respectively, but in terms of the particles and antiparticles defined in terms of ψ, we see that a photon is an antisymmetric combination of particle and antiparticle and an axion a symmetric combination, since

$$\phi = \frac{1}{\sqrt{2}}(\psi^* + \psi), \; A = \frac{1}{i\sqrt{2}}(\psi - \psi^*), \tag{11}$$

so that the axion is even under charge conjugation, while the photon is odd. These two eigenstates of charge conjugation will propagate without mixing as long as no external magnetic field is applied. The interaction with the external magnetic field transforms under (11) as $S_I \to -S_I$. Therefore these symmetric and antisymmetric combinations, corresponding to axion and photon are not going to be maintained in the presence of B in the analog QED language, since the "analog external electric potential" breaks the symmetry between particle and antiparticle and therefore will not maintain in time the symmetric or antisymmetric combinations. In fact if the analog external electric potential is taken to be a repulsive potential for particles, it will be an attractive potential for antiparticles, so the symmetry breaking is maximal.

Even at the classical level these two components suffer opposite forces, so under the influence of an inhomogeneous magnetic field both a photon or an axion will be decomposed through scattering into their particle and antiparticle components, each of which is scattered in a different direction, since the analog electric force is related to the gradient of the effective electric potential, i.e., the gradient of the magnetic field, times the $U(1)$ charge which is opposite for particles and antiparticles.

For this effect to have meaning, we have to work at least in a 2+1 formalism [15], the 1+1 reduction [12, 14] which allows motion only in a single spacial direction is unable to produce such separation, since in order to separate particle and antiparticle components we need at least two dimensions to obtain a final state with particles and antiparticles going in slightly different directions.

This is in a way similar to the Stern Gerlach experiment in atomic physics [16], where different spin orientations suffer a different force proportional to the gradient of the magnetic field in the direction of the spin. Here instead of spin we have that the photon is a combination of two states with different $U(1)$ charge and each of these components will suffer opposite force under the influence of the external inhomogeneous magnetic field. Notice also that since particle and antiparticles are distinguishable, there are no interference effect between the two processes.

Therefore an original beam of photons will be decomposed through scattering into two different elementary particle and antiparticle components plus the photons that have not undergone scattering. These two beams are observable, since they have both photon components, so the observable consequence of the axion photon coupling will be the splitting by a magnetic field of a photon beam.

Acknowledgments

We would like to thank Keith Baker, Pierre Sikivie and Konstantin Zioutas for conversations and encouragement.

References

[1] R.D. Peccei and H.R. Quinn, Phys. Rev. Lett. **38**, 1440 (1977).

[2] S. Weinberg, Phys. Rev. Lett. **40**, 223 (1978).

[3] F. Wilczek, Phys. Rev. Lett. **40**, 279 (1978).

[4] For a very early proposal see: J.T. Goldman and C.M. Hoffman, Phys. Rev. Lett. **40**, 220 (1978).

[5] For a review see: G.G. Raffelt, arXiv: hep-th/06111118.

[6] P. Sikivie, Phys. Rev. Lett. **51**, 1415 (1983); **52**, 695(E) (1984); Phys. Rev. D **32**, 2988 (1985).

[7] E. Zavattini et. al. (PVLAS collaboration), arXiv: hex/0706.3419.

[8] T. Yanagida and M. Yoshimura, Phys. Lett. **202**, 301 (1988).

[9] See for example: K. Van Bibber et. al., Phys. Rev. Lett. **59**, 759 (1987).

[10] R. Rabadan, A. Ringwald and K. Singurson, Phys. Rev. Lett. **96**, 110407 (2006) and references therein. Several Techniques are studied in S.L. Adler et. al., arXiv: 0801.4739 [hep-th].

[11] S. Ansoldi, E.I. Guendelman and E. Spallucci, JHEP **0309**, 044 (2003).

[12] E.I. Guendelman, Mod. Phys. Lett. A **23**, 191 (2008); arXiv: 0711.3685 [hep-th].

[13] J. D. Bjorken and S. D. Drell, *Relativistic Quantum Mechanics* (McGraw-Hill, N.Y, 1964).

[14] E.I. Guendelman, arXiv:0711.3961 [hep-ph].

[15] E.I. Guendelman, Phys. Lett. B **662**, 445 (2008); arXiv: 0802.0311 [hep-th].

[16] W. Gerlach, O. Stern, *Z.Phys.* **8**, 110 (1922); W. Gerlach, O. Stern, *Z.Phys.* **9**, 349 (1922).

New Theoretical Ideas: Anomaly Induced Effects in Magnetic Field and at LHC

Alexey Boyarsky[1,2], *Oleg Ruchayskiy*[3]

[1]ETHZ, Zürich, CH-8093, Switzerland
[2]Bogolyubov Institute for Theoretical Physics, Kiev 03780, Ukraine
[3]ÉPFL, FSB/ITP/LPPC, BSP 726, CH-1015, Lausanne, Switzerland

DOI: http://dx.doi.org/10.3204/DESY-PROC-2008-02/lindner_axel

Anomaly cancellation between different sectors of a theory may mediate new interactions between the gauge boson of a theory. This may lead to effects, observable both at precision laboratory experiments and at accelerators. Such experiments may reveal the presence of hidden sectors or hidden extra dimensions.

It is well known that theories in which fermions have chiral couplings with gauge fields suffer from *anomalies* – a phenomenon of breaking of gauge symmetries of the classical theory at one-loop level. Anomalies make a theory inconsistent (in particular, its unitarity is lost). The only way to restore consistency of such a theory is to arrange the exact *cancellation* of anomalies between various chiral sectors of the theory. This happens, for example, in the Standard Model (SM), where the cancellation occurs between quarks and leptons within each generation [1]. Another well studied example is the Green-Schwarz anomaly cancellation mechanism [2] in string theory. In this case the cancellation happens between the anomalous contribution of chiral matter of the closed string sector with that of the open string.[1]

Particles involved in anomaly cancellation may have very different masses – for example, the mass of the top quark in the SM is much higher than the masses of all other fermions. On the other hand, gauge invariance should pertain in the theory at all energies, including those which are smaller than the mass of one or several particles involved in anomaly cancellation. The usual logic of renormalizable theories tells that the interactions, mediated by heavy fermions running in loops, are generally suppressed by the masses of these fermions [4]. The case of anomaly cancellation presents a notable counterexample to this famous "decoupling theorem" – the contribution of *a priori* arbitrary heavy particles should remain unsuppressed at arbitrarily low energies. As it was pointed out by D'Hoker and Farhi [5], this is possible because anomalous (i.e. gauge-variant) terms in the effective action have topological nature and therefore they are scale independent. As a result, they are not suppressed even at energies much smaller than the masses of the particles producing these terms via loop effects. This gives a hope to see at low energies some signatures generated by new high energy physics.

[1]Formally, the Green-Schwarz anomaly cancellation occurs due to the anomalous Bianchi identity for the field strength of the Neveu-Schwarz 2-form. However, this modification of Bianchi identity arises from the 1-loop contribution of chiral fermions in the open string sector. A toy model, describing microscopically Green-Schwarz mechanism was studied e.g. in [3].

If a non-trivial anomaly cancellation involves the electromagnetic $U(1)$ gauge group (c.f. e.g. [6–11]), observable effects may be present in optical experiments. Indeed, the 4-dimensional electromagnetic anomaly is related to the quantity $\tilde{F}_{\mu\nu}F^{\mu\nu} = 4\vec{E}\cdot\vec{H} \neq 0$, where $F_{\mu\nu}$ is the electromagnetic field strength and $\tilde{F}_{\mu\nu}$ its dual. The high precision optical experiments (e.g. those measuring the change of polarization of light propagating in a strong magnetic field) could in principle see the anomalous terms, proportional to $\tilde{F}\cdot F$. There exists a significant experimental activity searching for such signals (see e.g. [14]), as various axion-like particles (ALPs) are expected to couple to $\tilde{F}_{\mu\nu}F^{\mu\nu}$ and produce interesting signatures in parallel electric and magnetic fields. A different type of experiment using static fields, which may test effects caused by non-trivial anomaly cancellation in the electromagnetic sector, was suggested in [**?**].

However, to generate an anomaly involving the electromagnetic (EM) group, some fermions should have chiral couplings with EM fields. If these particles are *massless*, their existence is severely constrained experimentally (see e.g. [15] or the book [16]). If the particles are massive, they can acquire mass via Higgs mechanism. Such an (electrically charged) Higgs field will necessarily give mass to the photon which is strongly constrained experimentally. Current experimental bound is $m_\gamma < 6\times10^{-17}$ eV as quoted by [17]. It is based on the work [18] which uses a magnetohydrodynamics argument based on survival of the Sun's field to the radius of the Earth's orbit. The most robust, model-independent constrain $m_\gamma < 10^{-14}$ eV comes from direct measurements of deviations of Coulomb law from r^{-2} dependence [19]. There also exist much stronger experimental restrictions, $m_\gamma < 3\times10^{-27}$ eV [20], which are however model-dependent [21]. Therefore, such theories will necessarily involve a small parameter (mass of the photon or charge of milli-charged particles), which in general strongly suppresses any possible effects [7, 8].

Another possibility is to realize non-trivial anomaly cancellation in the electroweak (EW) sector of the SM. Here the electromagnetic $U(1)$ subgroup is not anomalous by definition. However, the mixed triangular hypercharge $U_Y(1)\times SU(2)^2$ anomalies and gravitational anomalies are non-zero for generic choice of hypercharges. If one takes the most general choice of hypercharges, consistent with the structure of Yukawa terms, one sees that it is parametrized by two independent quantum numbers Q_e (shift of hypercharge of left-handed lepton doublet from its SM value) and Q_q (corresponding shift of quark doublet hypercharge). All the anomalies are then proportional to *one* particular linear combination: $\epsilon = Q_e + 3Q_q$. Interestingly enough, ϵ is equal to the sum of *electric charges* of the electron and proton. Experimental upper bound on the parameter ϵ, coming from checks of electro-neutrality of matter is rather small: $\epsilon < 10^{-21}e$ [17, 22]. If it is non-zero, the anomaly of the SM has to be cancelled by additional anomalous contributions from some physics beyond the SM, possibly giving rise to some non-trivial effects in the low energy effective theory.

A very interesting possibility may be realized in theories with extra dimensions. In this case, additional contribution to the anomaly may come from the higher-dimensional modes, which are separated from the 4-dimensional physics by a mass gap. Such a mechanism of anomaly cancellation is called "*anomaly inflow*" [23]. If an anomaly of EW gauge symmetry of the SM is cancelled by anomaly inflow, this may give rise to very interesting observable effects, making the 4-dimensional low energy effective theory non-local [6]. To see this, however, one needs to use an explicit mechanism of the localization of gauge fields in the presence of non-compact extra dimensions. This makes the theory rather complicated. For example, it may suffer from a strong coupling problem in the bulk at the "non-compact end" of an extra dimension. The model of Ref. [6] offers a way to overcome the strong coupling problem. It admits a non-perturbative solution in an external magnetic field. The solution is sharply localized in the 5th dimension so that it does not enter the strong coupling region. One can then build a perturbation theory around this localized solution and solve Maxwell equations in case of static charges or a stationary propagation (e.g. electromagnetic wave) in the external magnetic field. The analysis shows that the propagation of light, polarized parallel to the external magnetic field, acquires the "magnetic mass" $m_{\gamma H} \sim \sqrt{\epsilon |H_{\text{ext}}|}$, similarly to the static case of [6]. The propagation of orthogonal polarization remains unchanged. This leads to the birefringence of light in the magnetic field. This effect can be probed in the experiments, searching for the ALPs [14]. However, as the model of [6] does not contain any new light degrees of freedom, the effect of dichroism and "shining light through the wall" will not be present in this case.

In all scenarios described above the anomaly-induced effects are proportional to a very small parameter, which makes their experimental detection very difficult. One may consider another situation, where anomalous charges and therefore, anomaly-induced effects, are $\mathcal{O}(1)$. To reconcile this with existing experimental bounds, such an anomaly cancellation should take place between SM and "hidden" sector, with corresponding new particles appearing at relatively high energies. Namely, many extensions of the SM add extra gauge fields to the SM gauge group (see e.g. [24] and refs. therein). For example, additional $U(1)$s naturally appear in models in which $SU(2)$ and $SU(3)$ gauge factors of the SM arise as parts of unitary $U(2)$ and $U(3)$ groups (as e.g. in D-brane constructions of the SM [25]). In this paper, we consider extensions of the SM with an additional $U_X(1)$ factor, so that the gauge group becomes $SU(3)_c \times SU(2)_W \times U_Y(1) \times U_X(1)$. As the SM fermions are chiral with respect to the EW group $SU(2)_W \times U_Y(1)$, even choosing the charges for the $U_X(1)$ group so that the triangular $U_X(1)^3$ anomaly vanishes, still this may easily give rise to the appearance of mixed anomalies: $U_X(1)U_Y(1)^2$, $U_X(1)^2U_Y(1)$, $U_X(1)SU(2)^2$. In this work we are interested in the situation when only (some of these) *mixed anomalies* with the electroweak group $SU(2) \times U_Y(1)$ are non-zero. A number of works have already discussed such theories and their signatures (see e.g. [7, 8, 25–27]).

The question of experimental signatures of such theories at LHC should be addressed differently, depending on whether or not the SM fermions are charged with respect to the $U_X(1)$ group:

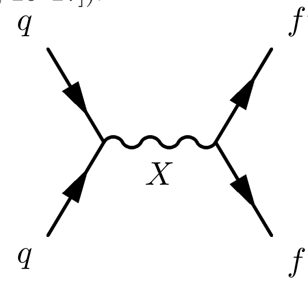

Figure 1: Direction production of neutral X boson in pp collision.

• If SM fermions are charged with respect to the $U_X(1)$ group, and the mass of the new X boson is around the TeV scale, we should be able to see the corresponding resonance in the forthcoming runs of LHC (in processes like those shown on Fig. 1). In this case an important question is to distinguish between theories with non-trivial cancellation of mixed anomalies, and those which are anomaly free.

• On the other hand, one is present with a completely different challenge if the SM fermions are *not charged* with respect to the $U_X(1)$ group. This makes direct production of the X boson impossible. Therefore, the question of whether an anomalous gauge boson with mass $M_X \sim 1$ TeV can be detected at LHC becomes especially interesting.

A theory in which the cancellation of the mixed $U_X(1)SU(2)^2$ anomaly occurs between some heavy fermions and Green-Schwarz (i.e. *tree-level gauge-variant*) terms was considered in [27]. The leading non-gauge invariant contributions from the triangular diagrams of heavy fermions, unsuppressed by the fermion masses, cancels the Green-Schwarz terms. The triangular diagrams also produce subleading (gauge-invariant) terms, suppressed by the mass of the fermions running in the loop. This leads to an appearance of dimension-6 operators in the effective action, having the general form $F^3_{\mu\nu}/\Lambda^2_X$, where $F_{\mu\nu}$ is the field strength of X, Z or $W^\pm$ bosons. Such terms contribute to the XZZ and XWW vertices. As the fermions in the loops are heavy, such vertices are in general strongly suppressed by their mass. However, motivated by various string constructions, [27] has assumed two things: *(a)* these additional massive fermions are above the LHC reach but not too heavy (e.g. have masses in tens of TeV); *(b)* there are many such fermions (for instance Hagedorn tower of states) and therefore the mass suppression can be compensated by the large multiplicity of these fermions.

In [28] we consider another possible setup, in which the anomaly cancellation occurs *only within a high-energy sector* (at scales not accessible by current experiments), but at low energies there remain terms XWW and XZZ unsuppressed by masses of heavy particles. Such a theory possess unique experimental signatures and can be tested at LHC. Similar setup (with completely different phenomenology) has been previously considered in [7, 8].

References

[1] D. J. Gross and R. Jackiw, Phys. Rev. **D6**, 477 (1972); C. Bouchiat, J. Iliopoulos, and P. Meyer, Phys. Lett. **B38**, 519 (1972); H. Georgi and S. L. Glashow, Phys. Rev. **D6**, 429 (1972).

[2] M. B. Green and J. H. Schwarz, Phys. Lett. **B149**, 117 (1984).

[3] A. Boyarsky, J. A. Harvey, and O. Ruchayskiy, Annals Phys. **301**, 1 (2002), `hep-th/0203154`.

[4] T. Appelquist and J. Carazzone, Phys. Rev. **D11**, 2856 (1975).

[5] E. D'Hoker and E. Farhi, Nucl. Phys. **B248**, p. 59 (1984); *ibid.* p. 77.

[6] A. Boyarsky, O. Ruchayskiy, and M. Shaposhnikov, Phys. Rev. **D72**, 085011 (2005); Phys. Lett. **B626**, 184 (2005).

[7] I. Antoniadis, A. Boyarsky, and O. Ruchayskiy (0600), `hep-ph/0606306`.

[8] I. Antoniadis, A. Boyarsky, and O. Ruchayskiy, Nucl. Phys. **B793**, 246 (2008), `arXiv:0708.3001[hep-ph]`.

[9] H. Gies, J. Jaeckel, and A. Ringwald, Phys. Rev. Lett. **97**, 140402 (2006), `arXiv:hep-ph/0607118`.

[10] M. Ahlers, H. Gies, J. Jaeckel, and A. Ringwald, Phys. Rev. **D75**, 035011 (2007), `hep-ph/0612098`.

[11] A. Ringwald (2005), `hep-ph/0511184`.

[12] J. Jaeckel and A. Ringwald, Phys. Lett. **B659**, 509 (2008), `0707.2063`.

[13] M. Ahlers, J. Jaeckel, J. Redondo, and A. Ringwald, Phys. Rev. **D78**, 075005 (2008), `0807.4143`.

[14] R. Cameron et al. (**BFRT**), Phys. Rev. **D47**, 3707 (1993); E. Zavattini et al. (**PVLAS**), Phys. Rev. Lett. **96**, 110406 (2006); S.-J. Chen, H.-H. Mei, and W.-T. Ni (**Q&A**) (2006), `hep-ex/0611050`; E. Zavattini et al. (**PVLAS**) (2007), `arXiv:0706.3419[hep-ex]`; P. Pugnat *et al.* (**OSQAR**), Phys. Rev. D **78** (2008) 092003 K. Ehret et al. (**ALPS**) (2007), `hep-ex/0702023`, `arXiv:0812.3495[hep-ex]`; C. Rizzo (**BMV**) (2007), `arXiv:0710.1703`; A. V. Afanasev, O. K. Baker, and K. W. McFarlane (**LIPPS**) (2006), `hep-ph/0605250`.

[15] S. Davidson, B. Campbell, and D. C. Bailey, Phys. Rev. **D43**, 2314 (1991); S. Davidson, S. Hannestad, and G. Raffelt, JHEP **05**, 003 (2000); G. G. Raffelt, Ann. Rev. Nucl. Part. Sci. **49**, 163 (1999).

[16] G. G. Raffelt, *Stars as laboratories for fundamental physics: The astrophysics of neutrinos, axions, and other weakly interacting particles* (University of Chicago Press, Chicago, USA, 1996).

[17] W.-M. Yao and et al., Journal of Physics G **33**, 1+ (2006), URL `http://pdg.lbl.gov`.

[18] D. Ryutov, Plasma Physics Control Fusion **39**, A73 (1997).

[19] E. R. Williams, J. E. Faller, and H. A. Hill, Phys. Rev. Lett. **26**, 721 (1971).

[20] G. V. Chibisov, Sov. Phys. Usp. **19**, 624 (1976); R. Lakes, Phys. Rev. Lett. **80**, 1826 (1998).

[21] E. Adelberger, G. Dvali, and A. Gruzinov (2003), `hep-ph/0306245`.

[22] M. Marinelli and G. Morpurgo, Phys. Lett. **B137**, 439 (1984).

[23] L. D. Faddeev and S. L. Shatashvili, Theor. Math. Phys. **60**, 770 (1985); J. Callan, Curtis G. and J. A. Harvey, Nucl. Phys. **B250**, 427 (1985).

[24] J. L. Hewett and T. G. Rizzo, Phys. Rept. **183**, 193 (1989).

[25] I. Antoniadis, E. Kiritsis, J. Rizos, and T. N. Tomaras, Nucl. Phys. B **660**, 81 (2003); P. Anastasopoulos, M. Bianchi, E. Dudas, and E. Kiritsis, JHEP **11**, 057 (2006); L. E. Ibanez, F. Marchesano, and R. Rabadan, JHEP **11**, 002 (2001).

[26] C. Coriano, N. Irges, and S. Morelli, JHEP **07**, 008 (2007); R. Armillis, C. Coriano, and M. Guzzi, AIP Conf. Proc. **964**, 212 (2007); C. Coriano, N. Irges, and S. Morelli, Nucl. Phys. **B789**, 133 (2008).

[27] J. Kumar, A. Rajaraman, and J. D. Wells (2007), `arXiv:0707.3488[hep-ph]`.

[28] I. Antoniadis, A. Boyarsky, S. Espahbodi, O. Ruchayskiy, and J. Wells, (2009), `arXiv:0901.0639[hep-ph]`.

Chapter 7

New Ideas and Experimental Approaches

The Enigmatic Sun*

Konstantin Zioutas[1,2], *Mary Tsagri*[1], *Yannis Semertzidis*[1,3], *Thomas Papaevangelou*[4], *Annika Nordt*[5,6], *Vassilis Anastassopoulos*[1]

[1]University of Patras, Greece
[2]CERN, 1211 Geneve 23, Switzerland
[3]Brookhaven National Laboratory, USA
[4]DAPNIA, CEA-SACLAY, Gif-sur-Yvette, France
[5]IKP/TU Darmstadt, Germany
[6]Max Planck Institute for Extraterrestrial Physics, Garching, Germany

DOI: http://dx.doi.org/10.3204/DESY-PROC-2008-02/zioutas_konstantin

The nearest star to Earth harbours a surprising number of unexplained phenomena, despite its proximity. Could astroparticle physics, and in particular particles like the charismatic axion, hold the key?

The Sun, a typical middle-aged star, is the most important astronomical body for life on Earth, and since ancient times its phenomena have had a key role in revealing new physics. Answering the question of why the Sun moves across the sky led to the heliocentric planetary model, replacing the ancient geocentric system and foreshadowing the laws of gravity. In 1783 a Sun-like star led the Revd. John Mitchell to the idea of the black hole, and in 1919 the bending of starlight by the Sun was a triumphant demonstration of general relativity. The Sun even provides a laboratory for subatomic physics. The understanding that it shines by nuclear fusion grew out of the nuclear physics of the 1930s; more recently the solution to the solar neutrino "deficit" problem has implied new physics.

This progress in science, triggered by the seemingly pedestrian Sun, seems set to continue, as a variety of solar phenomena still defy theoretical understanding. It may be that one answer lies in astroparticle physics and the curious hypothetical particle known as the axion. Neutral, light, and very weakly interacting, this particle was proposed more than 25 years ago to explain the absence of charge-parity (CP) symmetry violation in the strong interaction. So what are the problems with the Sun? These lie, perhaps surprisingly, with the more visible, outermost layers, which have been observed for hundreds, if not thousands, of years.

First, why is the corona -the Suns atmosphere with a density of only a few ngr/m^3- so hot, with a temperature of millions of degrees? This question has challenged astronomers since Walter Grotrian, of the Astrophysikalisches Observatorium in Potsdam, discovered the corona in the 1930s. Within a few hundred kilometres, the temperature rises to be about 500 times that of the underlying chromosphere, instead of continuing to fall to the temperature of empty space (2.7 K). While the flux of extreme ultraviolet photons and X-rays from the higher layers is some five orders of magnitude less than the flux from the photosphere (the visible surface), it is nevertheless surprisingly high and inconsistent with the spectrum from a black body with the temperature of the photosphere (Fig. 2). Thus, some unconventional physics must be at

*Extracted from CERN Courier May 20 (2008), http://cerncourier.com/cws/article/cern/34259.

work, since heat cannot run spontaneously from cooler to hotter places. In short, everything above the photosphere should not be there at all.

Another question is how does the corona continuously accelerate the solar wind of some thousand million tonnes of gas per second at speeds as high as 800 km/s? The same puzzle holds for the transient but dramatic coronal mass ejections (CMEs). How and where is the required energy stored, and how are the ejections triggered? This question is probably related to the mystery of coronal heating. And what is it that triggers solar flares, which heat the solar atmosphere locally up to about 10 to 30 million degrees, similar to the high temperature of the core, some 700,000 km beneath? These unpredictable events appear to be like violent "explosions" occurring near sunspots in the lower corona. This suggests magnetic energy as their main energy source, but how is the energy stored and how is it released so rapidly and efficiently within seconds? Even though many details are known, new observations call into question the 40-year-old standard model for solar flares, which 150 years after their discovery still remain a major enigma.

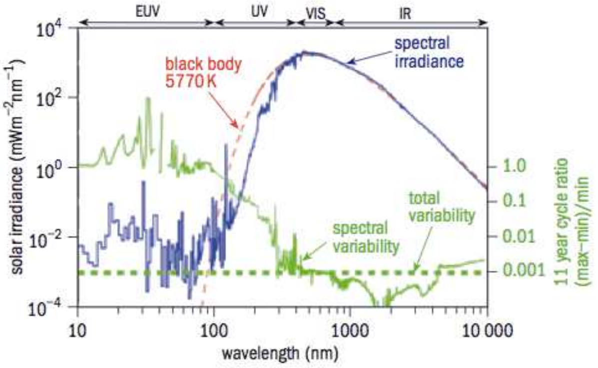

Figure 1: The unexpected deviation from the thermal distribution in the extreme ultraviolet (EUV) and shorter wavelengths (not shown) in the solar spectrum constitutes the celebrated solar corona problem discovered by Walter Grotrian in 1939. The green curve shows the wavelength dependence of the 11-year solar cycle, indicating a threshold-like effect around visible UV energies. The non-thermal part in short wavelengths is much more pronounced in young Sun-like stars.

Figure 2: Solar observatories past and present *Left:* Stonehenge in Wiltshire, southern England, left, constructed around 3000 BC. *Right:* The CERN Solar Axion Telescope (CAST), which started operation in 2002 and is based on a LHC dipole magnet.

On the Suns surface, what is it that causes the 11-year solar cycle of sunspots and solar activity? This seems to be the biggest of all solar mysteries, since it involves the oscillation of the huge "magnets" of a few kilogauss on the face of the Sun, ranging from 300 to 100,000 km in size. The origin of sunspots has been one of the great puzzles of astrophysics since Galileo Galilei first observed them in the early 1600s. Their rhythmic comings and goings, first measured by the apothecary Samuel Heinrich Schwabe in 1826, could be the key to understanding the unpredictable Sun, since everything in the solar atmosphere varies in step with this magnetic cycle. Beneath the Sun's surface, the contradiction between solar spectroscopy and the refined solar interior models provided by helioseismology has revived the question about the heavy-element composition of the Sun, with new abundances some 25 to 35% lower than before.

Abundances vary from place to place and from time to time in the Sun, and are enhanced near flares, showing an intriguing dependence on the square of the magnetic intensity in these regions. The so-called “solar oxygen crisis” or “solar model problem” is thus pointing at some non-standard physical process or processes that occur only in the solar atmosphere, and with some built-in magnetic sensor.

These are just some of the most striking solar mysteries, each crying out for an explanation. So can astroparticle physics help? The answer could be “yes”, using a scenario in which axions, or particles like axions, are created and converted to photons in regions of high magnetic fields or by their spontaneous decay. The expectation from particle physics is that axions should couple to electromagnetic fields, just as neutral pions do in the Primakoff effect known since 1951, which regards the production of pions by high-energy photons as the reverse of the decay into two photons. Interestingly, axions could even couple coherently to macroscopic magnetic fields, giving rise to axion-photon oscillation, as the axions produce photons and vice versa. The process is further enhanced in a suitably dense plasma, which can increase the coherence length. This means that the huge solar magnetic fields could provide regions for efficient axionphoton mutation, leading to the sudden appearance of photons from axions streaming out from the Sun’s interior. The photosphere and solar atmosphere near sunspots are the most likely magnetic regions for this process to become “visible”, as the material above is transparent to emerging photons. According to this scenario, the Sun should be emitting axions, or axion-like particles, with energies reflecting the temperature of the source. Thus one or more extended sources of new low-energy particles ($\lesssim 1$ keV), and the ubiquitous solar magnetic fields of strengths varying from around 0.5 T, as measured at the surface, up to 100 T or much more in the interior, might together give rise to the apparently enigmatic behavior of a star like the Sun. Conventional solar axion models, inspired by QCD, have one small source of particles in the solar core, with an energy spectrum that peaks at 4 to 5 keV. They therefore exclude the low energies where the solar mysteries predominantly occur. This immediately suggests an extended axion “horizon”. Experiments to detect solar axions axion helioscopes such as the CERN Solar Axion Telescope (CAST) should widen their dynamic range towards lower energies, in order to enter this new territory. The revised solar axion scenario must also accommodate two components of photon emission, namely, a continuous inward emission together, occasionally, with an outward radiation pressure. Massive and light axion-like particles, both of which have been proposed, can provide these thermodynamically unexpected inward and outward photons respectively. They offer an exotic but still simple solution, given the Sun’s complexity. The emerging picture is that the transition region (TR) between the chromosphere and the corona (which is only about 100 km thick and only some 2000 km above the solar surface) is the manifestation of a space and time dependent balance between the two photon emissions. However, the almost equally probable disappearance of photons into axion-like particles in a magnetic environment must also be taken into account in understanding the solar puzzles. The TR could be the most spectacular place in the Sun, since it is where the mysterious temperature inversion appears, while flares, CMEs and other violent phenomena originate near the TR. Astrophysicists generally consider the ubiquitous solar magnetism to be the key to understanding the Sun. The magnetic field appears to play a crucial role in heating up the corona, but the process by which it is converted into heat and other forms of energy remains an unsolved problem. In the new scenario, the generally accepted properties of the radiative decay of particles like axions and their coupling to magnetic fields are the device to resolve the problem -in effect, a real “$\alpha\pi\acute{o}\ \mu\eta\chi\alpha\nu\eta\zeta$” (the *deus ex machina* of Greek tragedy). The magnetic field is no longer the energy source, but is just the catalyst for the axions to become photons, and viceversa. The precise mechanism for enhancing axion-photon mutation in the Sun that this picture requires remains elusive and challenging. One aim is to reproduce it in axion experiments. CAST, for example, seeks to detect photons created by the conversion of solar axions in the 9 T field of a prototype superconducting LHC dipole. However, the process depends on the unknown mass of the axion. Every day the CAST experiment changes the density of the gas inside the two tubes in the magnet in an attempt to match the velocity of the solar axion with that of the emerging photon propagating in the refractive gas.

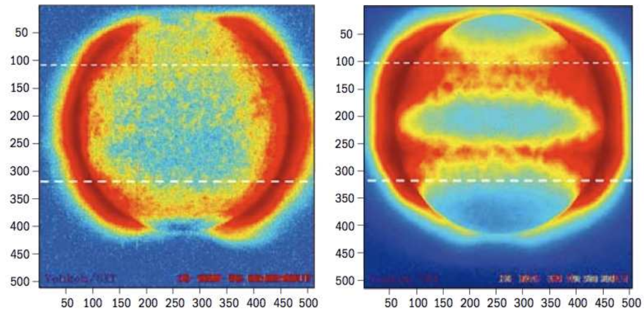

Figure 3: Solar images at photon energies from 250 eV up to a few keV from the Japanese X-ray telescope Yohkoh (19912001). *Left:* composite of 49 of the quietest solar periods during the solar minimum in 1996. *Right:* solar X-ray activity during the last maximum of the 11-year solar cycle. The dashed lines show the part of the solar disk where most activity takes place, indicating a different behavior between the quiet and active Sun.

It is reasonable to assume that fine tuning of this kind in relation to the axion mass might also occur in the restless magnetic Sun. If the energy corresponding to the plasma frequency equals the axion rest mass, the axion-to-photon coherent interaction will increase steeply with the product of the square of the coherence length and the transverse magnetic field strength. Since solar plasma densities and/or magnetic fields change continuously, such a "resonance crossing" could result in an otherwise unexpected photon excess or deficit, manifesting itself in a variety of ways, for example, locally as a hot or cold plasma. Only a quantum electrodynamics that incorporates an axion-like field can accommodate such transient brightening as well as dimming (among many other unexpected observations). These ideas also have implications for the better tuning not only of CAST, but also of orbiting telescopes such as the Japanese satellite Hinode (formerly Solar B), NASAs Reuven Ramaty High Energy Solar Spectroscopic Imager and the NASAESA Solar and Heliospheric Observatory, which have been transformed recently to promising axion helioscopes, following suggestions by CERNs Luigi di Lella among others. The joint Japan-US-UK mission Yohkoh has also joined the axion hunt, even though it ceased operation in 2001, by making its data freely available (Fig. 4). The revised axion scenario therefore seems to fit as an explanation for most (if not all) solar mysteries. Such effects can provide signatures for new physics as direct and as significant as those from laboratory experiments, even though they are generally considered as indirect; the history of solar neutrinos is the best example of this kind. Following these ideas and others on millicharged particles, paraphotons or any other weakly interacting sub-electron-volt particles, axion-like exotica will mean that the Sun's visible surface and probably not its core holds the key to its secrets. As in neutrino physics, the multifaceted Sun, from its deep interior to the outer corona and the solar wind, could be the best laboratory for axion physics and the like. The Sun, the most powerful accelerator in the solar system, whose working principle is not yet understood, has not been as active as it is now for some 11,000 years. Is this an opportunity not to be missed?

Pulsed Plasma Generator as Laboratory Source of Axions or ALPs

Joachim Jacoby[1], *Christian Teske*[1], *Mary Tsagri*[2], *Konstantin Zioutas*[2,3]

[1]University of Frankfurt (Main), Germany
[2]University of Patras, Greece
[3]CERN, 1211 Geneve 23, Switzerland

DOI: http://dx.doi.org/10.3204/DESY-PROC-2008-02/jacobi_joachim

A lately investigated pulsed plasma source known as Low Frequency Inductively Coupled Plasma with power ratings of more than 1 MW is suggested as a novel source for exotic particles like axions. The apparatus uses high magnetic AC fields (∼1 T) with gradients of ∼1 T/cm and generates high power radiation with a significant percentage in the blue and UV range. Therefore the discharge could function as a catalyst for the emitted photons to become axions. These low cost and easy to handle devices could utilize CAST or other axion helioscopes as detectors in a parasitic way, i.e. while they are not tracking the Sun. The working principle and the performance of such an axion source we propose here for the first time.

Introduction Recently a low frequency inductively coupled plasma (LF ICP) has been introduced [1]. One of the principal advantages of this concept is the generation of high electron densities up to $10^{21}\mathrm{m}^{-3}$ which is well beyond the maximum limit of $10^{19}\mathrm{m}^{-3}$ for RF discharges [2]. The LF ICP device is a pulsed high density source which eliminates electrode contact by inductive coupling to the plasma. Inductively coupled pulsed plasmas are common in fusion research where they are known as θ-pinch devices. A relative new approach are LF ICPs which represent a compact design and can be seen as a linkage between conventional RF operated ICPs and the θ-pinch devices, which are to cumbersome for technical applications. One of the primary attractions of the LF ICP is the elimination of contact electrodes, which mitigates issues with material erosion while still achieving high pulsed power levels of more than 1 MW inside the plasma. Moreover the high magnetic AC fields involved in the discharge generation are in the Tesla range [1]. Therefore a research goal in conjunction with the CAST experiment would be to confirm a proposed axion production at the discharge edge, where the combination of photon intensity, magnetic field and magnetic field gradient culminate, making the generation of axions most likely.

Inductive Discharge Generation Generally in an ICP, the power is transferred from the induction coils to the plasma within a skin depth of scale length thickness δ by transformer action [2, 3]. In order to initiate and maintain an inductively coupled discharge for a given discharge volume there is a minimum requirement for the induced electric field $\mathbf{E}_{ind}$ [4]. Because of the nature of the induced electric field $\mathbf{E}_{ind}$, there being no space charge limit on its value, the ionization by collision in the volume of the gas can be increased by higher current densities [5].

The induced electromotoric force U_{emf}, required for dielectric breakdown is dependent on the gas pressure and the gas used and given by a modified version of the Paschen law [4]:

$$U_{emf} = \frac{C_2 p \Lambda}{\ln (C_1 p \Lambda^2)} \tag{1}$$

with the diffusion length Λ, the gas pressure p and two gas dependent constants C_1 and C_2. Analogous to the classical Paschen law, Eq. (1) can be derived from the diffusion equation though without the presence of electrode phenomena represented by the Townsend coefficient γ [4]. Numerical values and experimental data on C_1 and C_2 can be found in [4]. The measured electromotoric force for inductive discharge generation as a function of the gas pressure inside the spherical volume of the LF ICP setup described in [1] can be seen in Fig.1.

The measurements are consistent with the theory of dielectric breakdown at a gas pressure between 2 and 100 Pa showing a minimum current rise time at 4 Pa. It should be noted here that the law for dielectric breakdown represented by (1) does not include the effect of magnetic fields which give rise to a higher effective diffusion length of the charged particles if the discharge comes into the collisionless regime [2, 3]. In the current LF ICP setup, the induction fields of up to 0.6 T lead to a temporal magnetic confinement of the charged particles [1]. As a consequence of this the effective diffusion length for charged particles gets considerable larger, which should accord for the difference between the measured current rise time for discharge generation and the theoretical model of [4].

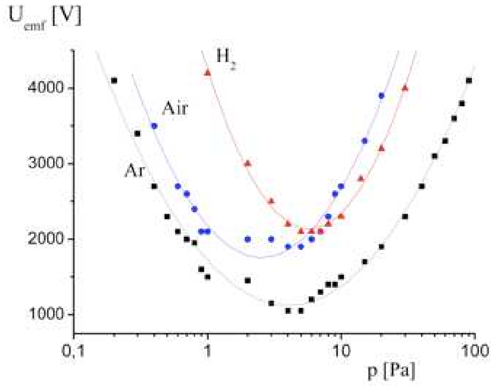

Figure 1: Electromotoric force necessary to initiate a dielectric breakdown as a function of gas pressure.

Measurements Experiments were performed to determine the electrical characteristics of the resonant circuit and the amplitude of the current flowing through the induction coils. The ohmic resistance of the induction coil R_0 was measured through the exponential damping of the current waveform without the plasma acting as a load. Further a fast photo diode was used to compare the electrical signals with the beginning of the discharge and to measure the discharge duration. The presence of a discharge plasma leads to a considerable enhancement of the damping of the circuit through transformer action. With the ohmic resistance of the coils being a known quantity the energy fraction dissipated in the coils during the discharge generation can be estimated. For an arbitrary current $I(t)$ the energy dissipated by the ohmic coil resistance is given by [1]:

$$W_c = R_0 \left[\int_0^{t_p} dt |I_1(t)|^2 + \int_{t_p}^{\infty} dt |I_2(t)|^2 \right] \tag{2}$$

Here t_p is the elapsed time period until discharge initiation starts, I_1 is the current waveform without the discharge plasma and I_2 is the current waveform with the discharge plasma acting as a transformer load. Subtracting W_c from the energy stored inside the capacitors gives the energy dissipated inside the Plasma W_p, leading to:

$$W_p = \frac{1}{2}CU_0^2 - W_c\,, \tag{3}$$

where U_0 is the load voltage of the capacitors and $I(t)$ is the current waveform measured with a Rogowski coil. By comparing the damping of the circuit with and without the presence of the plasma and using energy balance the coupling efficiency η between the primary and the plasma could be determined. Maximum current amplitudes of 4.2 kA were achieved during the ringing of the circuit. The measured results for η as a function of the gas pressure can be seen in Fig. 2.

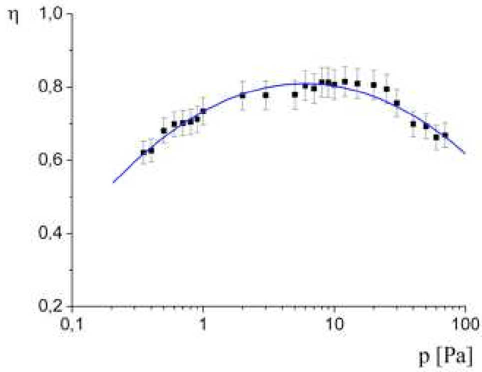

Figure 2: Energy transfer efficiency η of the coil-plasma configuration as a function of gas pressure p.

From the experimental data in Fig. 2, it is found that with maximum efficiency approximately 16% of the stored Energy is dissipated inside the induction coils and the transmission line including the stack assembly. Approximately 84% is dissipated inside the plasma due to the induced ohmic currents. This culminates to an energy transfer efficiency of 84% [1]. The vertical errors represent the uncertainty of the exponential fitting of the current waveform $I(t)$ and the measured coil resistance R_0. Energy transfer efficiency of the current experimental configuration varied between 0.61 up to 0.84. Maximum values were achieved at a gas pressure between 7 Pa and 15 Pa. With discharge duration of 120 μs and a stored energy of 100 J the transfer efficiency of 0.84 leads to a mean power dissipation of 680 kW inside the discharge. It should be noted that this is the integrated power dissipation over the damped discharge period. Peak values during the high intensity period could easily reach 1 MW of pulsed power. Beside the diagnostic of the electrical parameters the line intensities of the emitted spectra was measured. Due to the dynamic nature of the discharge the line intensities must be interpreted as time averaged quantities over a time scale of $\tau = 160\mu$s. Most of the emitted lines can be attributed to ArII. The dominant lines identified for the LF ICP where the ArII 488 nm, ArII 480 nm, ArII 461 nm and ArII 437 nm. This was also confirmed using the data obtained by the monochromator measurements. Emission lines from neutral Argon where scarce. At pressures between 8 Pa and 15 Pa, where maximum energy transfer efficiency was achieved, the UV ArII 359 nm line appeared at its maximum intensity. Higher power densities shift the emission spectra to the UV end. This was confirmed in [1] by comparing the relative intensity of the ArII 359 nm emission line with the most dominant emission lines between 437 nm and 488 nm. The broad band spectroscopic diagnosis was assisted by monochromator measurements for the accurate identification of the emission lines. For the density measurement the stark broadening of the H_β emission line was investigated as a function of the gas pressure. The monochromator measurements presented in this paper are averaged over the entire discharge duration period.

Applying VCS theory, the time averaged electron density could be determined from the spectroscopic data. According to Evans, Aeschliman and Hill [6] VCS (Vidal-Cooper-Smith) theory gives reliable results for the estimated density near $10^{21}\mathrm{m}^{-3}$. The resulting electron density achieved during the discharge generation is shown in Fig. 3. Maximum electron density correlates with the maximum energy transfer efficiency and the maximum line intensity. This is in agreement with the theory of inductive discharge generation which confirms a linear dependence between the electron density and the power density [2, 3]. In terms of achievable electron density the LF ICP is well beyond the limit of $10^{19}\mathrm{m}^{-3}$ given by Lieberman as the current threshold for RF ICPs [3].

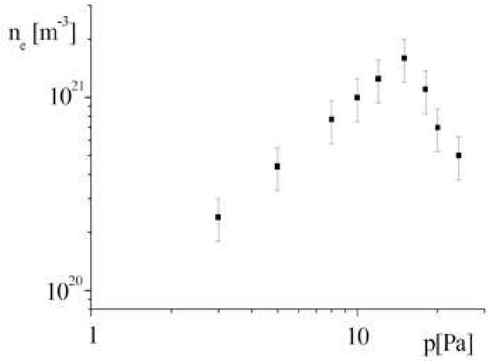

Figure 3: Time averaged electron density of the LF ICP.

Summary The experimental setup discussed in this publication can be seen as a linkage between conventional RF operated ICPs and the θ-pinch devices, which are too cumbersome for most applications. Compared to its high frequency pendant the LF ICP leads to some promising results in terms of achievable electron density and emitted light spectrum. Most of the emitted light was in the blue and violet wavelength with a considerable UV contribution and energy densities of 1 kW/cm^3. The maximum electron density achieved with the current experimental setup was in the range of $10^{21}\mathrm{m}^{-3}$, which is two orders of magnitude higher than the limit for RF ICPs [3]. Electron temperatures for the first experimental apparatus were 2 eV though more than 20 eV seems feasible with a more sophisticated device [1].

Summing up the principal advantages of the LF ICP concept, the setup should be suitable for the generation of axions in the laboratory. The strong magnetic AC fields generated at the edge of the discharge with field gradients of more than 1 T/cm would function as a catalyst for the emitted photons to become axions. A research goal involving the CAST experiment would be to confirm the proposed axion production at the discharge edge, where the combination of photon intensity and magnetic field (gradient) culminate, making the generation of axions most likely. It is also intended to use an optical resonator to increase the path length of the photons passing through the regions with a high magnetic field (gradient). This has the additional advantage that we can enhance accordingly also the potential axion emission towards the detector, e.g. the magnetic pipes of CAST. This resembles somehow the performance of a LASER. We also note here that the LF ICP provides a combination of strong magnetic fields ($\sim$1 T) and very strong magnetic field gradient ($\sim$1 T/cm), which is a promising new aspect of this proposed scheme. In summary the performance of such a device is characterized by its high pulsed power of more than 1MW with a measured energy conversion efficiency into photons of approximately 84%. Further a repetition rate up to 10 Hz seems feasible, while a cluster of several ($\sim$10) of such low cost devices is also possible.

References

[1] C. Teske and J. Jacoby, IEEE Trans. on Plasma Science, **36**(4) 1930-1936 (2008).

[2] M. A. Lieberman and A. J. Lichtenberg, "Principles of Plasma Discharges and Materials Processing" (Wiley & Sons, New Jersey, 2005).

[3] J. R. Roth, "Industrial Plasma Engineering" Volume 1 (IoP Publishing, Bristol and Philadelphia, 1995).

[4] T. Kihara, Rev. Mod. Phys. **24** 45-61 (1953).

[5] K. Chandrakar, J. Phys. **D11** 1809-1813 (1978).

[6] D. L. Evans, D. P. Aeschliman and R. A. Hill, Phys. Rev. **A 10** 6 (1974).

Free-electron Lasers at DESY: Status, Challenges and Opportunities

Tim Laarmann for the FLASH team

DESY, Notkestraße 85, 22607 Hamburg, Germany

DOI: http://dx.doi.org/10.3204/DESY-PROC-2008-02/laarmann_tim

An overview of the current status and future plans of Free-electron Lasers at DESY is presented. Information on the worldwide first FEL operating in the soft X-ray spectral range, called FLASH, is given in a nutshell. Advanced technologies that will be incorporated in the near future in order to further develop the machine are highlighted, such as seeding the FEL using high-harmonic generation (HHG). The valuable experience gained in the past with FLASH paves the way towards the future European XFEL on the DESY site.

The Free-electron LASer in Hamburg (FLASH) has started regular user operation in summer 2005 [1, 2]. This is a unique facility built for the vacuum-ultraviolet and soft X-ray region. The lasing wavelength can presently be tuned from 47 nm to 6.9 nm. Peak and average brilliance of the machine exceeds both that of the brightest synchrotron and laser plasma sources by orders of magnitude. Up to 10^{13} photons per pulse with durations of 10-50 fs result in intensities of more than 10^{16} W/cm^2 by using appropriate focusing optics [3]. Due to its unprecedented characteristics FLASH opens up exciting research opportunities allowing fundamental studies on atoms, ions, molecules and clusters, plasma formation, diffraction imaging of nanoparticles, spectroscopy of bulk solids and surfaces, photochemical reactions, spin dynamics, and the development of advanced photon diagnostics and experimental techniques [4-26]

This laser works on the principle of Self-Amplified Spontaneous Emission (SASE). Here, the lasing medium is a high-density bunch of electrons accelerated to relativistic velocity passing the periodic magnetic field of an undulator. The interaction between the generated undulator radiation and the electrons induce a periodic charge density modulation across the bunch that cause many electrons ($\sim 10^6$) to radiate in phase and thereby greatly enhancing the intensity of the radiation. Its routine operation paves the way to similar sources capable of working in the limit of hard X-rays that are currently proposed or under construction worldwide [1]. The European XFEL at the DESY site is expected to deliver first photons in 2013 [2]. The technical challenge is the preparation and accurate steering of a high quality electron beam over very long distances. Some of the most fascinating proposals for applications that have been made are the investigation of femtosecond structural changes during chemical reactions, or the structure determination of large single macromolecular assemblies.

In a SASE-FEL the intensity strongly fluctuates from pulse to pulse. The fluctuations are inherent to the SASE process and result from start of the amplification process from shot noise. One possibility to reduce these fluctuations is to produce much longer radiation pulses. In 2009,

[1] see e.g. http://hasylab.desy.de/facilities/sr_and_fel_labs/index_eng.html

[2] see e.g. http://www.xfel.eu

DESY plans to install a new acceleration section for the production of electron bunches with 10 times larger pulse durations while retaining the present peak current. An alternative approach is to operate the FEL as an amplifier of injected seed pulses from a high-harmonic generation (HHG) source by overlapping the seed and the electron bunch in the undulator section with μm and fs precision. This way, not only a higher shot-to-shot stability at GW power but a pulse duration of the order of 20 fs can be obtained. An experiment recently performed at the SPring-8 Compact SASE Source (SCSS) has successfully demonstrated HHG seeding at ~ 160 nm [27]. At FLASH, an experiment ("sFLASH") to study the feasibility of seeding at shorter wavelength (30 nm and below) is in preparation at a dedicated commissioning beamline, while SASE pulse trains are simultaneously delivered to the present FEL user beamlines [28].

Currently there are five beamlines for XUV radiation in operation. The layout of the experimental area is schematically depicted in Fig. 1.

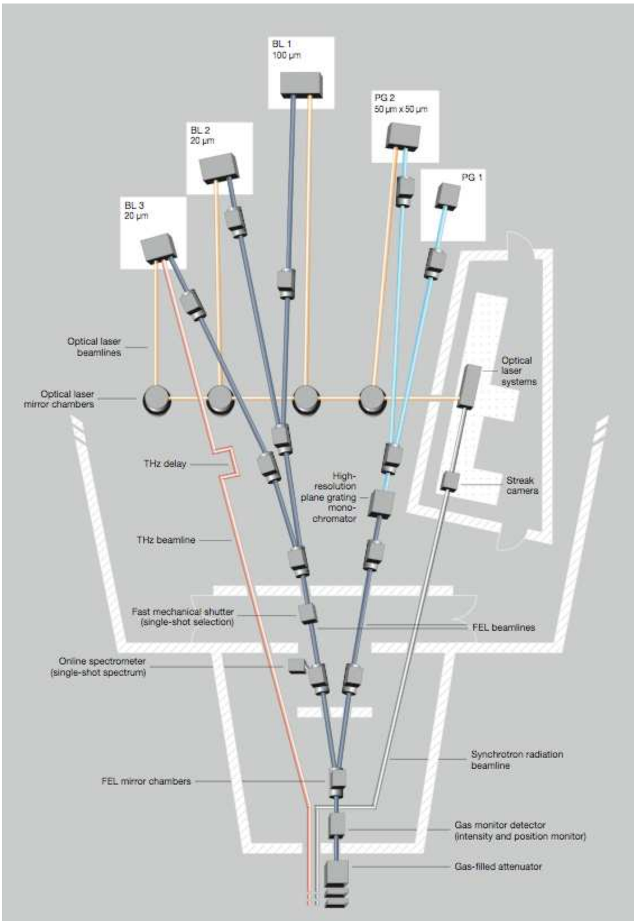

Figure 1: Overview of the FLASH facility including direct (BL1, BL2 and BL3), monochromatised (PG1 and PG2), optical and Teraherz (THz) FEL beamlines. Approximated focal sizes are given next to the station name. Various photon diagnostic tools are installed at different places in the experimental hall

The direct "non-monochromatized" beam is delivered to the beamlines BL1, BL2 and BL3. The high-resolution plane grating monochromator beamlines PG1 and PG2 are selecting a narrow bandwidth of the FEL pulse [29, 30]. For inelastic scattering experiments PG1 is equipped with a high resolution, two-stage spectrometer which is permanently installed in this station. Femtosecond time-resolved pump-probe studies using an optical laser synchronized to the FEL can be performed at BL1-BL3 and PG2 [31-34]. In addition THz radiation can be generated on demand in an electromagnetic undulator located behind the SASE undulator and transported to the endstation of BL3 [35]. Since both, the XUV and the THz pulses are generated by the same electron bunch they are naturally synchronized which opens another window of opportunities for time-resolved studies in the far-infrared spectral range in particular since the generated THz pulses are carrier envelope phase stable.

In summary, the operation of the FLASH facility has made very good progress during the past years pointing towards a bright future with the European XFEL. The author thanks the FLASH team at DESY and all collaboration partners for their contributions.

References

[1] W. Ackermann *et al.*, Nature Photonics **1**, 336-342 (2007).

[2] V. Ayvazyan *et al.*, Eur. Phys. J. D, **37**, 297-303 (2006).

[3] A. A. Sorokin, S. V. Bobashev, T. Feigl, K. Tiedtke, H. Wabnitz, and M. Richter, Phys. Rev. Lett. **99**, 213002 (2007).

[4] S. W. Epp, J. R. Crespo López-Urrutia, G. Brenner, V. Mäckel, P. H. Mokler, R. Treusch, M. Kuhlmann, M. V. Yurkov, J. Feldhaus, J. R. Schneider, M. Wellhöfer, M. Martins, W. Wurth and J. Ullrich, Phys. Rev. Lett. **98**, 183001 (2007).

[5] A. A. Sorokin, S. V. Bobashev, K. Tiedtke, and M. Richter, J. Phys. B: At. Mol. Opt. Phys. **39**, L299-L304 (2006).

[6] A. Pietzsch, A. Föhlisch, M. Beye, M. Deppe, F. Hennies, M. Nagasono, E. Suljoti, W. Wurth, C. Gahl, K. Döbrich, A. Melnikov, New Journal of Physics **10**, 033004 (2008).

[7] K. Tiedtke, J. Feldhaus, U. Hahn, U. Jastrow, T. Nunez, T. Tschentscher, S. V. Bobashev, A. A. Sorokin, J. B. Hastings, S. Möller, L. Cibik, A. Gottwald, A. Hoehl, U. Kroth, M. Krumrey, H. Schöppe, G. Ulm, and M. Richter, J. Appl. Phys. **103**, 094511 (2008).

[8] C. Bostedt, H. Thomas, M. Hoener, E. Eremina, T. Fennel, K.-H. Meiwes-Broer, H. Wabnitz, M. Kuhlmann, E. Plönjes, K. Tiedtke, R. Treusch, J. Feldhaus, A. R. B. de Castro and T. Möller, Phys. Rev. Lett. **100**, 133401 (2008).

[9] A. A. Sorokin, A. Gottwald, A. Hoehl, U. Kroth, H. Schöppe, G. Ulm, M. Richter, S. V. Bobashev, I. Domracheva, D. Smirnov, K. Tiedtke, S. Düsterer, J. Feldhaus, U. Hahn, U. Jastrow, M. Kuhlmann, T. Nuñez, E. Plönjes, and R. Treusch, Appl. Phys. Lett. **89**, 221114 (2006).

[10] M. J. Bogan, W. H. Benner, S. Boutet, U. Rohner, M. Frank, A. Barty, M. M. Seibert, F. Maia, S. Marchesini, S. Baijt, B. Wodds, V. Riot, S. P. Hau-Riege, M. Svenda, E. Marklund, E. Spiller, J. Hajdu, H. N. Chapman, Nano Letters **8**, 310-316 (2008).

[11] H. N. Chapman *et al.*, Nature Physics **2**, 839-843 (2006).

[12] N. Stojanovic, D. von der Linde, K. Sokolowski-Tinten, U. Zastrau, F. Perner, E. Förster, R. Sobierajski, R. Nietubyc, M. Jurek, D. Klinger, J. Pelka, J. Krzywinski, L. Juha, J. Cihelka, A. Velyhan, S. Koptyaev, V. Hájková, J. Chalupsky, J. Kuba, T. Tschentscher, S. Toleikis, S. Düsterer, and H. Redlin, Appl. Phys. Lett. **89**, 241909 (2006).

[13] A. R. B. de Castro, C. Bostedt, E. Eremina, M. Hoener, H. Thomas, T. Laarmann, T. Fennel, K.-H. Meiwes-Broer, E. Plönjes, M. Kuhlmann, H. Wabnitz, and T. Möller, J. Electron Spectrosc. Relat. Phenom. **156**, 25-29 (2007).

[14] M. Kirm, V. Babin, E. Feldbach, V. Nagirnyi, S. Vielhauer, S. Guizard, B. Carr, M. De Grazia, H. Merdji, A. N. Belsky, N. Fedorov, and P. Martin, phys. stat. sol. (c) **4**, No. 3, 870-876 (2007).

[15] S. Cunovic, N. Müller, R. Kalms, M. Krikunova, M. Wieland, M. Drescher, Th. Maltezopoulos, U. Frühling, H. Redlin, E. Plönjes-Palm, and J. Feldhaus, Appl. Phys. Lett. **90**, 121112 (2007).

[16] A. A. Sorokin, M. Wellhöfer, S. V. Bobashev, K. Tiedtke, and M. Richter, Phys. Rev. A **75**, 051402(R) (2007).

[17] S. P. Hau-Riege, H. N. Chapman, J. Krzywinski, R. Sobierajski, S. Bajt, R. A. London, M. Bergh, C. Caleman, R. Nietubyc, L. Juha, J. Kuba, E. Spiller, S. Baker, R. Bionta, K. Sokolowski-Tinten, N. Stojanovic, B. Kjornrattanawanich, E. Gullikson, E. Plönjes, S. Toleikis, and T. Tschentscher, Phys. Rev. Lett. **98**, 145502 (2007).

[18] M. Nagasono, E. Suljoti, A. Pietzsch, F. Hennies, M. Wellhöfer, J.-T. Hoeft, M. Martins, W. Wurth, R. Treusch, J. Feldhaus, J. R. Schneider, and A. Föhlisch, Phys. Rev. A **75**, 051406(R) (2007).

[19] R. Moshammer, Y. H. Jiang, L. Foucar, A. Rudenko, Th. Ergler, C. D. Schröter, S. Lüdemann, K. Zrost, D. Fischer, J. Titze, T. Jahnke, M. Schöffler, T. Weber, R. Dörner, T. J. M. Zouros, A. Dorn, T. Ferger, K. U. Kühnel, R. Treusch, P. Radcliffe, E. Plönjes, and J. Ullrich, Phys. Rev. Lett. **98**, 203001 (2007).

[20] H. B. Pedersen, S. Altevogt, B. Jordon-Thaden, O. Heber, M. L. Rappaport, D. Schwalm, J. Ullrich, D. Zajfman, R. Treusch, N. Guerassimova, M. Martins, J.-T. Hoeft, M. Wellhöfer, and A. Wolf, Phys. Rev. Lett. **98**, 223202 (2007).

[21] A. Föhlisch, M. Nagasono, M. Deppe, E. Suljoti, F. Hennies, A. Pietzsch, and W. Wurth, Phys. Rev. A **76**, 013411 (2007).

[22] H. N. Chapman *et al.*, Nature **448**, 676-680 (2007).

[23] S. Düsterer, P. Radcliffe, G. Geloni, U. Jastrow, M. Kuhlmann, E. Plönjes, K. Tiedtke, R. Treusch, J. Feldhaus, P. Nicolosi, L. Poletto, P. Yeates, H. Luna, J. T. Costello, P. Orr, D. Cubaynes and M. Meyer, Opt. Lett. **31**, 1750-1752 (2006).

[24] A. Höll *et al.*, High Energy Density Phys. **3**, 120-130 (2007).

[25] S. P. Hau-Riege, R. A. London, R. M. Bionta, M. A. McKernan, S. L. Baker, J. Krzywinski, R. Sobierajski, R. Nietubyc, J. B. Pelka, M. Jurek, L. Juha, J. Chalupsky, J. Cihelka, V. Hájková, A. Velyhan, J. Krása, J. Kuba, K. Tiedtke, S. Toleikis, Th. Tschentscher, H. Wabnitz, M. Bergh, C. Caleman, K. Sokolowski- Tinten, N. Stojanovic, and U. Zastrau, Appl. Phys. Lett. **90**, 173128 (2007).

[26] J. Chalupský, L. Juha, J. Kuba, J. Cihelka, V. Hájková, S. Koptyaev, J. Krása, A. Velyhan, M. Bergh, C. Caleman, J. Hajdu, R. M. Bionta, H. N.,Chapman, S. P. Hau-Riege, R. A. London, M. Jurek, J. Krzywinski, R. Nietubyc, J. B. Pelka, R. Sobierajski, J. Meyer-ter-Vehn, A. Tronnier, K. Sokolowski-Tinten, N. Stojanovic, K. Tiedtke, S. Toleikis, T. Tschentscher, H. Wabnitz, and U. Zastrau, Optics Express **15**, 6036-6043 (2007).

[27] G. Lambert *et al.*, Nature Physics **4**, 296-300 (2008).

[28] A. Azima, J. Bödewadt, M. Drescher, H. Delsim-Hashemi, S. Khan, T. Maltezopoulos, V. Miltchev, M. Mittenzwey, J. Rossbach, R. Tarkeshian, M. Wieland, H. Schlarb, S. Düsterer, J. Feldhaus and T. Laarmann, Proceedings of EPAC 2008.

[29] M. Martins, M. Wellhöfer, J. T. Hoeft and W. Wurth, Rev. Sci. Instr. **77**, 115108 (2006).

[30] M. Wellhöfer, M. Martins, W. Wurth, A. A. Sorokin and M. Richter, J. Opt. A. **9**, 749 (2007).

[31] M. Meyer, D. Cubaynes, P. O'Keeffe, H. Luna, P. Yeates, E.T. Kennedy, J.T. Costello, P. Orr, R. Taïeb, A. Maquet, S. Düsterer, P. Radcliffe, H. Redlin, A. Azima, E. Plönjes, and J. Feldhaus, Phys. Rev. A **74**, 011401(R) (2006).

[32] P. Radcliffe, S. Düsterer, A. Azima, H. Redlin, J. Feldhaus, J. Dardis, K. Kavanagh, H. Luna, J. Pedregosa Gutierrez, P. Yeates, E. T. Kennedy, J. T. Costello, A. Delserieys, C. L. S. Lewis, R. Taïeb, A. Maquet, D. Cubaynes and M. Meyer, Appl. Phys. Lett. **90**, 131108 (2007).

[33] C. Gahl, A. Azima, M. Beye, M. Deppe, K. Döbrich, U. Hasslinger, F. Hennies, A. Melnikov, M. Nagasono, A. Pietzsch, M. Wolf, W. Wurth, and A. Föhlisch, Nature Photonics **2**, 165-169 (2007).

[34] T. Maltezopoulos, S. Cunovic, M. Wieland, M. Beye, A. Azima, H. Redlin, M. Krikunova, R. Kalms, U. Frühling, F. Budzyn, W. Wurth, A. Föhlisch and M. Drescher, New Journal of Physics **10**, 033026 (2008).

[35] M. Gensch, L. Bittner, A. Chesnov, H. Delsim-Hashemi, M. Drescher, B. Faatz, J. Feldhaus, U. Frühling, G. A. Geloni, C. Gerth, O. Grimm, U. Hahn, M. Hesse, S. Kapitzki, V. Kocharyan, O. Kozlov, E. Matyushevsky, N. Morozov, D. Petrov, E. Plönjes, M. Röhling, J. Rossbach, E. L. Saldin, B. Schmidt, P. Schmüser, E. A. Schneidmiller, E. Syresin, A. Willner and M. V. Yurkov, Infrared Phys. Techn.**51**, 423-425 (2008).

Polarization Measurements and their Perspectives: PVLAS Phase II

Giovanni Cantatore[1], *Roberto Cimino*[2], *Marin Karuza*[1], *Valentina Lozza*[1], *Giancarlo Raiteri*[1]

[1]Universitá and INFN Trieste, Via Valerio 2, 34127 Trieste, Italy
[2]INFN Lab. Naz. di Frascati, Via E. Fermi 40, 00044, Frascati, Italy

DOI: http://dx.doi.org/10.3204/DESY-PROC-2008-02/cantatore_giovanni_pvlasII

We sketch the proposal for a PVLAS-Phase II experiment. The main physics goal is to achieve the first direct observation of non-linear effects in electromagnetism predicted by QED and the measurement of the photon-photon scattering cross section at low energies (1-2 eV). Physical processes such as ALP and MCP production in a magnetic field could also be accessible if sensitive enough operation is reached. The short term experimental strategy is to compact as much as possible the dimensions of the apparatus in order to bring noise sources under control and to attain a sufficient sensitivity. We will also briefly mention future perspectives, such as a scheme to implement the resonant regeneration principle for the detection of ALPs.

1 Introduction

The polarization of light plays an important role in many phenomena where photons interact with matter and other electromagnetic fields. It is well known from Quantum Electrodynamics (QED), and, more broadly, from particle physics, that photons impinging on a pneumatic vacuum region where an external magnetic field is present, are subject to various interactions at the microscopic level [1], such as photon-photon scattering [2] and real, or virtual, production of Axion Like Particles (ALPs) and Mini Charged Particles (MCPs) coupled to two photons [3]. By carrying out sensitive polarization measurements, it is possible to gain direct access to the physical quantities regulating these processes: photon-photon scattering and virtual particle production both result in an ellipticity acquired by the light beam, while real production results in a dichroism, that is an apparent rotation of the polarization plane. Taking into account experimental parameters available in a laboratory, one must detect, as in the case of photon-photon scattering, acquired ellipticities of the order of 10^{-11} or less. It is apparent, then, the crucial need for a high sensitivity ellipsometer in all these measurements. This kind of experimental investigation was started at CERN by the group led by E. Zavattini [4]. Later on, the BFRT experiment, based on an ellipsometer equipped with a multipass optical cavity and a pair of 4 T, horizontally placed, dipole magnets, reached a sensitivity just below 10^{-6} $1/\sqrt{\text{Hz}}$ [5]. BFRT set the first limits on the quantities involved in the physical processes described above, especially on particle production. The PVLAS experiment, at the Legnaro National Laboratories of INFN, Italy, used a high-finesse (≈100000) Fabry-Perot (FP) optical resonator and a 5 T super-conducting dipole magnet, placed vertically and capable of rotating around its own axis, and has reached a sensitivity of $\approx 5 \cdot 10^{-7}$ $1/\sqrt{\text{Hz}}$ [6]. The study of magneto-optical effects in vacuo is also presently under way by several groups of researchers, among which the BMV project at the University of Toulouse, France [7], the Q&A experiment in Taiwan [8], and the OSQAR experiment at CERN [9]. All these efforts have common features: a low energy (1-2 eV), low flux ($\approx 10^{18}$ ph/s) photon beam probes a pneumatic vacuum region subject to a magnetic field, the sought-after effect is made time-varying in order to employ signal extraction techniques, and the length of the optical path in the magnetic region is amplified by means of an optical resonator. They also share a common problem: how to minimize the noise background.

2 PVLAS Phase II

After an effort lasting several years, the possibilities of the "phase I" of PVLAS can be considered exhausted. The positive signal published in 2006 has subsequently been proven to be an instrumental effect, and the best sensitivity reached is $\approx 5 \cdot 10^{-7}\ 1/\sqrt{\mathrm{Hz}}$ [6], meaning that detecting QED effects would take about 80 years of measurement time. In fact, the original PVLAS apparatus was not completely optimized from an optics point of view. The large dimensions of the granite tower holding the optical components were actually dictated by the necessity of enclosing a 4 m high, 5 ton cryostat, and not by an optimal optics design. During operation it has been found that the tower actually moves, transferring this movement to the optics, especially the resonator mirrors. For instance, the induced birefringence due to beam movement on mirror surfaces has been measured to be $\approx 0.4\ \mathrm{m}^{-1}$. A sensitivity in ellipticity of $5 \cdot 10^{-7}\ 1/\sqrt{\mathrm{Hz}}$ then means that relative movement between the top and bottom optical benches must be $< 2 \cdot 10^{-7}\ \mathrm{m}/\sqrt{\mathrm{Hz}}$. This is impossible to achieve unless, perhaps, the entire PVLAS apparatus is rebuilt from scratch. With such a large apparatus it is also very hard to control overall thermal and acoustic noises. The main point we wish to make here, is that there is no reason of principle to keep a large optics tower.

The basic problem one must attack in order to progress with ellipsometric techniques is the reduction of the noise background. With this in mind we have started *"PVLAS Phase II"*, based on the following ideas. Abandon the large optics tower and compact the apparatus down to table-top size, mounting all components on a single optical bench in a well tested vacuum system. Carefully characterize the apparatus step by step and implement from the start all "passive" means of noise reduction, such as vibration isolation, environmental shields, solid and remotely controlled optics mounts. Reduce the number of optical components by developing a new ellipticity modulator which can be integrated on a resonator mirror. Use rotating permanent magnets in order to obtain a large duty cycle, fringe-field free operation, and the possibility to rotate the magnets at relatively large frequencies, up to 10-20 Hz. We are at present operating, in the INFN Laboratories in Trieste, Italy, a prototype table-top ellipsometer with these characteristics: a frequency-doubled Nd:YAG CW laser emitting 900 mW at 1064 nm and 20 mW at 532 nm; a 50 cm long, 2.3 T permanent magnet; a 1 m long high-finesse FP resonator (a finesse of 170000 has been reached during tests). The vacuum system is capable of reaching a base pressure of $\approx 10^{-8}$ mbar and the composition of the residual gas can be dynamically sampled. Preliminary noise tests at atmospheric pressure, with the FP removed, indicate a promising sensitivity of $\approx 2 \cdot 10^{-8}\ 1/\sqrt{\mathrm{Hz}}$ at 1 Hz, in slight excess of shot-noise limited operation. We envision a two-three year effort on a three step approach.
Prototype ellipsometer (already existing) - 900 mW - 1064 nm laser and 20 mW - 532 nm laser, stress-birefringence ellipticity modulator, 1 m long 220000 finesse FP, with 2.3 T - 50 cm long rotating permanent magnet, environmental screens, analog frequency-locking feedback on FP

Config.		IR		GREEN		
		Prot.	Adv.	Prot.	Adv.	Adv. pow. upg.
	Sens. $[1/\sqrt{\text{Hz}}]$	10^{-8}	$6 \cdot 10^{-10}$	10^{-8}	$6 \cdot 10^{-9}$	10^{-9}
One mag.	Meas. time (8-hr. days)	188	0.675	47.1	16.9	0.471
Two mag.	Meas. time (8-hr. days)	47.1	0.169	11.7	4.2	0.12

Table 1: Minimum measurement times necessary to detect QED photon-photon scattering for several apparatus configurations (see text).

resonator.
Advanced ellipsometer - prototype plus intensity stabilization to reduce laser Residual Intensity Noise (RIN), stress-birefringence modulation directly on the cavity mirrors, lower noise electronic detection chain, improved acoustic isolation, digital frequency-locking feedback on FP resonator.
Advanced ellipsometer with power upgrade - power upgraded laser to 600 mW or more at 532 nm, light injection and extraction from the cavity via optical fiber.
All three configurations could in principle be instrumented with a second 2.3 T, 50 cm long, permanent magnet to gain a factor 2 in signal and to allow zero-field equivalent measurements by crossing the two magnets at 90°.

It is important to note that the table-top ellipsometer is not just a test apparatus to research noise sources, rather, if a good enough sensitivity is reached (at least $\approx 10^{-8}\ 1/\sqrt{\text{Hz}}$) it could actually achieve the first detection of the vacuum magnetic birefringence due to photon-photon scattering. Table 1 gives the integration times, in units of 8-hour standard days, needed to achieve detection of QED ellipticity using a 220000 finesse FP resonator and one or two magnets. "IR" refers to 1064 nm, while "GREEN" refers to 532 nm. Also, the three ellipsometer advancement steps are considered. Notice the worst case of a measurement time of 188 days, which is difficult to achieve, but by no means impossible.

3 Future perspectives

In addition to observing QED, a sensitive ellipsometer could be used, for instance, to set very stringent laboratory bounds on ALP mass and coupling constant to two photons. Figure 1 shows the mass [m]-inverse coupling [M] plane for ALPs. Upper bounds from completed/projected polarization experiment are shown along with the "axion line", roughly corresponding to the currently accepted models for QCD axions. Notice how, even in the best case, polarization measurements cannot reach the "CAST barrier", that is the limit obtained by the CAST helioscope at CERN [10].

A suggestive proposal has been put forth in Ref. [11], where the authors envision a regeneration experiment with a FP cavity used to enhance ALP production in a first magnet, and a second FP enhancing ALP reconversion in a second magnet. The technical challenge is quite steep, involving the attainment of complete coherence of two high-finesse FP resonators. However, using a scheme based on a double-wavelength emitting laser [12], we believe that such a goal is ultimately reachable. The graph in Figure 1 reports the bound which could be set by a

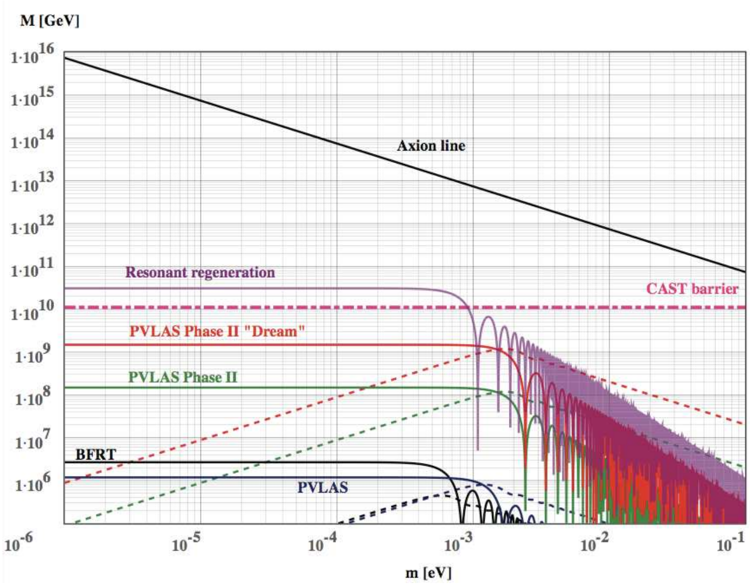

Figure 1: Upper bounds from laser experiments on ALP production. The CAST limit is shown, along with the axion line given by current models for QCD axions. An upper bound corresponding to successful measurement based on the resonant regeneration principle is also plotted (see text).

successful resonant regeneration measurement. In our view this represents the only hope by a laboratory laser experiment of beating the "CAST barrier" .

References

[1] H. Euler and K. Kochel, Naturwissenschaften **23**, 246 (1935);
W. Heisenberg and H. Euler, Z. Phys. **98**, 714 (1936) [arXiv:physics/0605038];
J. S. Schwinger, Phys. Rev. **82**, 664 (1951);
S. L. Adler, Annals Phys. **67**, 599 (1971).

[2] D. Bernard *et al.*, Eur. Phys. J. D **10** 141 (2000).

[3] P. Sikivie, Phys. Rev. Lett. **51**, 1415 (1983), ibid. **52**, 695 (1984);
G. Raffelt and L. Stodolsky, Phys. Rev. D **37** (1988) 1237;
M. Ahlers, H. Gies, J. Jaeckel, J. Redondo and A. Ringwald, Phys. Rev. D **77**, 095001 (2008).

[4] E. Iacopini and E. Zavattini, Phys. Lett. B **85**, 151 (1979);
E. Iacopini, B. Smith, G. Stefanini and E. Zavattini, Nuovo Cim. B **61**, 21 (1981).

[5] Y. Semertzidis *et al.*, Phys. Rev. Lett. **64**, 2988 (1990);
R. Cameron *et al.*, Phys. Rev. D **47**, 3707 (1993).

[6] E. Zavattini *et al.* [PVLAS Collaboration], Phys. Rev. Lett. **96**, 110406 (2006);
E. Zavattini *et al.*, Phys. Rev. D **77** 032006 (2008);
M. Bregant *et al.* [PVLAS Collaboration], Phys. Rev. D **78**, 032006 (2008).

[7] R. Battesti *et al.*, Eur. Phys. J. D **46**, 323 (2008);

[8] W.T. Ni, Chinese J. Phys. **34** 962 (1996).

[9] P. Pugnat *et al.*, Czech. J. Phys. A **56** C193 (2006).

[10] S. Andriamonje *et al.* [CAST Collaboration], JCAP **0704** (2007) 010.

[11] P. Sikivie, D. B. Tanner and K. van Bibber, Phys. Rev. Lett. **98** (2007) 172002.

[12] See for instance `http://axion-wimp.desy.de/e30/e258/talk-21-cantatore.pdf`

Lasers for the Axion-like Particle Search

Matthias Hildebrandt, Maik Frede, Bastian Schulz, Dietmar Kracht

Laser Zentrum Hannover e.V., Hollerithallee 8, 30419 Hannover, Germany

DOI: http://dx.doi.org/10.3204/DESY-PROC-2008-02/matthias_hildebrandt

A couple of promising experiments on the axion-like particle search (ALPS) are currently ongoing, reaching a level of high interest in the field of light particle research. In all kind of these experiments lasers are used to directly produce ALP or detect indirect ALP effects like polarization changes. For the direct production the number of produced ALP scales with the number of photons interacting with a strong magnetic field. Therefore, high power laser systems are needed to produce a detectable number of ALP. Laser parameters like wavelength, beam quality and operation regimes (cw or pulsed) directly effect the experiments sensitivity. The design considerations for different laser systems as well as some suitable laser systems for the ALPS will be presented.

1 Introduction

In recent years several research groups have addressed the search for theoretically predicted light particles such as ALP. In principle, laser light propagating through a magnetic field B undergoes a conversion and reconversion from photons to ALPs. These light particles are not supposed to interact with dense matter and can therefore hardly be detected directly. However, the so called "shining light through a wall" experiments take advantage of this phenomenon. After a certain interaction length l a beam-block is placed inside the magnet. ALPs that propagate through this barrier get reconverted to photons in a second magnetic field. This regenerated light can then be detected with low-noise photo-detectors. A second predicted effect that accompanies the ALP conversion process is a slight rotation between the incident and regenerated light polarization which can be detected to provide evidence for the generation of these particles.

$$P_{\gamma\to a} = \frac{4B_{ext}^2\omega^2}{M^2 m_a^4}\sin^2\left(\frac{m_a^4 l}{4\omega}\right) \tag{1}$$

$$R = (P_{\gamma\to a})^2\left(\frac{P_l}{\omega}\right)\eta \tag{2}$$

The conversion probability and regeneration rate are described by Eq. 1 and 2 for light polarized parallel to the magnetic field ($E||B$) with the inverse axion coupling coefficient M and the axion mass m_a [1]. Parameters that are related to the laser source being used are the photon energy ω, detector efficiency η and the optical power P_l. The laser power inside the magnetic field determines the number of photons that can possibly be converted.

Nowadays, fiber based lasers with 400 W of output power in linear polarized continuous-wave (cw) operation are commercially available with nearly diffraction limited beam quality at a

wavelength around 1 μm [2]. Although CO_2 gas lasers with even more output power and good beam quality are on the market, the emission wavelength of 10.6 μm would not allow for a straightforward detection. Fiber and solid-state lasers can deliver significantly more output power up to several kW, with degraded beam quality and unpolarized output [3]. The beam quality does not directly effect the ALP conversion efficiency, but is of some concern when mechanical apertures formed by magnet tubes limit the maximum size and divergence of the laser beam and small focus spots of only a few μm diameter on the photo-detector array are needed. Continuous-wave laser sources with up to 18 W have been installed in ALPS experiments with single- and multiple passes through the magnet [1, 4]. These were argon-ion based gas lasers emitting at 514 nm. An emission in this wavelength range is favorable for ALPS experiments due to smaller costs and better performance of photo-detectors available for this wavelength.
Pulsed lasers offer significantly lower average powers and consequently a relatively low time-integrated photon flux. Still they have been applied very successfully in ALPS experiments [5]. Commercial systems deliver a few hundred mJ pulse energy in the infrared and offer an excellent conversion efficiency into visible and ultraviolet wavelength ranges [6]. A temporal synchronization of laser pulses and detector exposure-time increases the signal to noise ratio.

2 Single-frequency laser for cavity-locking

In recent years the highest output power demonstrated from a laboratory fiber laser with linear polarization and close to diffraction limited beam quality was 633 W [7] showing the current limitation to increase the ALP detection sensitivity by scaling the laser power. An attractive alternative for ALPS experiments are Fabry-Pérot cavities installed inside the magnet that provide a large resonant power buildup [8, 9]. These cavities can either be operated with an active laser material placed inside the resonator or as passive high finesse cavities with a frequency coupling to an external laser, also referred to as injection-locking. The intra-cavity power in standing wave laser cavities depends on the mirror transmission and additional parasitic losses, the available laser gain and the saturation intensity of the laser material [10]. Intra-cavity powers of several kW should be feasible with minimized cavity losses and high laser gain. The power buildup in passive Fabry-Pérot cavities and their application for ALPS experiments is reviewed in detail by T. Meier *et al.* [11]. For an efficient resonant coupling of a laser to the fundamental transverse mode of a Fabry-Pérot cavity a laser source with diffraction limited beam quality and a stable narrow-linewidth emission spectrum is needed. Narrow-linewidth laser emission has been demonstrated from distributed feedback or external-cavity semiconductor lasers, ytterbium and erbium doped fiber lasers with integrated fiber Bragg gratings and solid-state micro-chip or non-planar ring oscillators (NPRO). Stable single-frequency operation with only one resonant longitudinal laser mode and a minimization of external and internal noise sources enable a free-running operation with a linewidth of only a few kHz. With a linewidth of 1 kHz (measured over 100 ms) and a frequency stability of less than 1 MHz per minute, NPROs provide one of the most stable single-frequency laser emission with typically 2 W of output power at 1064 nm [12]. NPROs have been installed in large-scale interferometers for gravitational-wave detection. These interferometers also comprise Fabry-Pérot cavities to enhance laser power and improve detector sensitivity. For the next stage Laser Interferometer Gravitational-Wave Observatory (Advanced LIGO) a power buildup to 830 kW was proposed [13]. Such high intra-cavity powers are obtained by resonantly coupling a single-frequency laser with 200 W of output power, linear polarization and nearly diffraction limited beam quality to a series of high finesse cavities. Due to thermo-optical restrictions, this output power can not be extracted directly from a NPRO. The Advance LIGO laser system comprises a four-stage Nd:YVO amplifier, delivering 35 W of output power, and a Nd:YAG based laser oscillator resonantly coupled to the NPRO master-oscillator [14]. This laser system is perfectly suited for an application in ALPS experiments and is currently installed up to the amplifier stage at DESY in Hamburg, for an ongoing “light shining through a wall” experiment named “ALPS” with a HERA dipole magnet [15]. A schematic representation of the laser system is shown in Fig. (1). The NPRO emission is passed through a pair of wave-plates to

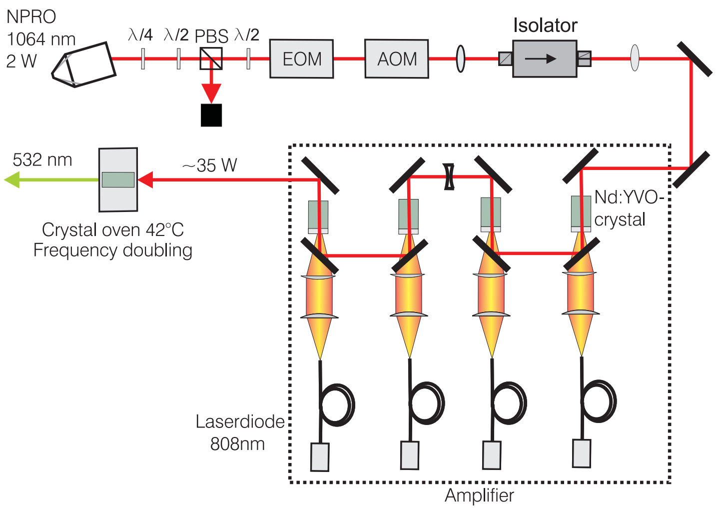

Figure 1: Schematic setup of the single-frequency laser system installed at ALPS (DESY). (PBS polarizing beam splitter, EOM electro-optic modulator, AOM acousto-optic modulator.

linearize the elliptical polarization. Electro-optic and acousto-optic modulators are installed for frequency and amplitude stabilization and a Faraday isolator protects the NPRO against backward propagating radiation. The amplifier consists of four Nd:YVO crystals pumped by four fiber-coupled laser diodes. An amplified output of more than 35 W with a fundamental mode TEM_{00} content of more than 95% is obtained with excellent long term stability. For the ALPS experiment the 1064 nm emission is frequency doubled in a periodically poled KTP crystal. Currently in single-pass configuration 0.8 W at 532 nm are achieved. With a resonant cavity for power enhancement, conversion efficiencies of 40-50% are expected.
An alternative amplification scheme for single-frequency radiation has been presented in the past using ytterbium doped large mode-area (LMA) fibers. Although nonlinear effects such as Brillouin scattering exacerbate the amplification of narrow-linewidth signals due to the long interaction length and small core size, impressive results have been obtained with 402 W of output power with linear polarization and good beam quality [16]. Extremely high gain allows for single-pass amplification to high power levels with good efficiency. Ytterbium doped fiber amplifiers are very promising candidates for future single-frequency laser applications with more than a kW of optical power.

3 Summary

We have presented considerations on the selection of laser sources and parameters for axion-like particle search experiments. Depending on the experimental approach different parameters such as emission wavelength, output power and pulsed or continuous-wave operation come into consideration. The use of resonantly coupled Fabry-Pérot cavities to enhance the laser power inside the dipole magnets has been studied intensely in the past. This approach includes the need for single-frequency laser radiation. Nonplanar ring oscillators offer extremely frequency stable radiation which can be amplified using solid-state or ytterbium doped fiber amplifiers and used as input sources for resonant cavity-locking.

References

[1] R. Cameron *et al.*, "Search for nearly massless, weakly coupled particles by optical techniques BFRT," Phys. Rev. D **47** (1993).

[2] IPG Laser GmbH.

[3] Trumpf Laser GmbH.

[4] P. Pugnat *et al.*, "First results from the OSQAR photon regeneration experiment: No light shining through a wall," arXiv:0712.3362 (2007).

[5] A.S Chou, "Search for axion-like particles using a variable baseline photon regeneration technique," arXiv:0710.3783v2 (2007).

[6] Continuum Inc.

[7] Y. Jeong *et al.*, "Single-mode plane-polarized ytterbium-doped large-core fiber laser with 633-W continuous-wave output power," Opt. Lett. **30** (2005).

[8] M. Bregnant *et al.*, "Limits on Low Energy Photon-Photon Scattering from an Experiment on Magnetic Vacuum Birefringence," arXiv:0805.3036 (2008).

[9] R. Battesti *et al.*, "The BMV experiment: a novel apparatus to study the propagation of light in a transverse magnetic field" arXiv:0710.1703v1 (2007).

[10] A.E. Siegman, *Lasers*, University Science Books (1986).

[11] T. Meier *et al.*, "Raising WISP production rate by use of optical cavities" Proc. 4th Patras Workshop (2008).

[12] T.J. Kane *et al.*, "Monolithic, unidirectional single-mode Nd:YAG ring laser" Opt. Lett. **10** (1985).

[13] A. Weinstein, "Advanced LIGO optical configuration and prototyping effort" Class. Quantum Grav. **19** (2002).

[14] M. Frede *et al.*, "195 W Injection-Locked Single-Frequency Laser System," CLEO Conference CMA1 (2005).

[15] K. Ehret *et al.*, "Production and Detection of Axion-Like Particles in a HERA Dipole Magnet - Letter-of-Intent for the ALPS experiment," DESY 07-014 (2006).

[16] Y. Jeong *et al.*, "Power Scaling of Single-Frequency Ytterbium-Doped Fiber Master-Oscillator Power-Amplifier Sources up to 500 W," J. Quantum Elect. **13** (2007).

WISP Hunting - some New Experimental Ideas

Joerg Jaeckel

Institute for Particle Physics and Phenomenology, Durham University, Durham DH1 3LE, UK

DOI: http://dx.doi.org/10.3204/DESY-PROC-2008-02/jaeckel_joerg

We present several new ideas on how to search for weakly interacting sub-eV particles in laboratory experiments. The first experiment is sensitive to minicharged particles. It exploits that in strong electric fields particle - antiparticle pairs are produced by the Schwinger mechanism. The charged particles move along the lines of the electric field and generate a current that can be measured. The other two experiments are designed to search for hidden-sector photons. They are based on photon - hidden photon oscillations and resemble classic light shining through a wall experiments. One uses (nearly) constant magnetic fields instead of the laser light. Photon - hidden photon mixing would allow these magnetic fields to leak through superconducting shielding which would ordinarily eliminate all magnetic fields. The other one replaces the laser light with microwaves inside cavities. The latter can achieve much higher quality factors than optical cavities increasing the sensitivity.

1 Introduction

Over the last few years it became increasingly clear that low energy experiments can provide a powerful tool to explore hidden sectors of particles which interact only very weakly with the ordinary standard model particles. Such hidden sectors appear in many extensions of the standard model. In fact, it may be exactly those hidden sectors that give us crucial information on how the standard model is embedded into a more fundamental theory as, e.g., string theory.

The key observation from the viewpoint of low energy experiments is that, due to their feeble interactions with the standard model particles, the hidden sector particles are relatively unconstrained allowing them to be light possibly even in the sub-eV range. This opens the possibility for observable effects in low energy but high precision experiments.

In this note we will focus on two particular classes of such light 'hidden-sector' particles: minicharged particles and hidden sector photons. The former are particles interacting with the ordinary electromagnetic field via the usual minimal coupling induced by the covariant derivative,

$$D_\mu = \partial_\mu - \mathbf{i}Q_f e A_\mu \tag{1}$$

where Q_f is the electric charge of the particle of a particle f. For example if f is a fermion the interaction term reads $Q_f e\bar{f}\not{A}f$.

The crucial point for a minicharged particle is now simply that the charge is much smaller than 1,

$$Q_f \ll 1. \tag{2}$$

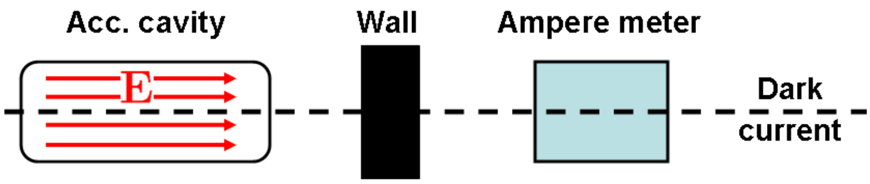

Figure 1: Schematic illustration of an *accelerator cavity dark current* (AC/DC) experiment for searching minicharged particles.

In particular it is not necessarily integer. Indeed it does not even have to be a rational number. Minicharges can arise in theories with kinetic mixing [1] (see also below) but also in scenarios with extra dimensions [2]. Typical predicted values, e.g., in realistic string compactifications range from 10^{-16} to 10^{-2} [2, 3].

The second class of particles we are concerned with in this note are massive hidden sector photons. These are extra U(1) gauge bosons which can mix with the ordinary electromagnetic photons via a so-called kinetic mixing term [1] in the Lagrangian,

$$\mathcal{L} = -\frac{1}{4}F^{\mu\nu}F_{\mu\nu} - \frac{1}{4}X^{\mu\nu}X_{\mu\nu} - \frac{1}{2}\chi\, F^{\mu\nu}X_{\mu\nu} + \frac{1}{2}m^2_{\gamma'}X_\mu X^\mu + j_\mu A^\mu, \tag{3}$$

where $F_{\mu\nu}$ is the field strength tensor for the ordinary electromagnetic $\mathrm{U}(1)_{\mathrm{QED}}$ gauge field A^μ, j^μ is its associated current (generated by electrons, etc.) and $X^{\mu\nu}$ is the field strength for the hidden-sector $\mathrm{U}(1)_{\mathrm{h}}$ field X^μ. The first two terms are the standard kinetic terms for the photon and hidden photon fields, respectively. Because the field strength itself is gauge invariant for U(1) gauge fields, the third term is also allowed by gauge and Lorentz symmetry. This term corresponds to a non-diagonal kinetic term, the kinetic mixing [1]. This term is a renormalizable dimension four term and does not suffer from mass suppressions. It is therefore a sensitive probe for physics at very high energy scales. Kinetic mixing arises in field theoretic [1] as well as in string theoretic setups [2, 3] and typical predictions for its size range between 10^{-16} and 10^{-2}. The second to last term is a mass term for the hidden photon. This could either arise from a Higgs mechanism or it could be a Stückelberg mass term [4].

2 AC/DC an experiment to search for minicharged particles

The basic setup [5] is depicted in Fig. 1. In a strong electric field a vacuum pair of charged particles gains energy if the particles are separated by a distance along the lines of the electric field. If the electric field is strong enough (or the distance large enough) the energy gain can overcome the rest mass, i.e. the virtual particles turn into real particles. This is the famous Schwinger pair production mechanism [6]. After their production the electric field accelerates the particles and antiparticles according to their charge in opposite directions. This leads to an electric current (dashed line in Fig. 1). If the current is made up of minicharged particles the individual particles have very small charges and interact only very weakly with ordinary matter. Therefore, they can pass even through thick walls nearly unhindered. An electron current, however, would be stopped. After passage through the wall we can then place an ampere meter to detect the minicharged particle current.

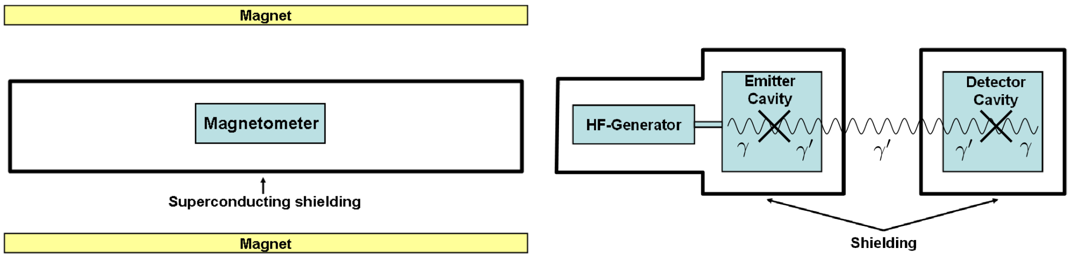

Figure 2: **Left panel:** Sketched setup for the *superconducting box* experiment. **Right panel:** Schematic illustration of a *microwaves permeating through a shielding* experiment for the search for massive hidden sector photons mixing with the photon (a high-frequency (HF) generator drives the emitter cavity).

Typical accelerator cavities achieve field strengths of $\gtrsim 25\,\mathrm{MeV/m}$ and their size is typically of the order of 10s of cm. Precision ampere meters can certainly measure currents as small as μA and even smaller currents of the order of pA seem feasible. Using the Schwinger pair production rate we can then estimate the expected sensitivity for such an experiment to be

$$\epsilon_{\rm sensitivity} \sim 10^{-8} - 10^{-6} \quad \text{for } m_\epsilon \lesssim \text{meV}. \tag{4}$$

Therefore such an experiment has the potential for significant improvement over the currently best laboratory[1] bounds [9, 10], $\epsilon \lesssim$ few 10^{-7}.

3 Searching hidden photons inside a superconducting box

The basic idea [11] of the proposed experiment is very similar to a classic *light shining through a wall experiment* [12]. However, instead of light it uses a static magnetic field and the wall is replaced by superconducting shielding (cf. Fig. 2). Outside the shielding we have a strong magnetic field. Upon entering the superconductor the ordinary electromagnetic field is exponentially damped with a length scale given by the London penetration depth $\lambda_{\rm Lon}$. Yet, due to the photon – hidden photon mixing a small part of the magnetic field is converted into a hidden magnetic field. After the superconducting shield is crossed the mixing turns a small fraction of the hidden magnetic field back into an ordinary magnetic field that can be detected by a magnetometer. Since the magnetometer measures directly the field (and not some probability or power output) the signal is proportional to the transition amplitude and therefore to the mixing squared, χ^2, instead of being proportional to χ^4.

High precision magnetometers can measure fields of the order of 10^{-13} T and even tiny fields of a few 10^{-18} T seem feasible. The expected sensitivity is shown as the blue area in Fig. 3.

4 A cavity experiment to search for hidden photons

Our final proposal [13] (see [14] for a similar proposal for axions [2]) is another setup searching for signatures of photon – hidden photon oscillations which resembles a classic *light shining through*

[1]Astrophysical bounds are much stronger [7] but are also somewhat model dependent [8].

[2]The only change necessary for an axion search is that one applies an additional magnetic field which allows for the usual photon–axion conversion inside magnetic fields. One might be worried that in this case one cannot

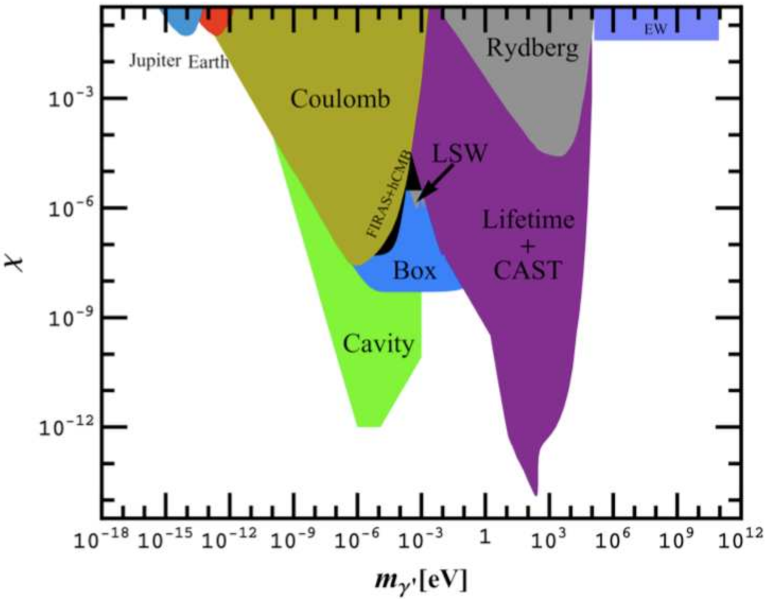

Figure 3: Current bounds on hidden-sector photons (cf., e.g., [16] and references therein). The *superconducting box* experiment could probe the blue region (Box). The estimated sensitivity for the *microwaves permeating through a shielding* is shown in green (Cavity). For details on the respective setups see [11, 13].

a wall [12] experiment, more precisely a resonant setup [15]. It consists of two microwave cavities shielded from each other (cf. Fig. 2). In one cavity, hidden photons are produced via photon – hidden photon oscillations. The second, resonant, cavity is then driven by the hidden photons that permeate the shielding and reconvert into photons. Due to the high quality factors achievable for microwave cavities (superconducting ones can reach $Q \sim 10^{11}$) and the good sensitivity of microwave detectors $\sim 10^{-26} - 10^{-20}$ W such a setup will allow for an unprecedented discovery potential for hidden sector photons in the mass range from μeV to meV (green area in Fig. 3).

5 Conclusions

We have presented several ideas for small scale laboratory experiments to search for weakly interacting sub-eV particles predicted in many extensions of the standard model. For minicharged particles an *accelerator cavity/dark current* experiment promises improvement over current laboratory bounds. Both the *superconducting box* and the *microwaves permeating through a shielding* experiment have the potential to improve not only upon the current laboratory but

use superconducting cavities because a magnetic field applied from outside the cavity cannot permeate through the superconductor to the inside of the cavity where it is needed for the conversion. This would allow only normal conducting cavities which have somewhat smaller Q. However, this may not be the case if one uses type II superconductors which allow for magnetic field penetration (via flux tubes) while maintaining their superconducting properties. Nevertheless, the magnetic field (and the flux tubes) can increase the surface resistance, again limiting the Q factor. Further investigation is needed to determine if one can achieve high Q with a strong magnetic field on the inside of the cavity.

also beyond existing astrophysical and cosmological bounds, thereby having significant discovery potential for new physics. Searching for extremely weakly interacting particles at small masses that would be missed in conventional colliders all these experiments provide for a new, complementary probe of fundamental physics.

Finally, we would like to point out that an experiment of the *microwaves permeating through a shielding* type is already in an initial stage [17] and will also be used to search for axions and axion-like particles.

Acknowledgements

The author wishes to thank the organizers of the *4th Patras Workshop on Axions, WIMPs and WISPs* for a very enjoyable and stimulating meeting. Moreover he is indebted to M. Ahlers, H. Gies, J. Redondo and A. Ringwald for many many interesting discussions and fruitful collaboration.

References

[1] B. Holdom, Phys. Lett. B **166** (1986) 196.

[2] B. Batell and T. Gherghetta, Phys. Rev. D **73** (2006) 045016 [hep-ph/0512356].

[3] K. R. Dienes, C. F. Kolda and J. March-Russell, Nucl. Phys. B **492** (1997) 104 [hep-ph/9610479]; D. Lüst and S. Stieberger, hep-th/0302221; S. A. Abel and B. W. Schofield, Nucl. Phys. B **685** (2004) 150 [hep-th/0311051]; R. Blumenhagen, S. Moster and T. Weigand, Nucl. Phys. B **751** (2006) 186 [hep-th/0603015]; S. A. Abel, J. Jaeckel, V. V. Khoze and A. Ringwald, hep-ph/0608248; S. A. Abel, M. D. Goodsell, J. Jaeckel, V. V. Khoze and A. Ringwald, 0803.1449 [hep-ph].

[4] E. C. G. Stückelberg, Helv. Phys. Acta **11** (1938) 225.

[5] H. Gies, J. Jaeckel and A. Ringwald, Europhys. Lett. **76** (2006) 794 [hep-ph/0608238].

[6] J. Schwinger, Phys. Rev. **82** (1951) 664.

[7] S. Davidson, S. Hannestad and G. Raffelt, JHEP **0005** (2000) 003 [hep-ph/0001179].

[8] E. Masso and J. Redondo, JCAP **0509**, (2005) 15, hep-ph/0504202; Phys. Rev. Lett. **97**, (2006) 151802, hep-ph/0606163; J. Jaeckel, E. Masso, J. Redondo, A. Ringwald, and F. Takahashi, hep-ph/0605313; Phys. Rev. **D75**, (2007) 013004, hep-ph/0610203; P. Brax, C. van de Bruck, and A.-C. Davis, Phys. Rev. Lett. **99**, (2007) 121103, hep-ph/0703243.

[9] H. Gies, J. Jaeckel and A. Ringwald, Phys. Rev. Lett. **97** (2006) 140402 [hep-ph/0607118]; M. Ahlers, H. Gies, J. Jaeckel and A. Ringwald, Phys. Rev. D **75** (2007) 035011 [hep-ph/0612098]; M. Ahlers, H. Gies, J. Jaeckel, J. Redondo and A. Ringwald, Phys. Rev. D **77** (2008) 095001 [0711.4991 [hep-ph]].

[10] A. Badertscher *et al.*, Phys. Rev. D **75** (2007) 032004 [hep-ex/0609059]; S. N. Gninenko, N. V. Krasnikov and A. Rubbia, Phys. Rev. D **75** (2007) 075014 [hep-ph/0612203].

[11] J. Jaeckel and J. Redondo, 0806.1115 [hep-ph].

[12] P. Sikivie, Phys. Rev. Lett. **51**, 1415 (1983) [Erratum-ibid. **52**, 695 (1984)]; A. A. Anselm, Yad. Fiz. **42**, 1480 (1985); M. Gasperini, Phys. Rev. Lett. **59**, 396 (1987); K. Van Bibber, N. R. Dagdeviren, S. E. Koonin, A. Kerman and H. N. Nelson, Phys. Rev. Lett. **59**, 759 (1987).

[13] J. Jaeckel and A. Ringwald, Phys. Lett. B **659** (2008) 509 [0707.2063 [hep-ph]].

[14] F. Hoogeveen, Phys. Lett. B **288** (1992) 195.

[15] F. Hoogeveen and T. Ziegenhagen, Nucl. Phys. B **358** (1991) 3; P. Sikivie, D. B. Tanner and K. van Bibber, Phys. Rev. Lett. **98** (2007) 172002 [hep-ph/0701198].

[16] M. Ahlers, J. Jaeckel, J. Redondo and A. Ringwald, 0807.4143 [hep-ph].

[17] P. L. Slocum, talk at the *4th Patras Workshop on Axions, WIMPs and WISPs* 2008, Hamburg, http://axion-wimp.desy.de/e30

Pictures


Have fun !

List of Authors

List of Participants

Anastassopoulos, Vassilis, University of Patras
Baker, Oliver, Yale University
Baudis, Laura, University of Zurich
Boyarsky, Alexey, CERN
Bruch, Tobias, University of Zurich
Giovanni, Cantatore, INFN
Cerdeno, David, University of Madrid
Chelouche, Doron, Princeton
Chou, Aaron, Fermilab
Davenport, Martyn, CERN
De Angelis, Alessandro, University of Udine
Ehret, Klaus, DESY
Fouch, Mathilde, Universit de Toulouse
Frede, Maik, LHZ, Hannover
Galaverni, Matteo, University of Ferrara
Guendelman, Eduardo, Ben Gurion University, Israel
Guthoerk, Tillmann, University of Freiburg
Hildebrandt, Matthias, LHZ, Hannover
Huber, Patrick, CERN
Incicchitti, Antonella, INFN
Jaeckel, Joerg, Durham University
Karuza, Marin, INFN
Kim, Seung Cheon, Seoul National University
Knabbe, Axel, DESY
Koehler, Martin, DESY
Kotthaus, Rainer, MPI, Munich
Kuster, Markus, Technical University of Darmstadt
Laarmann, Tim, DESY
Lanfranchi, Jean-Come, University of Munich
Lubimov, Valentin, DESY
Lindner, Axel, DESY
Meier, Tobias, MPI, Hannover
Meyer, Hinrich, DESY
Minowa, Makoto, University of Tokyo
Mirizzi, Alessandro, MPI, Munich
Nordt, Annika, Technical University of Darmstadt

Pugnat, Pierre, CERN
Quast, Guenter, University of Karlsruhe
Raffelt, Georg, MPI, Munich
Redondo, Javier, DESy
Regenfus, Christian, CERN
Riemer-Soerensen, Signe, Niels Bohr Institute
Ringwald, Andreas, DESY
Ripken, Joachim, University of Hamburg
Roncadelli, Marco, INFN
Ruchayskiy, Oleg
Russenschuck, Stephan, CERN
Ruz Armendariz, Jaime, CERN
Sakharov, Aleksandre, CERN
Schleper, Peter, University of Hamburg
Schumann, Marc, Rice University, Houston
Siemko, Andrzej, CERN
Sigl, Guenter, University of Hamburg
Sikivie, Pierre, University of Florida
Slocum, Penny, Yale University
Solanki, Sami K., MPI, Katlenburg-Lindau
Spooner, Neil, University of Sheffield
Tajuddin, Nurhana, University of Zurich
Tziaferi, Eirini, University of Zurich
Vogel, Julia, University of Freiburg
Wantz, Olivier, University of Cambridge
Weltman, Amanda, University of Cambridge
Wester, William, FNAL
Willke, Benno, MPI, Hannover
Zioutas, Konstantin, CERN